Self-assembly, study and applications of metalosupramolecular capsules based on Subphthalocyanines

Irene Sánchez-Molina Santos

Tesis Doctoral

Mayo 2013

Universidad Autónoma de Madrid

Realmente nada hay en el mundo más noble y raro que una amistad verdadera.

(Oscar Wilde)

El presente trabajo ha sido realizado en el Departamento de Química Orgánica de la Universidad Autónoma de Madrid bajo la dirección de los profesores Tomás Torres Cebada y Christian G. Claessens, a quienes quiero expresar mi más sincero agradecimiento

Agradecimientos

En primer lugar me gustaría dar las gracias a mis dos directores de tesis, *Tomás Torres* y *Christian Claessens.* Gracias a Tomás por su implicación durante este último año, por el buen trato, la confianza, y por su disposición a escuchar siempre. Gracias a Christian la confianza depositada en mí para hacer este trabajo.

En cuanto al grupo, gracias tanto a los que trabajan actualmente en el laboratorio como a los que ya se han ido de postdoc o los que han pasado fugazmente unos meses, por el compañerismo y la profesionalidad que han demostrado.

Thanks to *Dirk Guldi* and *Bruno Grimm* for their help during my stay in Erlangen. And a million thanks to all the people in Guldi's group for the great moments I spent there, not only during the stay but also when I've gone back to enjoy the Berg and their company.

Thanks also to *Peter Stang* and coworkers for the excellent experience in his research group. Especially, I'd like to thank *Tim*, *Bryant,* and *Margaret*, for their help with chemistry or administrative stuff while I was in Utah and because after more than one year they still find time to answer my emails.

También quiero dar las gracias a *Germán* y *Guillermo* por ser tan buenos compañeros de vitrina, seguramente mejores y más ordenados que yo. Gracias a *Anaïs* por ser el buen rollo personificado y porque las personas como ella son las que mejoran la calidad media de la raza humana.

Muy especialmente, *Olga, María "Pequeña", María, Carol, Eva, Laura* (algún día de verdad que iré a visitarte a Colombia) *y Jaramillo* son responsables de la mayoría de los buenos ratos dentro y fuera del laboratorio. Gracias por todo vuestro apoyo y ánimos para la química y las impurezas del día a día. Muchísimas gracias al "equipo piscina y compañía", *Emilie, Arturo, Mariam, Cinthya, Abraham*, *Satoko, Jose, Ricardo, Laura* porque sois la mejor sorpresa que me podía traer este último año de tesis. Gracias también a *Laura*, que aquí o en Murcia siempre me transmite su alegría vital.

Tanto en Erlangen como Salt Lake City conocí a muchas personas increíbles que a pesar de la distancia y el tiempo siempre serán un poco especiales. A ellos quiero darles las gracias por acordarse de escribir de vez en cuando y porque siempre ha sido y será un placer volver a verlos y recordar la huella que me han dejado. Gracias a *Noelia, Leandro, Oana, Eduard, Anna, Vito, Andrés, Susi, Ines, Sabrina* –en Erlangen- y *Tom, Lisa, Hauke, Mariano, Josh, Matt, Carolina, Georgia, Clayton, Linda, Luke*, *Karolina y David* (gracias a éste último por la iniciación a la guitarra)- en Salt Lake City.

Gracias a cada uno de esos amigos que siempre se acuerdan de mí y de los que siempre me acuerdo para lo bueno y para lo malo, *María, Ana, Juanjo, Carlos, Mery, Bárbara, Miguel (Pichi), Sandra, Juan, Claudio, Kristina, Rita, Pamela y* a mi hermana *Sara* por ser las personas con las que puedo compartir desde las risas más absurdas hasta el pensamiento más profundo, porque si es verdad eso de que *la carretera desemboca en el puerto donde me esperan los buenos amigos*, allí estáis vosotros seguro (… *y todo lo demás no importa* ♪).

Muchísimas gracias, por último, a mis padres, por su apoyo incondicional para todo, por ayudarme a no perder el equilibrio mental, por su amor y porque sin unos padres tan estupendos como ellos no sería la persona que soy.

Parte del trabajo descrito en esta memoria ha servido como contribución a los siguientes artículos:

- ***"Self-sorting among the diastereoisomers of a M_3L_2 subphthalocyanine capsule",*** C.G. Claessens, I. Sánchez-Molina, T.Torres*, Supram. Chem.* **2009***, 21,* 44-47.
- ***"Trapping fullerenes with Jellyfish-like Subphthalocyanines".*** I. Sánchez-Molina, C. G. Claessens, B. Grimm, D. M. Guldi, T. Torres. *Chemi. Sci., **2013**, 4,* 1338-1344.
- ***"On the stability of Subphthalocyanine-based capsules studied by ESI-QTOF tandem mass spectrometry experiments".*** I. Sánchez-Molina, M. J. Vicente-Arana, C. G. Claessens, T. Torres. *J. Mass. Spectrom.* (accepted, in press).
- ***"Self-assembly, host-guest chemistry and photophysical properties of subphthalocyanine-based metallosupramolecular capsules".*** I. Sánchez-Molina, B. Grimm, C. G. Claessens, D. M. Guldi, T. Torres. (submitted)
- ***"Incorporation of a tricationic subphthalocyanine in an organic photovoltaic device"***, I. Sánchez-Molina, A. Soriano C. G. Claessens, T. Torres, H. Bolink (submitted).

Pre-doctoral stays

- Photophysical measurements were carried out during a pre-doctoral (November-January 2010) stay in the group of Dirk M. Guldi (Friedrich-Alexander Universität Erlangen-Nürnberg), in close collaboration with Bruno Grimm.

- The work on porphyrin prisms described in Chapter 2 was carried out during a pre-doctoral stay (Sepetember-December 2011) in the group of Peter J. Stang (University of Utah), with the unvaluable guidance and advice of Timothy R. Cook.

- During the last year, I spent two weeks (March 2013) in Miguel A. Miranda's group, where I received training on photochemistry. I would like to express here my acknowledgements to all the people in his group for their help and patience.

Abreviations

QSM	Química Supramolecular
SubPc	Subphthalocyanine
Pc	Phthalocyanine
S-BINAP	*S*-1,1'-bis(diphenylphosphinodinaphthalene)
dppp	1,1'-bis(diphenylphosphinopropane)
dppf	1,1'-bis(diphenylphosphinoferrocene)
en	ethylendiamine
Chls	Chlorophills
COD	Ciclooctadiene
tpyP	5,10,15,20- tetra-(4-pyridyl)porphyrin
OPVs	Organic photovoltaics
HTL	Hole transporting layer
PEDOT	poly (3,4-ethylendioxy)tiophene
PSS	polystyrene sulphonate
BCP	Bathocuproine

Table of contents

Self-assembly, study and applications of metalosupramolecular capsules based on Subphthalocyanines

Resumen en español

Introducción

El progresivo agotamiento de combustibles fósiles hace imprescindible la búsqueda de fuentes de energía alternativas. Entre ellas, la energía solar destaca como una de las más prometedoras para cubrir la demanda energética mundial.

Por otro lado, el desarrollo de sistemas supramoleculares que funcionen como dispositivos a escala molecular ha sido un área muy activa desde el nacimiento de la química supramolecular. La química supramolecular[1] (QSM) se ocupa del estudio de las interacciones que se producen entre distintas moléculas. Es decir, cuando hablamos de QSM nos estamos moviendo en el campo de las interacciones no covalentes, tales como enlaces de hidrógeno, fuerzas de Van der Waals, interacciones dipolo-dipolo, enlaces de coordinación, π-π stacking, etc. Al tratarse de fuerzas relativamente débiles, todos los procesos que tienen lugar en QSM dependen exclusivamente de la termodinámica, y no de la cinética. Esta es la principal ventaja de la QSM a nivel sintético, ya que para cualquier ensamblado que se quiera obtener, una vez mezclados los precursores el sistema evoluciona a través de varios equilibrios termodinámicos hasta dar el producto o productos más estables. Este proceso se conoce como autoensamblaje, e implica varios procesos de reconocimiento molecular (es decir, una combinación de unidades complementarias, por ejemplo un dador y un aceptor de enlace de hidrógeno) entre las distintas unidades básicas, que al combinarse mediante interacciones no covalentes darán lugar al ensamblado supramolecular.

En numerosos casos, los ensamblados supramoleculares poseen una cavidad en la cual, también mediante interacciones no covalentes, puede alojarse otra molécula. Este fenómeno, conocido como química host-guest,[2] también está basado en procesos de reconocimiento molecular. La estabilidad de los complejos formados mediante este proceso se estima mediante el cálculo de las constantes

[1] (a) J. M. Lehn, *Supramolecular chemistry: concepts and perspectives*, VCH, Weinheim 1995; (b) Y. S. Lee, *Self-assembly and nanotechnology: a force balance approach*, John Wiley &Sons, New Yersey 2008; (c) J. W. Steed, J. L. Atwood, *Supramolecular Chemistry*, 2nd edition, John Wiley & Sons, 2009.

[2] (a) K. A. Connors, *Binding Constants,* Wiley & Sons, New York, 1987; (b) J. Polster, H, Lachmann, *Spectrometric titrations*, VCH; Weinheim, 1989; (c) P. Thodarson, *Chem. Soc. Rev.*, **2011**, *40*, 1305-1323.

termodinámicas del equilibrio de asociación, que generalmente se lleva a cabo mediante valoraciones.

La química metalosupramolecular[3] utiliza como unidades básicas, por un lado, metales, y por otro, compuestos orgánicos que poseen grupos funcionales capaces de coordinarse a ellos. El uso de metales para dirigir el autoensamblaje de moléculas permite obtener compuestos de geometría y tamaño bien definidos, gracias a que los enlaces de coordinación se producen en direcciones determinadas.

En el contexto en que se enmarca esta tesis, las fuerzas intermoleculares se emplearán con el propósito de organizar de manera efectiva y sencilla ciertos cromóforos que podrían participar en procesos fotoinducidos, produciéndose así una conversión de luz visible.

Las subftalocianinas[4] (SubPcs) fueron descubiertas por Meller y Ossko en 1972, cuando estos investigadores intentaban obtener una ftalocianina de boro. Son compuestos aromáticos que presentan una estructura cóncava formada por la unión de tres unidades de 1,3-diiminoisoindol fusionadas alrededor de un átomo de boro.

La síntesis de las SubPcs se realiza mediante la condensación de ftalonitrilos en presencia de un haluro de boro. Cuando dichos ftalonitrilos poseen un sustituyente en la posición 4, la ciclotrimerización da lugar a dos regioisómeros, C_3 y C_1. Cada uno de estos regioisómeros posee, a su vez, dos enantiómeros, los cuales pueden separarse por HPLC quiral.[5]

Además de una intensa absorción en la región del UV-Visible (con dos bandas, a 300 nm (banda Q) y 580 nm (banda B), las SubPcs presentan propiedades fotofísicas y electroquímicas[6] que las hacen buenas candidatas para diversas aplicaciones en

[3] (a) R. Chakrabarty, P. S. Mukherjee, P. J. Stang, *Chem. Rev,* **2011**, *111*, 6810-6918; (b) M. M. J. Smulders, I. A. Riddell, C. Browne, J. R. Nitschke, *Chem. Soc. Rev,* **2013**, *42*, 1728-1754; (c) Wiester, M. J.; Ulmann, P. A.; Mirkin, C. A. *Angew. Chem., Int. Ed,* **2011**, *50*, 114; (d) T. R. Cook, Y-R. Zheng, P. J. Stang, *Chem. Rev*, **2012**, 734-777; (e) M. D. Ward, *Chem. Commun*. **2009**, 4487-4499

[4] (a)C. G. Claessens, D. Gonzalez-Rodriguez, T. Torres, *Chem. Rev,* **2002**, *102*, 835-853; (b) T. Torres, *Angew. Chem. Int. Ed*, **2006**, *45*, 2834-2837; (c) A. Meller, A. Ossko, *Monatsh. Chem.* **1972**, *103*, 150-155.

[5] (a) C. G. Claessens, T. Torres, *Tetrahedron Lett*, **2000**, *41*, 6361; (b) N. Kobayashi, T. Nonomura, *Tetrahedron Lett.*, **2002**, *43*, 4253-4255.

[6] B. del Rey, U. Keller, T. Torres, G. Rojo, F. Agulló-López, S. Nonell, C. Martí, S. Brasselet, I. Ledoux, J. Zyss, *J. Am. Chem. Soc*, **1998**, *120*, 12808-12817.

sistemas de transferencia de energía y de electrones (OLEDs, células solares, óptica no lineal, etc).[7]

Objetivos

El principal objetivo de la tesis es explotar las posibilidades que ofrece la estructura cóncava de las SubPcs en el área de la química supramolecular. Su versatilidad sintética permitirá incorporar sustituyentes que participen bien en la modificación de las propiedades electrónicas del macrociclo o bien en la organización supramolecular de las SubPcs. Además, la forma de las SubPcs es complementaria a la del fulereno C_{60}, lo cual permite explorar el reconocimiento molecular del mismo con receptores basados en SubPcs.

Así pues, los objetivos básicos son:

- El estudio y empleo de interacciones no covalentes para construir estructuras supramoleculares basadas en SubPcs

- Estudiar la capacidad de dichas estructuras para encapsular otras moléculas en su cavidad, y aprovechar esta propiedad para obtener sistemas fotoactivos supramoleculares.

- Estudiar las propiedades fotofísicas de estas estructuras así como de los aductos formados por encapsulación de huéspedes.

[7] (a) H. Xu, D-K. Ng, *Inorg. Chem*, **2008**, *47*, 7921-7927 ; (b) D.González-Rodríguez, T. Torres, D. M. Guldi, J. Rivera, M. A. Herranz, L. Echegoyen, *J. Am. Chem.Soc*, **2004**, *126*, 6301-6313; (c) D. González-Rodríguez, E. Carbonell, G. de Miguel Rojas, C. Atienza Castellanos, D. M. Guldi, T. Torres, *J. Am. Chem. Soc*, **2010**, *126*, 6301-6313; (d) D. González-Rodríguez, E. Carbonell, D. M. Guldi, T. Torres, *Angew. Chem. Int. Ed.* **2009** , *48*, 8032-8036; (e) C. Romero-Nieto, J. Guilleme, C. Villegas, D. González-Rodríguez, N. Martín, T. Torres, D. M. Guldi, *J. Mater. Chem,* **2011**, *21*, 15914-15918; (f) A. Medina, C. G. Claessens, G. M. A. Rahman, A. M. Lamsabhi, O. Mó, M. Yáñez, D. M. Guldi, T. Torres, *Chem. Commun.* **2008** , 1759-1761; (g)H. H. P Gommans, D. Cheyns, T. Aernouts, C. Girotto, J. Poortmans, P. Heremans, *Adv. Func. Mater*, **2007**, *17*, 2653-2658; (h) H. H. P. Gommans, T. Aernouts, B. Verreet, P. Heremans, A. Medina, C. G. Claessens, T. Torres *Adv. Funct. Mater.*, **2009**, *19*, 3435-3439; (i) B. Verreet, B. P. Rand, D. Cheyns, A. Hadipuor, T. Aernouts, P. Heremans, A. Medina, C. G. Claessens, T. Torres, *Adv. Energy Mat.*, **2012**, *1*, 565-568.

Capítulo 1: Estructuras basadas en Subftalocianinas para reconocimiento supramolecular de fullerenos: síntesis, caracterización, y estudio de sus propiedades.

Este capítulo se centra en el uso de la superficie π de las SubPcs para el reconocimiento molecular de fullerenos. [8]

En la primera parte del capítulo, se describe un estudio sistemático de las interacciones π- π entre SubPcs de diversa naturaleza electrónica y fullerenos C_{60} y C_{70}. Para ello se prepararon SubPcs con sustituyentes periféricos que les confieren carácter aceptor, neutro o dador; por otro lado, en éstas últimas se varió la longitud de las cadenas alquílicas.[9]

Los experimentos llevados a cabo, entre los que se cuentan ensayos de espectrometría de masas, Job Plots y valoraciones, permitieron determinar que la naturaleza electrónica de la SubPc determina la estequiometría del complejo. Por otro lado, la longitud de la cadena alquílica tiene una influencia sobre la cinética del equilibrio de formación del complejo, ralentizándose este al reducirse el número de carbonos de dicha cadena. De esta manera se puso de manifiesto la existencia de interacciones secundarias entre las cadenas alquílicas.

Todas las constantes de asociación calculadas son aproximadamente del mismo orden de magnitud (10^4 M^{-1}).

Por otro, lado, experimentos fotofísicos pusieron de manifiesto que una vez formado el complejo, se produce una transferencia de energía fotoinducida desde el primer singlete excitado de la SubPc al del fullereno.

En la segunda sección del capítulo se utilizan enlacen de coordinación metal-ligando para preorganizar las SubPcs en una estructura tipo cápsula. Se decidió emplear ligandos tipo fosfina para facilitar la caracterización de los ensamblados, y a su vez, se escogieron dichos ligandos de manera que presentasen un interés adicional. Por ejemplo, el ligando 1,1'-difenilfosfinoferroceno ofrece la posibilidad de incorporar dadores de electrones en la periferia del sistema, mientras que el *S*-BINAP permite

[8] (a) R. Ziessel, G. Ulrich, K. J. Elliott and A. Harriman, *Chem.–Eur. J.,* **2009**, *15*, 4980–4984; (b) S. Shimizu, S. Nakano, T. Hosoya and N. Kobayashi, *Chem. Commun.*, **2011**, *47*, 316–318.

[9] I. Sánchez-Molina, C. G. Claessens, B. Grimm, D. M. Guldi, T. Torres, *Chem. Sci,* **2013**, *4*, 1338-1344.

modificar las propiedades de autoensamblaje de la cápsula y abre una vía al posible reconocimiento selectivo de fullerenos quirales.

Así pues, se llevó a cabo la síntesis de una SubPc trisustituída con grupos piridina, que por coordinación a complejos metálicos de Pd o Pt se autoensambló posteriomente en una serie de cápsulas.

El ligando *S*-BINAP permitión estabilizar las cápsulas resultantes de la combinación de dos SubPcs de igual quiralidad, al contrario de lo que ocurre con ligandos no quirales.

Por otro lado, se llevó a cabo un estudio sistemático comparativo de la estabilidad de estos sistemas en función del metal y el ligando mediante espectrometría de masas-masas. Se pudo demostrar la mayor fortaleza del enlace metal-nitrógeno en el caso del Pt frente al Pd, y por otro lado se puso de manifiesto el efecto *trans* de los ligandos al encontrarse más desestabilizadas las cápsulas con ligandos tipo fosfina.

Además, algunas de estas cápsulas se estudiaron en el contexto de la química host-guest. Diversos experimentos demostraron su capacidad para albergar fullerenos y derivados de fullerenos en su cavidad, con constantes de asociación de 10^4 M^{-1}. Mediante estudios de fluorescencia se determinó el efecto del metal así como del fullereno en la fotofísica de la SubPc, viéndose que ambos desactivan la fluorescencia del macrociclo, y pudiéndose establecer la tendencia que sigue esa desactivación en función del huésped, metal, o el disolvente.

Más tarde, los experimentos de espectroscopía de especies transitorias revelaron que dicha desactivación de la fluorescencia se debe a una transferencia de energía que se produce del primer singlete excitado de la SubPc al del fullereno. Tras producirse la conversión de éste a su primer estado triplete excitado, se produce nuevamente una transferencia de energía al triplete de la SubPc.

Capítulo 2: Autoensamblaje multicomponente de porfirinas y subftalocianinas.

En este capítulo se estudia el autoensamblaje de porfirinas y subftalocianinas en estructuras tridimensionales. El estudio relacionado con las primeras corresponde a una estancia de investigación realizada por la candidata en el laboratorio del Profesor Stang en la Universidad de Utah, y que sirvió de base al estudio de las segundas. En este caso, se emplea el protocolo de autoensamblaje multicomponente desarrollado

en los últimos años por el grupo de Stang,[10] en el que se ha demostrado que la coordinación de un ligando carboxilato y una piridina a un centro de Pt (II) está termodinámicamente favorecida frente a la formación de un complejo homoléptico.

Partiendo de esta premisa, se llevó a cabo en la primera parte del capítulo la construcción de prismas basados en porfirinas. Variaciones en la flexibilidad y longitud del ligando dicarboxilato se reflejan en propiedades de los prismas tales como su solubilidad y simetría.

Se prepararon tres series de prismas en las que varía el metal situado en la cavidad de la porfirina con el objetivo futuro de estudiar la actividad de estos autoensamblados como catalizadores en reacciones redox. Además, se desarrolló un nuevo protocolo experimental que permite realizar el autoensamblaje de estructuras multicomponente en un solo paso.

La segunda sección de este capítulo está dedicada a las propiedades de autoensamblaje de una SubPc sustituída con seis piridinas en la periferia.

Se comenzó estudiando su autoensamblaje con un complejo de Pt (II), pudiéndose aislar algunos productos de control cinético además del producto termodinámicamente más estable. A continuación se llevó a cabo el ensamblaje de una cápsula con dicha SubPc y ligandos dicarboxilato. Dicha cápsula se obtuvo como una mezcla de isómeros, cómo se pudo observar en ^{31}P-RMN que procede de las distintas configuraciones que pueden adoptar las piridinas.

Apéndice

En este apartado se reflejan los resultados de un trabajo realizado en colaboración con la Universidad de Valencia (Grupo del Dr. Bolink) consistente en la incorporación de una subfthalocianina tricationica en un dispositivo fotovoltaico de naturaleza orgánica.

[10] Y.-R. Zheng, Z. Zhao, M. Wang, K. Ghosh, J. B. Pollock, T. R. Cook, P. J. Stang, *J. Am. Chem. Soc*, **2010**, *132*, 16873-16882.

Conclusiones

Capítulo 1:

-Los experimentos con el método de la variación continua permitieron comparar las SubPcs según su naturaleza electrónica, que determina la formación o no del complejo y su estequiometría. De estos resultados se concluye que la complementariedad de forma de las superficies π por sí misma no es suficiente para que se produzca reconocimiento molecular. Además se ha comprobado que las interacciones hidrofóbicas entre cadenas alquílicas en las SubPcs con sustituyentes tipo tioeter son las principales responsables de la formación de complejos 2:1. Además se observó que la longitud de dichas cadenas influye en la cinética del equilibrio.

-Cuando las SubPcs se encuentran preorganizadas en una cápsula mediante coordinación a metales, la falta de complementariedad electrónica se encuentra compensada por éste parámetro, y se alcanzan constantes de complejación del mismo orden que en el caso anterior con las SubPcs dadoras (10^4 M^{-1}).

-Por otro lado, se han llevado a cabo estudios preliminares de complejación de fullerenos sustituidos con otras unidades fotoactivas (Pcs en este caso); una estrategia que ofrece la posibilidad de introducir otros cromóforos de interés para obtener sistemas más complejos. Además, la formación de cápsulas con un ligando quiral ofrece la posibilidad de reconocer selectivamente fullerenos quirales.

-Los estudios fotofísicos de ambos tipos de complejos (fullerenos con SubPcs dadoras y con cápsulas metalosupramoleculares basadas en SubPcs) demostraron que se produce una transferencia de energía fotoinducida en ambos casos.

Capítulo 2:

- En la primera sección se prepararon una serie de ensamblados multicomponente basados en porfirinas, en los cuales se pudo variar tanto la flexibilidad como la distancia entre dichas profirinas mediante la modificación del ligando dicarboxilato. Para la obtención de este tipo de compuestos se desarrolló una nueva metodología que permite realizar el autoensamblaje multicomponente en un solo paso.

-Además, en el caso particular de los dicarboxilatos alquílicos, el éxito del auto-ensamblaje depende del número par o impar de carbonos en dicho ligando, debido a la mayor facilidad de las cadenas alquílicas con número par de carbonos para ordenarse de acuerdo a la geometría de coordinación del Pt.

-Se ha estudiado además en la segunda parte del capítulo el autoensamblaje de una SubPc hexasustituída con piridinas. Estudios de ^{31}P-RMN y masas han permitido identificar algunos de los productos resultantes, tanto en el caso de autoensamblaje de la SubPc únicamente con Pt como en el caso del autoensamblaje multicomponente, y se han podido ordenar cualitativamente de acuerdo a su estabilidad termodinámica.

Apéndice:

-Se ha preparado una SubPc tricatiónica, y su incorporación en un dispositivo fotovoltaico de naturaleza orgánica ha dado lugar a eficiencias del 0.5%. Aunque no es un valor muy alto, es un resultado prometedor que probablemente pueda mejorarse mediante modificaciones sintéticas de la SubPc.

Introduction and Objectives

Outline

1. Introduction

The development of supramolecular systems that can work as devices at the molecular scale has been a very active field since the birth of supramolecular chemistry.[1] This kind of systems can perform tasks as assorted as sensing of certain molecules, light conversion, catalysis, or transport.

The incoming depletion of fossil fuels has provoked in the last decades a timed race for the development of alternative and efficient sources of energy. Among them, solar energy is one of the most promising in the long term. Every hour, the Earth receives enough solar power to supply humans' energy consumption for one year.[2] The development of species that can harvest and convert sunlight efficiently is thus an extremely important mission. Supramolecular chemistry plays a crucial role in the search for such systems, as proper positioning of the active components is a key point for the achievement of efficient devices.

In this regard, the supramolecular photoactive device by excellence that has served as inspiration to many scientists is found in nature: the photosynthetic system. Much effort has been devoted to the understanding of the mechanism of light conversion in this system, with the aim of designing artificial systems that can behave similarly in human's profit. Photosynthesis[3] is the process employed by plants, algae and cyanobacteria to convert the radiant energy from the sun into chemical energy to fuel the activities of these organisms. The success of this conversion relies upon the efficient absorption and conversion of sunlight.

The main players in the process are chlorophylls (Chls, Figure 1) and carotenoids. While the latter play mainly a photoprotective role, Chls are involved in light harvesting and charge separation processes.[4] Photosynthetic systems present two basic components, an antenna complex for light harvesting, and a reaction center for charge separation, and both events are, as mentioned above, performed by Chls.

---

[1] (a) J. M. Lehn, *Supramolecular chemistry: concepts and perspectives*, VCH, Weinheim 1995; (b) Y. S. Lee, *Self-assembly and nanotechnology: a force balance approach*, John Wiley &Sons, New Yersey 2008.
[2] Q. Schiermeier, J. Tollefson, T. Scully, A. Witze, O. Morton, *Nature,* **2008**, *454*, 816-823.
[3] B. Gobets, R. van Grondelle, *Biochim. Biophys. Acta,* **2001**, *1507*, 80-99.
[4] R. Berera, R. van Grondelle, J. T. M. Kennis, *Photosynth. Res,* **2009***, 101*, 105-108.

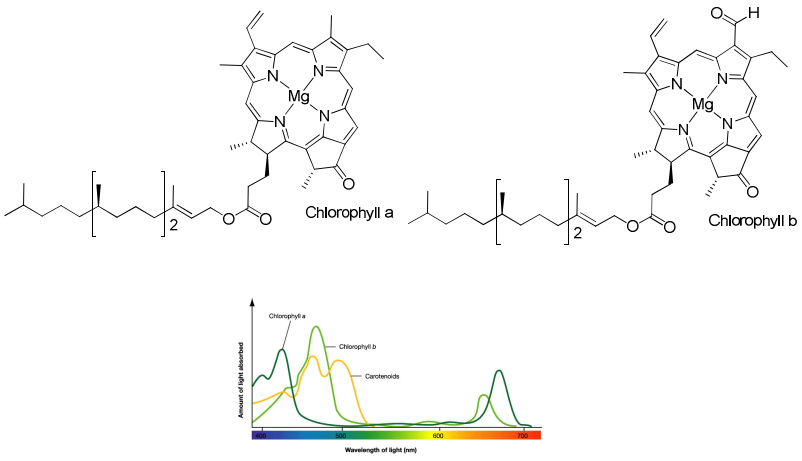

Figure 1. Structure of Chlorophylls a and b and UV-Vis absorption spectra of Chlorophylls (green lines) and carotenoids (yellow line).

The first step in photosynthesis is light absorption by the antenna complex. Photoinduced energy transfer is a process of great importance in the light harvesting complex, and, moreover, it acts as the trigger of charge separation process. The aim of this event is to progressively direct the energy from sunlight to the reaction centre. Energy transfer is a photophysical process where the excitation of a chromophore is transferred to another radiationless. Spectral overlap between the emission of the donor and the absorption of the acceptor is required for energy transfer to occur.

In the case of photosynthesis, energy transfer takes place through the dipolar coupling mechanism described by Theodore Förster in 1914. Förster resonance energy transfer (FRET) takes place when non-radiative excitation transfer occurs between two molecular entities separated by distances that exceed the sum of their Van der Waals radii.[5] This energy exchange happens via the electromagnetic field associated to the electron in the LUMO of the donor, which causes a perturbation on the electrons in the HOMO of the acceptor. The effectiveness of the energy transfer depends on the distance between the chromophores (the rate is proportional to R^{-6}) and the relative orientation of the chromophores. In this regard, organization of the chromophores is very important for an efficient photosynthetic process. A common feature of photosynthetic systems is a ring-like organization of the antenna (Figure 2) complex around the reaction center.[2] Such degree of organization of the photosynthetic pigments addressed to ensure formation of efficient antennas and reaction centers is

[5] *The IUPAC Golden book: http://goldbook.iupac.org/F02488.html*

based on supramolecular interactions involving not only the pigments but also proteins and protein dimers.

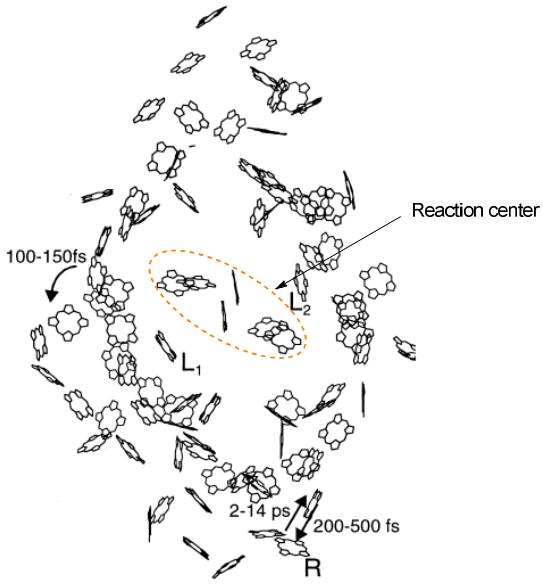

Figure 2. Distribution of chlorophylls in photosystem I.

Conversion of sunlight energy into chemical energy takes place through a cascade of unidirectional electron transfer reactions that will lead to the synthesis of carbohydrates. The success of this process relies on the effectiveness of these electron transfers and the lack of recombination reactions that would interrupt the process and cause a waste of the absorbed energy.

Electron transfer reactions are explained by the theory developed by Rudolph A. Marcus, who was awarded the Noble prize in 1992.[6] Photosynthetic systems achieve long-lived charge separation states because electron-transfer events are located in the "inverted region" of Marcus' parabola (Figure 3). This means charge separation reaction is thermodynamically and kinetically favourable, whereas charge recombination is not.

[6] (a)"Rudolph A. Marcus, 1992 Nobel Lecture: Electron Transfer Reactions in Chemistry: Theory and Experiment". http://www.nobelprize.org/nobel_prizes/chemistry/laureates/1992/marcus-lecture.html; (b) R. M. Metzger, *J. Mater, Chem,* **2008**,*18*, 4364-4396; (c) P. E. Schween, K. Gui, Y. Zhang, P. L. Burn, P. Meredith, B. J. Powell, *Organic Electronics,* **2012**, *13*, 2538-2545.

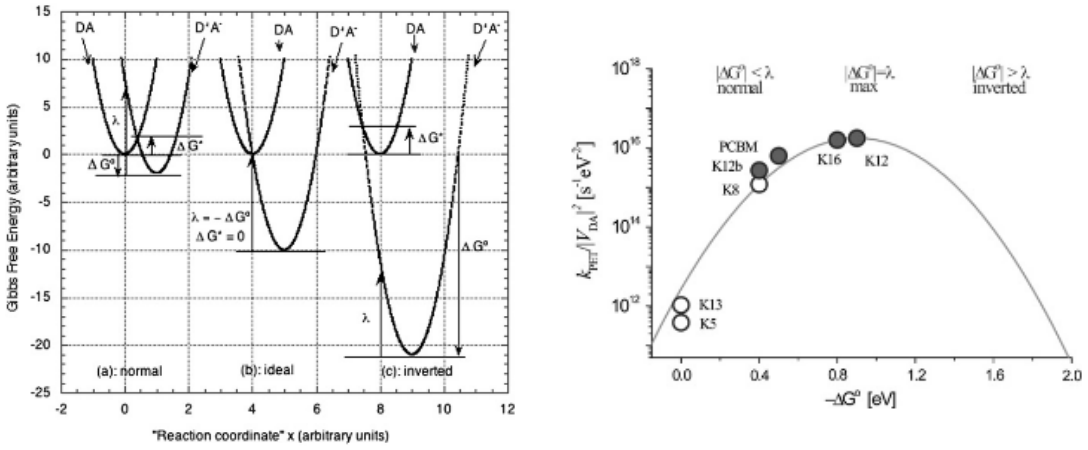

Figure 3. Left: Simplified representation of three cases for Marcus electron transfer theory.[5b] Right: Example of Marcus' parabola.[5c]

In a similar manner, artificial self-assembly of supramolecular structures from photoactive components may be expected to modify the ground-state and/or excited-state behaviour of the individual molecules. This fact may give rise to a number of processes (energy transfer, charge separation, perturbation of optical transitions and polarizabilities, modification of redox potentials, regulation of binding properties, photochemical reactions…) that will depend on the arrangement of components in the supramolecular structure.

Therefore, an accurate design of the components in order to get ensembles that can carry out effectively the desired functions is essential. Such design involves the knowledge and control of the basic principles operating in supramolecular chemistry.

1.1. Supramolecular chemistry

Supramolecular chemistry[7] is a young discipline that arose as a new field in chemistry in the late 60s and early 70s with the work of, among others, Cram,[8] Lehn,[9] and Pedersen,[10] (Figure 4) who were awarded with the Nobel Prize in 1987.

[7] J. W. Steed, J. L. Atwood, *Supramolecular Chemistry*, 2nd edition, John Wiley & Sons, 2009.
[8] D. J. Cram, *Angew. Chem.*, **1988**, *100*, 1041-1052.
[9] J. M. Lehn, *Eur. Rev.,* **2009**, *17*, 263-280.
[10] C. J. Pedersen, *J. Am. Chem. Soc,* **1967**, *26*, 7017-7036.

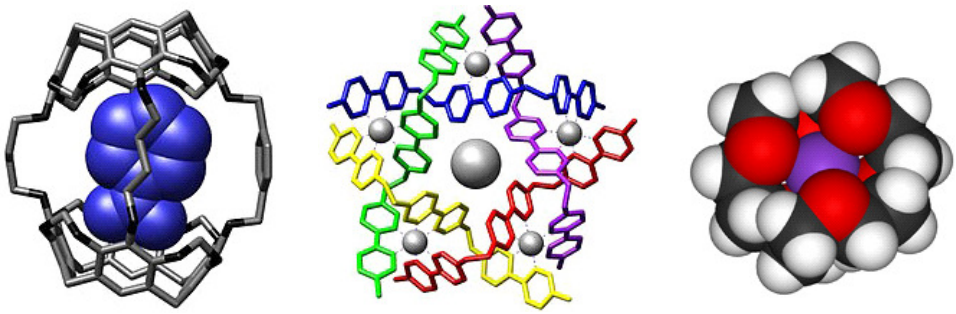

Figure 4. Examples of supramolecular systems reported (from left to right) by Cram, Lehn and Pedersen.[11]

Supramolecular chemistry deals with the study of molecular assembly and of the intermolecular bond. Thus, when talking about this area, we are referring to non-covalent interactions (Figure 5) such as hydrogen bonds, Van der Waals forces, dipole-dipole interactions or π-π stacking, for example.

Interaction	Image	Strength / kJ M^{-1}	Comments
Ion – ion		100–350	Comparable to a covalent bond in strength. However, non-directional and non-selective.
Ion – dipole		50–200	Strong attraction between a molecule with a permanent dipole and an ion.
Dipole – dipole	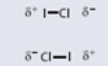	5–50	Electrostatic interaction between two molecules with permanent dipoles.
Hydrogen bonds	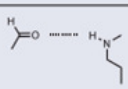	4–120	Arise between an atom bearing a lone pair of electrons (here, O) and a hydrogen atom bonded to an electronegative atom. Useful because of their high degree of directionality. Several H-bonds positioned correctly can add up to give very strong attractive forces.
π–π stacking		0–50	Arise from sharing of electron density between two aromatic (benzene-like) units. The effect is most powerful when there is a significant difference between the partial charges of the interacting units.
CH–π	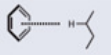	4–12	Arise from dispersion forces. Controversial forces which are not easy to differentiate from the hydrophobic effect.
Van der Waals		< 5	Arise from random fluctuations in electron density, leading to brief moments of electromagnetic attraction between molecules. Extremely weak and non-directional. Not generally useful to supramolecular designers.

Figure 5. Summary of intermolecular forces.[12]

All these interactions are relatively weak and thus, the activation energies for supramolecular transformations are generally low. As a consequence, the processes that take place in supramolecular chemistry depend almost exclusively on thermodynamics. The main advantage of supramolecular chemistry relies on this fact; once the individual constituents (building-blocks) of the final product are mixed, the

[11] (a) J. Yoon, C. B. Knobler, E. F. Maverick, D. J. Cram, *Chem. Commun,* **1997**, *14*, 1303-1304; (b) B. Hasenknopf, J. M. Lehn, B. O. Kneisel, G. Baum, D. Fenske, *Angew. Chem. Int. Ed. Engl,* **1996**, *35*, 1838-1840; C. J. Pedersen, *J. Am. Chem. Soc,* **1967**, *10*, 2495–2496.
[12] J. Howgego, *Education in Chemistry*, **2012**, *49*, 14-17.

system will spontaneously evolve through different thermodynamic equilibria until the most stable product or products are obtained. This process is known as self-assembly, and it is illustrated in Figure 6.

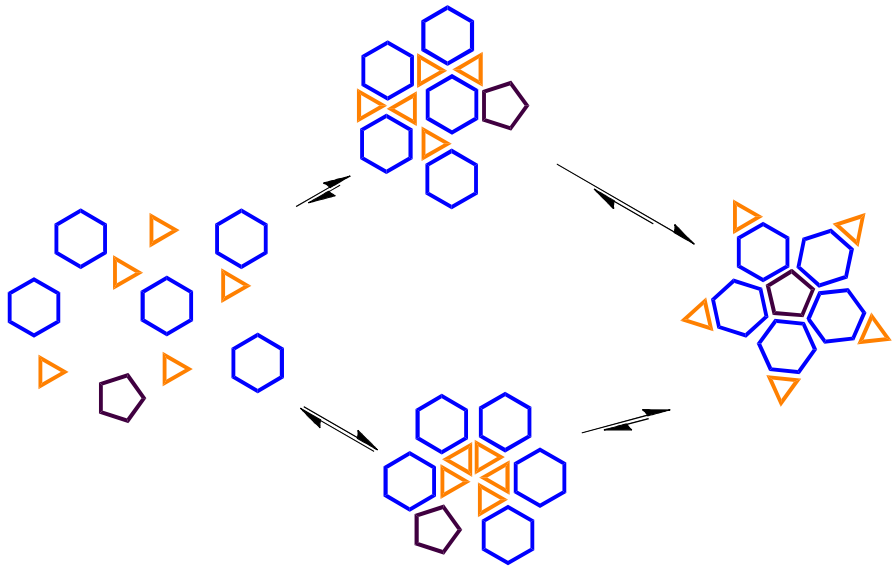

Figure 6. Self-assembly

Each equilibrium process taking place during the self-assembling process is a molecular recognition, where complementary functional groups on the building blocks search each other until the most energetically favorable combination of them is achieved. Every region or functional group in the building-blocks that is potentially able to take part in a non-covalent interaction is called binding site.

Molecular recognition via non-covalent interactions is employed often in covalent chemistry for pre-organizing reagents in situations where the desired reaction conformation is kinetic or thermodynamically unlikely. This event is known as template effect,[6] and it serves for purposes like inducing a determined stereochemistry, minimizing side-reactions, lowering the activation energy of a reaction, or obtaining large macrocycles as well as mechanically interlocked molecular architechtures.

Molecular recognition also plays a vital role in host-guest chemistry. Host-guest chemistry (Figure 7) takes place when one molecule (host) possesses a cavity where another one (guest) can fit, and as a result, a stable associate is obtained. More formally, the host is defined as the entity possessing convergent binding sites, whereas the molecule bearing divergent binding sites is identified as the guest (Figure 7a). Formation of a host-guest complex involves a complementary stereoelectronic arrangement of the binding sites of both the host and the guest.

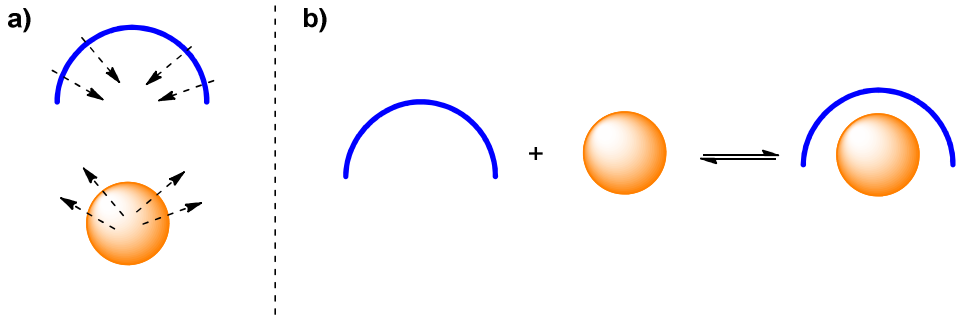

Figure 7. Schematic representation of a host, a guest, and the binding process.

The measurement of the binding constant between host and guest provides an evaluation of the strength of the non-covalent interactions acting, and thus, the thermodynamic stability of the complex at a given temperature.[13] Strictly, binding constants are dimensionless, but as they are commonly evaluated in variable-concentration experiments, they have units of, for example, in the case of 1:1 complexes, M^{-1}. Ignoring activity effects, the binding constant is equivalent to the equilibrium constant for the reaction showed in Figure 7b. As a consequence, large binding constants involve a high equilibrium concentration of host-guest complex, and thus, a more stable adduct.

When host-guest complex formation comprises sequential binding of more than one host or guest, a binding constant for any equilibrium may be measured. Under these circumstances, an overall binding constant, β, may be defined for the whole process:

$$\beta = K_{11} \cdot K_{12} \cdot K_{13} \cdots$$

In general, the affinity between a given couple of host and guest may be reported in terms of binding constant or free energy values, as these two parameters are related through Gibbs' equation:

$$\Delta G = -RT \cdot \ln K_{eq}$$

In principle, binding constants can be calculated by any experimental technique that yields information about the concentration of the host-guest complex as a function of the concentration of any of its components. However, the range of constants that can

[13] (a) K. A. Connors, *Binding Constants,* Wiley & Sons, New York, 1987; (b) J. Polster, H, Lachmann, *Spectrometric titrations*, VCH; Weinheim, 1989; (c) P. Thodarson, *Chem. Soc. Rev.*, **2011**, *40*, 1305-1323.

be measured in each technique is limited: the experiment requires the choice of concentration values where significant amounts of bound and free host and guest are present.

Currently, supramolecular chemistry has grown into new research lines that take advantage of self-assembly and self-organization for the construction of molecular devices and machines[14] and molecular containers.[15] It has expanded through the frontier of other disciplines, like, for example, nanochemistry. In this context, photo, electro or ionoactive devices built following the basic concepts of supramolecular chemistry are an important line of research nowadays.[16]

Supramolecular systems are often self-assembled not only employing non-covalent interactions, but also metal-ligand interactions,[17] which possess an important covalent component in their nature. The directionality of coordination bonds is highly defined, and thus, prediction and design of the structure resulting from self-assembly becomes more undemanding, as it is generally based in geometric principles; the metal coordination geometry, ligand structure and stoichiometry play vital roles in determining the shape of the final architecture.

Since the pioneering works of Lehn[16a] and Sauvage,[18] who employed coordination-driven self-assembly to build helicates, grids, knots, racks, catenanes, rotaxanes, etc, the topic has gained increasing attention. Research addressed to the understanding of the basic parameters that affect the result of a self-assembling process is still an active field, lead especially by the groups of Fujita and Stang.

An excellent example of how these principles operate has been recently reported by Fujita and coworkers. In 2004 they reported the formation of sphere-like M_nL_{2n}

[14] W. R. Browne, B. L. Feringa, *Nat. Nanotechnol*, **2006**, *1*, 25-35.
[15] H-J. Schneider, A. K. Yatsimirsky, *Chem. Soc. Rev*., **2008**, *37*, 263-277.
[16] See, for instance: (a) A. Mateo-Alonso, C. Ehli, G. M. A. Rahman, D. M. Guldi, G. Fioravanti, M. Marcaccio, F. Paolucci, M. Prato, *Angew. Chem. Int. Ed*., **2007**, *46*, 3521-3525; (b) K. Maurer, B. Grimm, F. Wessendorf, K. Hartnagel, D. M. Guldi, A. Hirsch, *Eur. J. Org. Chem,* **2010**, *26*, 5010-5029; (c) M. R. Wasielewski, *Chem. Rev,* **1992**, *92*, 435-461; (d) F. D'Souza, O. Ito, *Coord. Chem. Rev*, **2005**, *249*, 1410-1422; (e) F. Würthner, C. Thalacker, A. Sautter, W. Schärtl, W. Ibach, O. Hollricher, *Chem. Eur. J,* **2000**, *6*, 3871-3886.
[17] (a) R. Chakrabarty, P. S. Mukherjee, P. J. Stang, *Chem. Rev,* **2011**, *111*, 6810-6918; (b) M. M. J. Smulders, I. A. Riddell, C. Browne, J. R. Nitschke, *Chem. Soc. Rev,* **2013**, *42*, 1728-1754; (c) Wiester, M. J.; Ulmann, P. A.; Mirkin, C. A*. Angew. Chem., Int. Ed,* **2011**, *50*, 114; (d) T. R. Cook, Y-R. Zheng, P. J. Stang, *Chem. Rev*, **2012**, 734-777; (e) M. D. Ward, *Chem. Commun*. **2009**, 4487-4499.
[18] J.-P. Sauvage, C. Dietrich-Buchecker, Eds. *Molecular Catenanes, Rotaxanes, and Knots: A Journey Through the World of Molecular Topology*, Wiley-VCH; Weinheim, Germany, 1999.

structures[19] upon combination of rigid bent ligands (Figure 8) and square planar metal centers, namely, Pd (II). The resulting spherical ensemble may be obtained as $M_{12}L_{24}$ or $M_{24}L_{48}$ cage (Figure 8) depending on the M/L ratio and the angle of the ligand.[20]

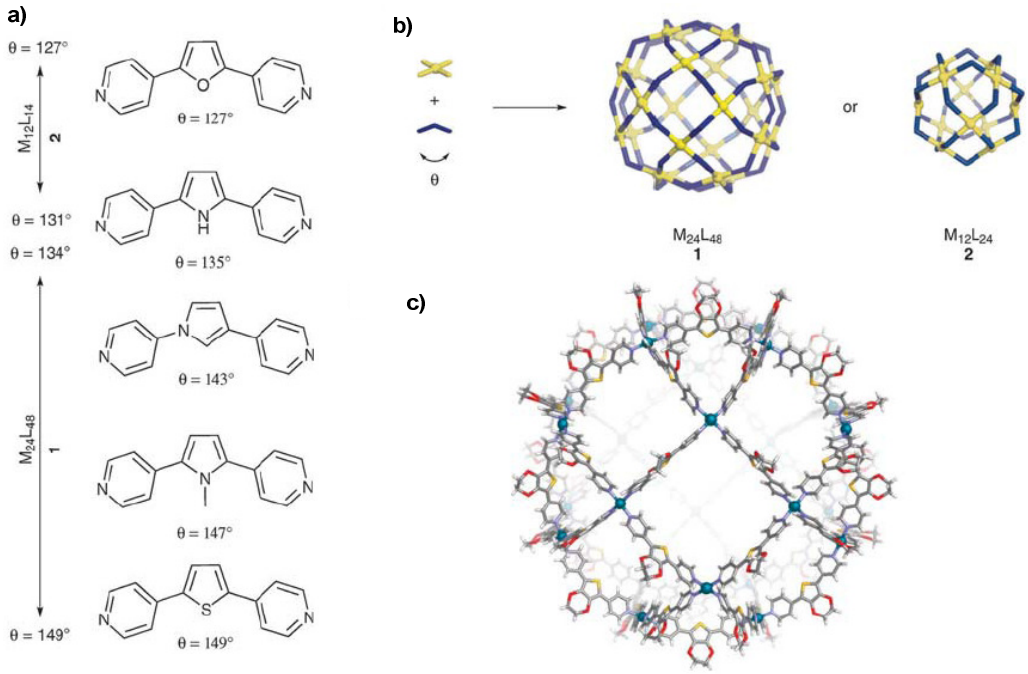

Figure 8. a) Ligands employed for the self-assembly of sphere-like metalosupramolecular assemblies. b) Scheme of self-assembly and the two possible products. c) X-Ray diffraction of an $M_{24}L_{48}$ self-assembly.

If the same self-assembling process is carried out employing Pt (II) instead of Pd (II), the inertness of Pt-N bonds prevents the progress of the reaction.[21] Addition of 2,2,2-trifluoroethanol (TFE) to the mixture provoked temporary labilization of the coordination bonds, and in consequence, error-checking and self-healing events took place until the thermodynamically most stable product was achieved.

The research group of Stang has also achieved self-assembly of many two and three dimensional species through the careful design of the building-blocks (Figure 9), giving rise to many species possessing optical properties that arise from the combination of

[19] M. Tominaga, K. Suzuki, M. Kawano, T. Kusukawa, T. Ozeki, S. Sakamoto, K. Yamaguchi, M. Fujita, *Angew. Che, Int. Ed,* **2004**, *43*, 5621-5625.
[20] (a) Q. F. Sun, J. Iwasa, D. Ogawa, Y. Ishido, S. Sato, T. Ozeki, K. Yamaguchi, M. Fujita, *Science*, **2010**, *328*, 1144-1147; (b) J. Bunzen, J. Iwasa, P. Bonakzardeh, E. Numata, K. Rissanen, S. Sato, M. Fujita, *Angew. Chem. Int. Ed*, **2012**, *51*, 3161-3163.
[21] D. Fujita, A. Takahashi, S. Sato, M. Fujita, *J. Am. Chem. Soc,* **2011**, *133*, 13317-13319.

the metals and the organic ligands,[22] or three-dimensional cage-like compounds that can act as hosts for other molecules.[23] The distinct feature of Stang's research group is the use of phosphine ligands and Pt (II) centers, which, combined, give rise to characteristic sets of signals in ^{31}P-NMR; becoming this a powerful tool for quick characterization of self-assemblies. Recently, a new stabilization effect has been observed upon coordination of a pyridine and a carboxylate to Pt (II) centers.[24] This event has allowed the construction of several multi-component self-assembled structures.

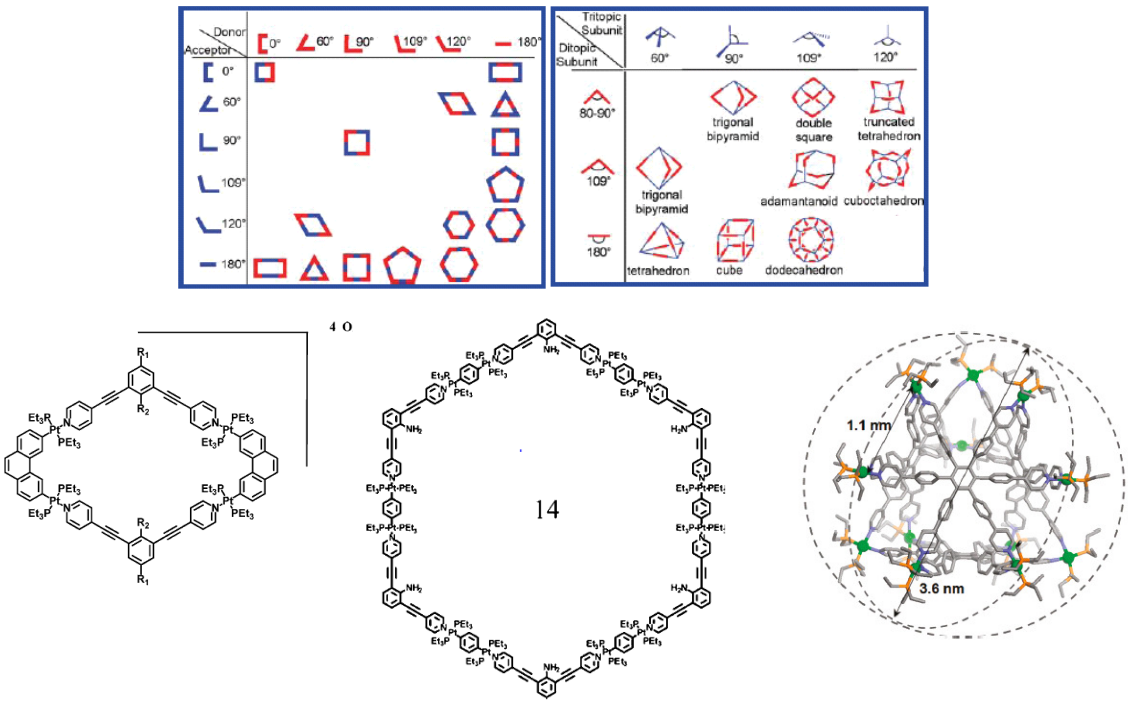

Figure 9. Tables showing the basic geometric priciples for the design of metalosupramolecular structures and representative examples of compounds reported by Stang and coworkers.

Many other groups' efforts are directed to the study of these metal-organic species as catalysts, containers, molecular materials or anticancer drugs.[25] The examples are of great abundance and variety (Figure 10).

---

[22] (a) A. Mishra, S. Lee, H. Kim, T. R. Cook, P. J. Stang, K-W. Chi, *Chem. Asian J,* **2010**, *7*, 2461; (b) J-S. Chen, G-J. Zhao, T. R. Cook, X-F. Sun, S-Q. Yang, M-X. Zhang, K-L. Han, P. J. Stang, *J. Phys. Chem. A*, **2012**, *116*, 9911-9918; (c) J-S. Chen, G-J. Zhao, T. R. Cook, K. L. Han, P. J. Stang, *J. Am. Chem. Soc*, **2013**, DOI:10.1021/ja402421w; (d) J. B. Pollock, T. R. Cook, P. J. Stang, *J. Am. Chem. Soc*, **2012**, *134*, 10607-10620.

[23] (a) Y-R. Zheng, Z. Zhao, H. Kim, M. Wang, K. Ghosh, J. B. Pollock, K-W. Chi, P. J. Stang, *Inorg. Chem*, **2010**, *49*, 10238-10240.

[24] (a) Y. R. Zheng, Z. Zhao, M. Wang, K. Ghosh, J. B. Pollock, T. R. Cook, P. J. Stang, *J. Am. Chem. Soc*, **2010**, *132*, 16873-16882.

[25] See, for instance: (a) C. J. Hastings, M. D. Pluth, R. G. Bergman, K. N. Raymond, *J. Am. Chem. Soc*, **2010**, *132*, 6938-6940; (b) T. Murase, Y. Nishijima, M. Fujita, *J. Am. Chem. Soc,*

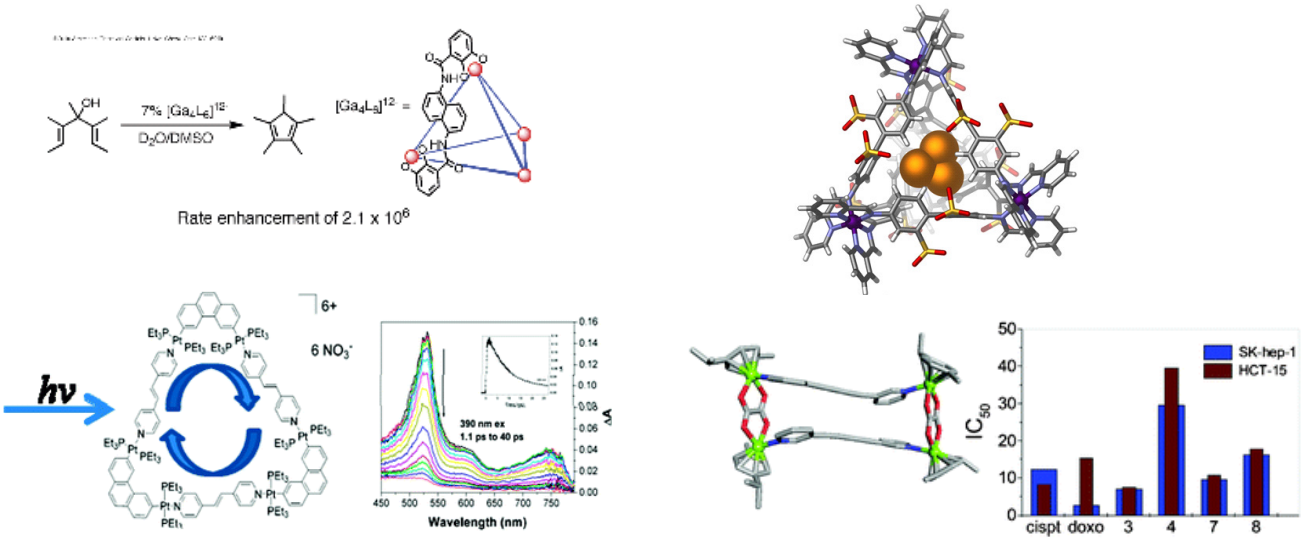

Figure 10. Examples of metallosupramolecular systems and their applications.

1.2. Subpthalocyanines

Subphthalocyanines[26] (SubPcs, Figure 11) are non-planar aromatic compounds composed of three units of 1,3-diiminoisoindol *N*-fused around a boron atom. They were discovered in 1972 by Meller and Ossko [27] when they were trying to obtain a boron Pc. Their concave structure arises from the sp^3 hybridation of the central boron atom. While the cavity of Pcs can host more than 70 elements, SubPcs are only known as boron derivatives. Actually, they represent an example of template effect in covalent chemistry.

2012, *134*, 162-164; (c) P. Mal, B. Breiner, K. Rissanen and J.R. Nitschke, *Science,* **2009**, *324*, 1697-1699; (d) F. Xu, R. A. Scullion, J. Yan, H. N. Miras, C. Busche, A. Scandurra, B. Pignataro, D-L. Long, L. Cronin, *J. Am. Chem. Soc*, **2011**, *133*, 4684-4686; (e) D. C. Flynn, G. Ramakrishna, H-B. Yang, B. H. Northrop, P. J. Stang, T. Goodson, *J. Am. Chem. Soc*, **2010**, *132*, 1348-1358; (f) M. D. Ward, *Dalton Trans,* **2010**, *39*, 8851-8867; (g) V. Vajpayee, Y. H. Song, Y. J. Jung, S. C. Kang, H. Kim, I. S. Kim, M. Wang, T. R. Cook, P. J. Stang, K-W. Chi, *Dalton Trans*, **2012**, *41*, 3046-3052.

[26] (a) C. G. Claessens, D. Gonzalez-Rodriguez, T. Torres, *Chem. Rev,* **2002**, *102*, 835-853; (b) T. Torres, *Angew. Chem. Int. Ed*, **2006**, *45*, 2834-2837.

[27] A. Meller, A. Ossko, *Monatsh. Chem.* **1972**, *103*, 150-155.

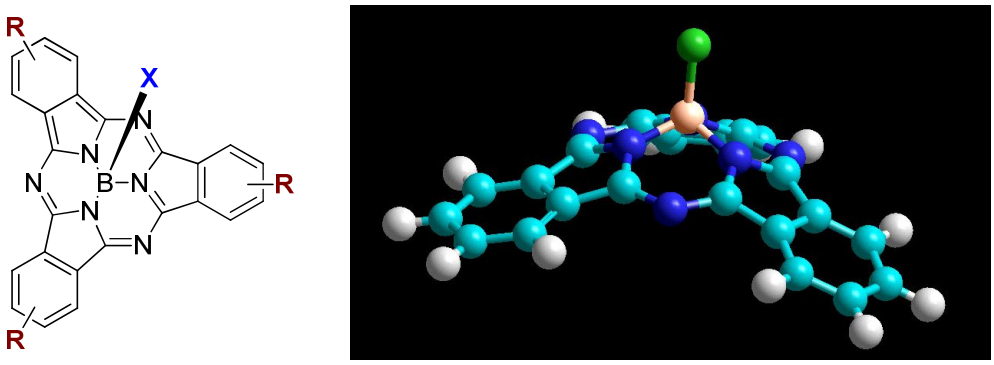

Figure 11. Structure of SubPcs.

SubPcs are synthesized by condensation of phthalonitriles in the presence of a boron halide in reluxing *p*-xylene. When the starting phthalonitrile lacks C_{2v} symmetry, SubPcs are obtained as a mixture of two regioisomers (Figure 11), C_3 and C_1, in 1:3 proportions. SubPc regioisomers can be generally separated by column chromatography in silica gel. Moreover, each regioisomer presents two enantiomers, *M* and *P* (Figure 12). Chiral HPLC allowed separation of SubPc enantiomers and obtention of their circular dichroism spectra. [28]

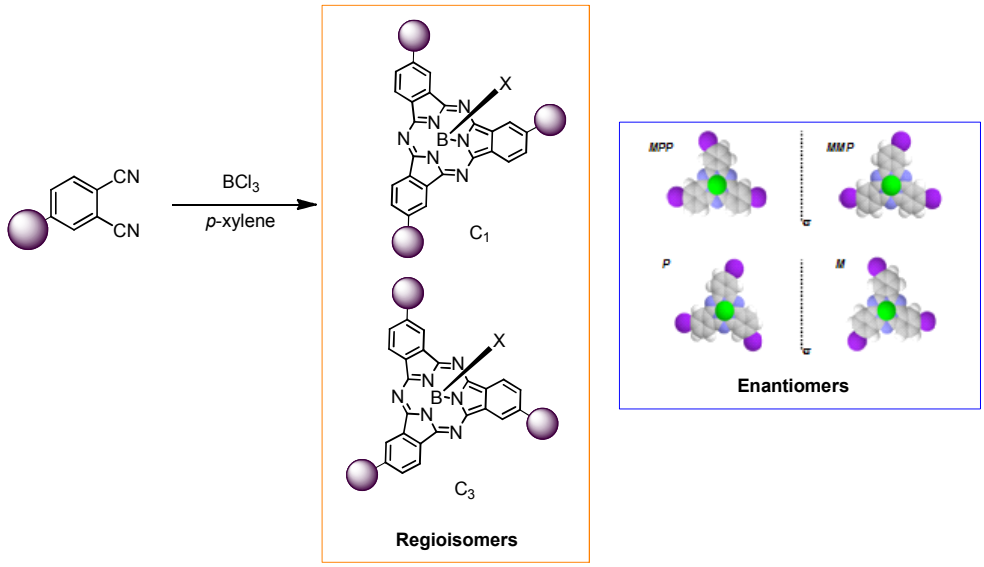

Figure 12. Synthesis of SubPcs and isomers resulting from monosubstituted starting material.

Reactivity of SubPcs

- Axial reactivity (Figure 13): it consists in the exchange of the group in the axial position of boron with another nucleophile that usually increases solubility of the macrocyle, and provides stability versus hydrolysis (a kinetically slow process that

[28] (a) C. G. Claessens, T. Torres, *Tetrahedron Lett*, **2000**, *41*, 6361; (b) N. Kobayashi, T. Nonomura, *Tetrahedron Lett.*, **2002**, *43*, 4253-4255;

usually takes place on halide SubPcs). The most common method for exchange of the axial group involves adding an excess of the nucleophile (usually a phenol or alcohol) and refluxing the mixture in toluene till the reaction is complete.[29] The reaction also proceeds at the melting point temparture of the phenol. However, some methods have been recently developed that employ activation of the boron-halide bond with triflate[30] or aluminium chloride,[31] and allow the incorporation of other groups like amines, thioeters or alkyl chains.

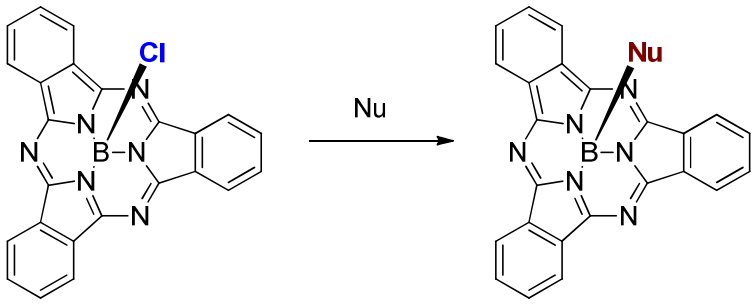

Figure 13. Axial substitution

- Peripheral reactivity:[32] the reactive centers in this case are the groups attached to the aromatic carbon atoms (Figure 14). In general, the SubPc macrocyclic core is unstable in the presence of nucleophiles at high temperatures or in acidic or basic media, due to its constrained structure. Moreover, the conditions employed in the formation of the macrocycle limit the functional groups that can be incorporated in the starting phthalonitrile. Because of all these reasons, peripheral functionalization of SubPcs is generally carried out by means of cross-coupling Pd-catalyzed reactions.

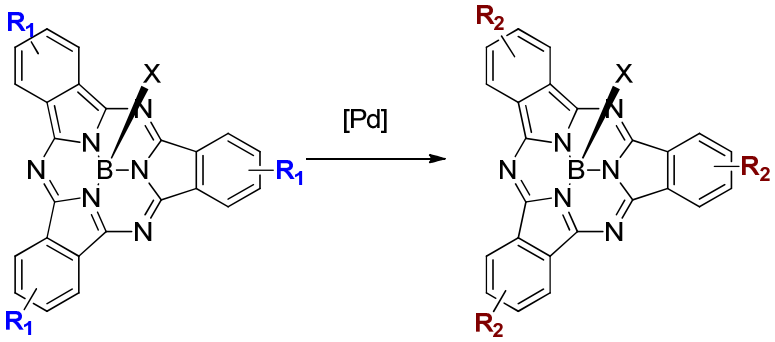

Figure 14. Peripheral functionalization of SubPcs

[29] C. G. Claessens, D. Gonzalez-Rodriguez, B. del Rey, T. Torres, G. Mark, H-P. Schuchmann, C. von Sonntag, J. G. McDonald, R. S. Nohr, *Eur. J. Org. Chem,* **2003**, *14*, 2547-2551.
[30] J. Guilleme, D. Gonzalez-Rodriguez, T. Torres, *Angew. Chem. Int. Ed*, **2011**, *15*, 3506-3509.
[31] G. E. Morse, T. P. Bender, *Inorg. Chem*, **2012**, *51,* 6460–6467.
[32] D. Gonzalez-Rodriguez, T. Torres, *Eur. J. Org. Chem,* **2009**, 1871-1879.

-Ring-expansion (Figure 15):[33] this reactivity, studied firstly by Kobayashi *et al.*, has been widely used for the synthesis of non-symmetrical A_3B Pcs, that otherwise are difficult to access through statistical condensation of phthalonitriles. The main cause for this reactivity is the constrained structure of the macrocyle.

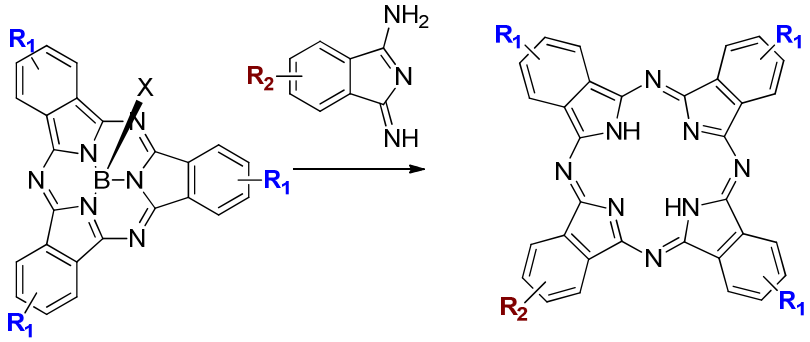

Figure 15. Ring-expansion reactivity of SubPcs

Photophysical and electrochemical properties of SubPcs [34]

UV-visible absorption spectra of SubPcs and Pcs (Figure 16) show two bands; B or Soret, around 300 nm, which corresponds to the π-π* transition, and the Q band, which corresponds to n-π* transition and appears in the visible region (around 560 nm for SubPcs and 660 nm for Pcs). SubPcs' absorption bands are shifted to shorter wavelengths with respect to Pcs, due to the decrease of the π-conjugated system.

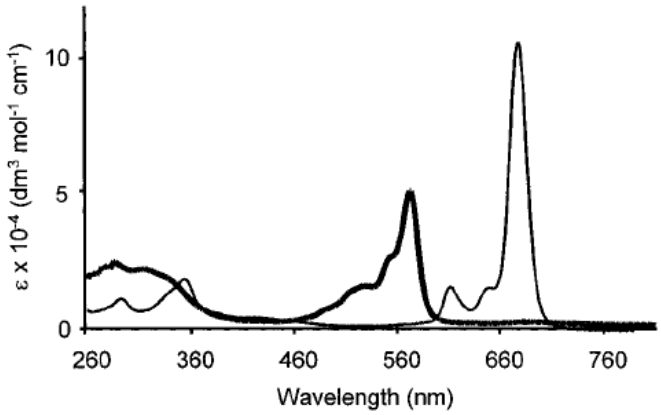

Figure 16. UV-visible spectra of a SubPc (thick line) and a Pc (thin line).

The first oxidative and reductive potentials of SubPcs are observed around 1V and -1V, *vs* Ag/AgCl electrode. They are both one-electron processes. First oxidation is usually irreversible, whereas first reduction generally appears to be reversible.

---

[33] (a) N. Kobayashi, R. Kondo, S. Nakajima, T. Osa, *J. Am. Chem. Soc,* **1990**, *112*, 9640; (b) M. Geyer, F. Plenzig, J. Rauschnabel, M. Hanack, B del Rey, A. Sastre, T. Torres, *Synthesis,* **1996**, 1139; A. Sastre, B. del Rey, T. Torres, *J. Org. Chem,* **1996**, *61*, 8591-8597.

[34] B. del Rey, U. Keller, T. Torres, G. Rojo, F. Agulló-López, S. Nonell, C. Martí, S. Brasselet, I. Ledoux, J. Zyss, *J. Am. Chem. Soc*, **1998**, *120*, 12808-12817.

Donor or acceptor substituents in the periphery of the SubPc have a great influence on the optical and electrochemical properties of the macrocycle, in sharp contrast with the axial substituent, whose influence is almost negligible. Absorption bands bathochromically shift upon substitution of the SubPc ring with donor or acceptor groups. Moreover, the nature of the peripheral substituents may strongly affect the values of the redox potentials (Table 1).

Table 1. UV-visible and electrochemistry data of some SubPcs (all data extracted from reference number 24, except entry 6[35])

	R peripheral	**X axial**	λ_{max} (nm, B band)	$\mathbf{E_{ox1}}$ **(V)**	$\mathbf{E^{1/2}_{red1}}$ **(V)**
1	12H	Cl	565	1.04	-1.05
2	12H	Br	567	1.03	-1.06
3	12H	OPh	562	1.09	-1.05
4	12F	Cl	570	1.50	-0.53
5	$3NO_2$	Cl	580	1.34	0.57
6	$6SC_8H_{17}$	OPh*t*Bu	600	0.89	-1.12
7	3I	Cl	574	1.13	-0.92

Redox potentials follow the expected trend according to the peripheral substitution: donor substituents make the macrocycle easier to oxidize, and acceptor substituents make it easier to reduce.

Regarding the photophysical properties, SubPcs are fluorescent, exhibiting quantum yields around 0.25. Non-radiative deactivation pathways of the first singlet excited state are more efficient than in the case of Pcs (φ_F = 0.60), especially intersystem crossing. The quantum yield for this process approaches 0.68. However, and although they can produce singlet oxygen in large quantities, as they are transparent in the region above 600 nm (the wavelength of highest tissue penetration), SubPcs are not suitable for biological applications.

SubPcs have been widely studied in the field of molecular materials. Many covalent donor-acceptor systems where a SubPc has been combined with other photo or

[35] D. D. Díaz, H. J Bolink, L. Capelli, C. G. Claessens, T. Torres, *Tetrahedron Lett.* **2007**, *48*, 4657–4660

electroactive moieties like Porphyrins, Pcs, C_{60} fullerene, ferrocene, cyanine dyes, etc. have been reported.[36] In contrast, only a few examples of equivalent supramolecular sytems can be found in literature.[37]

Research has also progressed towards the synthesis of SubPc-related structures as fused dimers and trimers.[38] These species, as well as their counterparts, SubPcs, have been probed as donor or acceptor materials in organic photovoltaic devices, displaying efficiencies up to 4%.[39]

Self-organization of SubPcs has been studied in crystals, surfaces and Langmuir-Blodgett films.[40]

[36] (a) H. Xu, D-K. Ng, *Inorg. Chem*, **2008**, *47*, 7921-7927 ; (b) D.González-Rodríguez, T. Torres, D. M. Guldi, J. Rivera, M. A. Herranz, L. Echegoyen, *J. Am. Chem.Soc*, **2004**, *126*, 6301-6313; (c) D. González-Rodríguez, E. Carbonell, G. de Miguel Rojas, C. Atienza Castellanos, D. M. Guldi, T. Torres, *J. Am. Chem. Soc*, **2010**, *126*, 6301-6313; (d) D. González-Rodríguez, E. Carbonell, D. M. Guldi, T. Torres, *Angew. Chem. Int. Ed.* **2009** , *48*, 8032-8036; € C. Romero-Nieto, J. Guilleme, C. Villegas, D. González-Rodríguez, N. Martín, T. Torres, D. M. Guldi, *J. Mater. Chem,* **2011**, *21*, 15914-15918; (f) A. Medina, C. G. Claessens, G. M. A. Rahman, A. M. Lamsabhi, O. Mó, M. Yáñez, D. M. Guldi, T. Torres, *Chem. Commun.* **2008** , 1759-1761

[37] (a) C. G. Claessens, T. Torres, *J. Am. Chem. Soc*. **2002**, *124*, 14522-1452; (b) C. G. Claessens, M.J. Vicente-Arana, T. Torres, *Chem. Commun*., **2008**, 6378-6380 ; (c) C. G. Claessens, I. Sanchez-Molina, T. Torres, *Supram. Chem*., **2009**, *21*, 44-47 ; (e) C. G. Claessens, T. Torres, *Chem. Commun*., **2004**, 1298–1299; (f) R. Ziessel, G. Ulrich, K. J. Elliott, A. Harriman, *Chem.–Eur. J.,* **2009**, *15*, 4980–4984; (g) S. Shimizu, S. Nakano, T. Hosoya and N. Kobayashi, *Chem. Commun*., **2011**, *47*, 316–318.

[38] (a) C. G. Claessesn, T. Torres, *Angew. Chem. Int. Ed*, **2002**, *41*, 2561-2565; (b) R. S. Iglesias, C. G. Claessens, T. Torres, M. A. Herranz, V. R. Ferro, J. M. Garcia de la Vega, *J. Org. Chem,* **2007**, *72*, 2967-2977.

[39] (a)H. H. P Gommans, D. Cheyns, T. Aernouts, C. Girotto, J. Poortmans, P. Heremans, *Adv. Func. Mater*, **2007**, *17*, 2653-2658; (b) H. H. P. Gommans, T. Aernouts, B. Verreet, P. Heremans, A. Medina, C. G. Claessens, T. Torres *Adv. Funct. Mater*., **2009**, *19*, 3435-3439; (c) B. Verreet, B. P. Rand, D. Cheyns, A. Hadipuor, T. Aernouts, P. Heremans, A. Medina, C. G. Claessens, T. Torres, *Adv. Energy Mat*., **2012**, *1*, 565-568.

[40] (a)A. Medina, C.G. Claessens, *J. Porphyrins Phthalocyanines,* **2009** *, 13,* 447-454; (b) M. Trelka, A. Medina, D. Ecija, C. Urban, J. M. Gallego, C. G. Claessens, R. Otero, T. Torres, R. Miranda, *Chem. Commun,* **2011**, *47*, 9986-9988; (c) M. V. Martinez-Diaz, B. del Rey, T. Torres, B. Agricole, C. Mingotaud, N. Cuvillier, G. Rojo, F. Agullo-Lopez, *J. Mater. Chem.* **1999**, *9*, 1521-1526.

2. Objectives

2.1. General objectives

The main objective is to explore the possibilities offered by the concave structure of SubPcs within the field of supramolecular chemistry. Their synthetic versatility allows the introduction of substituents which can participate as structuring partners or to modify the electronic nature of the macrocycle. Moreover, the complementary shape of SubPcs with C_{60} fullerene, a molecule that has arised great interest in the field of molecular materials since its discovery, states the possibility of exploring molecular recognition.

The basic objectives are the following:

a) Study and exploit the possibilities of non-covalent interactions for the construction of supramolecular architectures based on SubPcs.
b) Explore the host-guest chemistry of the aforementioned structures and take advantage of these properties to obtain supramolecular photoactive systems.
c) Study the photophysical and electrochemical properties of the SubPc-based supramolecular ensembles itselves as well as the complexes with encapsulated guests.

2.1. Methodology

In order to reach the aforementioned objectives, development of the following tasks is necessary:

a) Design, synthesis and functionalization of SubPcs

The synthesis of SubPcs will be carried out by cyclotrimerization reaction of the proper phthalonitriles in the presence of boron trichloride. This will generate the desired macrocyclic structure as chloro-derivative. SubPcs thus obtained will be functionalized axially and/or peripherally if required.

Axial functionalization of the chloro-SubPcs will be performed by nucleophilic substitution with 4-*tert*-buthylphenol in refluxing toluene.

Peripheral functionalization of SubPcs will be carried out in order to convert them in suitable building-blocks for metal-directed self-assembly. Pyridines will be incorporated as coordinating groups through cross-coupling reactions.

b) Choice of other building-blocks

Metal complexes bearing phosphine ligands were preferred for the construction of SubPc ensembles due to the possibility of quick characterization offered by ^{31}P-NMR. Additional properties will be introduced in the systems through the phosphine ligands.

c) Self-assembly

Stoichiometric amounts of building-blocks in the proper conditions are expected to give rise to the desired compounds in high to quantitative yields.

d) Study of host-guest properties

Encapsulation of fullerenes by the SubPc-based structures will be checked with a wide variety of techniques. Job Plot experiments will allow determination of stoichiometry and titrations will afford information on the binding constants.

e) Study of photoinduced and electrochemical processes

Photophysical and electrochemical studies of the self-assembled systems as well as the host-guest complexes will be carried out in order to retrieve information on the interactions between the different components. Fluorescence quenching experiments, fluorescence quantum yields, time-resolved fluorescence and transient absorption spectroscopy will be carried out in the group of Prof. Dirk M. Guldi (Friedrich-Alexander Univertität Erlangen-Nürnberg).

2.3. Thesis' distribution

The present Thesis has been organized in three chapters: *Chapter 1* (*Introduction and objectives*), presents the inspiration and background of the work, as well as the current state-of-the-art of supramolecular chemistry and phthalocyanine-related macrocycles, with special emphasis on metal-directed self-assembly and subphthalocyanines,

respectively, that will hold the leading roles along the discussion. *Chapter 2* is centered on the use of SubPcs as recognition motifs for fullerenes and the study of the properties of the host-guest systems thus obtained. This chapter is, at the same time, divided in two sections, the first one dealing with free SubPcs –jellyfish type- and the second one with metallosupramolecular capsules where the macrocycles are arranged in a fashion that makes favourable the interaction with fullerenes. *Chapter 3* contains the description of multicomponent self-assembled capsules containing Porphyrins (this work was carried out in Professor Peter J. Stang's research group, University of Utah) and SubPcs, and some insights into the kinetics and thermodynamics of this self-assembling process that has been derived from this work. Finally, the *Appendix* shows the synthesis of four cationic SubPcs and preliminary results on their application into organic photovoltaic devices.

Subphthalocyanine-based structures for supramolecular recognition of fullerenes: synthesis, characterization and study of their properties

Outline

1. Introduction

Fullerenes and fullerene derivatives are being widely used as active components in optoelectronic devices such as photovoltaic cells due to their outstanding photophysical and electrochemical properties.[1] They are good electron acceptors and show a low reorganization energy, which is desirable to prevent charge recombination in photoinduced electron transfer processes.[2]

Much effort has been devoted to the understanding of the interactions between fullerenes and other chromophores, which coexist within photovoltaic devices, in order to improve their performances.[3] One possible approach towards a better understanding of the morphology of fullerene-based devices is to study their interactions with supramolecular receptors which, moreover, are also chromophoric species.

The design of fullerene receptors is based on three principles:[4]

- Shape complementarity: fullerenes present a large curved aromatic surface that can be recognized by other molecules through π-π stacking. In this context, optimization of the recognition site of the π-system of the receptor is an important parameter in order to get stable associates.

- Electrostatic complementarity: fullerenes show inside-outside polarization due to the curvature of the aromatic surface. Thus, the external part of the molecule is electron deficient. As a consequence, electron rich molecules are better candidates to act as fullerene receptors.

---

[1] (a) Fullerenes, ed. A Hirsch, M Brettreich, Wiley-VCH Verlag GmbH & Co. KGaA, Weinheim, 2005; (b) S. Fukuzumi and D. M. Guldi, Electron-Transfer Chemistry of Fullerenes, in Electron Transfer in Chemistry (ed V. Balzani), Wiley-VCH Verlag GmbH, Weinheim, 2008; (c) R. Taylor, D. R. M. Walton, *Nature*, **1993**, *363*, 685 – 693. (d) M. Prato, *J. Mater. Chem.*, **1997**, *7*, 1097-1109. G. Bottari, G. de la Torre, D. M. Guldi, T. Torres, *Chem. Rev.*, **2010**, *110*, 6768-6816.

[2] "Rudolph A. Marcus, 1992 Nobel Lecture: Electron Transfer Reactions in Chemistry: Theory and Experiment". http://www.nobelprize.org/nobel_prizes/chemistry/laureates/ 1992/marcus-lecture.html

[3] (a) K. Tashiro, T. Aida, J.-Y. Zheng, K. Kinbara, K. Saigo, S. Sakamoto, K. Yamaguchi, *J. Am. Chem. Soc.*, **1999**, *121*, 9477–9478; (b) K. Tashiro, T. Aida, *Chem. Soc. Rev.*, **2007**, *36*, 189–197. (c) A. M. V. M. Pereira, A. R. M. Soares, A. Hausmann, M. G. P. M. S. Neves, A. C. Tomé, A. M. S. Silva, J. A. S Cavaleiro, D. M. Guldi, T. Torres, *Phys. Chem. Chem. Phys.* **2011**, *13*, 11858-11863. (d) H. Imahori, Y. Sakata, *Adv. Mater.*, **1997**, *9*, 537-546. (e) P. D. W. Boyd, C. A. Reed, *Acc. Chem. Res*, **2005**, *38*, 235-242.

[4] E. M. Pérez, N. Martín, *Chem. Soc. Rev*, **2008**, *37*, 1512-1519.

- Entropic factors like solvophobic effect or preorganization of the recognition sites in the receptors.

Many receptors for fullerenes[5] have been prepared following the aforementioned principles (Figure 1). For example, shape complementarity is observed in calyx-arenes,[5a] corannulene-based receptors[5b] or nanorings.[5c] Extended-TTF derivatives can also bind fullerene, being in this case the main driving force the donor ability of tetrathiafulvalene.[5d,e] Aza-crown ethers and γ- ciclodextrines are examples where fullerene is encapsulated by means of solvophobic effects.[5f,g]

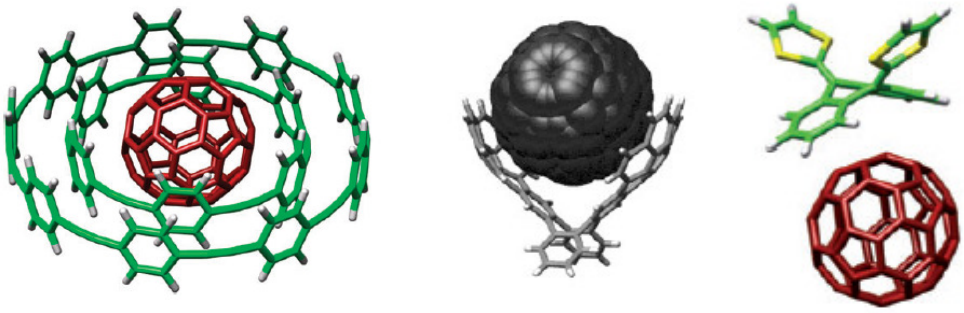

Figure 1. Some fullerene receptors

Nevertheless, many planar chromophores, like porphyrins, have been shown to interact favorably with fullerenes in spite of the surface shape mismatch. Moreover, remarkable results have been realized in the area of porphyrin-based receptors,[6] owing to the preorganization of the host. The strategy of preorganization is very powerful, especially in the context of enhancing fullerene encapsulation.

1.1. Background and Objectives

SubPcs inherently possess a curve-shaped aromatic surface, perfectly adapted to the shape of the fullerene, at least from a geometric point of view. Furthermore, their electronic properties can be tuned with the choice of the proper peripheral substitution.

---

[5] (a) S. Shinkai, A. Ikeda, *Pure Appl. Chem.*, **1999**, *71*, 275–280. (b) A. Sygula, F. R. Fronczek, R. Sygula, P. W. Rabideau, M. M. Olmstead, *J. Am. Chem. Soc.*, 2007, **129**, 3842–3843. (c) T. Kawase, H. R. Darabi, M. Oda, Angew. *Chem., Int. Ed. Engl.*, **1996**, *35*, 2664–2666. (d) E. M. Pérez, L. Sánchez, G. Fernández, N. Martín, *J. Am. Chem. Soc.*, **2006**, *128*, 7172–7173; (e) G. Fernández, E. M. Pérez, L. Sánchez, N. Martín, *Angew. Chem., Int. Ed.*, **2008**, *47*, 1094–1097. (f) F. Diederich, J. Effing, U. Jonas, L. Jullien, T. Plesnivy, H. Ringsdorf, C. Thilgen, D. Weinstein, *Angew. Chem., Int. Ed. Engl.*, **1992**, *31*, 1599–1602; (g) T. Andersson, K. Nilsson, M. Sundahl, G. Westman, O. Wennerström, *J. Chem. Soc., Chem. Commun.*, **1992**, 604–606.

[6] (a) P. D. W. Boyd, C. A. Reed, *Acc. Chem. Res.*, **2005**, *38*, 235–242; (b) K. Tashiro, T. Aida, J.-Y. Zheng, K. Kinbara, K. Saigo, S. Sakamoto, K. Yamaguchi, *J. Am. Chem. Soc.*, **1999**, *121*, 9477–9478

Moreover, photoinduced processes have been previously observed in covalently linked SubPc-C_{60} dyads. If the fullerene was attached to the axial position of the SubPc, and thus close to its convex face, energy transfer occurred unless the periphery of the SubPc was substituted with donor groups.[7] However, when the fullerene moiety was linked to the SubPc core so that it was exposed to the concave face of the macrocycle (Figure 2), distance was proved to be a decisive factor that determines if electron or energy transfer takes place.[8] The study of similar processes in supramolecular ensembles might help in the elucidation of the interaction of SubPcs and C_{60} at the interface between two layers, which is also crucial for device optimization.

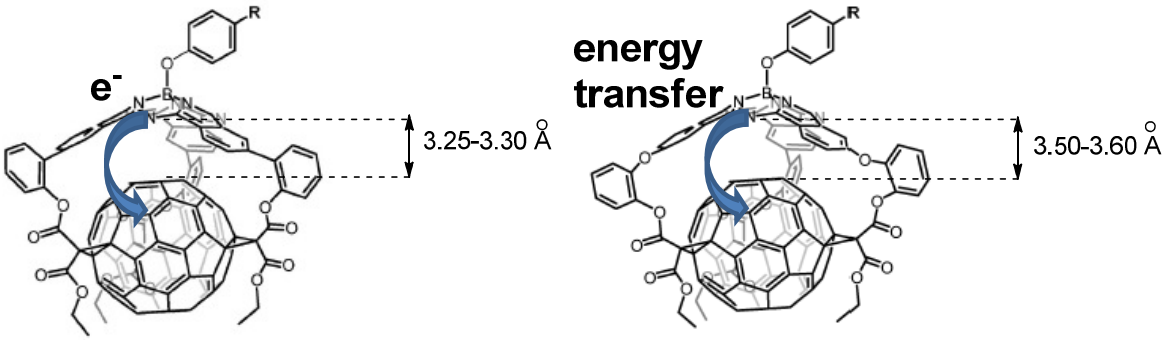

Figure 2. Covalently linked SubPc-fullerene dyads

The main aim of this chapter, as stated in the previous section, is the preparation and study of supramolecular SubPc-fullerene ensembles, and the determination of their binding constants as well as their photophysical properties.

Actually, SubPc-C_{60} supramolecular π-π stacking has been previously observed by Ziessel *et al.*[9] in solution, although no quantitative data were reported. Kobayashi *et al.*[10] also showed this π-π stacking between an extended SubPc and C_{60} in the solid state (Figure 3).

[7] D. González-Rodríguez, T. Torres, D. M. Guldi, J. Rivera, M. A. Herranz, L. Echegoyen, *J. Am. Chem. Soc.*, **2004**, *126*, 6301-6313.
[8] D. González-Rodríguez , E. Carbonell, G. de Miguel Rojas, C. Atienza Castellanos, D. M. Guldi, T. Torres , *J. Am. Chem. Soc*. **2010**, *132*, 16488-16500.
[9] R. Ziessel, G. Ulrich, K. J. Elliott and A. Harriman, *Chem.–Eur. J.,* **2009**, *15*, 4980–4984.
[10] S. Shimizu, S. Nakano, T. Hosoya and N. Kobayashi, *Chem. Commun.*, **2011**, *47*, 316–318.

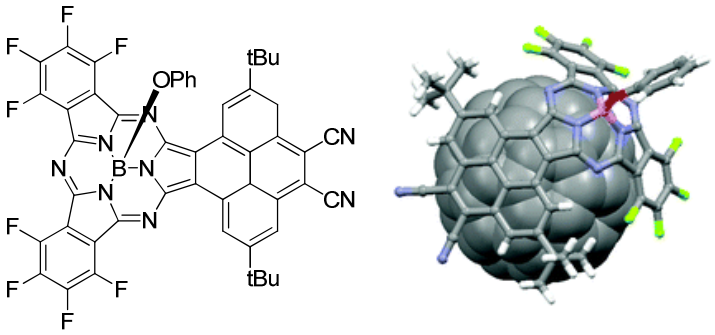

Figure 3. Pirene-fused SubPc and X-Ray structure of its co-crystal with C_{60}

Thus, we intended firstly to perform a systematic and quantitative study of the nature and scope of the supramolecular interactions between SubPcs and fullerenes. In order to do so, we describe in the first section of this chapter the synthesis of a series of donor, neutral and acceptor subphthalocyanines (Figure 4) and the careful study of their complexing ability towards C_{60} and C_{70} fullerenes in solution. In the first instance we expect to control the intensity of the interaction with fullerene through the modification of the electronic nature of the SubPc macrocycle.

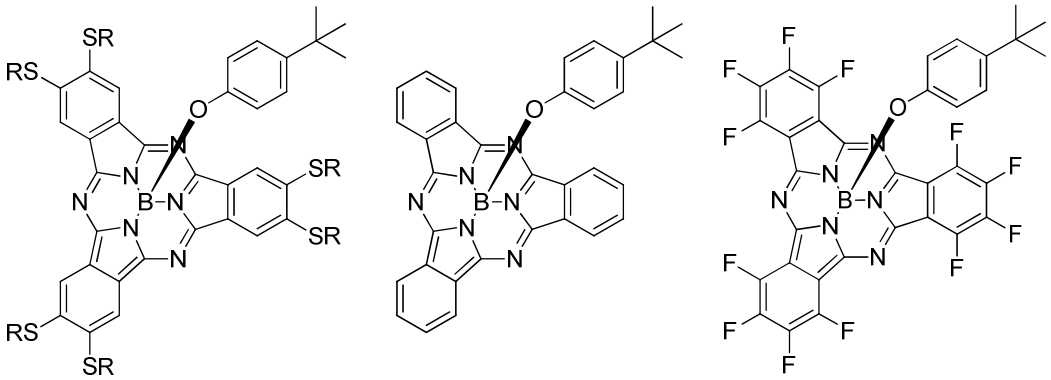

Figure 4. SubPcs employed as fullerene receptors.

We chose dodecafluorosubphthalocyanine **6f** as acceptor, unsubstituted SubPc **6e** as neutral, and hexathioether SubPcs **6a-d** as donor components. Furthermore, the donor SubPcs bear alkyl chains which may strengthen the complexation of C_{60} and C_{70} fullerenes through additional van der Waals interactions. The alkyl chains of the hexaalkylthio-substituted SubPcs are expected to mutually interact and, thereby, to cooperate in the encapsulation of fullerenes. Thus, four different SubPcs **6a-d** with

increasing chain-length (C2, C4, C8 and C16, respectively) were synthesized with the aim of determining the role and importance of these moieties in the formation of the complexes.

Finally, photoinduced processes occurring in the complexes were studied with pump probe experiments.

On the other hand, the curve-shaped structure and the synthetic versatility of SubPcs make them ideal building-blocks for the construction of functional homodimeric capsules. Thus, the tritopic C_3-symmetric receptor shown in Figure 5, which combines both the preorganization of the rigid SubPc skeleton and three pyridyl units, was self-assembled into a heterochiral cage of C_{3h} symmetry in the presence of a stoichiometric amount of $Pd(en)(NO_3)_2$. Remarkably, this high degree of symmetry was found to be the result of chiral self-discrimination between the enantiomers of the SubPc (Figure 5a) during the self-assembling process.[11]

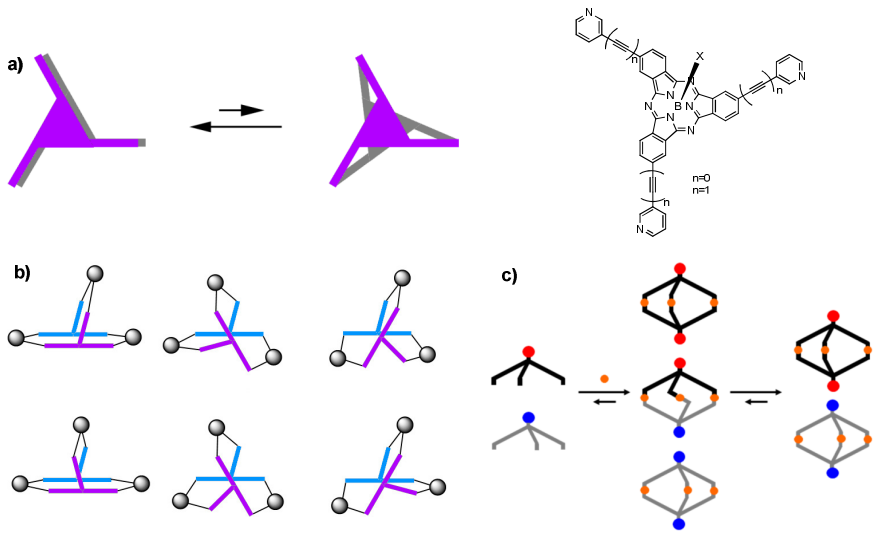

Figure 5. Structure of SubPcs employed as building blocks of homodimeric capsules and schematic representations of dynamic properties of self assembly: (a) between the enantiomers of C_3 symmetric SubPc; (b) between the enantiomers of C_1 symmetric SubPc; and (c) between regioisomers of SubPc.

Metallosupramolecular capsules built with a SubPc that bear a triple bond as spacer between the coordinating unit and the core (Figure 5), were also found to be excellent for the study of dynamic processes associated with the formation of

[11] C. G. Claessens, T. Torres, *J. Am. Chem. Soc.* **2002**, *124*, 14522-1452.

metalosupramolecular assemblies.[12] Namely, it was possible to observe discrimination between regioisomers and determine the kinetics of the process with mass spectrometry, as well as self-sorting between the enantiomers of C_1-symmetric SubPc (Figure 5).

Regarding the context of this chapter, fullerene encapsulation in SubPc-based metallosupramolecular structures has been also proved in our group in 2004.[13] Nevertheless, in this case, no quantitative data were reported since C_{60} was extracted from acetone, a solvent in which it is barely soluble.

The second section of this chapter deals with the preparation and study of new SubPc-based metallosupramolecular capsules and the study of their properties. Hence, the first objective is the self-assembly of new cage-compounds bearing different metal centers –Pd (II) and Pt (II)- and ligands (Figure 6). Representative capsules of the library thus obtained were compared to determine the influence of any parameter (metal, ligand) on their relative stabilities.

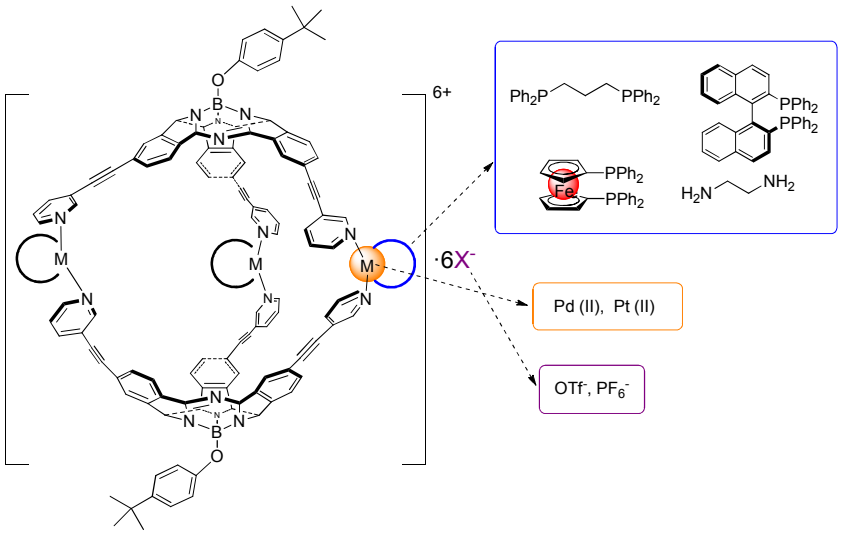

Figure 6. Capsule compounds studied in the second section of this chapter.

Phosphine ligands were chosen to allow a quick characterization of the self-assembled capsules by ^{31}P-NMR, which provides more simple spectra than ^{1}H-NMR. Such ligands were selected so that they presented an additional interest. For example, 1,1'-bis(diphenylphosphino)ferrocene was employed with the aim of incorporating

[12] (a) C. G. Claessens, M.J. Vicente-Arana, T. Torres, *Chem. Commun.*, **2008**, 6378-6380 ; (b) C. G. Claessens, I. Sanchez-Molina, T. Torres, *Supram. Chem.*, **2009**, *21*, 44-47 .
[13] C. G. Claessens and T. Torres, *Chem. Commun.*, **2004**, 1298–1299.

secondary donor moieties at the periphery of the system. A chiral phosphine was employed to obtain capsules containing two *M* or *P* isomers of the SubPc, instead of the usually more stable [*M, P*] cage.

Furthermore, and as we mentioned above, preorganization is a powerful and interesting tool to construct effective fullerene receptors. Thus, we intended to employ SubPc based capsules to complex fullerenes and fullerene derivatives in solution, and to perform a complete study of the encapsulation process.

Again, the presence of photo- and electroactive chromophores in the systems motivated the photophysical study of the capsules as well as the adducts they form with the fullerenes.

1.2. Experimental Techniques

Along this chapter, a series of photoactive supramolecular systems will be discussed. Their study involves basically two disciplines: supramolecular chemistry and phtotophysics. In the next pages the necessary experiments for determination of quantitative aspects of the binding equilibrium (stoichiometry, binding constant) are firstly described. Secondly, a short explanation of the techniques usually employed for the study of photophysical properties of organic molecules is made.

Method of Continuous variation

The method of continuous variation is a commonly used procedure to determine the stoichiometry of a binding event. Although the basic principle of the method had been employed before,[14] it is generally associated with P. Job, who applied the procedure to the study of many coordination compounds.[15]

The experimental procedure consists of preparation of a series of samples containing both components (metal and ligand or host and guest, for example), in different ratios, while the total concentration is kept constant. Then, a property of the system that changes upon complex formation is measured, and plotted versus the mole fraction of one of the components. The resulting curve (Figure 7) held a maximum that indicates

[14] I. Osstromesslinsky, *Berichte*, **1911**, *44*, 268; R. B. Denison, *Trans. Faraday Soc.*, **1912**, *8*, 35.
[15] P. Job, *Ann. Chim.,* **1928**, *9,* 113.

the ratio of components in the complex. For example, a maximum at 0.5 mole fraction corresponds to 1:1 complex, 0.33 corresponds to 1:2 complex, and so on.

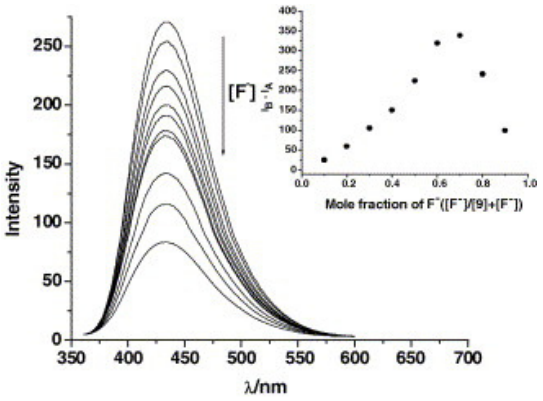

Figure 7. Example of a Job Plot.[16]

Some limitations must be taken into account when applying Job's method:

- If UV-visible spectroscopy is employed to study the samples (as it generally happens), the system must conform Lambert-Beer's law.
- One complex must be predominant under the experimental conditions
- pH and ionic strength must be maintained constant

A usually recommended crosscheck of the technique, to ensure complete reliability of the results, is to carry out the experiments at different values of total concentration.

Moreover, Job Plots of 1:1 complexes allow approximate determination of the binding constants.[17] For that purpose, the slope of the tangent lines to the Job Plot's curve at mole fraction = 0 and 1 must be determined, and then, binding constants are derived from the following equations:

$$a_0 = \frac{m}{(m+1)}$$

$$a_1 = \frac{-m}{(m+1)}$$

where: a_0 y a_1=slopes of tangent lines at χ=0 and χ=1; m=K_{eq}·$[C]_0$

[16] H-Y. Hu, C-F. Chen, *Tetrahedron. Lett.*, **2006**, *47*, 175-179.
[17] E. Bruneau, D. Lavabre, G. Levy, J. C. Micheau, *J. Chem Educ.*, **1992**, *69,* 833-837

Titrations

A titration is a volumetric technique in which a solution of one reactant (called "the titrand") is added to a solution of a second reactant (analyte) until the equivalence point is reached. The equivalence point is the point at which titrant has been added in exactly the right quantity to react stoichiometrically with the analyte.[18]

Titrations are the most common approach in supramolecular chemistry to quantify interactions between host and guest.[19] The changes in some physical property that is affected upon addition of the titrand are monitored by NMR, UV-vis, fluorescence or other techniques. The accuracy of the results relies on the right choice of concentration range (and thus the appropriate technique), acquisition of a reasonable number of data points, and careful work during the experimental procedure as well as on the data analysis.

In general, it is worthwhile to obtain as much information as possible (stoichiometry, estimated value of binding constant) prior to the titration experiment, in order to ease the choice of the above mentioned issues.

Supramolecular titration experiments are usually carried out maintaining the concentration of one component (H) fixed. Then, the physical changes observed on the system are plotted versus the added concentration of guest (G). The resulting titration curve is known as binding isotherm (Figure 8), and its points can be fitted to a mathematical model which is deduced from the equilibrium we assume is taking place.

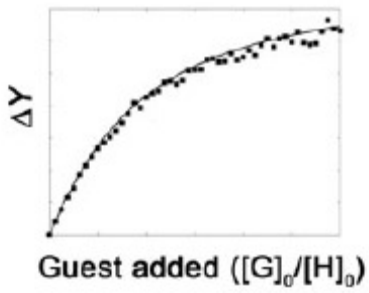

Figure 8. Example of binding isotherm for 1:1 complexes.

For example, if we carry out a titration of a 1:1 complex and follow the changes upon UV-vis spectroscopy, we can deduce an equation that describes the changes of

[18] http://chemed.chem.wisc.edu/chempaths/GenChem-Textbook/Titrations-875.html
[19] P. Thodarson, *Chem. Soc. Rev.*, **2011**, *40*, 1305-1323.

absorbance upon addition of, for example, the guest, by combination of Lambert-Beer's law and mass balance.[20]

$$K_{eq} = \frac{[HG]}{([H]\cdot[G])}$$

$$[H]_{tot} = [H] + [HG] \rightarrow [H]_{tot} = K_{eq}\cdot[H]\cdot[G] + [H] = (K_{eq}\cdot[G] + 1)[H] \rightarrow [H] = \frac{[H]_{tot}}{(K_{eq} + 1)}$$

$$[G]_{tot} = [G] + [HG]$$

$$\Delta A = \Delta\epsilon\cdot[HG]\cdot b$$

$$\Delta A = \Delta\epsilon\cdot[H]\cdot[G]\cdot b$$

$$\frac{(\Delta A)}{b} = \frac{(\Delta\epsilon)\cdot[G]\cdot[H]_{tot}}{(K_{eq}\cdot[G] + 1)}$$

In a similar manner, mathematical models for other techniques and stoichiometries can be derived and applied to mathematical treatment of the data according to the case.

Electrochemistry

Electrochemical measurements[21] of organic molecules in solution are employed to determine the energies of their frontier orbitals (HOMO and LUMO) and the bandgap between them (corresponding to the energy of the first singlet excited state), which are crucial parameters for the study of photoinduced transfer processes.

The material of which an electrode is made (usually a metal, or in the case of the working electrode we used, graphite) does not possess the individual well defined electron energy levels that would be found in a single atom of the same material. Instead, a continuum of levels is created with the available electrons filling a certain number of states. The Fermi-level corresponds to the energy at which the 'top' electrons sit. This level is not fixed, and its energy can be modified by supplying electric energy. That means, if we apply a positive potential, we are removing electrons from the material and, thus, the Fermi level will descend. When the Fermi level of the electrode goes below the energy of the HOMO of the analyte, the first oxidation of the molecule occurs (figure 9a). In contrast, when applying a negative potential, we are injecting electrons into the empty levels of the electrode, and thus, the Fermi level goes

[20] K. A. Connors, *Binding Constants,* Wiley & Sons, New York, 1987.
[21] Electrochemical Methods: Fundamentals and Applications, A.J. Bard, L. R. Faulkner, Wiley & Sons, 2nd Ed., January 2001.

up. When it reaches a value of energy higher than the LUMO of the molecule, the first reduction takes place (figure 9a).

-Cyclic Voltammetry: [22]

Cyclic voltammetry (CV) is a type of potentiodynamic electrochemical measurement based on variation of the applied potential at a working electrode in both forward and reverse directions, at a determined scan rate, while monitoring the current (Figure 9b). A three-electrode setup is employed (Figure 9c). CV measurements must be carried out in quiescent solutions to ensure diffusion control.

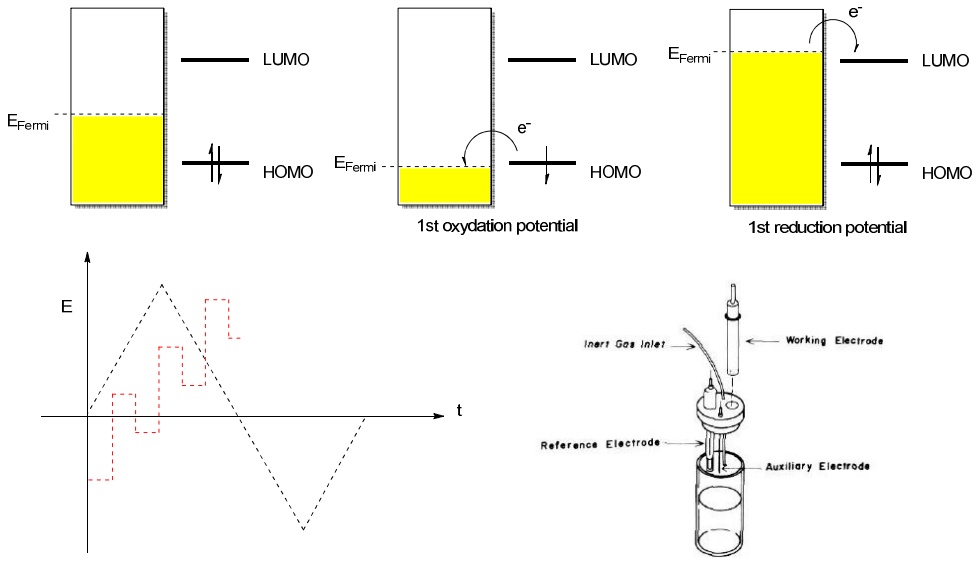

Figure 9. a) Representation of the relationship between electrochemistry and frontier orbitals. b) Variation of applied potential *vs* time in cyclic voltammetry (black) and square-wave voltammetry (red). c) Electrochemical cell.

During the experiment, the potential is applied between the reference and the working electrodes, while the current intensity is measured between the working and the counter electrode. The current at the working electrode will increase when reductions (injection of electrons from the electrode to the empty orbitals of the analyte) or oxydations (injection of electrons from occupied orbitals of the analyte to the electrode) of the molecule in solution occur. The current falls off again as the concentration of analyte close to the electrode surface is depleted.

[22] P. T. Kissinger, W. R. Heinemann, *J. Chem. Educ.,* **1983**, *60*, 702-706; Handbook of instrumental Techniques for Analytical Chemistry, F. A. Settle (Chapter 37, S. P. Kounaves), Prentice Hall, 1997.

Cyclic voltammetry can distinguish reversible and irreversible electrochemical processes. A redox process is said to be reversible if the system remains in equilibrium throughout the whole potential scan. A typical voltammogram for a reversible process is shown in Figure 10. Generally, two conditions must be fulfilled to consider an oxidation or reduction reversible, at 25°C and any scan rate:

$$(1)\ \Delta E_p = |E_{pc} - E_{pa}| = \frac{57}{n} mV$$

$$(2)\ \frac{i_{pa}}{i_{pc}} = 1$$

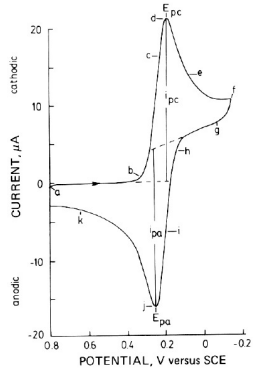

Figure 10. Typical voltammogram obtained with CV.

On the other hand, irreversibility is caused by slow exchange of electrons between the analyte and the working electrode.

- Square wave voltammetry:[22]

Square-wave voltammetry (SWV, Figure 9b) is a pulse technique. This type of potential modulation presents important advantages as increased speed and sensitivity. However, it does not distinguish between reversible and non reversible redox processes.

The excitation signal in SWV consists of a symmetrical square-wave pulse of amplitude E_{sw} superimposed on a staircase waveform of step height ΔE, where the forward pulse of the square wave coincides with the staircase step. The net current, i_{net}, is obtained by taking the difference between the forward and reverse currents. The peak height in the voltammogram is proportional to the concentration of the electroactive species, and

allows limits of detection up to 10^{-8} M. In general, it is employed to obtain the exact values of the redox potentials.

Study of photophysical properties

The absorption of UV or visible light by an organic molecule [23] causes the promotion of an electron from an initially occupied, low energy orbital to a higher energy, previously unoccupied orbital (Figure 11). When such event happens, an excited state of the molecule is generated. Following light absorption, several processes contribute to the relaxation of the molecule and its return to the ground state. These processes can be either radiative (a photon is emitted during the transition) or non-radiative (the loss of energy is emitted as heat- infrared radiation- instead of UV-visible light).

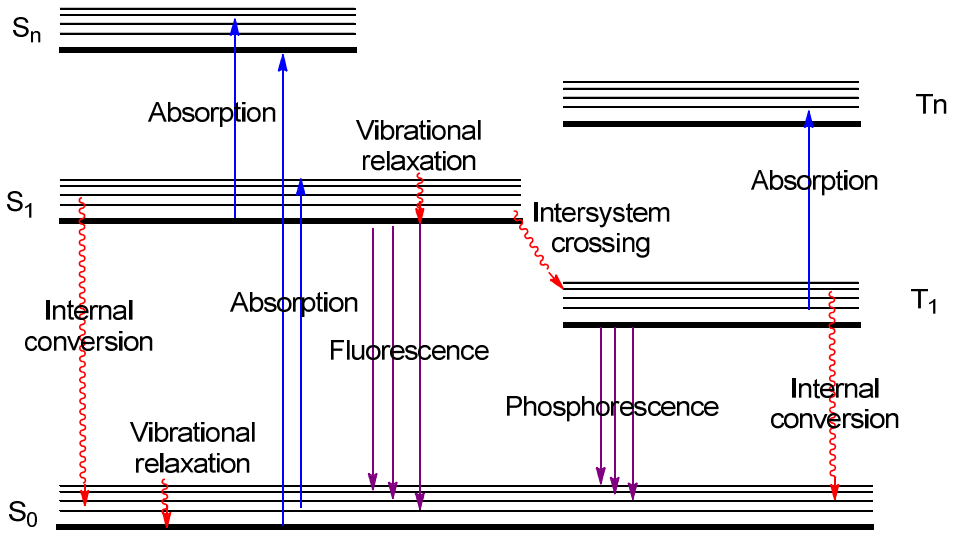

Figure 11. Jablonsky diagram.

Molecules in condensed phases rapidly relax to the lowest vibrational state of S_1 (typically in 10^{-12} s or less). Fluorescence then results from a thermally equilibrated excited state. This radiative transition to the ground state generally occurs to excited vibrational levels within the ground state, which then reaches thermal equilibrium again through vibrational relaxation. As a consequence, fluorescent emission is bathocromically shifted with respect to absorption. This wavelength difference between both bands is called Stokes shift. Moreover, when the shape of the fluorescence spectrum mirrors the one of the absorption band, it means that the vibrational structure in both the ground state and the first excited state are similar. Actually, all transitions

[23] Modern Molecular Photochemistry, N. J. Turro, University Science Books, 1991; Principles of Fluorescence Spectroscopy 3rd Ed, J. R. Lackowicz, Springer Science, 2006.

between electronic states occur without nuclear geometry being affected; they take place within times close to 10^{-15} s, which is a too short interval for nuclei displacement (Franck-Condon Principle).

Radiative emission from the first singlet excited state also occurs when the molecule interacts with an electromagnetic wave of the exact frequency of the transition. The photon thus generated has the same phase, frequency, polarization and direction of the incident light. In normal media at thermal equilibrium, absorption exceeds stimulated emission because there are more electrons in the lower energy states than in the higher energy states. However, when a population inversion is present the rate of stimulated emission exceeds that of absorption, and a net optical amplification can be achieved.

Molecules in the first singlet excited state can also undergo a spin flip of one electron to the first triplet state. This conversion is known as intersystem crossing (ISC). Spin flip is usually produced by spin-orbit coupling, and it is more favourable if the molecule possesses heavy atoms. Radiative emission from T_1 to the ground state is called phosphorescence*, and it is usually shifted to longer wavelengths than fluorescence. Transitions involving a change of spin are optically forbidden, and as a consequence the rate constants for phosphorescence are several orders of magnitude lower than for fluorescence.

Relaxation from the S_1 or the T_1 to the ground state can also occur non-radiatively through the vibrational levels, which is known as internal conversion.

All the photophysical events described above are defined by their quantum yield and their lifetime. The quantum yield is the number of times a specific event occurs per photon absorbed by the system. For example, fluorescence quantum yield is defined as the number of molecules decaying from S_1 to S_0 through emission with respect to the number of photons absorbed. As both radiative and non radiative transitions can depopulate the first singlet excited state, the fluorescence quantum yield is given by

$$\phi_f = \frac{\Gamma}{(\Gamma + k_{nr})}$$

* Actually, phosphorescence is the term applied for any radiative transition between states of different spin multiplicity, but since as the most common case in organic molecules is the T_1-S_0 emission, only this one is commented in the text.

Where Γ is the rate of fluorescence and k_{nr} contains the kinetic rates of all non radiative processes that deactivate the first singlet excited state.

The lifetime of an excited state is defined by the average time the molecule spends in that state prior to deactivation. Lifetime is the inverse of the total decay rate (sum of the kinetic rates corresponding to the processes that depopulate the excited state):

$$\tau = \frac{1}{(\Gamma + k_{nr})}$$

Time-resolved fluorescence is a technique in which the fluorescence of a sample is monitored as a function of time after excitation by a flash of light. The width of the excitation pulse is made as short as possible, preferably much shorter than the decay time of the sample. Fluorescence lifetime is determined fitting the data to exponential decay models. For a single exponential decay, around 63% of the molecules have emitted prior to t = τ.

Lifetime of triplet states can be determined with laser flash photolysis.[24] In this technique, a sample is firstly excited by a strong pulse of light of a laser. The pulse width ranges from nanoseconds to femtoseconds, depending on the laser. In this manner, an increased population of excited states is generated. Typically the light absorption of the sample (at the maximum of absorption of the triplet state) after excitation is recorded within short time intervals.

After light absorption, and in the presence of other molecules in solution, chromophores can also undergo transformations like energy transfer, photoinduced electron transfer or other chemical reactions. These events are among the fastest events in nature. They occur in time scales ranging from femtoseconds to nanoseconds. The development of ultrafast laser systems has enabled investigation of these events in real time. In particular, transient absorption spectroscopy[25] provides one of the most effective methods for studying the behaviour of transient species like radicals, ions and excited states.

The principle of transient absorption spectroscopy is shown in Figure 12a. Here, the absorbance at a particular wavelength or range of wavelengths of a sample is measured as a function of time after excitation by a flash of light. In a typical

[24] www.photophysics.com/tutorials/laser-flash-photolysis
[25] R. Berera, R. van Grondelle, J. T. M. Kennis, *Photosynth. Res.*, **2009**, *101*, 105-118.

experiment, both the light for excitation ('pump') and the light for measuring the absorbance ('probe') are generated by a pulsed laser. In each measurement, the absorbance of the probe pulse by the sample is recorded twice, the second time after a certain delay with respect to the pump pulse. Thus, in the first shot, the absorbance of the sample in the ground state is recorded. In contrast, the second time the probe pulse hits the sample a fraction of molecules has been promoted to an electronically excited state by means of the pump pulse. A difference absorption spectrum is then calculated. By changing the delay, a ΔOD profile as a function of time and wavelength is obtained (Figure 12b). This profile contains information on the dynamic processes occurring in the system we are studying. Specifically, the study of the spectra (ΔOD vs wavelength) allows identification of the excited states or transient species formed upon excitation of the chromophore. On the other hand, the study of decay profiles (ΔOD vs time) provides information on the kinetics of photophysical or photochemical processes.

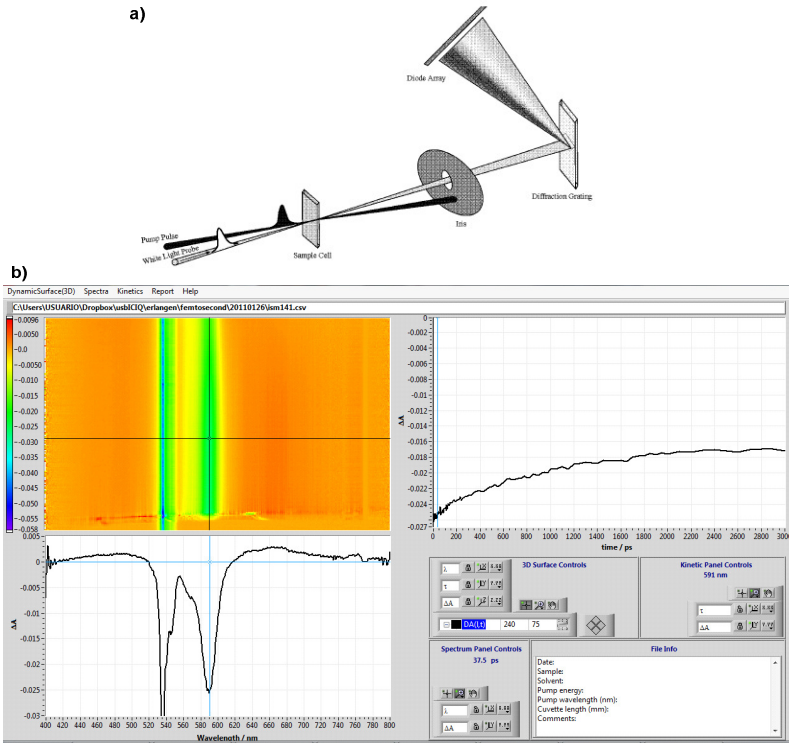

Figure 12. (a) Principle of transient absorption spectroscopy. (b) Data obtained in a pump probe experiment :ΔOD as a function of wavelength (spectrum) and as a function of time (decay).

In general, the bands observed in a transient absorption spectrum arise from four kinds of contributions:

- Ground-state bleach: as a fraction of molecules has been promoted to the excited state through the action of the pump pulse, population of the ground state has

decreased. As a consequence, ground state absorption of the excited sample is lower than the non-excited. Hence, a negative signal in the ΔOD spectrum is observed. This signal appears in the region of the ground state absorption (it mirrors the UV-Vis absorption band).

- Stimulated emission: Upon population of the first excited state, stimulated emission may take place when the second probe pulse passes through the sample. This process will occur only for optically allowed transitions (see above), and its spectral profile generally reflects the fluorescence spectrum of the chromophore. The photon thus generated is emitted in the same direction as the one of the probe pulse, and both are detected. Hence, stimulated emission produces a negative ΔOD signal. Many chromophores present such a low Stokes shift that both ground state bleach and stimulated emission bands overlap and merge into one band.

- Excited state absorption: Optically allowed transitions from the excited states (populated upon excitation with the pump pulse) to higher states might exist in certain wavelength regions. Absorption of the probe pulse at these regions is then observed as a positive band in the ΔOD spectrum.

-Product absorption: After excitation, photophysical or photochemical processes might give rise to long-lived states or *transients*, such as triplet, charge separation or isomerization states. These species appear as positive bands, and they are accompanied by bleaching at the bands corresponding to the excited states that lead to their formation. For example, as a triplet arises from intersystem crossing from a singlet excited state, bleaching will be observed in the bands of the latter.

2. Systematic study of Subphthalocyanines as receptors for C_{60} and C_{70} fullerenes

2.1. Synthesis of Subphthalocyanines

Tetrafluorophthalonitrile and 1,2-dicyanobencene were purchased from Aldrich and used without further purification. 4,5-dialkylthiophthalonitriles (Figure 13) were prepared starting from 4,5-dichlorophthalic acid,[26] with was treated with acetic anhydride to afford 4,5-dichloroftalic anhydride in 95% yield. Compound **1** was refluxed in formamide and 4,5-dichlorophthalimide was obtained. Opening of the phthalimide was achieved by means of a 48-hour treatment with ammonia. Finally, dehydration of **3** afforded 4,5-dichlorophthalonitrile in 66% (52% global yield).

Nucleophilic aromatic substitution of the chlorine atoms in **4** with the corresponding thiol in the presence of potassium carbonate gave rise to the desired precursor phthalonitriles.

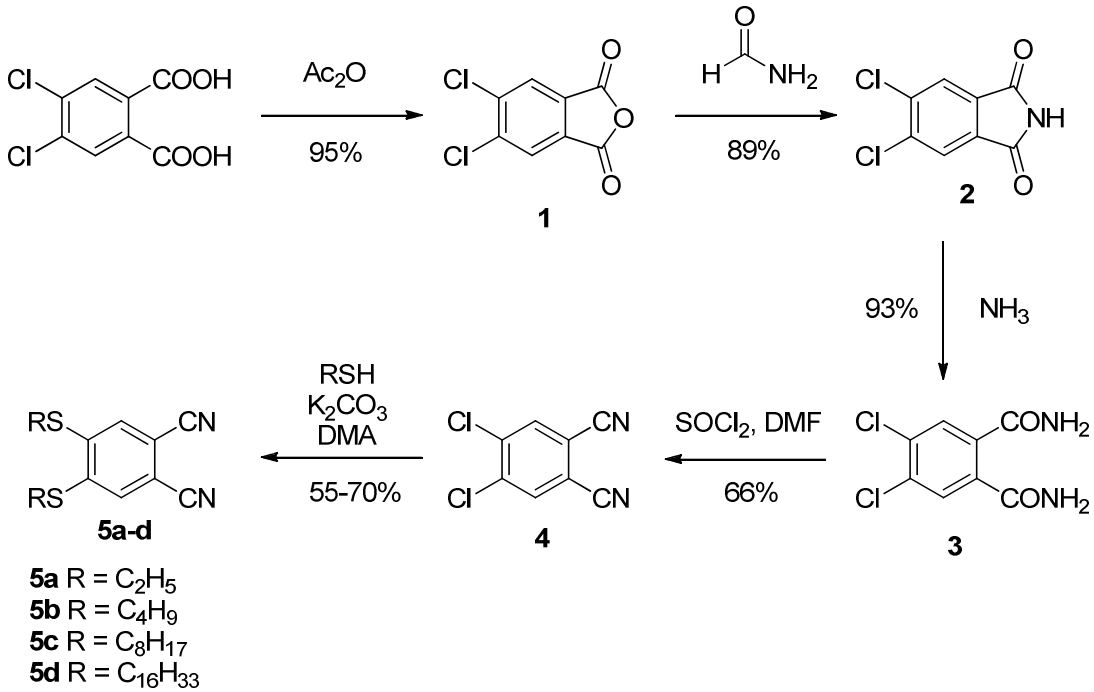

Figure 13. Synthesis of 4,5-dialkylthiophthalonitriles.

[26] (a) A.G. Gürek, Ö. Bekâroglü, *J. Chem. Soc. Dalton Trans.* **1994**, 1419-1423; (b) B. del Rey, U. Keller, T. Torres, G. Rojo, F. Agulló-López, S. Nonell, C. Martí, S. Brasselet, I. Ledoux, J. Zyss, *J. Am. Chem. Soc.* **1998**, *120*, 12808-12817.

Cyclotrimerization reaction of precursor phthalonitriles (Figure 14) in the presence of boron trichloride under an argon atmosphere gave rise to the desired SubPcs[27] as chloro-derivatives. Substitution of this chlorine atom on the axial position provides to the macrocycle more solubility as well as stability towards hydrolysis. Thus, such reaction was carried out through addition of 3 eq of 4-tertbuthylphenol upon the crude of the previous reaction. The mixture was refluxed in toluene till the reaction was complete or the major product was the phenoxy-substituted SubPc (checked by TLC). Axial-substitution reaction proceeded within 2-3 hours for hexaalkylthio-SubPcs (**6a-d**). On the other hand, 18-24 hours of reflux were required for dodecahydro and dodecafluoro-SubPc. In the last case, some unreacted material was still detected in the TLC.

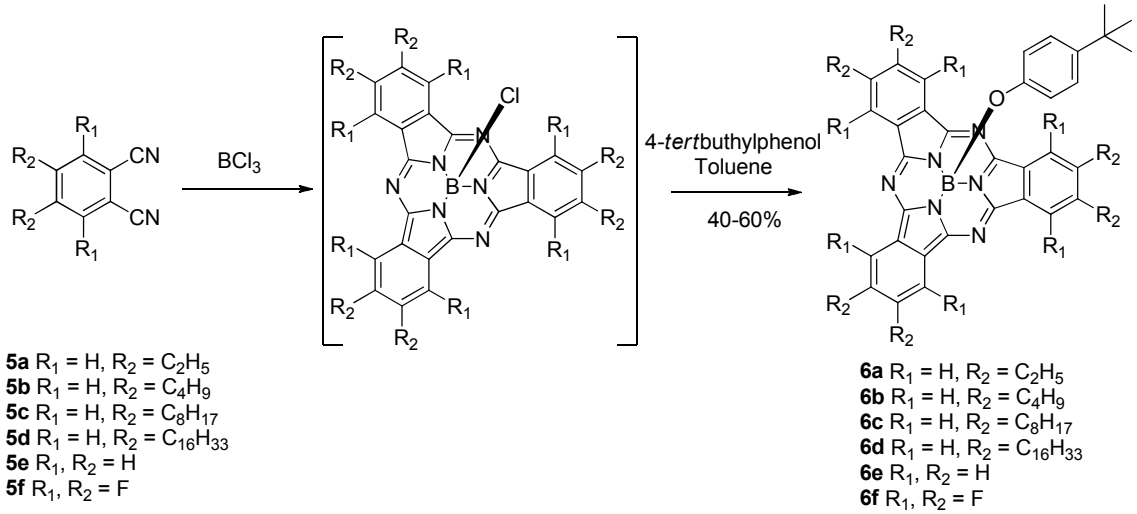

Figure 14. Synthesis of SubPcs **6a-f**.

2.2. Characterization

All compounds were characterized by ^{1}H, ^{19}F, ^{13}C-NMR spectroscopy, UV-vis spectrophotometry as well as mass spectrometry.

MALDI-TOF mass spectra of compounds **6a-f** show peaks at 760.14, 544.24, 904.26, 1072.42, 1408.64, 2082.36, respectively, corresponding to $[M]^{+}$. In the case of thioether-substituted SubPcs **6a-d** peaks corresponding to the loss of the axial tert-butylphenoxy group were more intense than in **6e** and **6f**. These observations confirm the higher lability of the axial ligands observed experimentally when the macrocycle is

[27] (a) D. D. Díaz, Henk J. Bolink, L. Capelli, C. G. Claessens, E. Coronado, T. Torres, *Tetrahedron Lett*, **2007**, *48*, 4657; (b) C. G. Claessens, T. Torres, *Angew. Chem. Int. Ed.* **2002**, *41*, 2561-2565.

peripherally substituted with donor groups (see previous page). Hence, mass spectrometry results are in good agreement with the reactivity observed in the macrocycles.

UV-vis spectra of SubPcs **6e** and **6f** show the expected B and Q bands at ca. 320 and ca. 580 nm; suffering the Q band of **6f** a small bathochromic shift due to the presence of the electron-attracting groups. In the case of donor subphthalocyanines **6a-d**, the Q band is bathochromically shifted from 570 to 605 nm (Figure 15). It is worth mentioning the presence of a weak absorption band at ca. 400 nm in these compounds which is most probably due to a n-π* transition between the lone pair of the sulphur atoms and the adjacent aromatic ring.

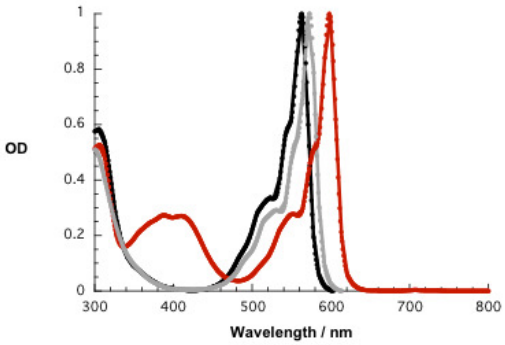

Figure 15. UV-vis absorption spectra of SubPcs **6d** (red), **6e** (black), and **6f** (grey).

In ^{1}H-NMR spectra, all the signals corresponding to the periphery of SubPcs **6a-e** are downfield-shifted with respect to the precursor phthalonitriles **5a-e**. The same change can be observed for the fluorine atoms of **5f** and **6f** in ^{19}F-NMR. Moreover, the AA'BB' system of the protons of 4-*tert*buthylphenoxy group in the axial position are observed at 6.7 and 5.3 ppm approximately. The low chemical shift for these signals is due to the shielding effect of the π-system of the macrocycle.

2.3. Host-guest chemistry

2.3.1. Mass spectrometry experiments

In order to achieve a fast evidence of the existence of an interaction between SubPcs **6a-f** and fullerenes (C_{60} and C_{70}), ESI-mass spectra of samples containing **6b-d** and C_{60} were registered. Acetone and chloroform were employed as solvents, and TCNQ was added to the samples to facilitate ionization of the SubPcs.

All cases showed 1:1 SubPc/C_{60} complex as the major product (Figure 16). Small amounts of 2:1 and 3:1 complexes were also detected in the case of **6d**.

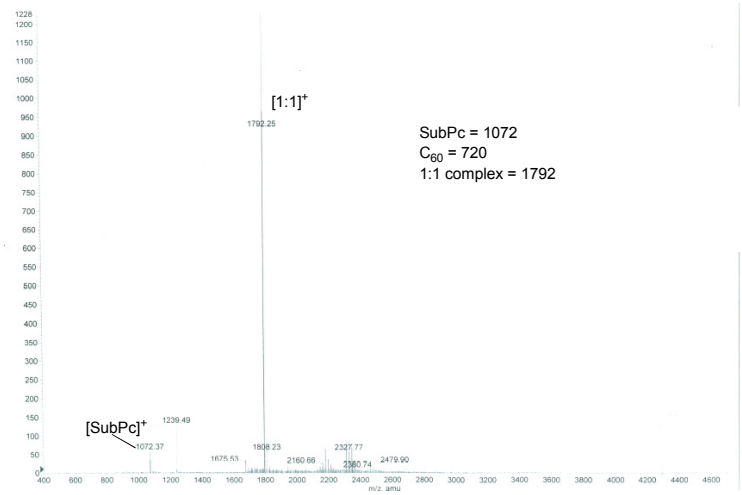

Figure 16. Mass spectrum of the mixture of **6c** and C_{60}.

Thus, the interaction of SubPcs with fullerene was confirmed with this technique. However, mass spectrometry could not provide information about the quantitative aspects of these complexes. Such aspects were studied by means of Job's Plots (to determine the stoichiometry) and titrations (to determine the binding constants). All these experiments were carried out in toluene and followed with UV-vis spectroscopy. The main reason to choose toluene as solvent was the solubility of the fullerene.

2.3.2. Stoichiometry of complexes

Perfluorinated SubPc **6f** and C_{60} or C_{70} were not expected to interact because their electronic nature is not complementary (both compounds are electronically deficient); Job's plot experiments carried out in toluene confirmed our hypothesis, as illustrated in Figure 17. These results indicate that shape complementarity alone is not enough for SubPcs to interact appreciably with fullerenes. In the case of unsubstituted SubPc **6e**, a 1:1 complex with either C_{60} or C_{70} was shown to form in toluene with a clear maximum at 0.5 molar fraction (Figure 17), which is in good agreement with the result previously reported.[9]

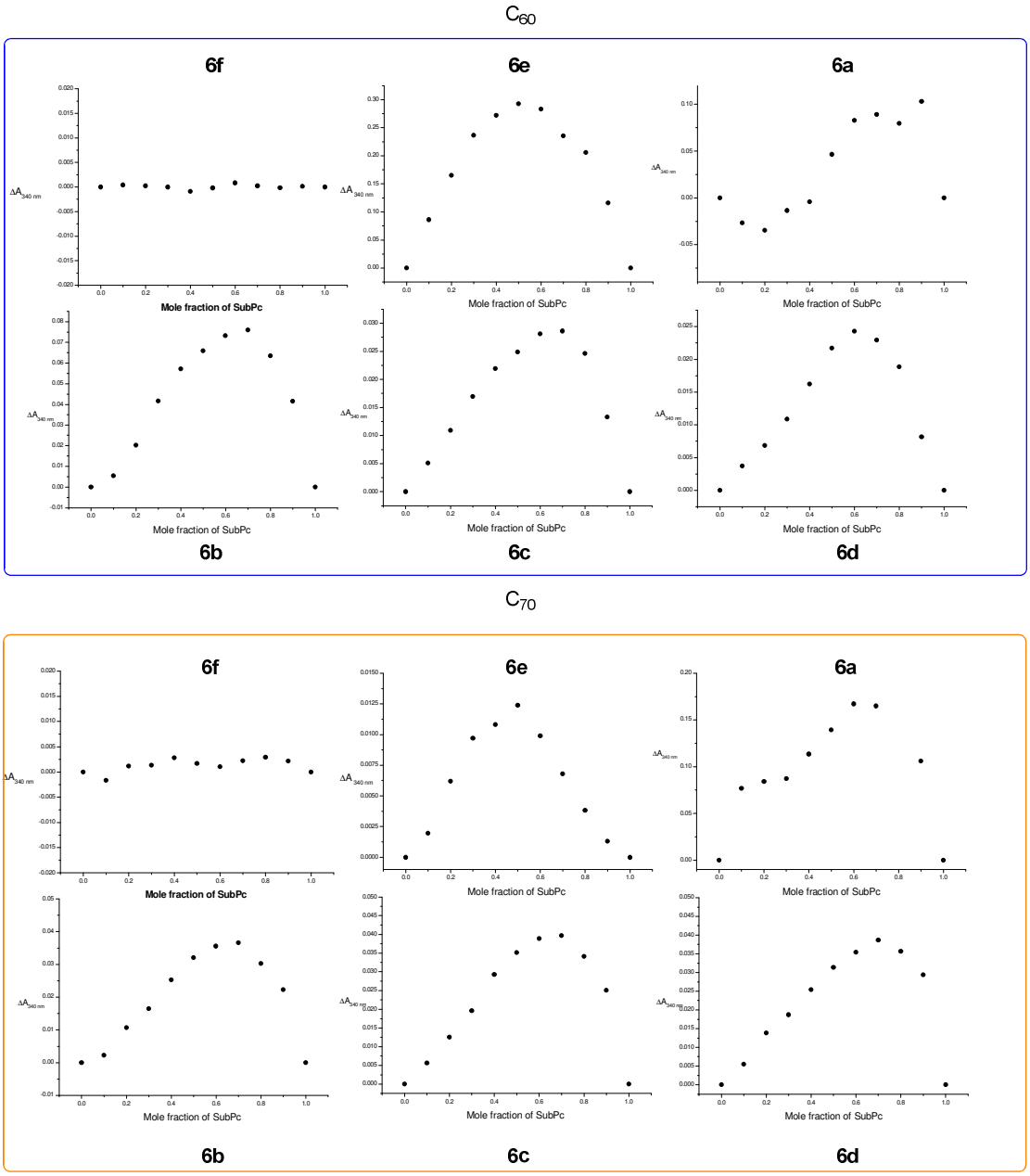

Figure 17. Job Plots for SubPcs **6a-f** with C_{60} (upper part) and C_{70} (lower part).

More strikingly, the introduction of six donor thioalkyl chains in the periphery of the macrocycles (**6a-d**) gave rise to the formation of 2:1 complexes. Here, two SubPcs encapsulate one fullerene. The length of the alkyl chain influences dramatically the time required for the binding process to reach equilibrium. For example, the latter occurred inmediately for lipophilic SubPcs **6c** and **6d**, but required some time for SubPc derivatives bearing short alkyl chains, that is, 15 minutes for **6b**, and around 45 minutes for **6a** with C_{60} fullerene. When studying the interactions with C_{70}, the time delay only evolved for SubPc **6a** (20 minutes). One can observe that the Job's plots corresponding to the formation of the 2:1 complex between SubPc **6a** and C_{60} are far

from perfect even after several attempts. From these experimental observations we infer that the alkyl chains have a structuring role in the formation of the complexes with fullerenes. In Figure 18, representation of the molecular structure of the 2:1 complexes between SubPcs **6b**, **6c** and **6d** and C_{60} confirm the necessary interactions between the alkyl chains when the number of carbon atoms of the alkyl chains exceed four.

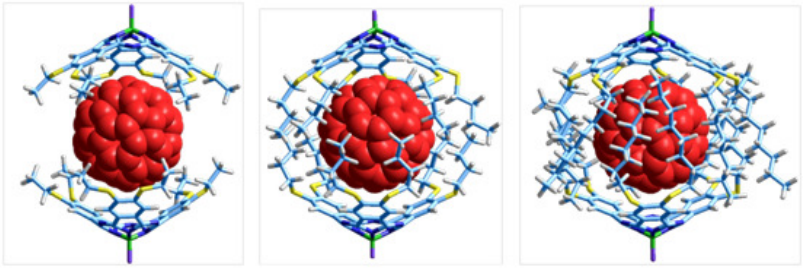

Figure 18. Molecular modeling of adducts of C_{60} with (from left to right) **6b**, **6c** and **6d**.

2.3.3. Binding constants

Binding constants for all of the previously described complexes were derived from titration experiments monitored by UV-visible spectroscopy. The only notable exception is **6e**, whose binding constants with C_{60} and C_{70} were obtained from the Job's plots (Figure 17).

At first glance, no changes appear in the spectra during the titration. However, the spectra differ from the sum of the individual spectra, that is, SubPc and C_{60}. This difference of absorbance around 360 nm was plotted versus increasing concentrations of SubPc, and curve fitting afforded the values of the binding constants. It is worth mentioning that, despite evidence for a 2:1 stoichiometry in the Job's plots of **6a-d** with C_{60} and C_{70}, the shape of the titration curves corresponds to the typical absorbance hyperbola for 1:1 complexes (Figure 19).

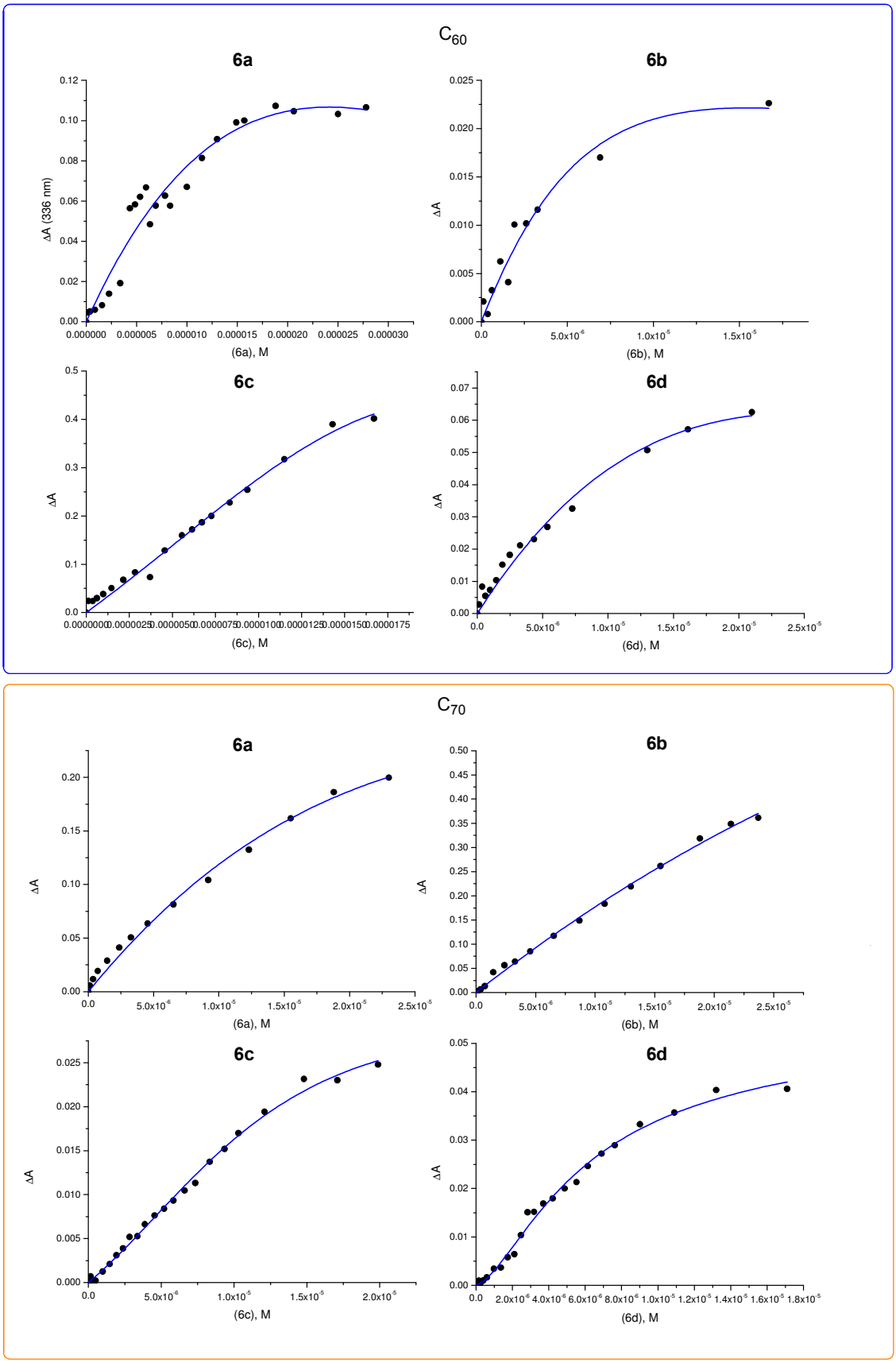

Figure 19. Binding isotherms for titrations of C_{60} and C_{70} with SubPcs **6a-d**.

On the one hand, this fact may be rationalized on the basis of a 1:1 complex, but, on the other hand, the stepwise formation of a 2:1 complex, where both binding constants have the same value, cannot be ruled out. The former interpretation was discarded, since, if true, it should be reflected in the Job's plot experiments. As a matter of fact, the latter interpretation was used for the curve fitting. The titration of C_{70} with SubPc **6d** (C_{16} alkyl chains) gave rise to a typical sigmoidal curve, from which different K_1 and K_2 values were derived (Table 1).

Table 1. Binding constants derived from titration experiments

SubPc	**with C_{60} (M^{-1})**	**with C_{70} (M^{-1})**
6a	$K_1 = K_2 = 2.1 \times 10^4 \pm 2.6 \times 10^3$	$K_1 = K_2 = 1.9 \times 10^4 \pm 1.9 \times 10^3$
6b	$K_1 = K_2 = 1.9 \times 10^5 \pm 5.2 \times 10^4$	$K_1 = K_2 = 1.1 \times 10^4 \pm 2.2 \times 10^3$
6c	$K_1 = K_2 = 2.9 \times 10^4 \pm 1.1 \times 10^3$	$K_1 = K_2 = 1.3 \times 10^4 \pm 3.6 \times 10^3$
6d	$K_1 = K_2 = 4.4 \times 10^4 \pm 2.6 \times 10^3$	$K_1 = 3.6 \times 10^5 \pm 2.7 \times 10^4$ $K_2 = 1.8 \times 10^5 \pm 3.8 \times 10^4$
6e	$K = 2.1 \times 10^4 \pm 1.1 \times 10^3$	$K = 6.6 \times 10^2 \pm 46$
6f[a]	—	—

Overall, the binding constants are quite high, with values ranging from 10^4 to 10^5 M^{-1} and, as such, attest the strong interactions between SubPcs and fullerenes. In spite of the different kinetic behaviour in terms of complex formation, no general trend in binding constants is observed. In fact, the differences between the binding constants are insignificant and, thus hinder to reach any meaningful conclusion.

2.4. Photophysics

Further insights into the interactions between SubPcs and fullerenes in the host-guest complexes came from femtosecond pump probe experiments. SubPcs **6b**, **6c** and **6d** were selected for the study and all of them showed a very similar behaviour. Common to the three of them is that photoexcitation at, for example, 540 nm generates a singlet excited state, whose characteristics involve minima at around 600 nm, corresponding to ground state bleaching, accompanied by maxima at 485, 680, and 870 nm, corresponding to $S_1 - S_n$ transitions (Figure 20). Singlet excited states, with a lifetime of

1250 ± 50 ps decay through intersystem crossing to the corresponding triplet states. The latter features minima at 600 nm as well as maxima at 490, 645, and 865 nm (T_1 – T_n transitions).

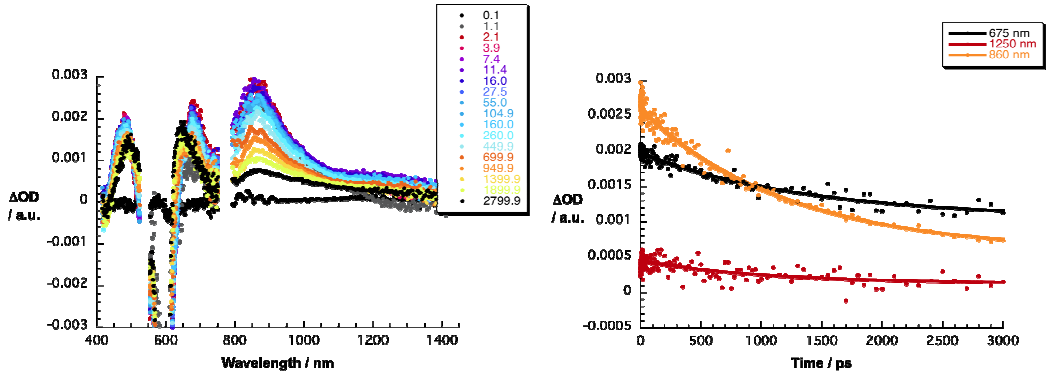

Figure 20. (a) Differential absorption spectra (visible and near-infrared) obtained upon femtosecond pump probe experiments (540 nm) of **6c** (2.5 x 10-5 M) in toluene with several time delays between 0 and 2800 ps at room temperature- see figure legend for details; (b) Time absorption profiles of the spectra at 675 (black spectrum), 860 (orange spectrum) and 1250 nm (red spectrum) monitoring the excited state dynamics. y (iii), Diagrama de Jablonsky para la SubPc.

SubPcs singlet excited state characteristics evolve despite the presence of C_{70} or C_{60} (Figures 21 and 22, respectively).

Nevertheless, in the presence of C_{70} a number of changes are discernable, especially in the near-infrared region (Figure 21). Firstly, instead of the 1250 ± 50 ps intersystem crossing dynamics, a 1240 nm maximum evolves with a lifetime of 5.5 ± 0.5 ps. This and the feature at 460 nm resemble those seen in reference experiments with just C_{70} and correlate with its singlet excited state. Secondly, no evidence that would corroborate the involvement of the one electron reduced form of C_{70} is gathered. Namely, the absence of the transient at 1370 nm (registered in spectroelectrochemical or pulse radiolytical experiments) rules the presence of C_{70} radical anion out. As a matter of fact, we conclude that energy transfer rather than electron transfer dominates the electronic interactions between SubPcs and C_{70} in the excited state. In line with this hypothesis is the observation that the triplet excited state of C_{70}, with its characteristic 945 nm fingerprint, evolves on the longer time scale (up to 3000 ps). Moreover, this 945 nm growth, corresponding to C_{70} triplet excited state, and the 1240 nm decay,

corresponding to C_{70} singlet excited state, mirror each other and feature the same lifetime of 1000 ± 50 ps.

Finally, the SubPc triplet-triplet maxima and the triplet-triplet minimum are noted at 490 and 645 and 600 nm, respectively. Their formation with 1250 ± 50 ps matches that seen in the absence of C_{70} and, as such, is rationalized on the basis of free SubPcs in solution, whose singlet excited state intersystem crosses to the corresponding triplet excited state. Variation of the C_{70} concentration, that is, either an increase or decrease, is key in terms of yielding different C_{70} triplet to SubPc triplet ratios, without, however, affecting the underlying energy transfer dynamics of 5.5 ± 0.5 ps.

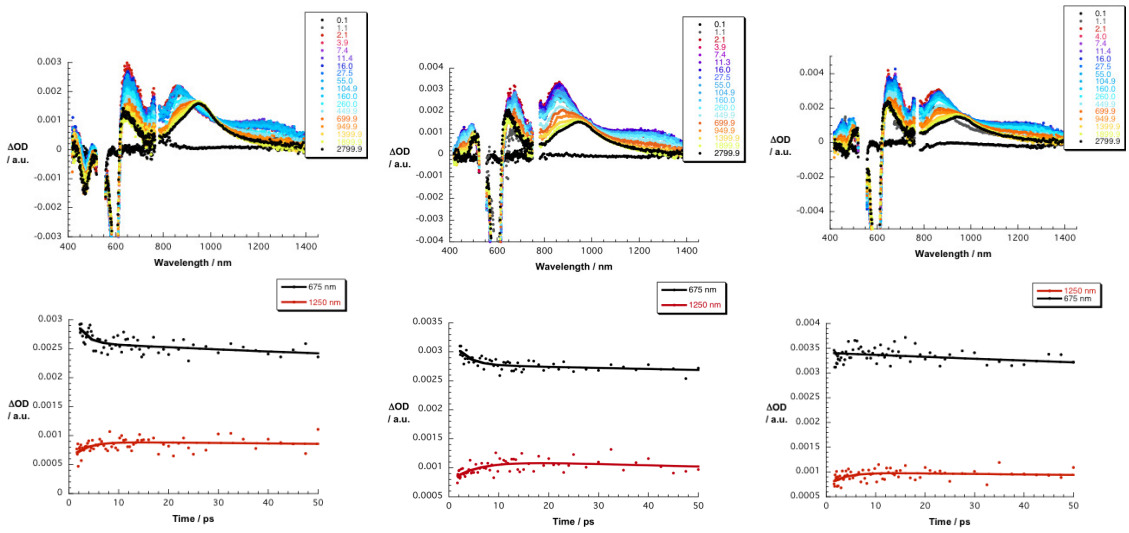

Figure 21 Upper part: differential absorption spectra (visible and near-infrared) obtained upon femtosecond pump probe experiments (540 nm) of (from left to right) **6b**, **6c**, and **6d** (2.5 x 10^{-5} M) and C_{70} (7.5 x 10^{-5} M) in toluene with several time delays between 0.1 and 2800 ps at room temperature- see figure legend for details. Lower part: time absorption profiles of the spectra at 675 (black spectrum) and 1250 nm (red spectrum) monitoring the excited state dynamics.

In the case of C_{60} the situation was less clear, due to the difficulty to distinguish the fingerprint of C_{60} singlet excited state. Its typical feature at 960 nm is partially masked by SubPc transitions, which dominate the differential absorption changes throughout the recorded region in the visible and the near-infrared.

Nevertheless, a closer analysis allowed identification of the 960 nm feature in the form of a shoulder. The presence of C_{60} like that of C_{70} evokes a rapid decay, namely 4.5 ± 0.5 ps, of the SubPc singlet excited state. As in the previous case (see discussion for C_{70}), an energy transfer scenario is operative upon SubPc / C_{60} complex formation.

The one electron reduced form of C_{60}, on the other hand, is not seen at 1080 nm even on longer time scales of up to 3000 ps. Instead, the formation of the C_{60} triplet excited state at 750 nm is noted as a consequence of an efficient intersystem crossing.

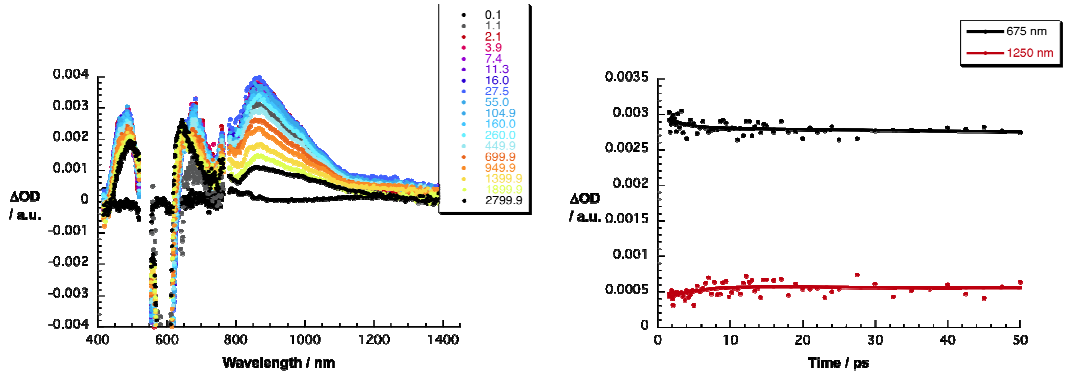

Figure 21. Left: Differential absorption spectra (visible and near-infrared) obtained upon femtosecond pump probe experiments (540 nm) of **6c** (2.5 x 10-5 M) and C_{60} in toluene with several time delays between 0.1 and 2800 ps at room temperature- see figure legend for details. Right: Time absorption profiles of the spectra at 675 (black spectrum) and 1250 nm (red spectrum) monitoring the excited state dynamics.

3. Metal-directed self-assembly of Subphthalocyanine based capsules

3.1. Synthesis of building blocks and self-assembly

3.1.1. Synthesis of building-blocks

The synthesis of the precursor phthalonitrile (Figure 22) was achieved following previously reported methods.[28] Compound **8** was obtained in two steps from 4-nitrophthalonitrile. Firstly, reduction of the nitro group was achieved with iron in acidic medium. 4-aminophthalonitrile was then treated with sodium nitrite to obtain the diazonium salt that was converted to the iodo-derivative by means of a nucleophilic aromatic substitution.

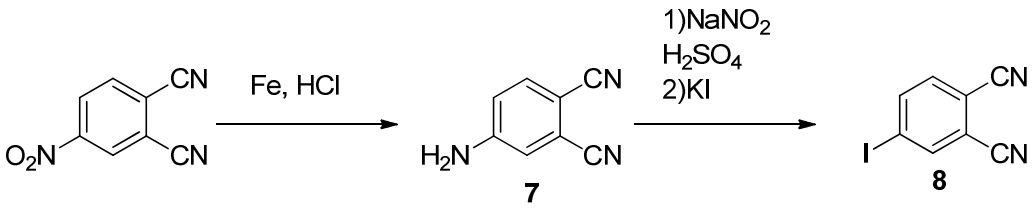

Figure 22. Synthesis of 4-iodophthalonitrile

The synthesis of SubPc **11** (Figure 23) was reported in 2008 with an overall yield of 35% starting from 4-iodophthalonitrile.[12a] However, it was necessary to develop an optimized version of this synthesis which may be scaled up to gram quantities of starting materials.[29] The first step of the synthetic route consists in the condensation of 4-iodophthalonitrile in the presence of boron trichloride in refluxing *p*-xylene. The crude product from this condensation reaction was directly treated with 2.2 equivalents of 4-*t*-butylphenol in a 1:1 mixture of THF and toluene in the presence of a substoichiometric amount of DBU at reflux for 18-24 h in order to complete, in a one pot process, the substitution of the axial chlorine atom. Subphthalocyanine **10** was obtained in an overall yield of 60%. C_3 and C_1 regioisomers were isolated by column chromatography on silica gel. Finally, the C_3 isomer was subjected to a triple Sonogashira cross coupling reaction with 3-ethynilpyridine in the presence of $PdCl_2(PPh_3)_2$ and copper

[28] (a) H. Lam, S. M. Marcuccio, P. I. Svirskaya, s. Greenberg, A. B. P. Lever, C. C. Leznoff, R. L. Cerby, *Can. J. Chem.*, **1989**, *67*, 1087-1097;(b) J. G. Young, W. Onyebuagu, *J. Org. Chem.,* **1990**, *55*, 2155-2159.

[29] (a) I. Sánchez-Molina, C. G. Claessens, B. Grimm, D. M. Guldi, T. Torres, *Chem. Sci,* **2013**, *4*, 1338-1344; (b) I. Sánchez-Molina, B. Grimm, C. G. Claessens, D. M. Guldi, T. Torres (submitted).

iodide, affording the desired SubPc **11** in 80% yield. Global yield of the synthetic route is 48%.

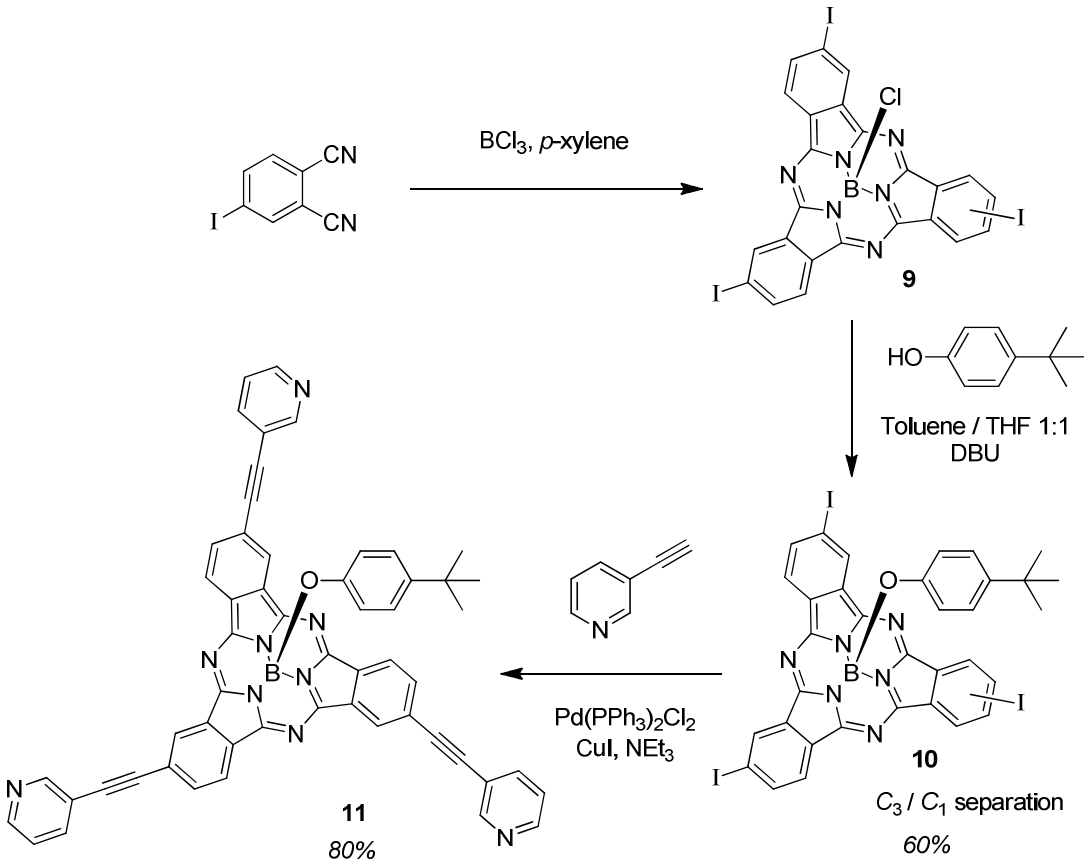

Figure 23. Synthesis of SubPc **11**

On the other hand, the metal complexes (Figure 24) bearing 1,1'-bisdiphenylphosphino propane (dppp), 1,1'-bisdiphenylphosphino ferrocene (dppf) or 1,1'-bisdiphenyl naphthalene (*S*-BINAP) were prepared as described in the literature.[30] Their synthesis was achieved preparing first the dichloro-derivative (from K_2MCl_4 in the case of dppp or *s*-BINAP and from $M(COD)Cl_2$ in the case of dppf), and then exchanging the chloride anions by treatment with silver triflate.

[30] (a) D. H. Cao; S. Saito; A. M. Arif, P. J. Stang, *J. Am. Chem. Soc*, **1995**, *117*, 6273-6283; (b) B. Olenyuc, J. Fan, A. M. Arif, P. J. Stang, *Organometallics*, **1996**, *15*, 904-908.

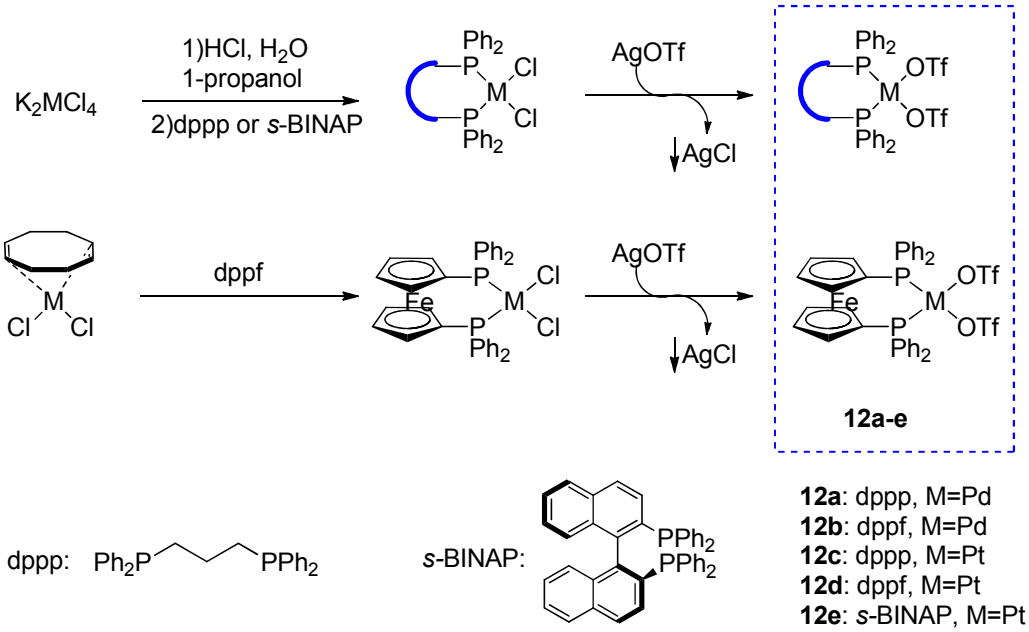

Figure 24. Preparation of metal complexes

3.1.2. Self-assembly

Stoichiometric mixtures of building-blocks in dichloromethane solution afforded the desired capsule compounds **13a-e** (Figure 25). The solutions were stirred first at 40ºC and then at room temperature in order to get the most thermodynamically stable product. Yields of self-assembly are shown in table **2**.

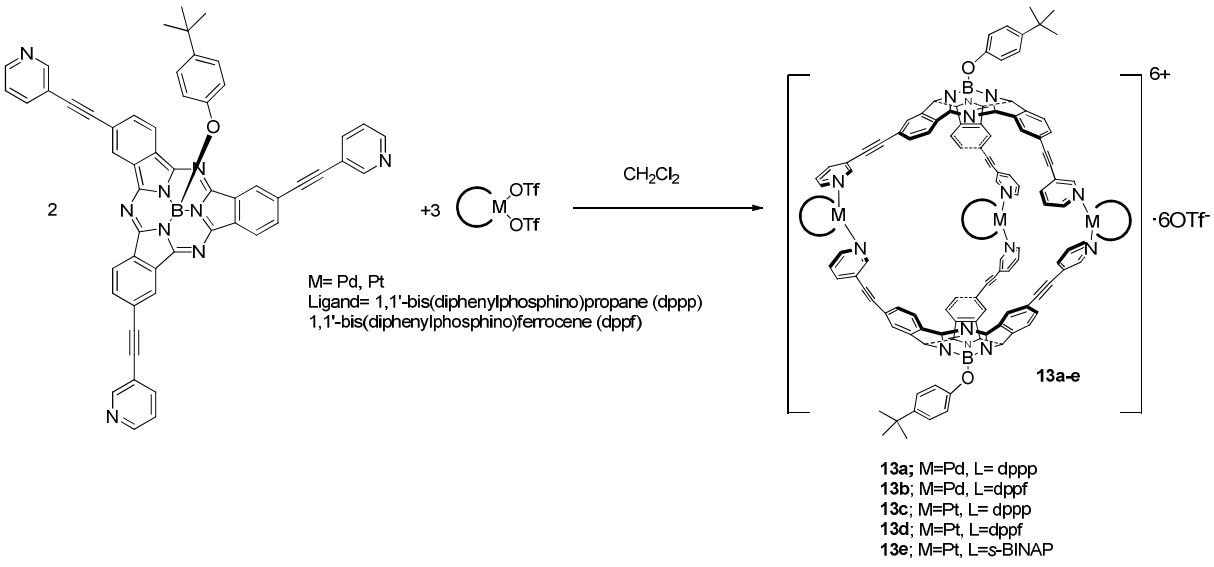

Figure 25. Self-assembly of capsules

Table 2. Yields of self-assembly

Ligand/Metal	Pd	Pt
dppp	>90% **13a**	>90% **13c**
dppf	17% **13b**	25% **13d**

Self-assembled capsules with dppp ligand were successfully obtained in quantitative yields. The low yields detected for **13b** and **13d** may be a consequence of the rigidity of both the SubPc and the ferrocene ligand, which, when combined, do not easily fulfil the required square-planar geometry of the metal. Higher yields for Pt compounds arise from the higher strength of the metal-nitrogen bond.

In addition, capsule **13f**, self-assembled from SubPc **11** and Pd ethylendiamine complex[12a] was prepared with the aim of establishing the influence of the different elements on the stability of the system. In this case, stoichiometric amounts of building-blocks were strirred in MeCN/MeOh 1:1 mixture for 24 h and, after concentration of the solution, aqueous KPF_6 solution was added to exchange counteranions.

3.1.3. Synthesis of flexible SubPcs

Some attempts to synthesize other precursor building blocks containing flexible linkages between the pyridine and the SubPc core were carried out (Figure 26). The objective was to stabilize the capsules bearing 1,1'-bisdiphenylphosphineferrocene ligand, because at this point of the process we thought it was interesting to introduce additional donor moieties at the periphery of the system.

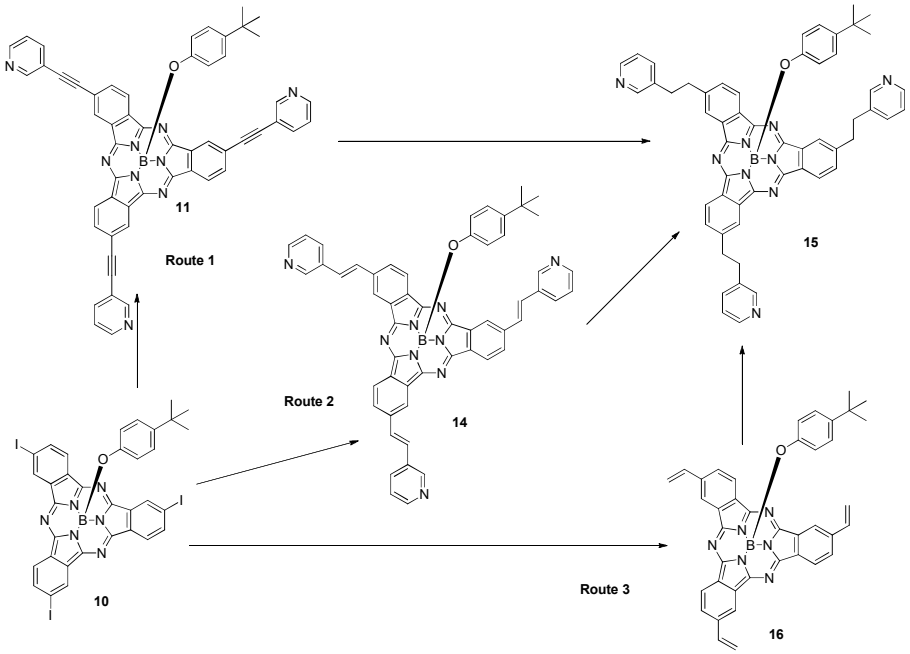

Figure 26. Synthetic routes designed for the obtention of flexible SubPc **15**

As a first synthetic approach to a flexible SubPc, hydrogenation of the triple bond was attempted (Figure 26). Although this reaction had been previously described[31] with Pd/C as catalyst and a mixture of dicholomethane and acetonitrile as solvent, we couldn't succeed in obtaining of the desired product. However, SubPc **15** was obtained when treated with H_2 in the presence of Pearlman's catalyst. The yield was, unfortunately, very low (<2%). Thus, the compound could not be fully characterized. Nevertheless, its synthesis was confirmed by UV-visible spectroscopy and mass spectrometry (Figure 27).

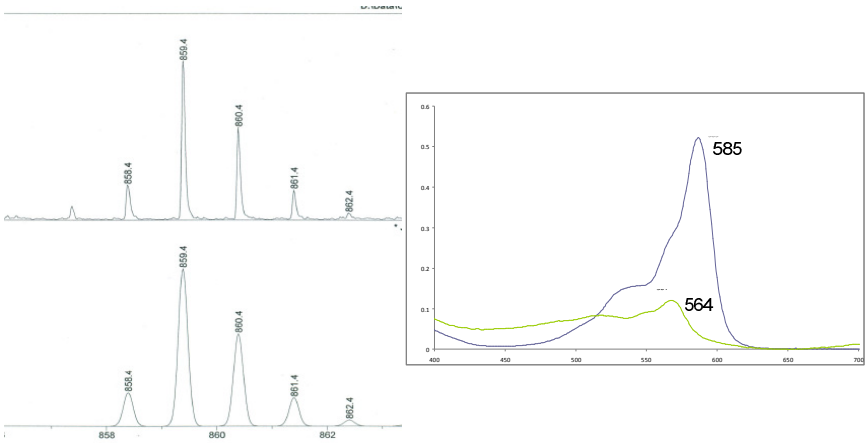

Figure 27. Exact mass and UV-visible spectra of SubPc **15** (green line) compared with its precursor, SubPc **11** (blue line).

[31] L. Lapok, C. G. Claessens, D. Whörle, T. Torres, *Tetrahedron Lett.*, **2009**, *50,* 2041-2044.

A second route (Figure 26) was then designed to obtain SubPc **15**. In this case, 4-vinylpyridine was attached to the SubPc core by means of a Heck reaction[32] that proceeded with high yield (70%). Position of pyridine nitrogen was altered from *meta* to *para* with respect to the linker. The reason for this change was the commercial unavailability of 3-vinylpyridine.

Tris(4-vinylpyridyl)SubPc **14** was successfully obtained, but hydrogenation failed again. SubPc **14** was employed to self-assemble a capsule with the metallic complex **12c**, but this product was obtained in low yield due to its lack of stability (caused again by the excess of rigidity of the building-blocks). ^{1}H-NMR of SubPc **14** and the corresponding capsule is shown in Figure 28, where shift of protons of both the pyridine and the double bond can be observed as a consequence of coordination of pyridines to Pt.

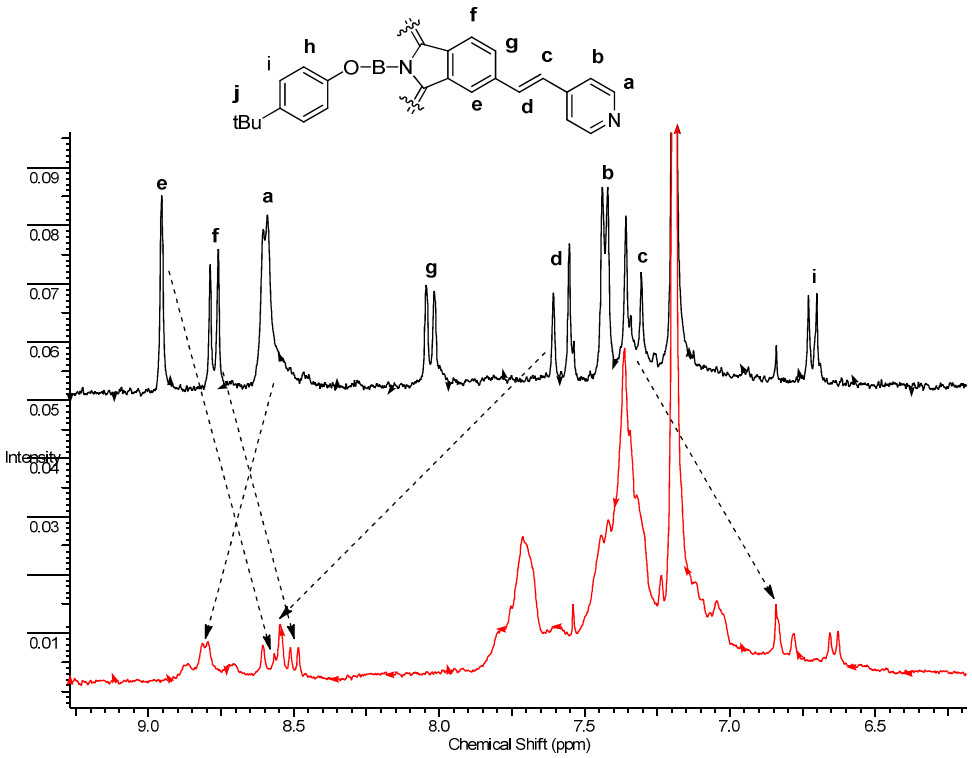

Figure 28. ^{1}H-NMR spectra of SubPc **14** (top) and capsule **13g** (bottom). Arrows show the shift of each signal upon coordination of the pyridine to Pt.

Finally, synthesis of SubPc **15** was addressed via a trivinyl precursor. Stille cross-coupling reaction on triiodoSubPc[33] afforded compound **16** in 70% yield. This product was then subjected to hydroboration of double bonds and subsequent Suzuki cross

[32] C. Allain, F. Schmidt, R. Lartia, G. Bordeau, C. Fiorini-Debuisschert, F. Charra, P. Tauc, M-P. Teulade-Fichou, *ChemBioChem* **2007**, *8*, 424.
[33] D. González-Rodríguez, T. Torres, *Eur. J. Org. Chem.*, **2009**, 1871-1879.

coupling reaction. Once more, conditions in which the desired product would be obtained were not found.

After all, synthesis of **15** was abandoned due to all these failed attempts together with the results of electrochemistry and photophysics (see discussion below).

3.1.4. Inversion of chiral self-discrimination in self-assembly

All the capsules described so far possess a plane of symmetry due to chiral self-discrimination during the self-assembling process. This equilibrium was observed in ^{1}H-NMR the first time our group prepared a SubPc-based capsule.[11]

Turning upside-down the equilibrium between the enantiomers of the SubPc would give rise to capsules containing each enantiomer of the SubPc, *M* or *P*. This might be a step forward in the separation of the enantiomers of SubPcs. So far, *M* and *P* enantiomers of SubPcs have been discriminated by chiral HPLC.[34] Thus, there is a strong need to develop a chiral discrimination approach that could potentially be applied to higher quantities of starting material.

To this end, a chiral ligand (*s*-BINAP) was chosen to arrange the coordination positions of the metal in a way that prevents the formation of the *meso* cage (Figure 29).

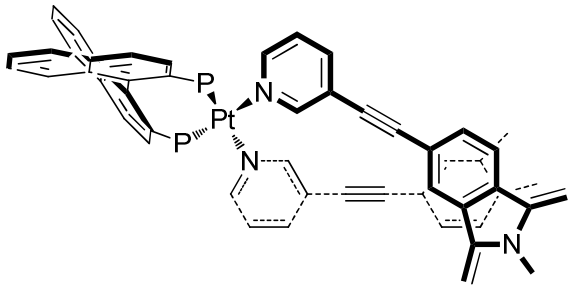

Figure 29. Schematic representation of Pt(*S*-BINAP) complex coordinating two SubPcs (only one pyridyl substituent of each one is shown). The distribution of the coordination positions prevents the formation of the capsule with a plane of symmetry.

In principle, two situations might be envisaged in self-assembly with this metallic complex:

[34] (a) C. G. Claessens, T. Torres, *Tetrahedron Lett.*, **2000**, *41*, 6361-6365 ; (b) N. Kobayashi, T. Nonomura, *Tetrahedron Lett.,* **2002**, *43*, 4253-4255.

- Stabilization of [*M,M*] and [*P,P*] capsules. In this case, we would obtain a mixture of the two capsules, each one containing only one kind of enantiomer. Thus, separation of *M* and *P* isomers could not be directly achieved, and further work addressed to selective crystallization of one of the capsules should be done.

- Stabilization of [*M,M*] or [*P,P*] capsule. That involves selectivity towards one of the enantiomers. The other one might remain in solution or might coordinate to Pt, but to afford specie(s) different from homodimeric capsules.

Self-assembly was carried out as described above, and ^{1}H and ^{31}P-NMR spectra of the product were recorded. ^{31}P-NMR spectrum showed two singlets at ~ -3 ppm. ^{1}H-NMR spectrum analysis was difficult due to the abundance and overlapping of signals in the aromatic region. These results, at first, made us think that equilibrium had not been reached.

Hence, self-assembly process was followed by ^{31}P-NMR. Pt(*S*-BINAP)OTf$_2$ was added portionwise to a solution of SubPc **11** until the right stoichiometry was reached. The mixture was allowed to equilibrate after each addition. Results are shown in Figure 30.

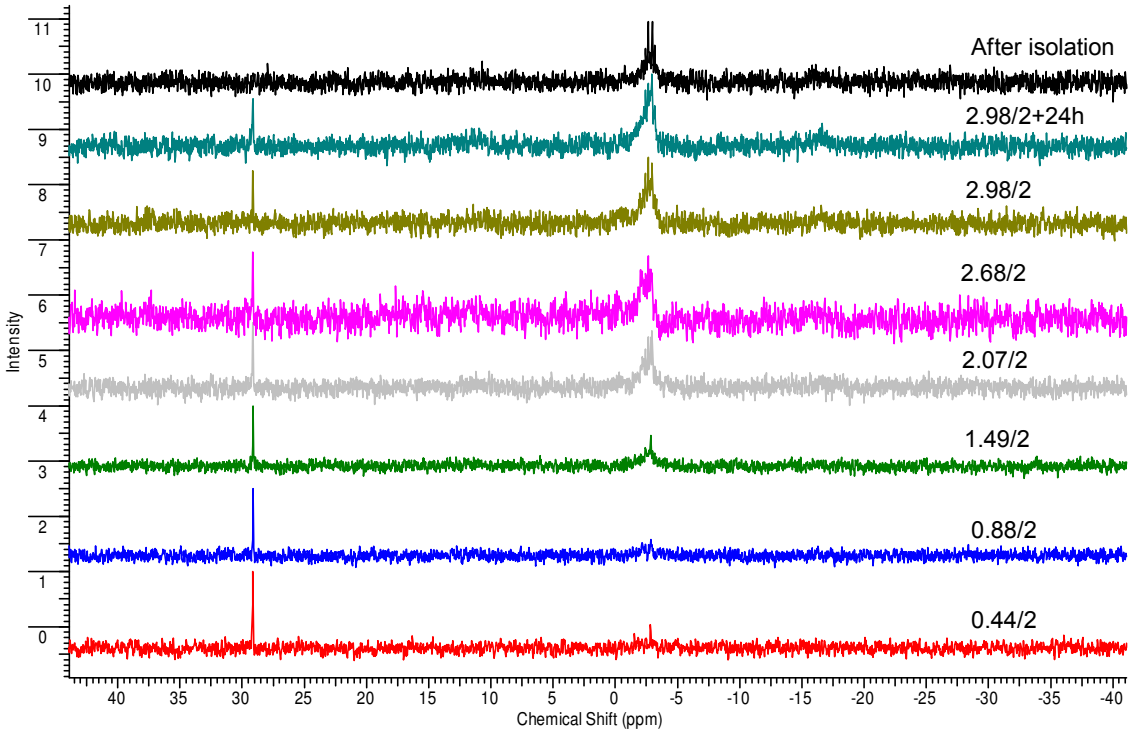

Figure 30. ^{31}P-NMR spectra of self assembly of **11** with increasing amounts of **12e**.

Coordination of SubPc **11** to Pt is observed in the growth of the signals around -3 ppm. When the amount of Pt complex **12e** approaches the accurate ratio, two peaks become

dominant in that region. Finally, the solution was stirred at room temperature overnight. After that period, almost total disappearance of the singlet corresponding to **12e** was observed. The solution was then concentrated, and upon addition of diethyl ether the product crashed out as a purple powder. Size exclusion chromatography of this solid was carried out, and two purple fractions were isolated. The major one was the heaviest compound and its ^{31}P-NMR spectra presented the two singlets previously observed in the reaction mixture. The second fraction was the starting SubPc (Figure 31).

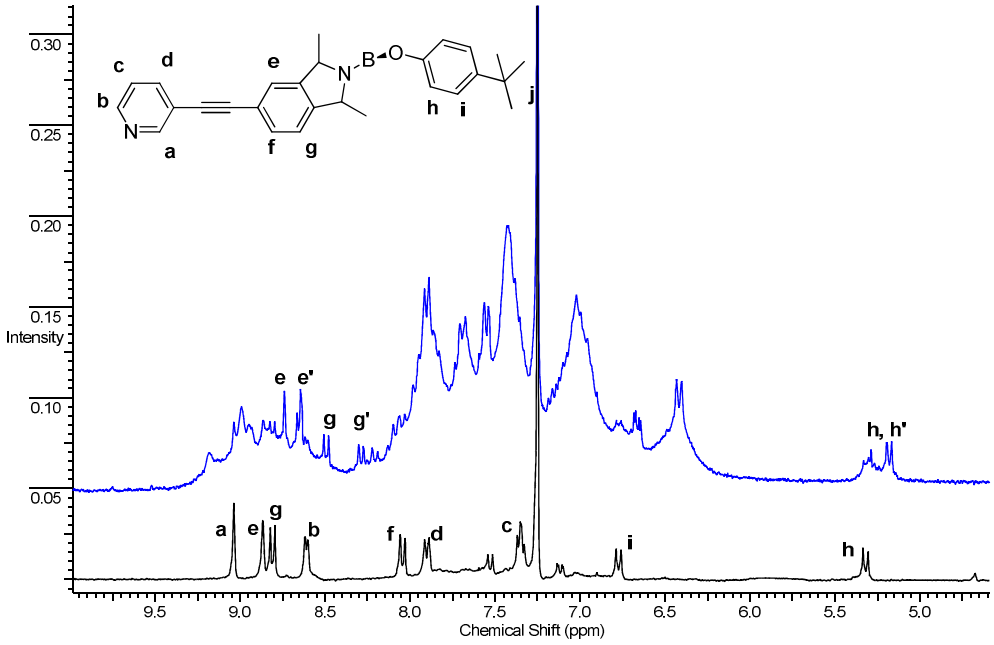

Figure 31. ^{1}H-NMR spectra of the products isolated in size-exclusion chromatography (blue line corresponds to fraction 1, capsule **13e**; and black line corresponds to fraction 2, SubPc **11**).

^{31}P-NMR spectrum of the first fraction might be explained by the presence of those two capsules. Besides, a closer analysis of ^{1}H-NMR spectrum allowed identification of some of the signals of the SubPc, and it could be seen that each signal is duplicated. This fact is also consistent with the hypothesis of formation of both [*M,M*] and [*P,P*] capsules.

A representation of [*M,M*] and [*P,P*] capsules is shown in Figure 32. In each of these capsules, there are elements of symmetry relating every atom in the upper SubPc with the lower one. For example, in Figure 32, some protons that are related through a improper rotation axis are indicated. Thus, each capsule has to give rise to only one set of signals in NMR. Moreover, as the relative disposition of SubPcs in each capsule is different, it should be possible to distinguish them in NMR spectroscopy.

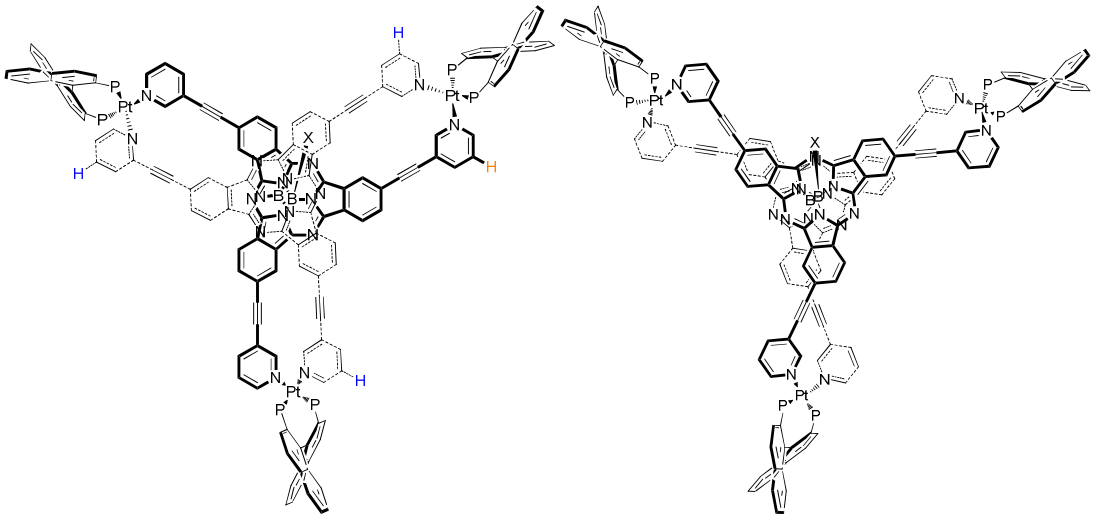

Figure 32. Representation of [*M,M*] (left) and [*P,P*] (right) capsules. In [*M,M*] isomer, protons marked in blue are related to the one marked in orange through symmetry elements.

Finally, and in order to completely discard the selectivity towards one of the enantiomers, capsule **13e** was decomposed by column chromatography in silica gel. SubPc **11** was thus recovered, and its optical rotation was measured, as well as the one of the starting material (racemic mixture). In both cases polarized light passed through the sample without appreciable deviation. From this result we conclude the SubPc recovered from the capsule contains both enantiomers. The conclusion is, thus, that stabilization of [*M,M*] and [*P,P*] capsules was achieved.

Attempts of crystallization of any of these capsules with slow vapour diffusion failed.

3.2. Characterization

All compounds were characterized by ^{1}H, ^{31}P and ^{19}F-NMR, IR, UV-visible spectroscopies and ESI-mass spectrometry.

The most remarkable feature of ^{1}H-NMR spectra is the downfield shift of the proton in *ortho* to the N of the pyridine due to the coordination of pyridine to the metal centre. This signal appears at 9.01 ppm in the free SubPc and shifts up to 9.65 ppm in the case of capsules bearing dppp ligand. This downfield shift is lower in the case of dppf-capsules. ^{1}H-NMR spectra also showed more defined signals for platinum capsules, revealing the less dynamic nature of the equilibria that occur in solution. In the case of **13b** and **13d**, bearing ferrocenyl secondary ligands, the loss of planar symmetry of the

ferrocene moiety in the capsules give rise to four signals (Figure 33). These results are consistent with the formation of the capsules.

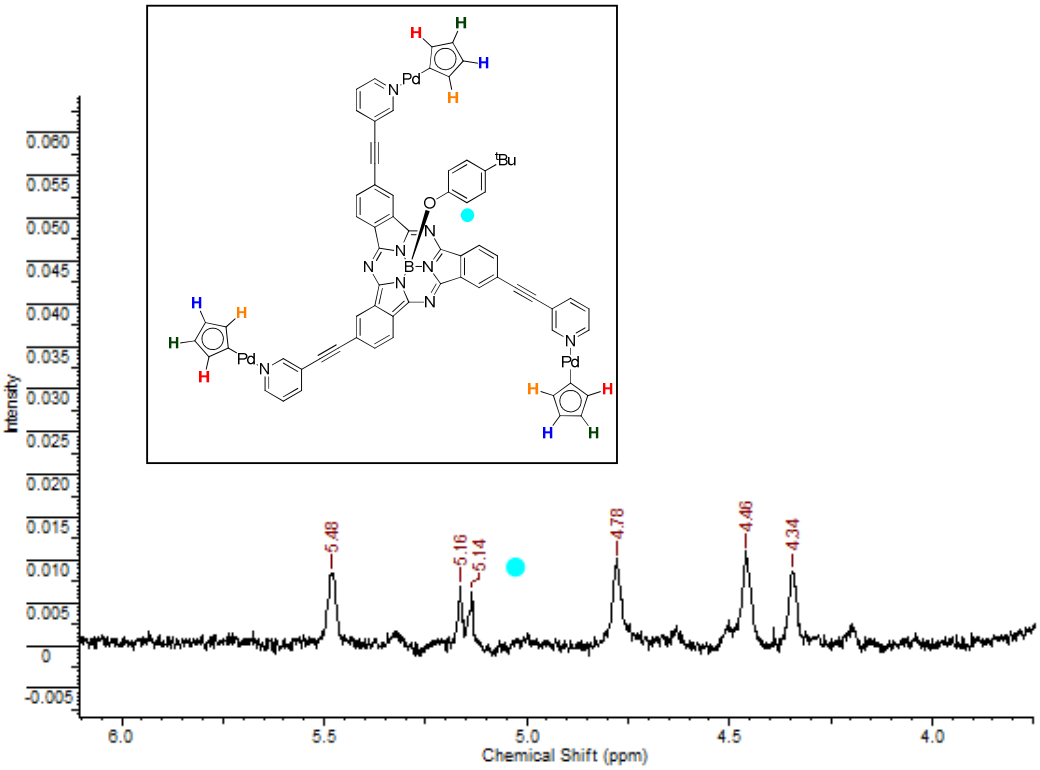

Figure 33. Signals corresponding to ferrocene moiety in the ^{1}H-NMR spectrum of **13b**.

^{31}P-NMR showed one singlet in all cases, accompanied by two ^{195}Pt satellites in the case of **13c** and **13d**. The chemical shift of these singlets was different from the ones in the original metal complexes, thus showing that the chemical environment of P has changed after the self-assembly process.

Table 3. ^{31}P-NMR chemical shifts for precursor metal complexes and capsules.

	δ ^{31}P (ppm)	J_{Pt-P} (Hz)
12a	15.01	--
12b	46.17	--
12c	-10.83	3818
12d	15.81	1074
13a	6.23	--
13b	27.89	--
13c	-15.28	2988
13d	16.11	2988

ESI-MS spectrometry experiments also confirmed the formation of the assemblies. Peaks corresponding to $[M\text{-}OTf]^+$, $[M\text{-}2OTf]^{2+}$, $[M\text{-}3OTf]^{3+}$ were found in the spectra of **13a** and **13c**. Unfortunately, spectra of **13b** and **13d** could not be obtained; most probably as a consequence of the lack of stability of these compounds during the ionization process.

3.3. Study of stability

The rapid development of mass spectrometry during the last decade has allowed its expansion into many scientific disciplines. Thus, for example, the advances made in Electrospray Ionization technique (ESI) permitted its extensive use in the Supramolecular Chemistry area, where it has been proved to be a useful tool for the study of the stability of host-guest complexes as well as to evaluate the strength of non-covalent interactions.[35] Electrospray technique allows to establish a relationship between the areas of the peaks and the stability of the compound in MS experiments, thus making possible the comparison of compounds of a similar nature. However, this comparison must be taken carefully, since the response factors might not be the same for all the compounds analysed. This problem can be overcome thanks to MS/MS experiments, where all interactions due to the presence of the solvent disappear, and hence, complexes' behaviour may vary from the one observed in simple MS spectrometry experiments.

Many supramolecular systems have been studied in mass spectrometry, as well as their relative stabilities.[36]

The strength of the coordination bonds depends not only on the atoms involved, but also on the nature of the additional ligands (phosphine or amine in our case) present in

---

[35] (a) D. V. Dearden, *Host-guest molecular recognition without solvents* (Ed.: L. Echegoyen, A. E. Kaiser), Kluwer, Dordrecht, 1996, pp 229-247; C. A. Schalley, *Int. J. Mass Spectrom.,* **2000**, *194* 11-39; (b) B. Baytekin, H. T. Baytekin, C. A. Schalley. *Org. Biomol. Chem,* **2006**, *4*, 2825-2841.

[36] (a) R. Zadmard, A. Kraft, T. Schrader, U. Linne. *Chem. Eur. J*, **2004**, *10*, 4233-4239; (b) C. A. Schalley, P. Weis., *Int. J. Mass Spectrom.*, **2002**, *221*, 9-19; (c) C. A. Schalley, P. Ghosh, M. Engeser. *Int. J. Mass Spectrom.*, **2004**, *232*, 249-258; (d) R. W. Troff, R. Hovorka, T. Weilandt, A. Lützen, M. Cetina, M. Nieger, D. Lentz, K. Rissanen, C. A. Schalley. *Dalton Trans.*, **2012**, *41*, 8410-8420; (e) C. L. Mazzitelli, J. Wang, S. I. Smith, J. S. Brodbelt. *J. Am. Soc. Mass Spectrom.,* **2007**, *18*, 1760–1773;(f) M. A. Kaczorowska, A. C. G. Hotze, M. J. Hannon, H. J. Cooper. *J. Am. Soc. Mass Spectrom.,* **2010**, *21*, 300-309

the coordination sphere. In order to study how these parameters affect the stability of SubPc-based capsules, three of them were chosen for MS/MS experiments. Comparison of their distinct elements allows the establishment of stability trends in terms of metals (Pd *vs* Pt) and ligands (amine *vs* phosphine). Interestingly, the importance of the response factor in mass spectrometry was highlighted in the case of +3 ions of each capsule.

The homodimeric capsules employed in this study are shown in Figure 34.

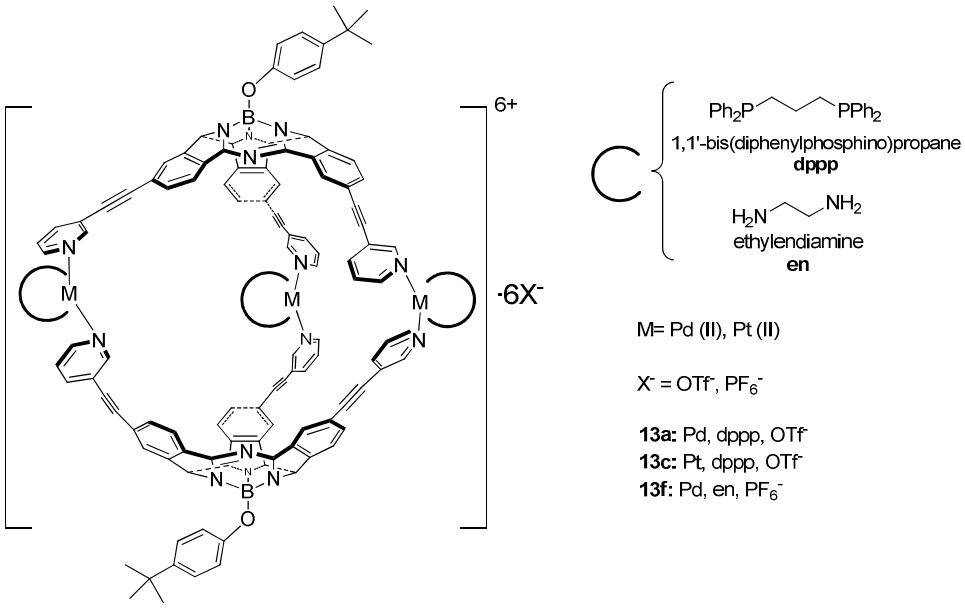

Figure 34. SubPc-based Capsules

For each capsule, a series of ESI-MS/MS spectra were registered where the collision energy was progressively increased. Then, the area of the peak of the corresponding ion was measured through integration of the signal (entire isotopic distribution was taken into account). Finally, these areas were plotted versus the applied collision energy (see Figure 35), and fitted according to a fourth order polynomial curve. Generally, this kind of plots require taking into account the internal energy acquired by the ions through collisions with the ionization gas, and not only the applied energy. However, in the case of our experiments, such value was negligible. From these graphs values for CE_{50} (value of the energy of collision necessary to dissociate 50% of the complex) were obtained in each case, and a close analysis of the data gave rise to the results discussed below.

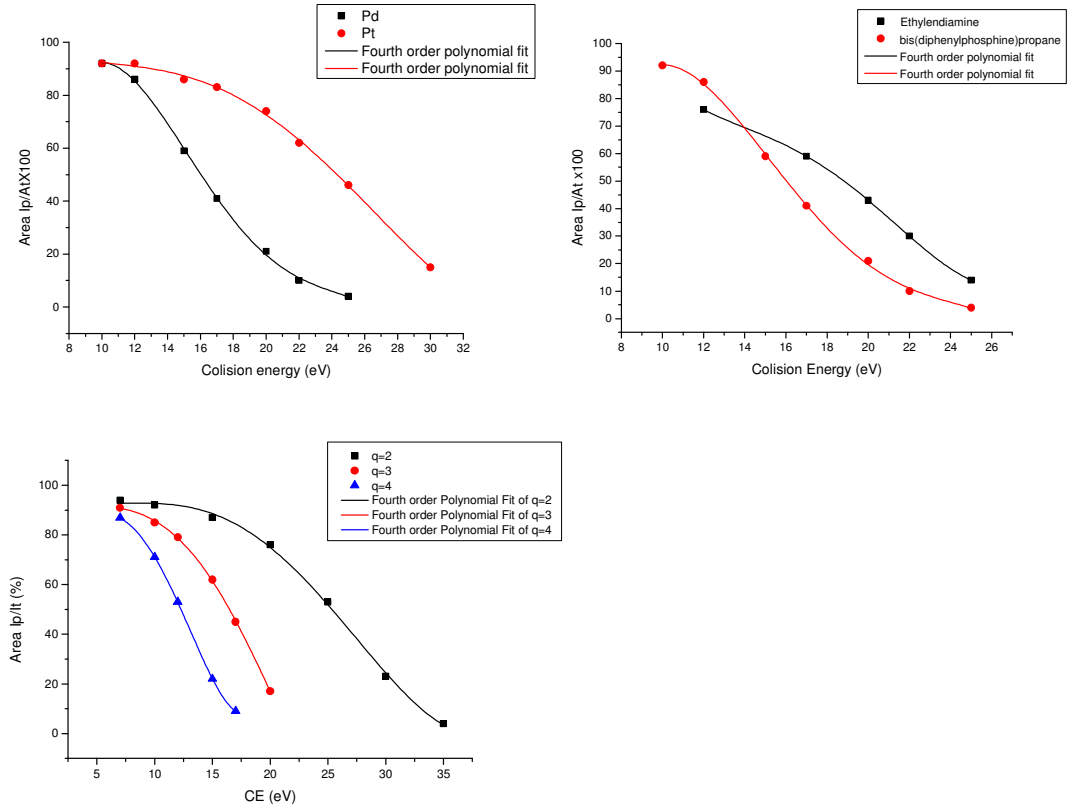

Figure 35. Stability diagrams comparing (from the top to the bottom) (i) Charge state +2 of cages **13a** and **13c**; (ii) Charge state +2 of cages **13a** and **13f**; (iii) Charge states +2, +3 and +4 of cage **13c**.

Analysis of ESI-MS and MS/MS spectra

Capsules **13a, 13c** and **13f** show similar fragmentations in mass spectra. Figure 36 shows the mass spectra of compound **13c**, where signals corresponding to loss of 2, 3 and 4 counteranions can be found at 2056.90, 1321.62 and 854.17.

MS/MS spectra of ion 2056.90 shows $[Pt(dppp)OTf]^+$ (755.06 Dalton) as the main product of fragmentation. Other small peaks appear at high collision energies. Namely, 1602.37 corresponds to the loss $Pt(dppp)(OTf)_2$ plus two additional counteranions. 3357.70 and 2507.38 correspond to the formation of a dimer-like structure of the cage with some missing metal centers (Figure 36b).

On the other hand, MS/MS spectra of tri- and tetracharged ions show only some fragments of the cage that involve the loss of $Pt(dppp)(OTf)_2$ moieties and counteranions (Figure 36c).

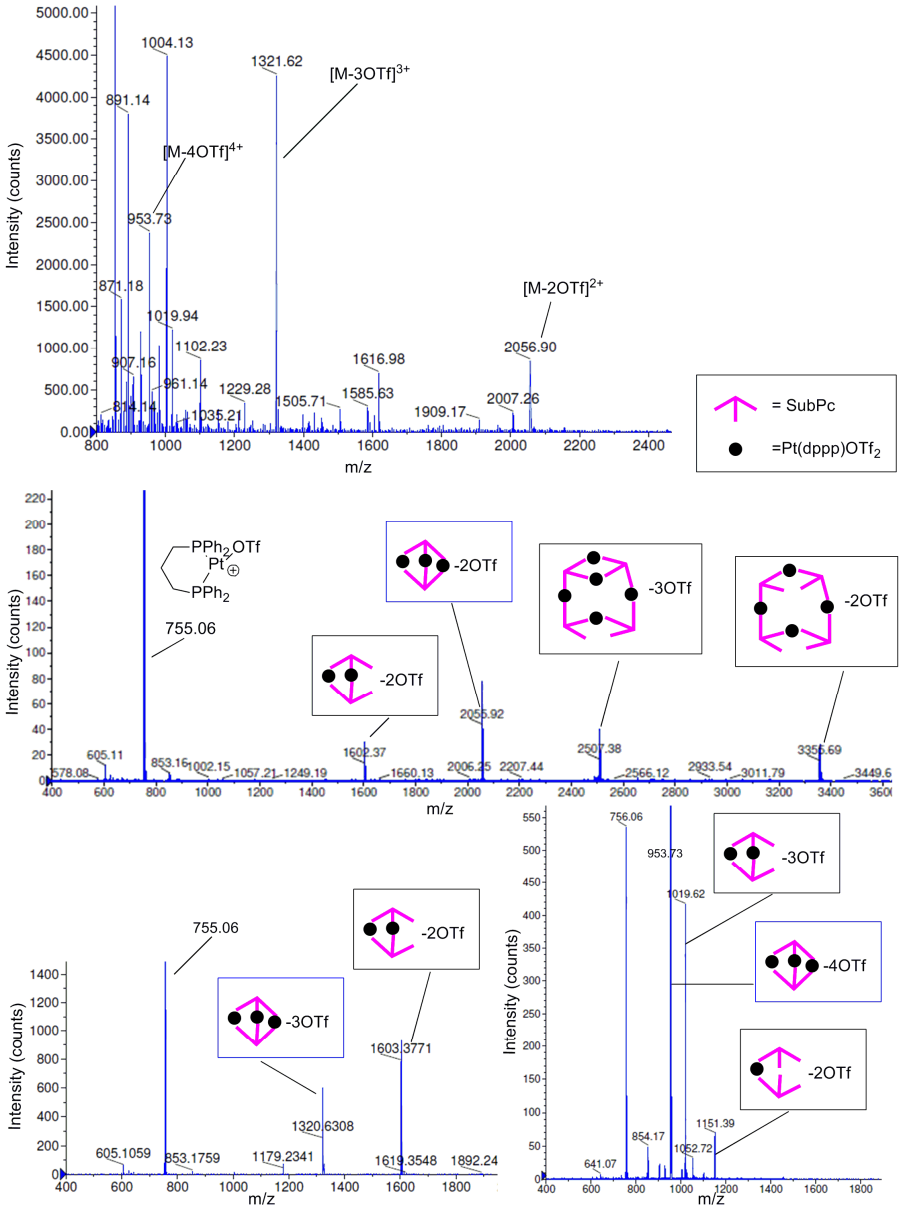

Figure 36. MS and MS/MS spectra of compound **2**, with assignation of the signals. In MS/MS spectra; precursor ions are indicated into a blue rectangle.

Trends in stability

- Influence of the metal: In order to establish which metal provides more stability to the capsules, CE_{50} for equally charged ions of **13a** and **13c** were compared (see Figure 35 and Table 4). Clearly, this value is higher for capsule **13c**, thus reflecting the stronger nature of metal-nitrogen bond in the case of Pt, as previously shown in many mass spectrometry studies of self-assembled compounds, as well as in infrared studies

of coordination compounds.[37] The effect of this parameter has been previously observed in the difficulty of self-healing in related capsule compounds.[38]

Table 4. Values of CE_{50} (collision energy required to fragment 50% of the ion) obtained from stability diagrams

Ion	**CE_{50} (eV)**
Pd/en +2	19
Pd/en +3	5
Pd/dppp +2	16
Pd/dppp +3	7
Pt/dppp +2	25
Pt/dppp +3	16
Pt/dppp +4	12

- Influence of the ligand: The stability of these capsule compounds is also dependent on the nature of the ligands the metal bears. We have previously observed huge differences in the intensity of signals (peaks corresponding to the loss of counterions) of compounds **13a** and **13f** when registering the ESI mass spectra. Although intensity of the peaks in mass spectra depends on many issues like instrument parameters, desolvation, ionization potentials, pH of solvent, counterions, etc, the differences mentioned above may be attributed mainly to the intrinsic characteristics of cage compounds **13a** and **13f** (i.e. ligand, counterion) **,** since all the mass spectra have been recorded in the same conditions.

Considering the EC_{50} of, for example, the charge state +2 of the above mentioned capsules, it can be observed that the capsule bearing the amine ligand is more stable than its counterpart. This fact has been interpreted as a manifestation of *trans* effect,[39] which is higher in the case of phosphorous than in nitrogen ligands, and hence, the Pd-$N_{pyridine}$ bond is more weakened in compound **13a**.

The fact that capsules **13a** and **13f** bear different counteranions must not be missed. Thus, the different stability of their ions cannot be exclusively attributed to the *trans*

[37] (a) C. A. Schalley, T. Müller, P. Linnartz, M. Witt, M. Schäfer, A. Lützen, *Chem. Eur. J.*, **2002**, *8*, 3538-3551;(b) S. J. Park, D. M. Shin, S. Sakamoto, K. Yamaguchi, Y. K. Chung, M. S. Lah, J.-I. Hong, *Chem. Eur. J.* **2005**, *11*, 235 – 241; (c) W. Klotzbücher, G. A. Ozin, *J. Am. Chem. Soc,* **1975**, 2672-2675; (d) R. J. H. Clark, C. H. Williams, *Inorg. Chem.*, **1965**, *3,* 350-357.
[38] P. S. Mukherjee, N. Das, P. J. Stang., *J. Org. Chem.*, **2004**, *69*, 3526-3529.
[39] R. H. Crabtree, *The Organometallic Chemistry of the transition metals* (4th Ed, 2005) New Jersey, Wiley Interscience, pp 6-8.

effect of the ligand. Nevertheless, as it has a direct influence on the strength of the coordination bonds, it might be the most determinant parameter.

- Influence of Charge State: Finally, different charge states of one of the capsules were compared in order to determine the stability of the ions according to this parameter. In all cases, the trend in stability was the same. As expected, double charged ions were more stable than tri- and tetra charged ions in MS/MS experiments, most likely due to the increase of coulomb repulsion from 2 to 4 charges. Remarkably, the importance of the response factor in mass spectrometry was shown in the particular case of tri-charged ion. As it could be observed in the ESI-mass spectra the most intense of the peaks considered is usually the charge state +3 (Figure 36). Meanwhile, charge state +2 is shown to be the most stable in MS/MS experiments. The unexpected stability of +3 ion in MS experiments might be explained in terms of a symmetric distribution of charges, which would make it more stable during the desolvation process. When electrospray process occurs, micrometric drops that carry the product are produced. Evaporation of these drops is promoted by N_2 flow. Surface tension progressively grows until ions of different charge appear. The coulomb repulsion within the drops makes the ions fly into the analyser. In our case +3 ion might be more resistant to decomposition during this process.

3.4. Host-guest chemistry

3.4.1. Mass spectrometry experiments

The host-guest properties of our systems were also studied. Firstly, ESI mass spectra of samples containing cage **13a** and different guests in acetone were registered (Figure 37). The experiment included a variety of guests that could interact with our host via π-π stacking and that presented some interest as potential electron or energy donors or acceptors. The guests chosen for the study were pentacene, ferrocene carboxylic acid, C_{60}, C_{70} and C_{60}-PCBM.

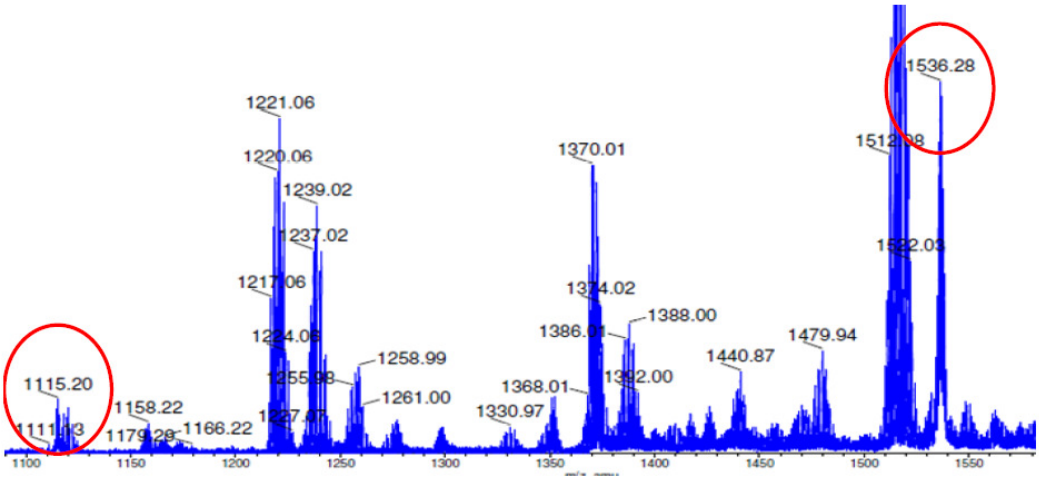

Figure 37. Mass spectrum of **13a** with C_{60}-PCBM.

Results of the mass spectra are summarized in table 5.

Table 5. Peaks detected in ESI-Mass spectra corresponding to encapsulation of guests.

Guest	+2	+3	+4
Pentacene	--	--	--
Ferrocene carboxylic acid	--	--	--
C_{60}	2282	1473	1067
C_{60}-PCBM	2344	1536	1115
C_{70}	--	1511	1097

Spectra of **13a** with fullerenes showed peaks for 1:1 complexes. Peaks for complex with C_{60}-PCBM were more intense than for the other fullerenes, probably because the guest is soluble in acetone. In the case of pentacene only the typical signals for the free capsule were observed, as well as some free guest. On the other hand, ferrocene carboxylic acid destroyed the capsule during the ionization process through coordination to Pd.

3.4.2. Template effect

To confirm that the fullerene is present inside the capsule, we took advantage of template effect (Figure 38). In this regard, the self-assembly was carried out in the presence of soluble fullerene guests to probe the pre-organization of SubPcs before they coordinate the metal centers. This pre-organization would arise from interactions of the fullerenes with the concave face of SubPcs, and will induce an increase of the

yield. Hence, experimental conditions, in which the yield of self-assembly was not optimum, were chosen (18 hours of reaction). The experimental procedure implied stirring first the SubPc and the guest together for 1h and subsequently adding the platinum complex. Notably, the expected increase in yields was observed with only 1.2 equivalents of guests (Table 6). Moreover, if the guest is not entirely removed during the work-up, the ^{1}H and ^{31}P-NMR spectra show the same signals of the stoichiometric mixture of host and guest.

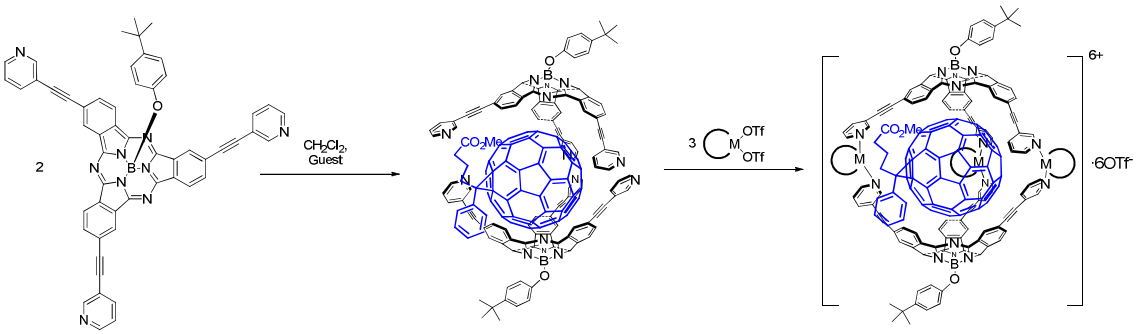

Figure 38. Self-assembly of capsules **13c** and **13d** in the presence of a guest.

Table 6. Yields of self-assembly in the presence of guests.

Cage	time	Yield (without template)	C_{60}-PCBM	C_{70}-PCBM
Pt/dppp	18h	28%	47%	53%
Pt/dppf	18h	11%	20%	89%

3.4.3. Stoichiometry of complexes

Stoichiometry of the complexes was calculated through Job's Plot experiments. Chloroform was chosen as solvent to record the UV-visible spectra. The experiments were carried out on **13c** and **13d**; C_{60}-PCBM being the guest in both cases.

No remarkable changes were observed in the spectra, so a wavelength where both host and guest absorb was chosen, and theoretical absorbance was substracted. Plotting this difference versus the mole fraction of cage gave rise to graphs showing a maximum at χ_{cage}= 0.5, which corresponds to 1:1 stoichiometry (Figure 39).

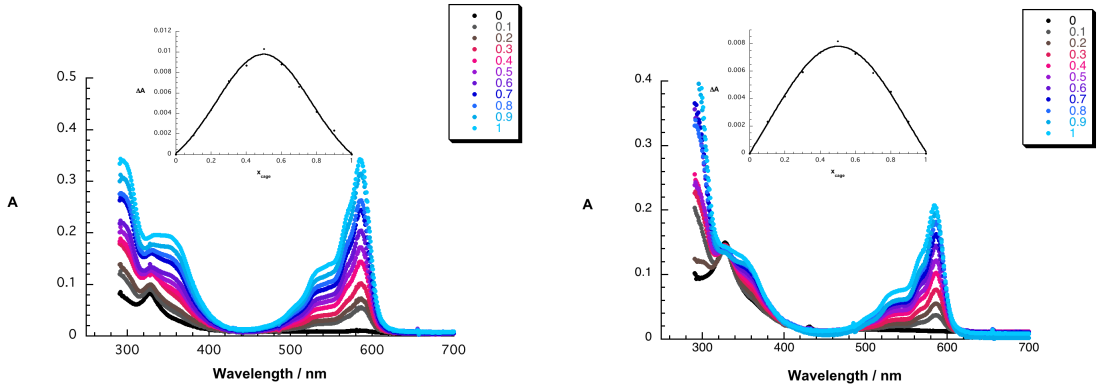

Figure 39. Job Plots obtained for **13c** and **13d** with C_{60}-PCBM.

Table 6. Binding constants (M^{-1}). Solvents: [a] $CHCl_3$, [b] CH_2Cl_2, [c] Toluene, [d] Toluene/MeCN 1:1. * Fluorescence quenching was observed but data could not be fitted to obtain K_{eq}. Maximum I/I_0 observed is indicated between brackets.

	Job Plot[a]		**^{1}H-NMR[a]**		**Fluorescence quenching**			
	5c	**5d**	**5c**	**5d**	**2**	**5a**	**5c**	**5d**
C_{60}-PCBM	$1.2\cdot10^4$	$7.7\cdot10^3$	$4.6\cdot10^4$	$3.2\cdot10^2$				
C_{70}-PCBM			$1.5\cdot10^5$	$2.2\cdot10^3$			$4.57\cdot10^4$ [b]	$6.15\cdot10^4$ [b]
C_{60}					(0.92)*,[c]	(0.94)*,[c] (0.88)*,[d]	$3.01\cdot10^4$ [c] (0.76)*,[c]	

3.4.4. Binding Constants

NMR experiments were carried out in order to obtain more reliable values for the binding constants.

A titration of capsule **13c** with C_{60}-PCBM, which was followed by ^{1}H and ^{31}P-NMR spectroscopy (Figure 40) indicates that the equilibrium is slow on the NMR time scale. Specifically, we can observe the signals of both the free cage and the complex. This fact is particularly evident for proton **a** and in the signal of ^{31}P. As a consequence, we are able to calculate the binding constants directly from the ^{1}H and ^{31}P NMR spectra of 1:1 mixtures of host and guest. The values obtained from the ^{1}H-NMR spectra are surveyed in Table 6. The latter reveal that C_{70}-PCBM forms more stable associates with our capsules. A likely rationale implies its size, which seems more appropriate for the encapsulation. Furthermore, ^{1}H and ^{31}P-NMR spectra give rise to a loss of symmetry regarding the capsule signals (three peaks are observed for each proton and phosphorous). From the latter we conclude that the guest has highly limited freedom inside the cage. Unfortunately, in the case of Pd cages the equilibrium is faster and no

remarkable shift of any signal was observed upon addition of the guest. Hence, binding constants could not be obtained from NMR experiments.

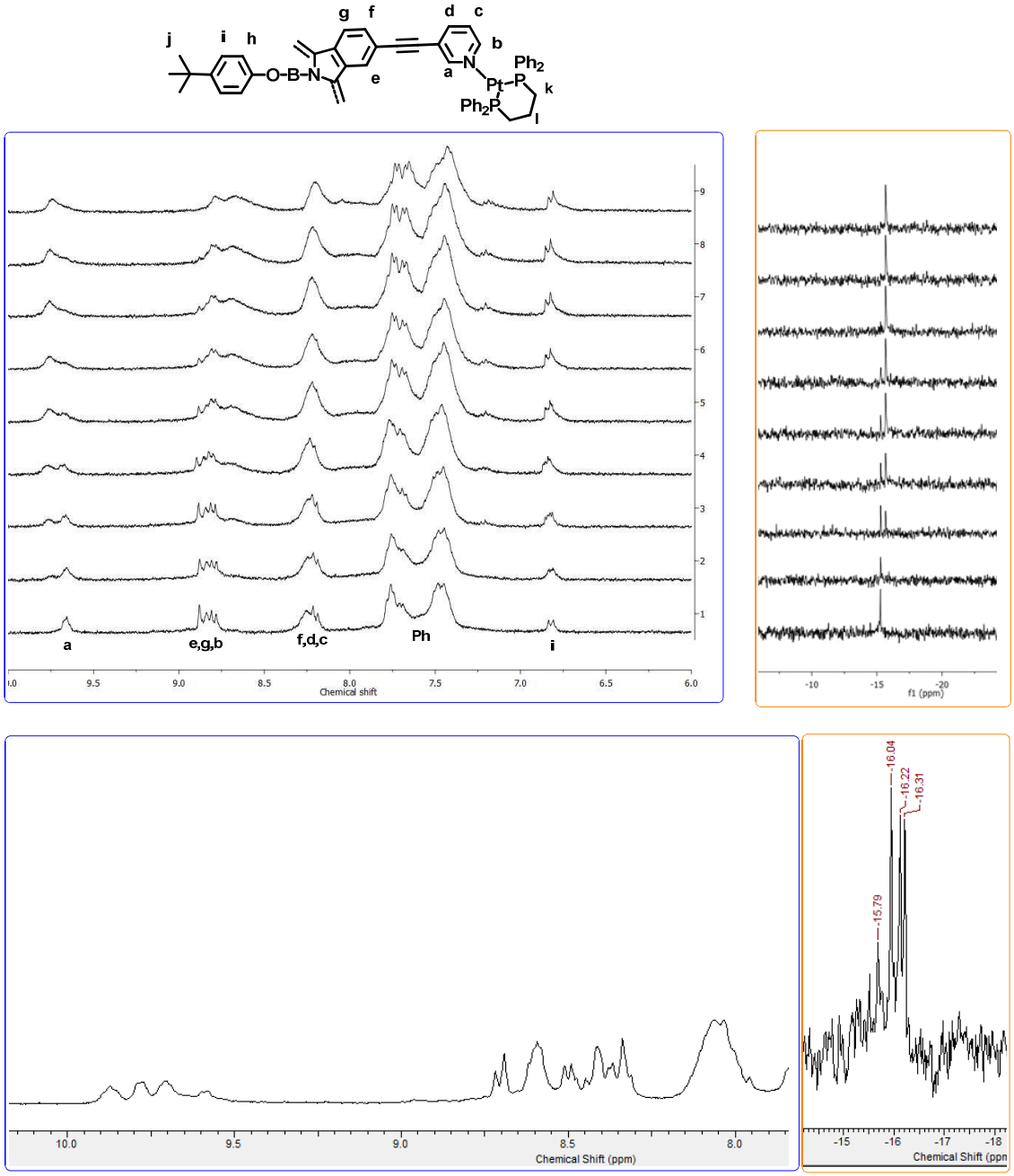

Figure 40. Upper part: ^{1}H and ^{31}P -NMR spectra of titration of **13c** with C_{60}-PCBM. From the bottom to the top, Spectra of **5c** + 0, 0.1,0.3, 0.5, 0.7, 0.8, 0.9, 1 and 3 eq of C_{60}-PCBM. Lower part: ^{1}H and ^{31}P -NMR spectra of 1:1 mixture of **13c** and C_{70}-PCBM.

Finally, and as an additional step towards supramolecular systems involving various chromophores, encapsulation of C_{60}-phthalocyanine dyads was probed. Both flexible

and rigid dyads were tested, and their binding constants were calculated employing ^{31}P-NMR. All of them were encapsulated by cage **13c** except dyad **B**. The dyads employed for the study are shown in Figure 41, and the binding constants determined for each one are listed in Table 7.

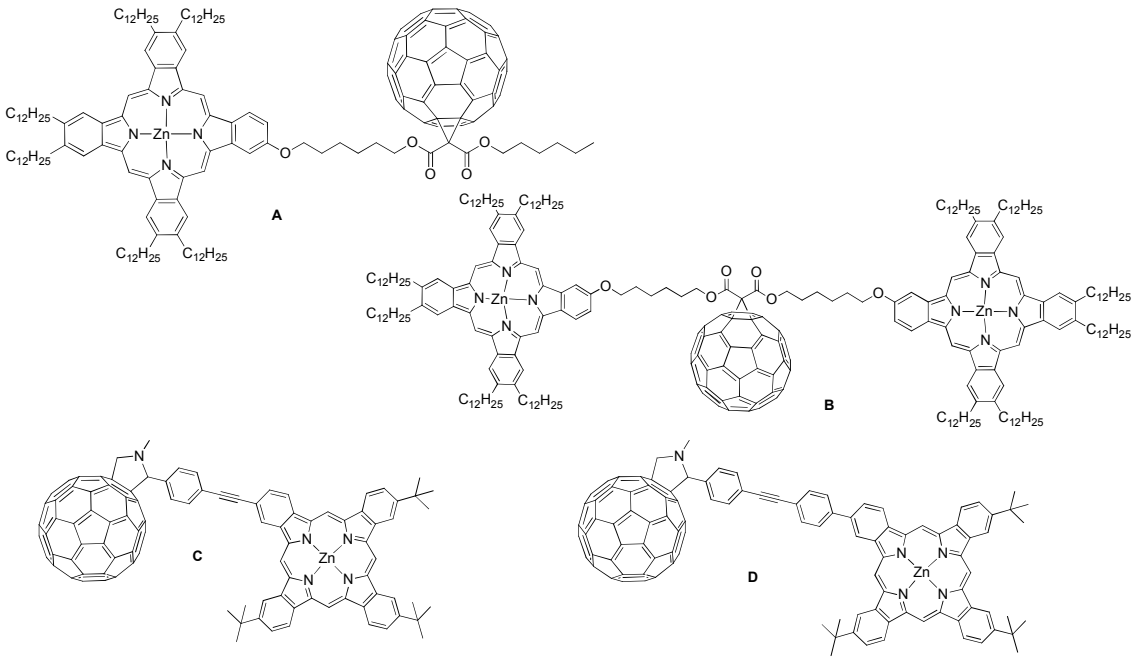

Figure 41. Pc-C_{60} dyads*

Table 7. Binding constants calcultated for Pc-C_{60} dyads. Solvents: [a] $CDCl_3$, [b] THF-d_8, [c] Toluene-d_8/THF-d_8 1:1

Pc-C_{60} dyad	**K_{eq} (M^{-1}) – ^{31}P-NMR**
A	$1.7 \cdot 10^{3}$ [a] $8.5 \cdot 10^{2}$ [b]
C	$1.10 \cdot 10^{3}$ [c]
D	$2.73 \cdot 10^{3}$ [c]

These preliminary studies highlight the possibility of including additional photo- and electroactive moieties of well-known photophysical properties.

3.5. Electrochemistry

Cyclic and square-wave voltammetry of building blocks as well as self-assembled capsules were measured (Figure 42 and Table 8).

* Pc-C_{60} dyads were prepared by Mine Ince (**A**, **B**) and Giovanni Bottari (**C**, **D**).

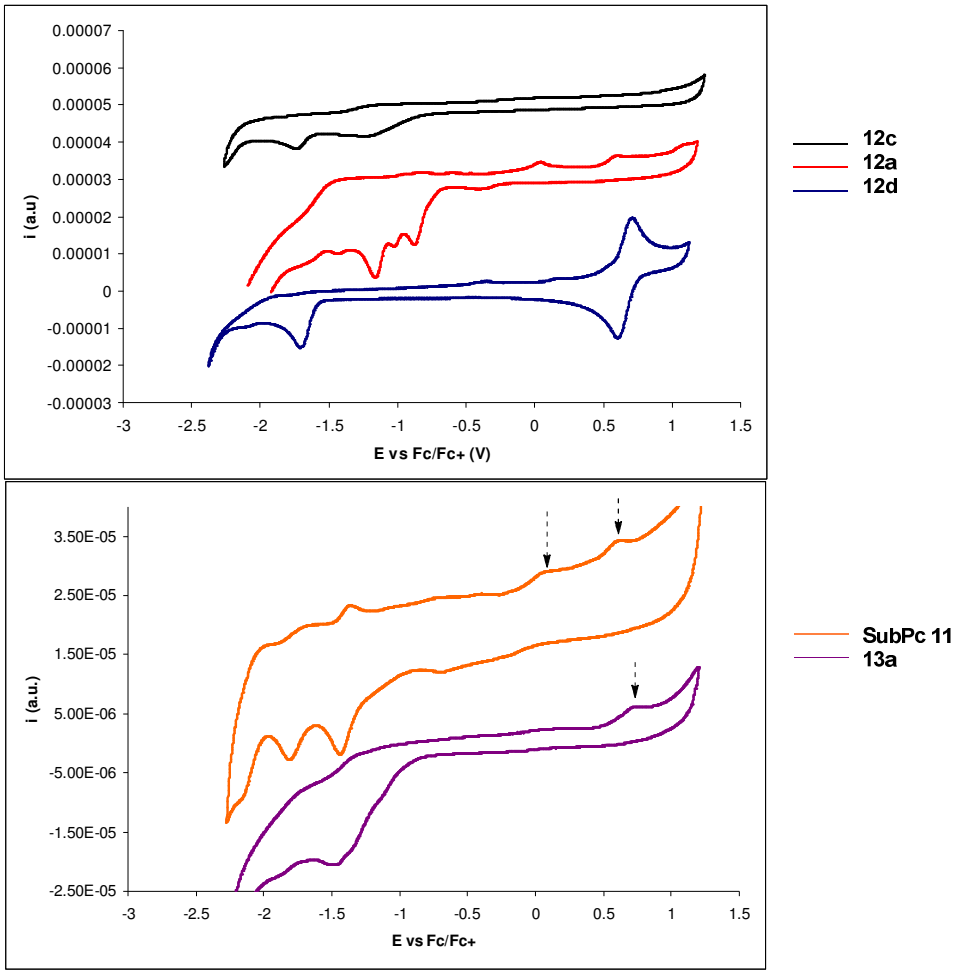

Figure 42. Cyclic voltammograms obtained for building blocks and capsule **13a**.

Table 8. Electrochemical data recorded for capsules and building blocks. Reversible processes in yellow, irreversible in grey.

Compound	E_{ox1}	E_{ox2}	E_{red1}	E_{red2}	E_{red3}	E_{red4}
11	0.119	0.632	-1.352	-1.717	-2.042	
12c			-1.254	-1.765		
12a			-0.891	-1.184	-1.406	-1.682
12d	0.713		-1.650			
13c		0.968	-1.442	-1.866	-2.221	
13a		0.725	-1.398	-1.828		
13d		0.639	-1.372	-1.870	-2.224	
3-etinilpyridine			-1.333			

Analysis of the cyclic voltammogram of metal complexes **12a**, **12c**, and **12d** showed that only **12d** presents a two-electron reversible oxidation, corresponding to the ferrocene ligand. This oxidation appears at 0.7 V, which is a much higher potential than the usual value for ferrocene (0.0 V). Thus, we shall not expect electron transfer from the ferrocene to the SubPc or the fullerene taking place. Two oxidations are also observable in the voltammogram of **12a**, but they only appear either in the second scan or if the voltage cycle is applied first to negative potentials. Thus, these oxidations were

assigned to the adsorption of reduced species of **12a** on the surface of the working electrode.

On the other hand, both Pt complexes **12c** and **12d** showed an irreversible reduction at -1.7 V that was assigned to the metal. **12c** presents an additional one-electron reversible reduction at -1.2 V, which may correspond to the phosphine ligand. Up to four reductions are present in the cyclic voltammogram of **12a**, the first ones at less negative potentials than the ones in **12c**. They overlap even at slow scan rates, so it was not possible to determine their reversibility with accuracy; although at first sight one might think all of them are irreversible. Nevertheless, a reduction process at -1.2 V appears again in **12a**, and by comparison, it was also assigned to dppp ligand.

Regarding SubPc **11**, the most interesting feature of its voltammogram is the presence of two irreversible oxidations at 0.1 and 0.6 V, the former one being an uncommon value for first oxidation potentials in SubPcs. Since this oxidation at 0.1 V disappears upon coordination of the pyridine units to the metal in all cases, it might arise from a conformational effect (the HOMO would have different energy if the three pyridine units are conjugated with the SubPc core or if, as in the capsules, they are not).

Capsules **13a** and **13c** show higher first oxidation potentials than SubPc **11**, due most probably to the interaction with the metal. As a matter of fact, Pt seem to affect more the position of this signal, which might be explained by the higher strength of metal-nitrogen bond, which also provokes more intimate contact of the π-system of the SubPc with the metallic centre. First reductions on these capsules follow the same trend, being the value of the potential more affected by the presence of Pt that by Pd.

Finally and in addition, the supramolecular interaction between capsule **13c** and C_{70}-PCBM was evidenced by this technique. Namely, we could observe the reduction potentials of both host and guest slightly shifted. Figure 43 shows the square cyclic voltammetry of a solution containing a 1:1 mixture of both components and the two reference compounds separated.

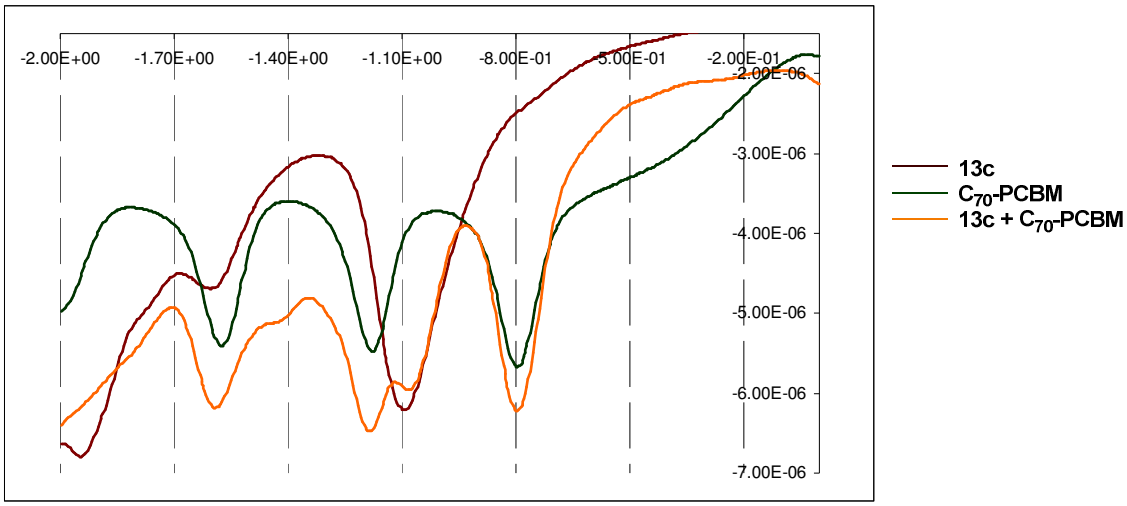

Figure 43. Square-wave voltammetry of the complex formed between **13c** and C_{70}-PCBM, and reference compounds.

3.6. Photophysics

Photophysical studies of the cages were carried out to determine the impact of metal coordination as well as fullerene encapsulation on SubPc. In particular, fluorescence quantum yields of **13a-d** as well as that of the precursor SubPc **11** were determined by comparison with rhodamine 6G, which was chosen as standard.[40] We noted that the presence of both Pd and Pt quench the SubPc fluorescence, which was not that unexpected considering heavy-atom effects, etc. However, in the case of Pd the quenching turned out to be appreciably stronger. Please note that metal-ligand charge transfer, that is, from Pt to the pyridine ligands, has been observed in related self-assembled triangles and squares.[41] Despite the fact that we have no sound evidence for a similar behaviour taking place in our systems, it is, nevertheless, likely to assist in explaining why Pd deactivates more strongly the fluorescence of SubPcs.

Subsequently, the cages were titrated with different guests. In any of the titrations, fluorescence spectroscopy was employed to monitor the changes. In general, the Pt containing cages gave rise to a weak SubPc fluorescence quenching upon addition of the guests. Nevertheless, we were able to derive binding constants of about 10^4 M^{-1} (Figure 44 and Table 6).

[40] R. F. Kubin, A. N. Fletcher, *J. Lumin.*, **1982**, *27*, 455-462
[41] D. C. Flynn, G. Ramakrishna, H-B. Yang, B. H. Northrop, P. J. Stang , *J. Am. Chem. Soc.*, **2010**, *132*, 1348-1358.

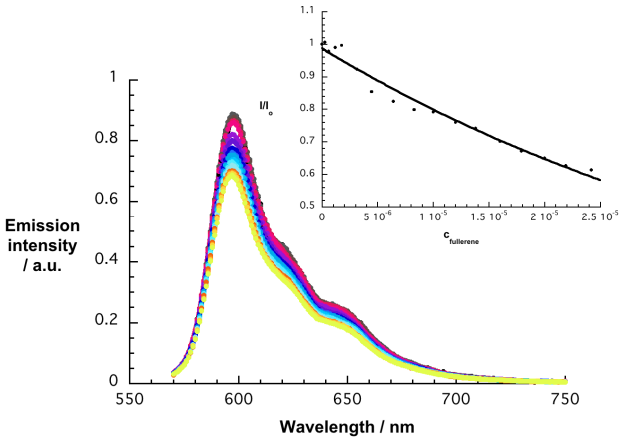

Figure 44. Titration of cage **13c** + C_{60} followed with fluorescence spectroscopy

Despite the weak fluorescence quenching, several interesting trends emerged. Comparing the different cages, fluorescence quenching was only observed when Pt is incorporated. Overall, this is not surprising considering that the presence of Pd causes a strong decrease of the SubPc fluorescence quantum yields. Regarding the guests, pristine C_{60} seems to interact more strongly than its derivative. A likely explanation infers the disruption of π-π stacking caused by the substituent on the fullerene. C_{70}-PCBM, on the other hand, showed higher binding constants than C_{60}-PCBM – a finding that is in good agreement with the NMR results. Finally, comparing the same guests in different solvents revealed that a stronger fluorescence quenching occurs in CH_2Cl_2 rather than in toluene. The origin of the latter implies a better desolvation of the fullerenes in CH_2Cl_2.

To examine the excited state interactions between the SubPc cages and encapsulated C_{60} we turned to pump probe measurements with C_{60}•**13c** and C_{60}•**13d**. However, we studied firstly, C_{60} and SubPc **11**. As a matter of fact, the differential absorption spectra, taken right after the excitation of C_{60} at 387 nm, show the instantaneous transformation –~1 ps– of high lying singlet excited states into the lowest vibrational state of the singlet excited state of C_{60}. In particular, marked transitions develop in the near infrared region with maxima at 960 nm. This singlet excited states (1.9 eV) deactivates slowly – 1.5 ± 0.1 ns – via intersystem crossing to the energetically lower lying triplet excited state (1.52 eV). Notably, the lifetime of intersystem crossing was determined from multi-wavelength analyses. A newly developing band at 750 nm reflects the diagnostic signature of the triplet excited state of C_{60}. Upon 540 nm excitation of SubPc **11** (Figure 45) its singlet excited state (2.1 eV) evolves, whose spectral characteristics include transient maxima at 460, 485, 640, 665, and 760 nm as well as transient bleaching between 510 and 610 nm. The latter features a minimum at

590 nm. From multiwavelength analyses a singlet excited state lifetime of 2.05 ± 0.1 ns was determined for **11**. For the correspondingly formed triplet excited state (1.45 eV) the most important spectroscopic feature is a 490 nm maximum.

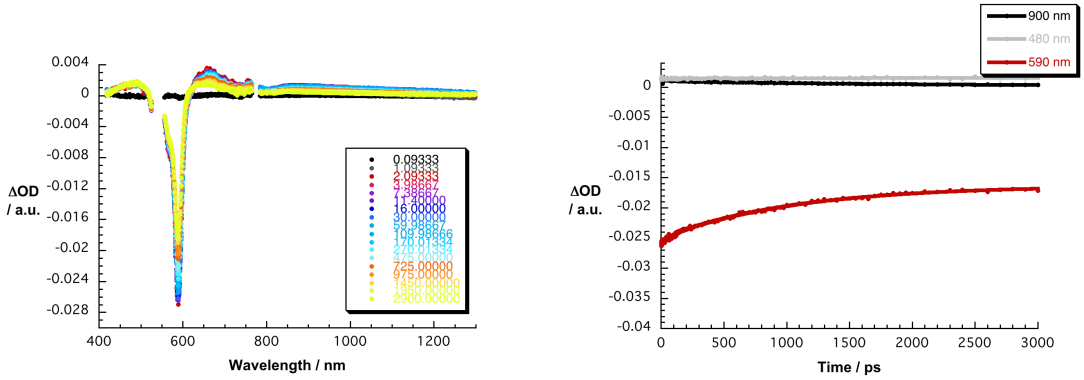

Figure 45. Left: differential absorption spectra (visible and near-infrared) obtained upon femtosecond pump probe experiments (540 nm) of SubPc **11** (8.3 x 10- M) in toluene with several time delays between 0.1 and 2800 ps at room temperature – see Figure Legend for details. Right: time absorption profiles of the spectra of 900 (black), 480 (light grey) and 590 (red) nm monitoring the excited state dynamics.

Next, we performed experiments with SubPc cages **13d** and **13c** (Figure 46), which were like SubPc **11** photoexcited at 540 nm. Similar to what is seen for SubPc **11**, photoexcitation results in the formation of SubPc centered singlet excited states. In particular, 465, 485, 640, 660, 760 nm maxima as well as 460, 485, 640, 670, 760 nm maxima evolve for SubPc cages **13d** and **13c**, respectively, next to a minimum for both at 590 nm. In comparison to **11**, the presence of platinum exerts, however, in **13d** and **13c** an acceleration of the singlet excited state decay – 1.1 ± 0.1 ns for **13d** and 1.2 ± 0.2 ns for **13c** – without yielding, however, a different photoproduct. Here, it is again the triplet excited state that is discernable by means of the 490 nm marker. But it is only the platinum that seems active, while ferrocene, which is present in **13d**, lacks any appreciable impact neither in a kinetic nor in a spectroscopic sense.

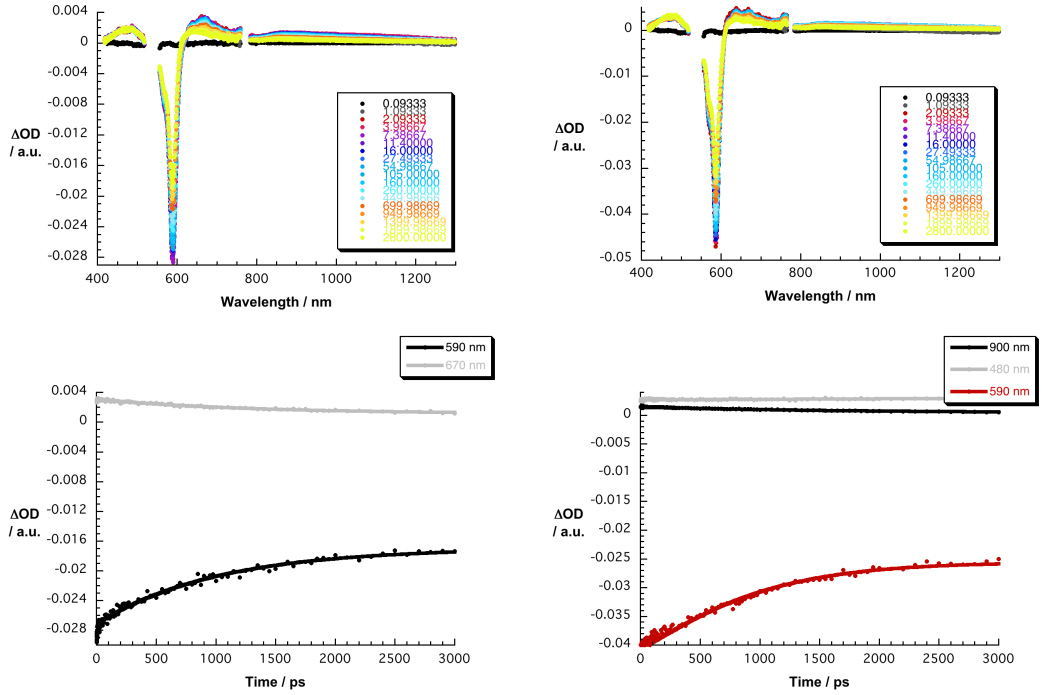

Figure 46. Upper part: differential absorption spectra (visible and near-infrared) obtained upon femtosecond pump probe experiments (540 nm) of **13c** (left) and **13d** (right) (1.3 x 10-5 M) in toluene with several time delays between 0.1 and 2800 ps at room temperature – see Figure Legend for details. Lower part: time absorption profiles of the spectra of 590 (black), and 670 (light grey) nm monitoring the excited state dynamics.

Finally, SubPc cages **13c** and **d** were treated with 1, 2, 5, 6, and 8 equivalents of C_{60} to yield C_{60}•**13c** and C_{60}•**13d**, respectively, and subjected to pump probe experiments (Figure 47). In sharp contrast to SubPc **11** as well as to SubPc cages **13d** and **13c**, upon 540 nm excitation, capsules give rise in the presence of different equivalents of C_{60} to a fast deactivation – 2 ± 1 ps for **13d** and 3 ± 1 ps for **13c** – of the SubPc singlet excited state. Simultaneous to the rapid decay in the visible, the C_{60} singlet-singlet features grow in the near infrared, revealing identical dynamics. From this we conclude the transduction of singlet excited state energy to yield the C_{60} singlet excited state. In C_{60}, intersystem crossing – 1.5 ± 0.1 ns – to the energetically lower lying C_{60} triplet dominates the deactivation of the singlet excited state – vide supra. In C_{60}•**13d** and C_{60}•**13c** the 960 nm transition – product of the initial transfer of singlet excited state energy – decays with kinetics, which are barely faster. In fact, the lifetimes are 1.4 ± 0.1 ns for C_{60}•**13d** and for C_{60}•**13c**. Interesting is, however, that we did not find the characteristic C_{60} triplet features, that is, a strong triplet-triplet transition at 750 nm, at the end of the C_{60} singlet excited state deactivation. Instead, a maximum around 490

nm and a minimum at 590 nm were concluded. The latter are excellent matches of the SubPc triplet excited state – vide supra. From this we infer that the C_{60} triplet excited state (1.52 eV), once formed, undergoes a thermodynamically allowed transfer of triplet energy to the SubPc (1.45 eV). Nearly, similar kinetics at the 590 nm minimum, which allowed us to follow the generation of the SubPc triplet, further furnishes the following kinetic assignment. The rate determining and, in turn, the slower step in the SubPc triplet formation is the C_{60} intersystem crossing.

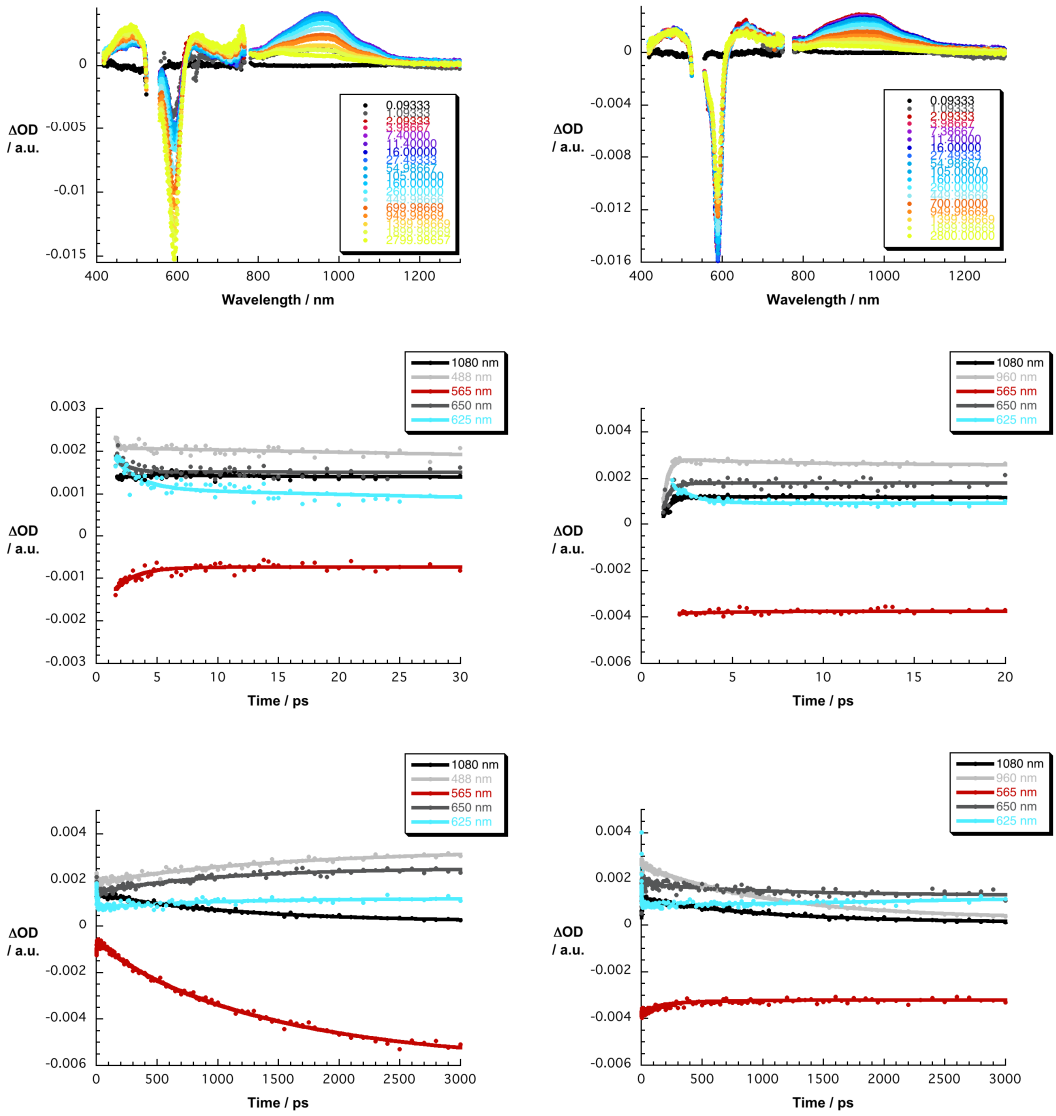

Figure 47. Upper part – differential absorption spectra (visible and near-infrared) obtained upon femtosecond pump probe experiments (540 nm) of **13c** (left) **13d** (right) (1.3 x 10^{-5} M) with 2 eq of C_{60} in toluene with several time delays between 0.1 and 2800 ps at room temperature – see Figure Legend for details. Central and lower part – time absorption profiles of the spectra of **13c** and **d** (central) and C_{60}•**13c** and C_{60}•**13d** (lower) at 1080 (black), 960 (light grey), 565 (red), 650 (dark grey) and 625 (light blue) nm monitoring the excited state dynamics.

4. Summary and Conclusions

Along this chapter, the study of SubPcs as supramolecular receptors for fullerenes has been discussed.

In the first section a systematic study involving six different SubPcs was carried out. Firstly, Job Plot experiments allowed comparison of SubPcs in terms of their electronic nature. While acceptor SubPc **6e** did no interact with C_{60} or C_{70}, SubPcs possessing an electron-rich π-system did. From these results, we inferred that shape complementarity is not enough to provide an effective π- π stacking between SubPcs and fullerenes, and therefore supramolecular recognition does not take place. Moreover, Job Plot experiments showed that the stoichiometry of the complexes was dependent on the peripheral substitution of the SubPc. To this end, hydrophobic interactions complemented by π-π interactions are the major driving forces behind a 2:1 complexation between two hexaalkylthioSubPcs and one C_{60} (or C_{70}), with binding constants as large as 10^5 M^{-1}. The length of the alkyl chain has a strong influence in the kinetics of the encapsulation equilibrium.

In the resulting 2:1 adduct and upon excitation of the SubPc, a photoinduced energy transfer takes place from the SubPc to the fullerene. Despite the lack of electron transfer in solution, such event may be expected in organic photovoltaic devices, considering the results of dodecahidro SubPc.[42]

In the second section, SubPc-based receptors for fullerenes have been constructed through preorganization of the macrocycles via metal-directed self-assembly. Excessive rigidity on the building-blocks seems to be an important drawback for the formation of the capsules, as highlighted in the case of **13b** and **13d**. Attempts to solve this issue including flexibility in the linker between the pyridine moiety and the macrocyclic core were unsuccessful.

A comparative study of the stability of capsules **13a**, **13c**, and **13e** with tandem-mass spectrometry allowed determination of the influence of various parameters (metal, ligand) in the stability of the capsule. The trends derived from the results of the study might bring up an interesting tool for the design of future SubPc-based capsules.

---

[42] H. H. P. Gommans, D. Cheyns, T. Aernouts, C. Girotto, J. Poortmans, P. Heremans, *Adv. Func. Mater*, 2007, **17**, 2653-2658.

Regarding the host-guest properties of these capsules, recognition of fullerene (C_{60} and C_{70}) and soluble fullerene derivatives was proved through an extensive series of experiments, including Job Plots, mass spectrometry experiments, and titrations performed in a rich variety of techniques. In general, the binding constants calculated show values of 10^4 M^{-1}. Interestingly, these values are in the same order of the ones obtained with hexaalkylthoieter SubPcs in the first section. From these result we can conclude that despite the non-donor electronic nature of SubPc **11** (specially compared to SubPcs **6a-d)**, preorganization provides a powerful strategy to balance lack of electronic complementarity.

Furthermore, preliminary studies on the encapsulation of fullerene derivatives bearing other chromophores have been carried out, which offers the possibility to introduce additional optically active units. On the other hand, capsules where the self-discrimination between the enantiomers of the SubPc was inverted by the introduction of a chiral phosphine might be capable of selectively recognize chiral fullerenes.

The impact of coordination to metals in the properties of the SubPc was observed in electrochemistry (shift of first oxidation and reduction potentials), fluorescence (quenching of SubPc fluorescence) and pump probe experiments (quicker deactivation of first singlet excited state). Transient absorption spectroscopy also allowed observation of ping-pong energy transfer processes upon photoexcitation of the SubPc: firstly from the SubPc to C_{60} and then from C_{60} to the SubPc.

Finally, the importance of fullerenes as materials in combination with other chromophores is highlighted by the great, and still increasing, amount of research carried out in this direction since they were discovered. Supramolecular recognition is an important field that may contribute to a better understanding of the interaction of C_{60} and other molecules in the interfaces of many devices. Moreover, supramolecular chemistry could potentially cooperate in device processing, for example, deaggregation of C_{60} by the chromophore might be a useful approach to the obtention of better architectures in bulk-heterojunction solar cells.

5. Experimental Section

General Remarks

Synthesis and Characterization: UV-vis spectra were recorded with a JASCO V-660 instrument. IR spectra were recorded on a Bruker Vector 22 spectrophotometer. ^{1}H, ^{13}C and ^{19}F-NMR spectra were recorded with a Bruker AC-300 equipment. Chemical shifts, δ, are indicated in ppm, using the solvent as a reference. MALDI spectra were obtained with a ULTRAFLEX III (Bruker) spectrometer; TCNQ was chosen as matrix. Electrochemistry was measured with an Autolab equipment, using carbon electrode (work electrode), Ag/Ag^{+} electrode (Reference electrode) and Pt electrode (Counterelectrode. Ferrocene was employed as internal reference. E is given in volts, vs Fc/Fc^{+}. Column chromatographies were carried out on sílica gel Merck-60 (230-400 mesh, 60 Å), and TLC on aluminium sheets coated with silica gel 60 F254 (Merck). Chemicals were purchased from Aldrich Chemical Co and Alfa Aesar and used as received without further purification.

MS/MS experiments

Mass spectrometry experiments were performed in a hybrid quadrupole-time of flight mass spectrometer (QTOF, QSTAR pulsar i, ABSciex) equipped with a micro electrospray ion source. Samples were dissolved in acetone (concentration 300 uM) and introduced in the spectrometer using a syringe infusion pump with a 10 ul/min flow. N_2 was employed as collision gas. Both MS and MS/MS experiments were registered: the MS experiment to identify the compound ions and the MS/MS experiment to measure stability of the cage. The experiments were performed in MCA mode (Multi Channel Acquisition) with positive ion detection. The instrumental parameters were set as follows: mass range 50-4700 Dalton; ion spray voltage (IS): 4500 V; ion source gas pressure (GS1): 35 psi; curtain gas pressure (Cur): 20 psi; declustering potencial (DP): 30 V; focusing potencial (FP): 280 V; declustering potencial 2 (DP2): 15 V; Collision gas: 3 psi in MS experiments and 5 psi in MS/MS experiments. In MS/MS experiments, the ions corresponding to loss of 2, 3 or 4 counterions, were selected and MS/MS spectra were registered with collision energies ranging from 7 eV until 35 eV. The spectra were recorded and averaged during 5 min. After each MS/MS experiment the relation A_{pi} (Area precursor ion) / A_{total} (Area precursor ion + Area product ions) x 100 was calculated and a representation to the different Collision Energies was built (the internal energy given to the ions by collisions with the gas was neglected. Its value was very low in comparison with the applied energy). The value of CE (collision energy),

when A_{pi}/A_{total} x 100= 50, was compared between different ions. The reproducibility of the experiments was estimated above 94%.

Data analyisis was carried out with Origin Pro 8 SR0 v8.0724 (B724), Copyright 1991-2007 OriginLab Corporation, Norhampton, MA 01060 USA.

4,5-dichlorofthalic anhydride (1) [26]

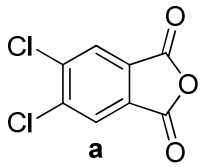

a

4,5-dichlorophthtalic acid (10 g, 0.043 mol) and acetic anhydride (17 mL, 0.18 mol) were placed in a round-bottomed flask, and refluxed for 4 hours, while the acetic acid formed in the reaction was distilled. Final traces of acetic acid were evaporated under vacuum, and the resulting solid was stirred 12 hours in hexane. Finally, the product was filtered and washed with hexane and diethyl ether (8.9 g, 95% yield). ^{1}H NMR (300 MHz, DMSO-d_6, 298 K): δ = 8.11 ppm (s, 2H, H*a*).

4,5-dichlorophthalimide (2) [26]

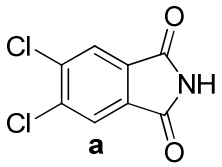

a

4,5-dichlorophthalic anhydride (9 g, 0.041 mol) was refluxed in formamide (13.8 mL) for 3 hours. The resulting mixture was allowed to cool down to room temperature. The product was filtered, washed with water and dried. 4,5-dichlorophthalamide was obtained as a white solid (7.9 g, 95%) ^{1}H NMR (300 MHz, DMSO-d_6, 298 K): δ = 8.44 (s, 2H, H*a*), 7.89 ppm (s, 1H, NH).

4,5-dichlorophthalamide (3) [26]

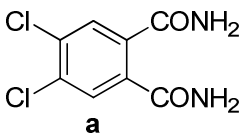

a

4,5-dichlorophthalimide (7 g, 0.034 mol) and 100 mL of NH_3 (25%) were placed in a round-bottomed flask, and the mixture was stirred 24 hours at room temperature. Then,

44 mL of NH_3 (33%) were added and the suspension was stirred for another 24 hours. Product was filtered, washed with water and dried under vacuum. 4,5-dichlorophthalamide was obtained as a white solid (5.8 g, 73%). ^{1}H NMR (300 MHz, DMSO-d_6, 298 K): δ = 7.87 (bs, 2H, NH_2), 7.71 (s, 2H, H*a*), 7.49 (bs, 2H, NH_2).

4,5-dichlorophthalonitrile (4) [26]

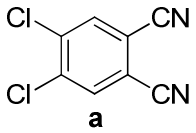

21 mL of thionyl chloride were slowly added over 30 mL of DMF at 0ºC. After 2 hours of stirring, 4,5-dichlorophthalamide (5.8 g, 0.025 mol) was added and the mixture was strirred overnight at room temperature. The resulting solution was poured onto crashed ice. The solid thus formed was filtered, washed with water and dried. Purification of 4,5-dichlorophthalonitrile was achieved by recrystalization from methanol. Product was obtained as white-yellowish crystals (3.35 g, 68 %). ^{1}H NMR (300 MHz, $CDCl_3$, 298 K): δ = 7.90 ppm (s, 2H, H*a*).

General method for the synthesis of 4,5-dialkylthiophthalonitriles [26]: 4,5-dichlorophthalonitrile (1g, 5.08 mmol), K_2CO_3 (2.1 g, 15.24 mmol) and degassed *N,N*-dimethylacetamide (13 ml) were placed in a round bottomed flask under argon atmosphere. The corresponding thiol (12 mmol) was added and the mixture was stirred at 90ºC for 12 h.

4,5-diethylthiophthalonitrile (5a)

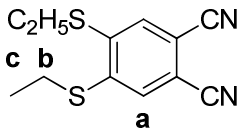

Work-up and purification: 20 mL of dichloromethane were added and the solution was extracted with bleach (2x15), water (5x15) and brine (1x15). The organic layer was dried with $MgSO_4$ and evaporated. The resulting brown solid was dissolved in diethyl ether and filtered off. The colourless solution was concentrated and left in the fridge. The precipitate was filtered and washed with cold diethyl ether. The desired compound

was obtained as a white solid (206 mg, 63%). If non-substituted or mono-substituted product remains, 4,5-diethylthiophthalonitrile can be isolated with column chromatography in silica gel (Hexane/AcOEt 7:1).
^{1}H NMR (300 MHz, $CDCl_3$, 298 K): δ = 7.4 (s, 2H, H*a*), 3.06 (q, J = 7.3 Hz 4H, H*b*), 1.42 ppm (t, J = 7.3 Hz, 4H, H*c*).

4,5-dibuthylthiophthalonitrile (5b)

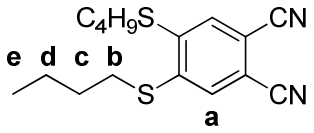

Work-up and purification: CH_2Cl_2 (20 ml) was added and the solution was extracted with bleach (2 x 10 ml), water (4 x 10 ml) and brine (1 x 10 mL). The organic layer is dried over $MgSO_4$ and the solvent was evaporated. The resulting brown solid was washed with methanol and filtered off. 4,5-dibuthylthiophthalonitrile was obtained as a white-greyish solid (1.04 g, 68%). ^{1}H NMR (300 MHz, $CDCl_3$, 298 K): *δ* = 7.40 (s, 2H, H*a*), 3.01 (t, *J* = 7.2 Hz, 4H, H*b*), 1.73 (q, *J* = 7.0, 4H, H*c*), 1.50 (m, *J* = 7.4, 4H, H*d*), 0.97 ppm (t, *J* = 7.3 Hz, 6H, H*e*).

4,5-dioctylthiophthalonitrile (5c)

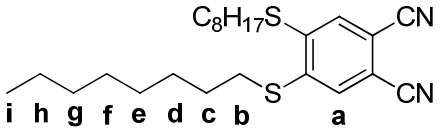

Work-up and purification: the resulting mixture was poured onto cold water. The precipitate was filtered and washed with bleach and water. 4,5-dioctylthiophthalonitrile was recrystallized in ethanol and obtained as white needles. (1.67 g, 79%). ^{1}H NMR (300 MHz, $CDCl_3$, 298 K): *δ* = 7.40 (s, 2H, H*a*), 2.94 (t, 4H, *J* = 7.2 Hz, H*b*), 1.66 (q5, 4H, *J* = 7.2 Hz, H*c*), 1.40 (m, 4H, H*d*), 1.22 (m, 12H, H*e,f,g*), 0.81 ppm (m, 10H, H*h, i*).

4,5-hexadecylthiophthalonitrile (5d)

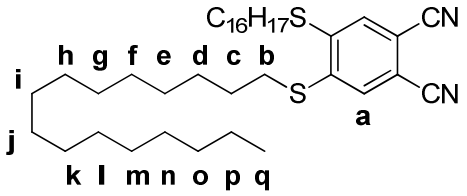

Work-up and purification: the resulting mixture was poured onto cold water. The precipitate was filtered and washed with bleach, water and methanol. 4,5-dihexadecyl thiophthalonitrilo was obtained as an off-white solid. (2.12 g, 65%). ^{1}H NMR (300 MHz, $CDCl_3$, 298 K): δ = 7.39 (s, 2H, H*a*), 3.00 (t, 4H, *J* = 7 Hz, H*b*), 1.74 (m, 4H, H*c*), 1.54 (m, 4H, H*d*), 1.25 (m, 44H, H*e-o*), 0.87 ppm (m, 10H, H*p,q*).

General method for the Synthesis of Subphthalocyanines 6a-f [27]: In a 25-ml round bottomed flask, BCl_3 (0.3 mmol, 1M solution in *p*-xylene) was added to the corresponding phthalonitrile (0.6 mmol) under an argon atmosphere. The reaction mixture was stirred under reflux for 2 h and then flushed with argon to remove volatiles. Subsequent axial substitution was carried out without isolation of chlorosubphthalocyanines intermediate. 4-*tert*-buthylphenol (1.8 mmol) and toluene (1 ml) were added and the mixture was refluxed till reaction was completed (check by TLC; see eluent below). Reaction was cooled down to room temperature, the solvent was evaporated under reduced pressure and the resulting purple-green solid was washed with a 4:1 mixture of methanol and water. Finally, compounds **6a-f** were purified by column chromatography in silica gel using as eluent: hexane/toluene (1:2.5) for **6a** and **6b**, hexane/CH_2Cl_2 (1:1) for **6c**, hexane/ethyl acetate (20:1) for **6d**, toluene/THF (20:1) for **6e** and hexane/$CHCl_3$ (2:1) for **6f**.

Phenoxy-[1,2,3,4,8,9,10,11,15,16,17,18-dodecafluoro-7,12:14,19-diimino,-21,5-nitrilo-5H-tribenzo[c,h,m][1,6,11]triazacyclopentadecinato-(2)-κN^{22},κN^{23},κN^{24}]-boron(III) (6f) [27]

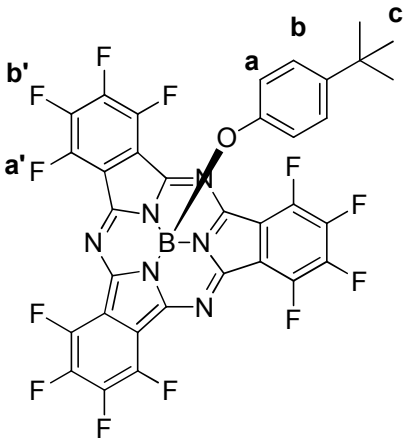

Dark pink solid (159 mg, 35%). ^{1}H NMR (300 MHz, CDCl3, 298 K): δ = 6.78 (d, 2H, *J* = 8.4 Hz, H*b*), 5.28 (d, 2H, *J* = 8.4 Hz, H*a*), 1.10 ppm (s, 9H, H*c*). ^{19}F NMR (470 MHz, $CDCl_3$): δ = -136.85 (AA'BB' system, F*a'*), -147.58 ppm (AA'BB' system, F*b'*) ^{13}C-NMR (300 MHz, CDCl3, 298 K): δ = 148.68, 148.47, 145.02, 144.48, 143.95, 141.06,140.61, 140.41, 126.18, 117.60, 114.93, 114.83, 33. 94, 31.25 ppm. UV-Vis (Toluene) : λ_{max} (log(ε)) = 300 (3.90), 573 nm (4.19).

Phenoxy-[7,12:14,19-diimino,-21,5-nitrilo-5H-tribenzo [c,h,m][1,6,11]triazacyclopentadecinato-(2)-κN^{22},κ N^{23}, κN^{24}]-boron(III) (6e) [27]

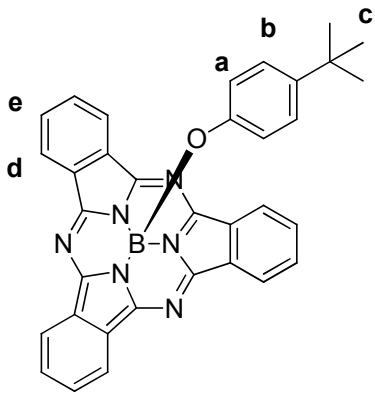

Dark pink solid (121 mg, 37%). ^{1}H NMR (300 MHz, CDCl3, 298 K): δ = 8.87-8.84 (AA'BB' system, H*d*), 7.91-7.88 (AA'BB' system, H*e*), 6.76 (d, 2H, *J* = 8.4 Hz, H*b*), 5.31 (d, 2H, *J* = 8.4 Hz, H*a*), 1.07 ppm (s, 9H, H*c*). ^{13}C-NMR (300 MHz, CDCl3, 298 K): δ =

151.46, 150.08, 143.53, 134.24, 130.97, 129.72, 125.65, 123.54, 122.14, 117.68, 33.79, 31.30 ppm. UV-Vis (Toluene) : λ_{max} (log(ε)) = 305 (4.03), 563 nm (4.24).

Phenoxy-[2,3,9,10,16,17-hexaethylthio-7,12:14,19-diimino,-21,5-nitrilo-5H-tribenzo[c,h,m][1,6,11]triazacyclopentadecinato-(2)-κN^{22},κN^{23},κN^{24}]-boron(III) (6a)

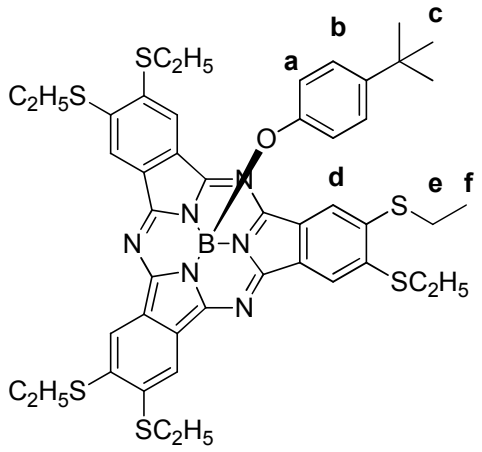

Dark green powder (282 mg, 52%). ^{1}H NMR (300 MHz, CDCl3, 298 K): δ = 8.60 (s, 6H, Ha), 6.79 (d, J = 8.5 Hz, 2H, He), 5.33 (d, J = 8.5 Hz, 2H, Hd), 3.25 (t, J = 7.6 Hz, 12H, Hb), 1.50 (t, J = 7.5 Hz, 18H, Hc), 1.07 ppm (s, 9H, Hd). ^{13}C NMR (300 MHz, $CDCl_3$, 298 K): δ = 140.04, 127.23, 126.42, 125.49, 120.06, 119.72, 118.87, 114.76, 58.54, 31.53, 27.59, 13.69 ppm. IR (KBr) v = 3057, 2297, 2195, 1587, 1481, 1436, 1223, 825, 750, 692 cm^{-1}. UV/vis (Toluene) : λ_{max} (log(ε))= 302 (4.67), 385 (4.41), 597 nm (4.80). MALDI (DCTB): 904.26 [M^{+}], 755.42 [M-tBufenoxy]$^{+}$. Electrochemistry (CH_2Cl_2, 200 mV/s, E vs Fc/Fc^{+}): E = 0.52 (irrev), 1.08 (irrev), -1.19 (rev), -1.45 (rev), -1.73 (rev), -2.18 V (irrev). Elemental Analysis: Calculated for $C_{46}H_{49}BN_6OS_6$: C, 61.04; H, 5.46; N, 9.28; S, 21.26. Found: C, 61.69; H, 5.88; N, 7.29; S, 16.38.

Phenoxy-[2,3,9,10,16,17-hexabuthylthio-7,12:14,19-diimino,-21,5-nitrilo-5H-tribenzo[c,h,m][1,6,11]triazacyclopentadecinato-(2)-κN^{22},κN^{23},κN^{24}]-boron(III) (6b)

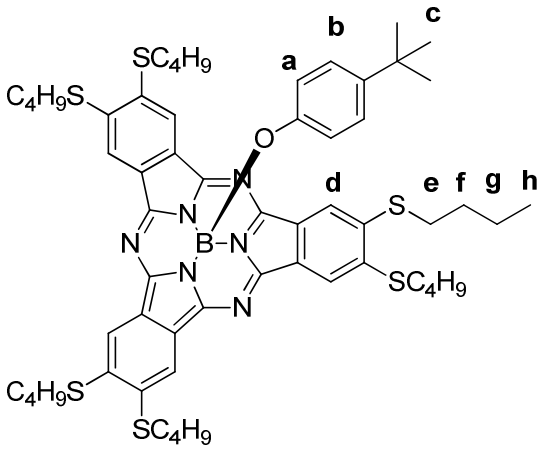

Dark green powder (456 mg, 71%). ^{1}H NMR (300 MHz, $CDCl_3$, 298 K): δ = 8.57 (s, 6H, H*a*), 6.71 (d, *J* = 8.1 Hz, 2H, H*g*), 5.27 (d, *J* = 8.1 Hz, 2H, H*f*), 3.23 (m, 12H, H*b*), 1.81 (m, 12H, H*c*), 1.59 (m, 12H, H*d*), 1.05 (s, 9H, H*h*), 0.98 ppm (t, *J* = 7.24 Hz, 18H, H*e*). ^{13}C NMR (300 MHz, $CDCl_3$, 298 K): δ = 150.79, 147.22, 140.34, 136.35, 128.34, 125.62, 119.60, 117.74, 33.76, 33.30, 28.74, 27.19, 22.18, 13.68 ppm. IR (KBr) : *v* = 3060, 2691, 1662, 1437, 1252, 1029, 692, 638 cm^{-1}. MALDI (DCTB) : 1072.42 [M^{+}], 923.28 [M-tBufenoxy]. UV/vis (Toluene) : λ_{max} (log(ε))= 286 (4.67), 385 (4.09), 598 nm (4.49). Electrochemistry (CH_2Cl_2, 200 mV/s, E vs Fc/Fc^{+}): E = 0.86 (irrev), -1.07 (rev), -1.44 V (rev). Elemental Analysis: Calculated for $C_{58}H_{73}BN_6OS_6$: C, 64.90; H, 6.85; N, 7.83; S, 17.92. Found: C, 63.03; H, 6.87; N, 6.25; S, 14.18.

Phenoxy-[2,3,9,10,16,17-hexaocthylthio-7,12:14,19-diimino,-21,5-nitrilo-5H-tribenzo[c,h,m][1,6,11]triazacyclopentadecinato-(2)-κN^{22},κN^{23},κN^{24}]-boron(III) (6c)[27]

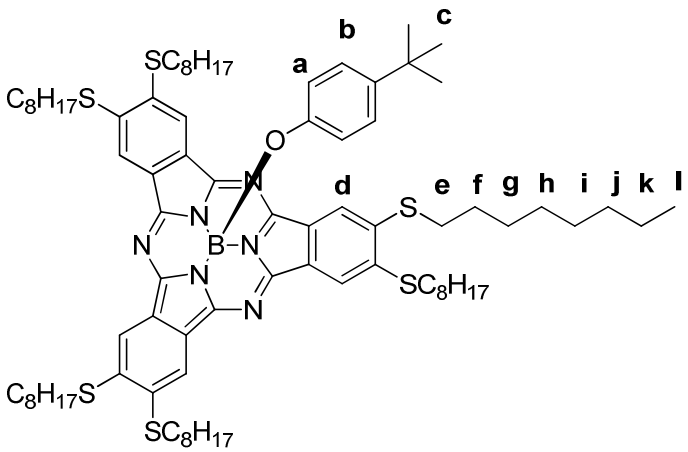

Dark green slurry solid (549 mg, 65%). ^{1}H NMR (300 MHz, CDCl3, 298 K): δ = 8.59 (s, 6H, H*d*), 6.75 (d, 2H, *J* = 8.5 Hz, H*b*), 5.33 (d, 2H, *J* = 8.5 Hz, H*a*), 3.23 (m, 12H, H*e*), 1.85 (m, 12H, H*f*), 1.57 (m, 12H, H*g*), 1.29 (m, 36H, H*h,i,j*), 0.87 ppm (m, 30H, H*k,l*). UV/vis (Toluene) : λ_{max} (log(ε))= 286 (4.47), 408 (4.09), 598 (4.53). Electrochemistry (CH_2Cl_2, 200 mV/s, E vs Fc/Fc^+): E = 0.88 (irrev), -1.13 (rev), -1.58 (rev).

Phenoxy-[2,3,9,10,16,17-hexakis(hexadecylthio)-7,12:14,19-diimino,-21,5-nitrilo-5H-tribenzo[c,h,m][1,6,11]triazacyclopentadecinato-(2)-κN^{22},κN^{23},κN^{24}]-boron(III) (6d) [27]

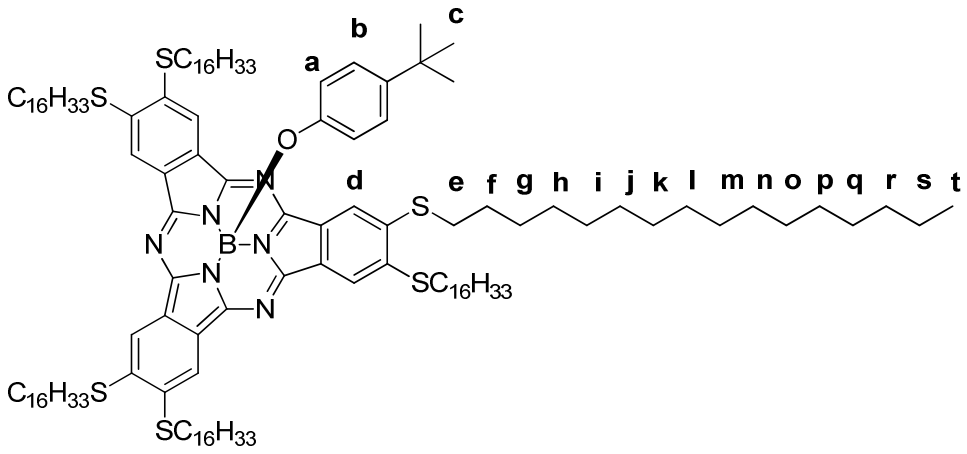

Dark green slurry solid (300 mg, 24%). ^{1}H NMR (300 MHz, CDCl3, 298 K): δ = 8.45 (s, 6H, H*d*), 6.60 (d, 2H, *J* = 8.3 Hz, H*b*), 5.16 (d, 2H, *J* = 8.3 Hz, H*a*), 3.09 (m, 12H, H*e*), 2.86 (t, 12H, *J* = 7.2 Hz, H*f*), 1.71 (m, 12H, H*g*), 1.60 (m, 12H, H*h*), 1.43 (m, 12H, H*i*), 1.34 (m, 12H, H*j*), 1.12 (m, 96H, H*k-r*), 0.94 (s, 9H, H*c*), 0.71 ppm (m, 24H, H*s,* H*t*). ^{13}C NMR (300 MHz, CDCl3, 298 K): δ = 150.83, 150.12, 144.25, 141.65, 140.58, 129.01, 128.43, 125.67, 119.73, 117.81, 115.63, 111.07, 38.15, 33.74, 31.84, 31.73, 29.69, 29.06, 28.53, 28.07, 22.66, 14.05 ppm. λ_{max} (log(ε))= 286 (4.36), 408 (3.89), 598 (4.46). Electrochemistry (CH_2Cl_2, 200 mV/s, E vs Fc/Fc^+): E = 1.02 (irrev), -1.10 (rev), -1.53 (rev).

4-aminophthalonitrile (7) [28]

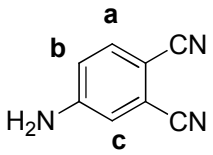

3g of 4-nitrophthalonitrile are gently warmed in 70 mL of methanol and 15 mL of HCl till complete solution of the product. Subsequently, 3.3 g of Fe are added portionwise and the reaction is refluxed for 1 h. The resulting solution is allowed to cool down to room temperature and cold water is added. 4-aminophthalonitrile crashes out as a white solid that is washed with water and dried under vacuum. Yield: 85%. m.p. 170-173ºC (reported: 172-174ºC); ^{1}H-NMR (300MHz, DMSO-d_6): δ = 7.65 (d, J_o = 8.7 Hz, 1H, H*a*), 7.00 (s, 1H, H*c*), 6.85 ppm (d, J_o = 8.7 Hz, 1H, H*b*), 6.70 (bs, 2H, NH_2).

4-iodophthalonitrile (8) [28]

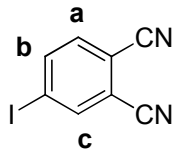

A suspension of 1.5 g of 4-aminophthalonitrile in 20 mL of H_2SO_4 is cooled down to -10ºC. A solution of 0.84 g of $NaNO_2$ in 3 mL of water is then added dropwise. The mixture is poured onto a cold solution of 1.6 mL of KI in 10 mL of water and stirred 2 h at room temperature. The brown solid is filtered, washed with water, a solution of $Na_2S_2O_3$, and water again, and then dried. The product is further purified by columna chromatography in silica gel employing CH_2Cl_2 as eluent. Yield: 65%. m. p. 141-143ºC (reported 142-143ºC). ^{1}H-NMR (300MHz, $CDCl_3$): δ = 8.15 (s, 1H, H*c*), 8.10 (d, J_o = 8.3 Hz, 1H, H*b*), 7.49 ppm (d, J_o = 8.2 Hz, 1H, H*a*).

Chloro [2,9,n*-triyodo-7,12:14,19-diimino-21,5-nitrilo-5H-tribenzo [c,h,m][1,6,11]triazaciclopentadecinate(2-)κN^{22},κN^{23},κN^{24}] boron (III) (9)

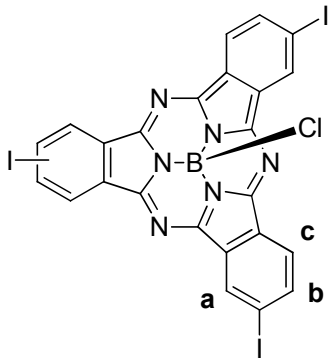

400 mg of 4-iodophthalonitrile are placed in a round-bottomed flask equiped with refrigerant and magnetic stirrer under argon atmosphere. 0.8 mL of BCl_3 1M-solution in *p*-xylene are added through a syringe and the mixture is refluxed for 2 h. The final purple mixture is flushed with an argon stream to remove volatiles and the solvent is eliminated under vacuum. Product can be obtained pure by column chromatography (silica gel, hexane/ ethyl acetate 1:2). Yield: 63%. ^{1}H-NMR (300MHz, $CDCl_3$): δ = 9.19 (s, 3H, H*a*), 8.55 (d, 3H, *J* = 8.9 Hz, H*c*), 8.20 ppm (d, 3H, *J* = 8.3 Hz, H*b*).

4-*terc*-butilfenolate[2,9,n*-triyodo-7,12:14,19-diimino-21,5-nitrilo-5H-tribenzo[c,h,m][1,6,11]triazaciclopentadecinate(2-) κN^{22},κN^{23},κN^{24}] boron(III) (10) [29]

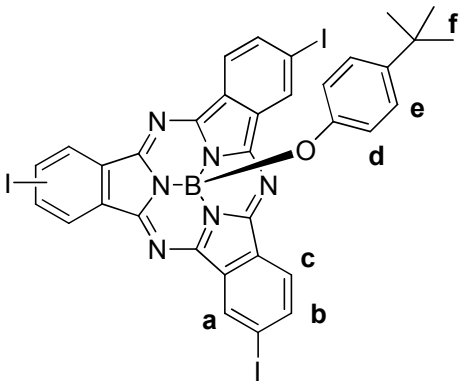

The crude of the previous reaction is disolved in 0.75 mL of toluene, and kept under argon atmosphere. 157 mg of 4-*tert*buthylphenol disolved in 0.75 mL of THF and 78 µl of DBU are added and the mixture is refluxed till the reaction is complete (check by TLC). Solvent is evaporated and the product is washed with methanol/water 1:1. Finally, the product is purified and its regioisomers (*C_3, **n**=16 y C_1, **n**=17) separated through column chromatography (silica gel, hexane/toluene 2:3). Yield (calculated from starting material 4-iodophthalonitrile): 60% ^{1}H-NMR (300MHz, $CDCl_3$): δ = 9.20 (s, 3H,

a), 8.53 (d, 3H, *J* = 8.0 Hz, H*c*), 8.22 (d, 3H, *J* = 8.0 Hz, H*b*), 6.73 (d, 2H, *J* = 8.2 Hz, H*e*), 5.24 (d, 2H, *J* = 8.2 Hz, H*d*), 1.08 ppm (s, 9H, H*f*).

4-*terc*-butilfenolato[2,9,16-tris(3-piridiletinil)-7,12:14,19-diimino-21,5-nitrilo-5H-tribenzo[c,h,m][1,6,11]triazaciclopentadecinato- κN22,κN23,κN24] boron (III) (11) [12a]

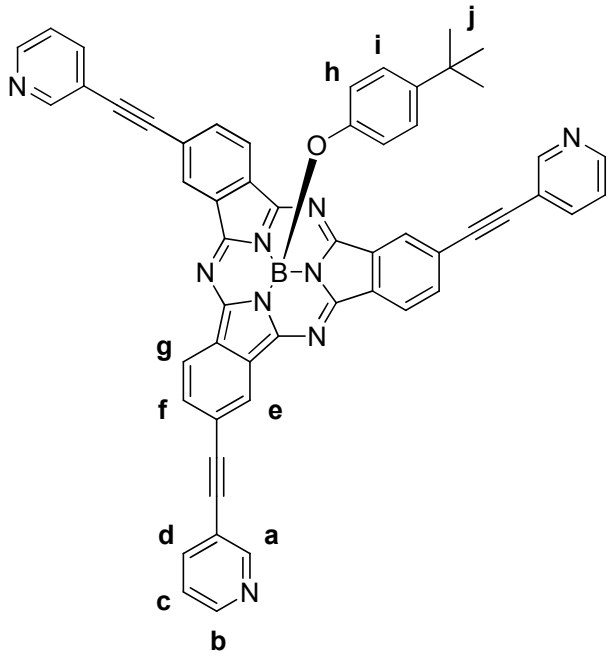

33 mg of triodo-SubPc, 13.4 mg of 3-ethynylpyridine, 5 mg of $Pd(PPh_3)Cl_2$ and 2 mg of CuI in 2 ml of degassed triethylamineare stirred at 40ºC overnight under argon atmosphere. Subsequently, 10 mL of water are added and the product extracted with CH_2Cl_2 (3x10mL), then the organic laye ris dried with Na_2SO_4 and solvent is evaporated under vacuum. Product is purified through column chromatography (silica gel, Hexane/acetone 2:3). Yield: 78%

^{1}H-RMN (300 MHz, $CDCl_3$, 298 K): δ = 9.01 (s, 3H, H*a*), 8.79 (s, 3H, H*e*), 8.76 (d, 3H, *J* = 8.17 Hz, H*g*), 8.52(d, 3H, *J* = 4.85 Hz, H*b*), 8.01(dt, 3H, J_o = 8.17, J_m =1.27 Hz, H*d*), 7.87(d, 3H, J_o = 7.9 Hz, H*f*), 7.29 (dd, 3H, J_o = 7.79 Hz, J_m = 4.82 Hz, H*c*), 6.72 (d, 2H, *J* = 8.14Hz, H*i*), 5.29 (d, 2H, *J* = 8.14Hz, H*h*), 1.09 (s, 9H, H*j*) ppm. UV/Vis (CH_3Cl): λ_{max}(log(ε))= 283 (4.65), 353 (4.38), 587 nm (4.72).

M(dppp)Cl_2 and Pt(*s*-BINAP)Cl_2[30]

100 mg of K_2MCl_4 are dissolved in 1 ml of hot H_2O/HCl 2:1 mixture. Then, 20mL of 1-propanol are added and the Light Pink mixture is stirred 15 min at room temperature. 1 eq of 1,3-bis(diphenylphosphino)propane (dppp) is added and the reaction is stirred 30

min at room temperature and refluxed for 2 h. The resulting solution is allowed to cool down and the product crashes out. The solid is filtered and washed with cold water and diethyl ether, and dried. Yield: M=Pd, 90% (beige solid); M=Pt, 93% (white solid); and Pt(*s*-BINAP)Cl_2, 90% (white solid).

Pd(dppp)Cl_2 : ^{1}H-RMN (300 MHz, $CDCl_3$, 298 K): δ = 7.81-7.42 (m, 20H, Ph), 2.38 (m, 2H, CH_2-$\underline{CH_2}PPh_2$), 2.07 ppm (m, 2H, $\underline{CH_2}$-CH_2PPh_2). ^{31}P NMR (119 MHz, $CDCl_3$, 298 K): δ = 11.18 ppm (s).

Pt(dppp)Cl_2 : ^{1}H-RMN (300 MHz, $CDCl_3$, 298 K): δ = 7.76 (m, 8H, Ph), 7.43 (m, 12H, Ph), 2.51 (m, 4H, CH_2-$\underline{CH_2}PPh_2$), 2.04 ppm (m, 2H, $\underline{CH_2}$-CH_2PPh_2). ^{31}P NMR (119 MHz, $CDCl_3$, 298 K): δ = -10.16 (s), 5.14 and -25.48 ppm (^{195}Pt satellites, $J_{Pt\text{-}P}$ = 3721 Hz).

Pt(*S*-BINAP)Cl_2 : ^{1}H-RMN (300 MHz, $CDCl_3$, 298 K): δ = 7.95-7.37 (m, 20H, Ph), 7.23-6.77 (m, 12H, Naphthalene). ^{31}P NMR (119 MHz, $CDCl_3$, 298 K): δ = 9.88 (s), 24.96 and 5.21 ppm (^{195}Pt satellites, $J_{Pt\text{-}P}$ = 3667 Hz).

M(dppp)OTf_2 and Pt(*s*-BINAP)OTf_2 (12a, 12c and 12e) [30]

To a solution of 0.07 mmol of M(dppp)Cl_2 in CH_2Cl_2 (7ml for M=Pd; 3.5 ml for M=Pt) 1.5 equivalents of AgOTf are added, and the mixture is stirred at room temperature and in absence of Light for 18 h. The AgCl is filtered off the mixture and the solution concentrated under vacuum. Dyethyl ether is added and the precipitated solid filtered and washed with water and ether. Yield: M=Pd, 74% (pale-yellow solid); M=Pt, 70%, (White solid).

12a: ^{1}H-RMN (300 MHz, $CDCl_3$, 298 K): δ = 7.66-7.02 (m, 20H, Ph), 2.77 (m, 4H, CH_2-$\underline{CH_2}PPh_2$), 2.30 ppm (m, 2H, $\underline{CH_2}$-CH_2PPh_2). ^{31}P NMR (119 MHz, $CDCl_3$, 298 K): δ = 15.01 ppm (s). ^{19}F NMR (282 MHz, $CDCl_3$, 298 K): δ = -98.71 ppm (s).

12c: ^{1}H-RMN (300 MHz, $CDCl_3$, 298 K): δ = 7.62-7.32 (m, 20H, Ph), 2.90-2.82 (m, 4H, $\underline{CH_2}$-CH_2PPh_2), 2.32 ppm (m, 2H, CH_2-$\underline{CH_2}PPh_2$). ^{31}P NMR (119 MHz, $CDCl_3$, 298 K): δ = -10.83 ppm (s), 4.69 and -26.73 ppm (^{195}Pt satellites, $J_{Pt\text{-}P}$ = 3818 Hz).

12e: ^{1}H-RMN (300 MHz, $CDCl_3$, 298 K): δ = 7.77-7.30 (m, 20H, Ph), 7.22-6.56 (m, 12H, Naphthalene). ^{31}P NMR (119 MHz, $CDCl_3$, 298 K): δ = 2.83 ppm (s), 18.01 and -12.33 ppm (^{195}Pt satellites, $J_{Pt\text{-}P}$ = 3687 Hz).

M(dppf)Cl_2[30]

100 mg MCl_2(COD) and 1,1´-bis(difenilfosfino)ferroceno (1 equivalent) disolved in 20 ml de CH_2Cl_2 are stirred 15 min at room temperature. The solution is concentrated and diethyl ether added to afford precipitation of the product, that is filtered, washed with

water and diethyl ether and dried. Yield=99%. M=Pd (orange solid); M=Pt (dark-yellow solid).

Pd(dppf)Cl_2 : ^{1}H-RMN (300 MHz, $CDCl_3$, 298 K): δ = 7.89 (m, 8H, Ph), 7.48-7.38 (m, 12H, Ph), 4.38 (s, 2H, Fc), 4.18 ppm (s, 2H, Fc). ^{31}P NMR (119 MHz, $CDCl_3$, 298 K): δ = 33.83 ppm (s).

Pt(dppf)Cl_2 : ^{1}H-RMN (300 MHz, $CDCl_3$, 298 K): δ = 7.87 (m, 8H, Ph), 7.46-7.18 (m, 12H, Ph), 4.36 (s, 2H, Fc), 4.18 (s, 2H, Fc). ^{31}P NMR (119 MHz, $CDCl_3$, 298 K): δ = 15.01 ppm (s).

[M(dppf)(H_2O)$_2$]OTf_2[30]

To a solution of 30 mg of M(dppf)Cl_2 3 equivalents of AgOTf are added and the mixture is stirred under argon at room temperature for 18 h. Subsequently, the AgCl is filtered off, and 1 mL of water is added to the solution under vigorous stirring for 10 min. The solution is then concentrated and dyethyl ether added to afford precipitation of the product, that is filtered and washed with water and diethyl ether and dried. Yield=55%. M=Pd (green solid); M=Pt, (yellow solid).

12b: ^{1}H-RMN (300 MHz, $CDCl_3$, 298 K): δ = 7.82-7.09 (m, 20H, Ph), 4.63 ppm (bs, 8H, Fc). ^{31}P NMR (119 MHz, $CDCl_3$, 298 K): δ = 46.17 ppm (s).

12d: ^{1}H-RMN (300 MHz, $CDCl_3$, 298 K): δ = 7.87, 7.46-7.18 (m, 20H, Ph), 4.36 (s, 4H, Fc), 4.18 ppm (s, 4H, Fc). ^{31}P NMR (119 MHz, $CDCl_3$, 298 K): δ = 15.81 ppm (s), 29.83 and -0.24 ppm (^{195}Pt satellites, J_{Pt-P} = 3818 Hz).

General procedure for self-assembly of compounds 13a-e

General: Subphthalocyanine **11** (1 eq) and the corresponding metal complex (1 eq) were dissolved in dry dichoromethane. The resuting purple solution was stirred under argon atmosphere and warmed at reflux for different periods of time depending on each case. After completion, the solution was concentrated and diethylether was

added. Finally, the resulting precipitate was filtered and washed sequentially with cold toluene, hexane and diethylether.

Compound 13a

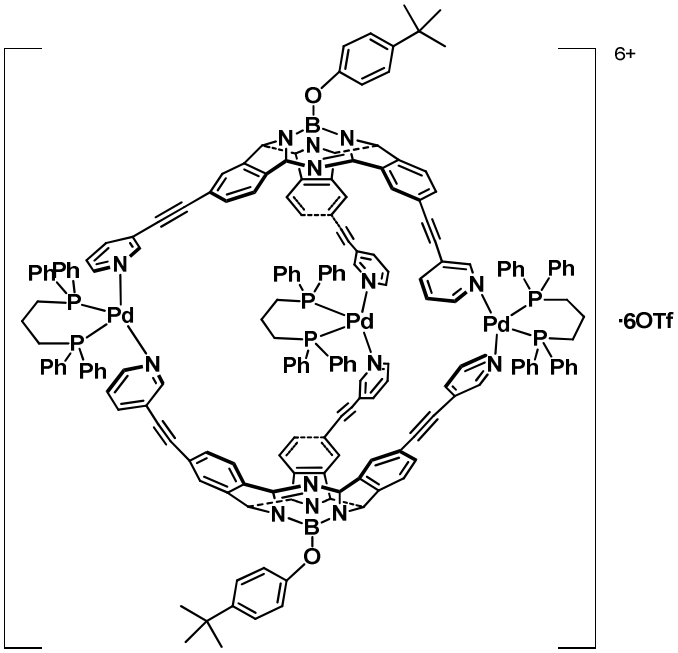

Subphthlocyanine **11** (7 mg, 0.011 mmol), [Pd(dppp)]OTf_2 (13 mg, 0.016 mmol), CH_2Cl_2 (7 ml). The solution was refluxed for 5 h and then left at room temperature overnight. Purification was carried out as described above. Compound **13a** was obtained as a purple powder (16 mg, 94%). m.p.>250 ºC; ^{1}H NMR (300 MHz, $CDCl_3$, 298 K): δ = 9.66 (s, 6H, H*a*); 8.75 (s, 6H, H*e*); 8.65 (d, 6H, *J* = 8 Hz, H*g*); 8.58 (bs, 6H, H*b*); 8.08 (m, 12H, H*d*, H*c*); 8.00 (d, 6H, *J* = 8 Hz, H*f*); 7.65-7.14 (m, 60H, H*Ph*); 6.70 (d, 4H, *J* = 8 Hz, H*h*); 5.23 (d, 4H, *J* = 8 Hz, H*i*); 3.74 (m, 6H, H*l*); 2.87 (m, 12H, H*k*); 1.04 (s, 18H, H*j*) ppm.

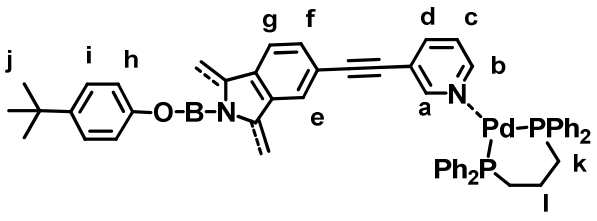

^{31}P NMR (119 MHz, $CDCl_3$, 298 K): δ = 6.23 (s); ^{19}F NMR (282 MHz, $CDCl_3$, 298 K): δ = -77.90 (s); IR (KBr): ν = 3059, 2959, 2868, 2218, 1614, 1485, 1437, 1250, 1157, 1028, 835, 764, 702, 638, 573, 513 cm^{-1}. UV/Vis (CH_3Cl): $\lambda_{max}(\log(\varepsilon))$= 293 (4.67), 348 (4.41, sh), 540 (4.21, sh), 588(4.65) nm. MS (ESI, Acetone): *m/z* = 1922.4 $[M\text{-}2OTf]^{2+}$,

1231.9 $[M\text{-}3OTf]^{3+}$, 1515.4 $[M\text{-}Pd(dppp)\text{-}4OTf]^{2+}$, 667.0 $[Pd(dppp)OTf]^{+}$. Elemental Analysis: Calculated for $C_{197}H_{146}N_{18}O_{20}P_6F_{18}S_6B_2Pd_3$: C, 57.06; H, 3.55; N, 6.08; S: 4.64. Found: C, 57.22; H, 3.59; N, 6.11; S, 4.67.

Compound 13b

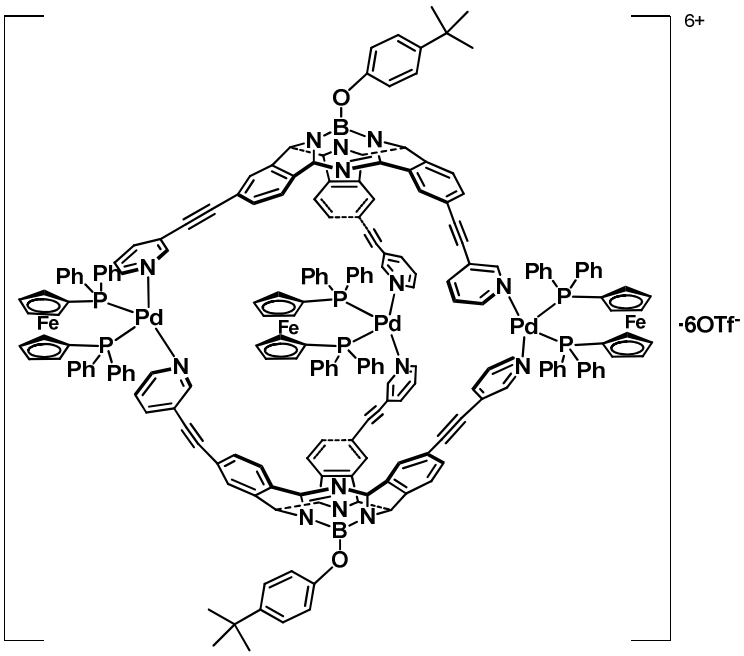

Subphthalocyanine **11** (6 mg, 0.007 mmol), $[Pd(dppf)(H_2O)_2]OTf_2$ (10 mg, 0.01 mmol), CH_2Cl_2 (3 ml). The solution was refluxed for 2 days and then left 12 hours at room temperature. The product was isolated as described above and further purification was carried out by gel permeation chromatography. Compound **13b** was obtained as a purple powder (2.3 mg, 17%). m.p.>250ºC; ^{1}H NMR ($CDCl_3$, 300 MHz, 298 K): δ = 9.38 (s, 6H, H*a*), 8.72 (s, 6H, H*e*), 8.67-8.62(m, 12H, H*g*, H*d*), 8.26(m, 12H, H*b*, H*c*), 8.12 (d, 6H, *J* = 8.4 Hz, H*f*), 7.5-7.8 (m, 60H, Ph), 6.69 (d, 4H, *J* = 8.7Hz, H*i*), 5.54 (bs, 6H, Fc), 5.22(d, 4H, *J* = 8.7Hz, H*h*), 4.84 (bs, 6H, Fc), 4.52 (bs, 6H, Fc), 4.42 (bs,6H, Fc), 1.04 (s, 18H, H*j*) ppm.

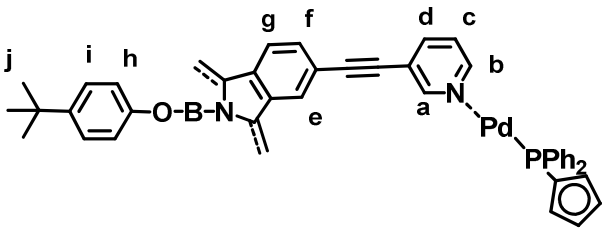

^{31}P NMR (119 MHz, $CDCl_3$, 298 K): δ = 27.89 ppm; ^{19}F NMR spectrum could not be recorded; IR (KBr): v = 3053, 2962, 2939, 2214, 1659, 1612, 1435, 1385, 1261, 1028, 804, 694, 636, 567, 492 cm^{-1}. UV/Vis ($CHCl_3$): λ_{max}(log(ε))= 295 (4.64), 344 (4.31, sh), 530 (4.05, sh), 587 (4.60) nm. ESI-MS spectrum could not be recorded. Elemental Analysis: Calculated for $C_{218}H_{152}N_{18}O_{20}P_6F_{18}S_6B_2FePd_3$: C, 57.27; H, 3.35; N, 5.51; S: 4.21. Found: C, 57.48; H, 3.41; N, 5.59; S, 4.57.

Compound 13c

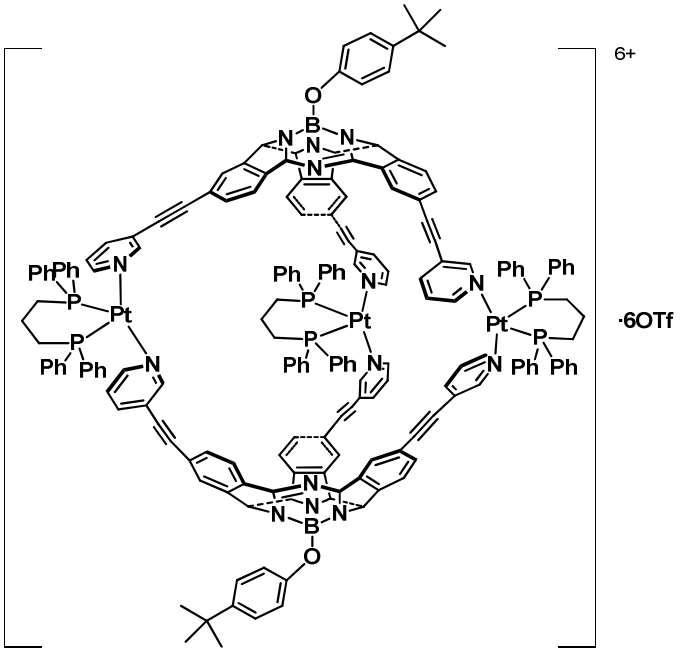

Subphthalocyanine **11** (15 mg, 0.018 mmol), Pt(dppp)OTf_2 (24 mg, 0.027 mmol), CH_2Cl_2 (7.5 ml). The solution was refluxed for 2 days and then left 24 hours at room temperature. Purification was carried out as described above. Compound **13c** was obtained as a purple powder (37.5 mg, 95%). m.p.>250ºC; ^{1}H NMR ($CDCl_3$, 300 MHz, 298 K): δ = 9.65 (s, 6H, H*a*), 8.76 (s, 6H, H*e*), 8.66 (d, 6H, J = 8.20 Hz, H*g*), 8.59 (s, 6H, H*b*), 8.08 (m, 18 H, H*f*, H*d*, H*c*), 7.66-7.20 (m, 60H, Ph), 6.71 (d, 4H, J = 8.7 Hz, H*i*), 5.22 (d, 4H, J = 8.7 Hz, H*h*), 2.79 (m, 12H, H*k*), 2.00 (m, 6H, H*l*), 1.05 (s, 18H, H*j*) ppm.

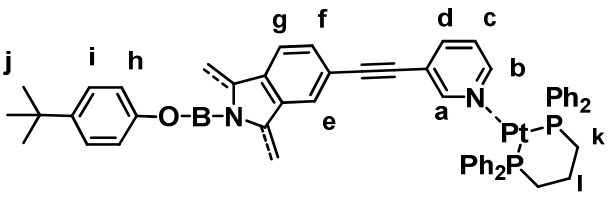

^{31}P NMR (119 MHz, $CDCl_3$, 298 K): δ = -15.28 ppm (s, $J_{Pt\text{-}P}$ = 1492 Hz); ^{19}F NMR (282 MHz, $CDCl_3$, 298 K): δ = -78.93 ppm (s). IR (KBr): ν = 3061, 2960, 2218, 1716, 1662, 1437, 1252, 1159, 1030, 748, 692, 517 cm^{-1} ; UV/Vis ($CHCl_3$): λ_{max}(log(ε))=292 (5.25), 340 (4.99, sh), 545 (4.83, sh), 585 (5.25) nm ; MS (ESI, Acetone): *m/z*= 1321.6 [M-3OTf]$^{3+}$, 953.9 [M-4OTf]$^{4+}$, 1604.3 [M-Pt(dppp)-4OTf]$^{2+}$, 1019.6 [M-Pt(dppp)-5OTf]$^{3+}$; Elemental Analysis: Calculated for $C_{197}H_{146}N_{18}O_{20}P_6F_{18}S_6B_2Pt_3$: C, 53.62; H, 3.34; N, 5.71; S: 4.36. Found: C, 53.75; H, 3.35; N, 5.54; S, 4.37.

Compound 13d

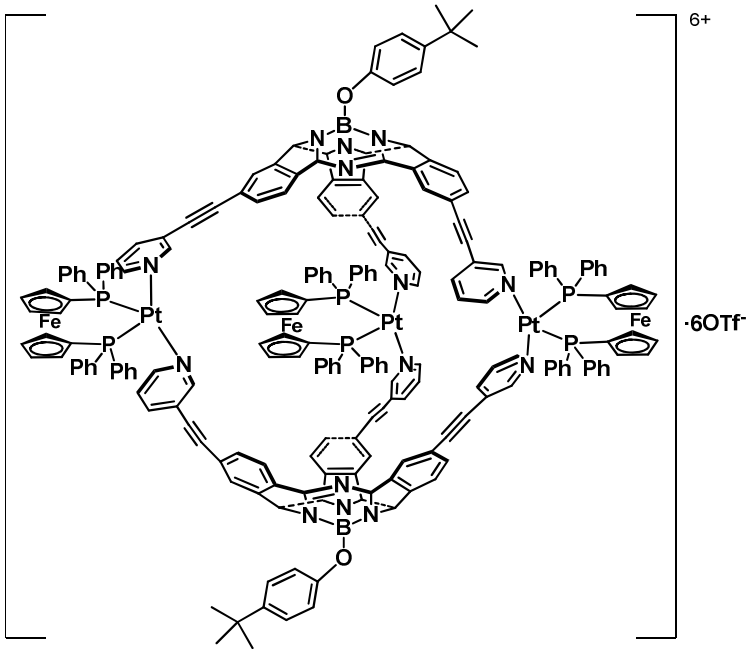

Subphthalocyanine **11** (15 mg, 0.018 mmol), [Pt(dppf)(H_2O)]OTf_2 (30 mg, 0.027 mmol), CH_2Cl_2 (9 ml). The solution was refluxed for 3 days and then left 24 hours at room temperature. The product was isolated as described above and further purification was carried out by gel permeation chromatography. Compound **13d** was obtained as a purple powder (11.1 mg, 25%). m.p.> 250ºC; ^{1}H-NMR ($CDCl_3$, 300MHz, 298K): δ = 9.04 (s, 6H, H*a*), 8.87 (s, 6H, H*e*), 8.82 (d, 6H, *J* = 8 Hz, H*g*), 8.61 (bs, 6H, H*b*), 7.1-8 (m, 78H, H*f*, H*d*, H*c*, Ph), 6.78 (d, 4H, *J* = 7.5 Hz, H*i*), 5.33 (d, 4H, *J* = 7.5 Hz, H*h*), 5.13 (s, 8H, Fc), 4.79-4.27 (m, 18H, Fc), 1.09 (s, 18H, H*j*).

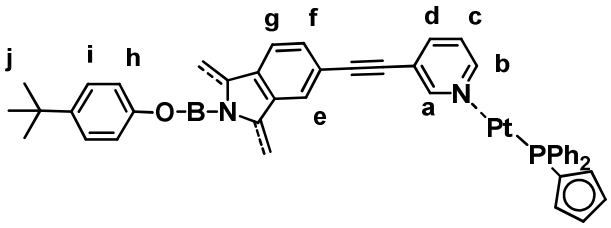

^{31}P NMR (119 MHz, $CDCl_3$, 298 K): δ = 16.11 ppm (s, $J_{Pt\text{-}P}$ = 1495 Hz); ^{19}F NMR (282 MHz, $CDCl_3$, 298 K): δ = -77.68 ppm (s). IR (KBr): ν =3057, 2959, 2216, 1663, 1612, 1483, 1437, 1259, 1153, 1030, 748, 694, 636, 563, 517, 494, 471, 440 cm^{-1}; UV/Vis ($CHCl_3$) λ_{max}(log(ε))= 292 (5.18), 360 (4.53, sh), 540 (4.33, sh), 585 (4.82); ESI/MS spectrum could not be recorded. Elemental Analysis: Calculated for $C_{218}H_{152}N_{18}O_{20}P_6F_{18}S_6B_2FePt_3$: C, 54.12; H, 3.17; N, 5.21; S: 3.98. Found: C, 54.28; H, 3.18; N, 5.23; S, 4.38.

Compound 13e

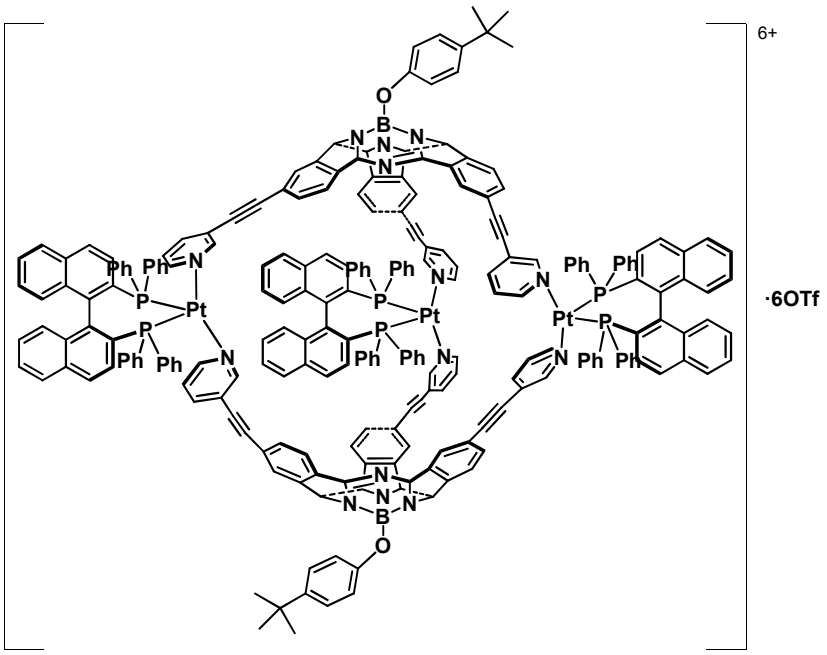

Subphthalocyanine **11** (5 mg, 0.006 mmol), [Pt(*S*-BINAP)]OTf_2 (10 mg, 0.009 mmol), $CDCl_3$ (0.5 ml). [Pt(*S*-BINAP)]OTf_2 was added portionwise to a solution of SubPc **11**. After each addition the mixture was refluxed for 1 hour and NMR was taken. Finally, the solution was stirred 24 hours at room temperature. The product was isolated as described above and further purification was carried out by gel permeation chromatography. Compound **13d** was obtained as a purple powder (7.8 mg, 51%).

m.p.> 250ºC; ^{1}H-NMR ($CDCl_3$, 300MHz, 298K): δ = 9.18-6.40 (m, 140H, H*a,b,c,d,e,f,g,i* Ph, Naphthalene), 5.29-5.19 (d+d, 2H, *J* = 7.7 Hz, H*h*), 1.02 ppm (s, 9H, H*j*).

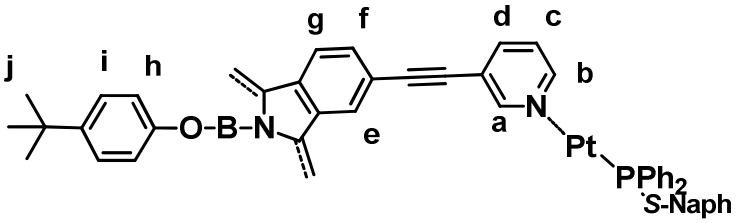

^{31}P NMR (119 MHz, $CDCl_3$, 298 K): δ = -2.65 (s), -2.98 ppm (s). UV/Vis ($CHCl_3$): λ_{max}(log(ε)) = 357 (4.94), 545 (sh, 4.57), 587 nm (5.07). ESI/MS spectra could not be recorded.

Compound 13f [12a]

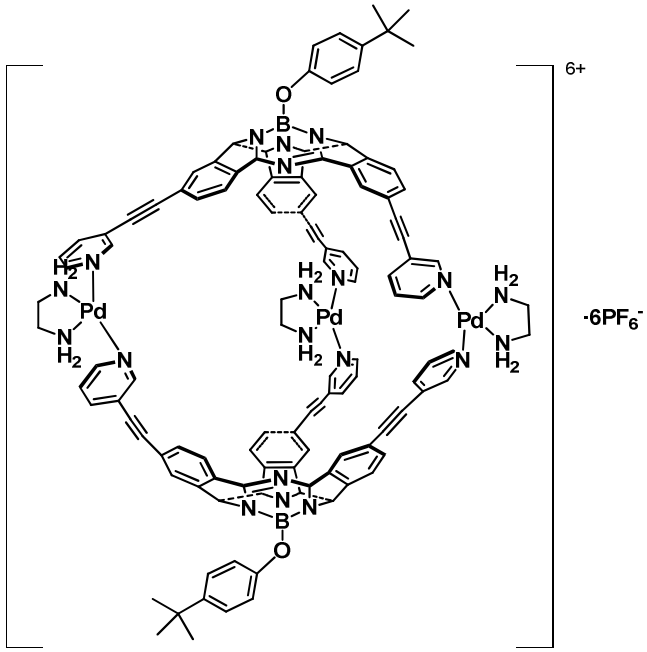

Firstly, $Pd(en)Cl_2$ (5 mg, 0.021 mmol) was dissolved in water (0.6 mL), and $AgNO_3$ (9 mg, 0.053 mmol) was added. After 10 min of stirring at room temperature, the mixture was filtered and the resulting yellow solution was poured onto a solution of SubPc **11** (10 mg, 0.012 mmol) in MeCN/MeOH 1:1 (1 mL). The mixture was stirred 24 hours at room temperature. The solution was concentrated under vacuum and KPF_6 was added. The purple precipitate was collected and washed with water, hexane and diethyl ether. product was obtained as a purple powder (15 mg, 83%). m.p.> 250ºC; ^{1}H-NMR ($CDCl_3$, 300MHz, 298K): δ = 9.37 (s, 3H, H*a*), 9.35 (s, 3H, H*a*), 9.23-9.19 (d+d, 6H, *J* = 8.5 Hz, H*e*), 8.85 (d, 3H, *J* = 8.5 Hz, H*g*), 8.75 (d, 3H, *J* = 8.3 Hz, H*g*), 8.42 (d, 3H, *J* = 8.3 Hz,

H*f*), 8.25-7.59 (m, 33H, H*f,d,c,b*), 7.23 (d, 3H, *J* = 7.9 Hz, H*c*), 6.77 (d, 4H, *J* = 7.6 Hz, H*i*), 5.50 (bs, 12H, NH_2), 5.26 (d, 4H, *J* = 7.6 Hz, H*h*), 3.64 (t, 12H, *J* = 6.9 Hz, H*k*), 1.04 ppm (s, 9H, H*j*).

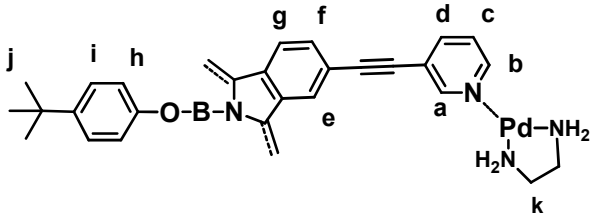

MS (ESI, acetone): *m/z* = 1386.22 $[M\text{-}2PF_6]^{2+}$, 875.82 $[M\text{-}3PF_6]^{3+}$.

4-*terc*-butilfenolate[2,9,n*-tris(pyridylethenyl)-7,12:14,19-diimino-21,5-nitrilo-5H-tribenzo[c,h,m][1,6,11]triazaciclopentadecinate(2-) $\kappa N^{22},\kappa N^{23},\kappa N^{24}$] boron (III) (14)

32

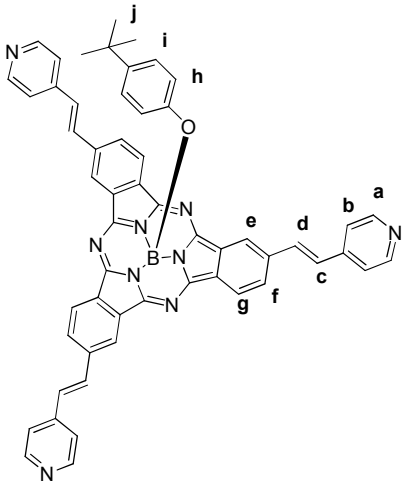

$PdCl_2$ (4 mg, 0.017 mmol) and tris(orthotolyl)phosphine (6 mg, 0.019 mmol) were placed in a 25 ml round-bottomed flask, and the system was subjected to three cycles of vacuum/Ar. Then, a dry and degassed 2:1 mixture of NEt_3 and DMF was added and the resulting solution was stirred for 20 minutes. Subsequently, tri-iodo-subphthalocyanine (100 mg, 0.11 mmol) was added and the mixture was degassed again and then heated up to 85-90ºC. Finally, 4-vinylpyridine was added through a syringe and the reaction was stirred at that temperature for 5 hours. After completion, 20 ml of dichloromethane were added and extracted with saturated solution of $NaHCO_3$ (1x20 ml) and water (4x20 ml). The organic layer was dried with $MgSO_4$ and the solvent was evaporated. Isolation of the product was carried out by means of column chromatography in silica gel ($CHCl_3$/AcOEt/MeOH 1:1:1). Compound **2** was obtained as a violet solid (75 mg, 80%). m.p.>250 ºC; ^1H NMR (300 MHz, $CDCl_3$, 298 K): δ = 9.02 (s, 3H, H*e*);8.84 (d, 3H, *J* = 8.2 Hz, H*g*); 8.67 (d, 6H, *J* = 4.5 Hz, H*a*), 8.10 (d, 3H,

J = 8.2 Hz, H*f*), 7.61 (d, 3H, *J* = 16.7 Hz, H*d*), 7.48 (d, 6H, *J* = 4.5 Hz, H*b*), 7.39 (d, 3H, *J* = 16.7 Hz, H*c*), 6.79 (d, 2H, *J* = 8.3 Hz, H*i*), 5.36 (d, 2H, *J* = 8.3 Hz, H*h*), 1.09 (s, 9H, H*j*). ^{13}C NMR (300 MHz, DMSO-d_6, 298 K): δ (ppm) = (cuaternary atoms are not observed) 150.19, 149.73, 146.98, 144.22, 138.15, 132.57, 128.38, 125.78, 123.85, 121.04, 117.85, 31.29. IR (KBr): ν (cm^{-1}) = 3028, 2962, 2924, 2853, 1593, 1450, 1261, 1049, 800. UV/Vis (CH_3Cl): λ_{max} (nm) (log(ε))= 297 (4.43), 360 (4.11, sh), 540 (sh), 595 (4.33). MS (MALDI, DCTB): *m/z* = 853.4 [M$^+$], 704.2 [M-tBuOPh]. Exact mass: 853.3 (Calculated), 853.4 (Experimental).

4-terc-butilfenolate[2,9,16-tris(3-pyridylethyl)-7,12:14,19-diimino-21,5-nitrilo-5H-tribenzo[c,h,m][1,6,11]triazaciclopentadecinate- κN22,κN23,κN24] Boron (III) (15)

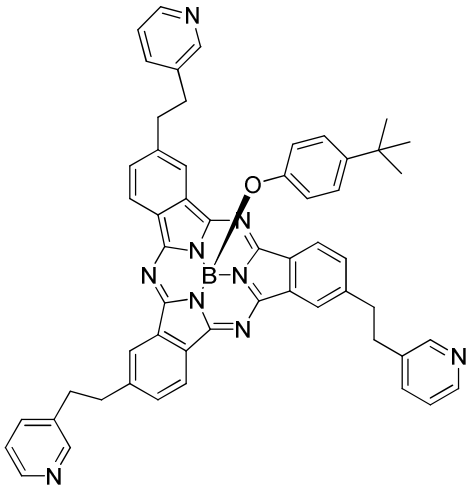

SubPc **11** (30 mg, 0.035 mmol) and $Pd(OH)_2/C$ (15 mg- 20% Pd, ≥50% H_2O- 30% mol in the reaction)were placed in a round-bottomed flask under argon atmosphere. 1.5 mL of degassed DMF/EtOH 3:2 were added. The system was then subjected to H_2 flow for 10 minutes. The reaction was stirred at room temperature for 2 hours in hydrogen atmosphere. Catalyst was then filtered and solvent was evaporated. Product was obtained as a red solid. UV-vis ($CHCl_3$): 564 nm; Mass (MALDI, Matriz DCTB): 859 (M$^+$)

4-terc-butilfenolate[2,9,16-triethenyl-7,12:14,19-diimino-21,5-nitrilo-5H-tribenzo[c,h,m][1,6,11]triazaciclopentadecinate- κN22,κN23,κN24] boron (III) (16) [33]

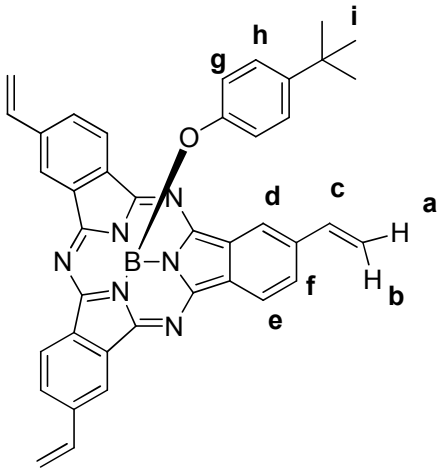

SubPc **11** (45 mg, 0.048 mmol), and $Pd(PPh_3)_4$ (8 mg, $7.2 \cdot 10^{-3}$ mmol), are placed in a round-bottomed flask under argon. Degassed toluene (3 mL) and tributhylvinyltin (69 µL, 0.24 mmol) were subsequently added through a syringe and the reaction was refluxed for 6 hours. Toluene was evaporated under vacuum and product was washed with hexane. Product was purified by column chromatography in silica gel (Hexane/THF 3:1). Compound **17** was obtained as a pink solid (23 mg, 77%). m.p.>250 ºC; ^{1}H NMR (300 MHz, $CDCl_3$, 298 K): δ = 8.84 (s, 3H, H*d*), 8.77 (d, 3H, J = 8.3 Hz, H*e*), 7.96 (d, 3H, J = 8.3 Hz, H*f*), 7.03 (dd, 3H, J_{cis} = 10.7 Hz, J_{trans} = 17.5 Hz, H*c*), 6.76 (d, 2H, J = 8.7 Hz, H*h*), 6.10 (d, 3H, J_{trans} = 17.5 Hz, H*b*), 5.52 (d, 3H, J_{trans} = 10.7 Hz, H*a*), 5.32 (d, 2H, J = 8.7 Hz, H*g*), 1.06 ppm (s, 9H, H*i*).

Multi-component self-assembly of porphyrins and subphthalocyanines

Outline

1. Introduction

For a long time, the design of coordination-driven self-assembled compounds has been mostly limited to two-component systems, where only one metallic and one organic building-blocks are combined.[1] Although this approach enables easy design and control of the resulting structures, the library of compounds that could be obtained is reduced by the lack of versatility in the building-blocks employed. Development of selective methods for metal-directed multi-component self assembly is essential in this context, since it will extend the diversity of self-assembled structures and the functionalities that can be incorporated in these systems.

Multi-component self-assembly is a process where multiple building-blocks can selectively recognize and combine to generate a single discrete structure.[2] Inclusion of sufficient information within the building-blocks in order to provide selectivity in molecular recognition still represents an active task in supramolecular chemistry.

In the field of coordination-driven self-assembly, topological information as well as steric constraints have already been employed for selective multi-component self-assembly.[3] However, any of these approaches usually requires an important synthetic effort. Template effect has also been employed in this field, providing a simple strategy for the self-assembly of molecular prisms.[4]

---

[1] (a) P. J. Stang, B. Olenyuk, *Acc. Chem. Res,* **1997**, *30*, 502-518; (b) B. J. Holliday, C. A. Mirkin, *Angew. Chem. Int. Ed*, **2001**, *40*, 2022-2043; (c) M. Fujita, M. Tominaga, A. Hori, B. Therrien, *Acc. Chem Res*, **2005**, *38*, 369-378; (d) J. R. Nitschke, *Acc.Chem. Res.* **2007**, *40*, 103-112; M. Ruben, J. Rojo, F-J. Romero-Salguero, L. H. Uppadine, J-M. Lehn, *Angew. Chem. Int. Ed.*, **2004**, *43*, 3644-3662.

[2] (a) J.-M. Lehn, *Science* **2002**, *295*, 2400-2403; (b) J.-M. Lehn, *Rep. Prog. Phys.* **2004**, 67–249; (c) J.-M. Lehn, *Chem. Soc. Re*v. **2008**, *36*, 151-160.

[3] (a) J-P. Sauvage, J. Weiss, *J. Am. Chem. Soc.* **1985**, *107*, 6108-6110; (b) J. F. Nierengarten, J. F.; C. O.Dietrich-Buchecker, J.-P.Sauvage, *J. Am. Chem. Soc.* **1994**, *116*, 375-376; (c) M. Schmittel, A. Ganz, D. Fenske, *Org. Lett.* **2002**, *4*, 2289-2292; (d) M. Schmittel, K. Mahata, *Inorg. Chem.* **2009**, *48*, 822-824; (e) Y. Yamauchi, M. Fujita, *Chem. Commun.* **2010**, *46*, 5897-5899; (f) M. Yamanaka, Y. Yamada, Y. Sei, K. Yamaguchi, K. Kobayashi, *J. Am. Chem. Soc.* **2006**, *128*, 1531-1539.

[4] (a) K. Kumazawa, K. Biradha, T. Kusukawa, T. Okano, M. Fujita, *Angew. Chem., Int. Ed.* **2003**, *42*, 3909-3913; (b) M. Yoshizawa, J. Nakagawa, K. Kurnazawa, M. Nagao, M. Kawano, T. Ozeki, M. Fujita, *Angew. Chem., Int. Ed.* **2005**, *44*, 1810-1813.

1.1. Background and objectives

Recently, Stang and coworkers have reported a new selective multi-component strategy for metal-directed self-assembly.[5] This methodology employs a Pt (II)-phosphine metal complex and pyridyl- and carboxylate-substituted organic ligands. Selectivity results from an energetic preference towards Pt-N,O coordination instead of Pt-O,O or Pt-N,N. This strategy has allowed direct self-assembly of two- and three-dimension structures, as well as their indirect construction through supramolecule-to-supramolecule transformations.

This selective self-assembly event was first reported in 2010, when a multi-component metallosupramolecular rectangle was directly obtained from the stoichiometric 2:2:1 mixture of sodium *tert*phthalate, 1,4-bis(4-pyridyl)ethynilbenzene and $Pt(PEt_3)OTf_2$ in quantitative yield. ^{31}P-NMR spectrum showed two doublets of equal intensity at 1.06 and 6.60 ppm (Figure 1), which is indicative of an heteroleptic coordination motif at the metal center.[6]

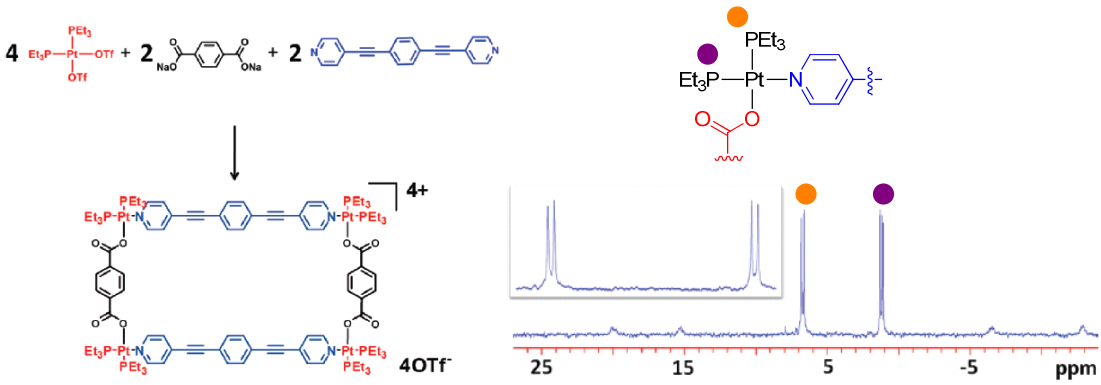

Figure 1. Example of multi-component self-assembly via heteroleptic coordination to Pt, and characteristic ^{31}P-NMR spectrum of this kind of compounds.

Selective self-assembly of these multi-component metallosupramolecular structures can be achieved not only by the conventional strategy of mixing the individual building-blocks, but also via supramolecule-to-supramolecule transformations. Such event takes

[5] Y.-R. Zheng, Z. Zhao, M. Wang, K. Ghosh, J. B. Pollock, T. R. Cook, P. J. Stang, *J. Am. Chem. Soc*, **2010**, *132*, 16873-16882.

[6] (a) K.-W Chi, C. Addicott, A. M. Arif, P. J. Stang, *J. Am. Chem.Soc.* **2004**, *126*, 16569-16574; (b) K.-W. Chi, C. Addicott, Y. K. Krishenko, P. J. Stang, *J. Org. Chem*, **2004**, *69*, 964-966.

place when a supramolecule alters its structure and composition as a consequence of an external stimulus; for example, photochemical, electrochemical or chemical signals.[7]

This event was investigated with two approaches. Firstly, the mixture of two different two-component structures (a symmetric self-assembly with pyridines and another one with carboxylates) gave rise, after equilibration, to the multi-component compound, as confirmed by the typical signals in ^{31}P-NMR spectrum.

Secondly, further evidence of this supramolecule-to-supramolecule transformation (Figure 2) was obtained upon portionwise addition of a carboxylate triangle onto a solution of pyridyl square. The transformation could be followed by ^{31}P-NMR, which showed progressive formation of the multi-component rectangle.

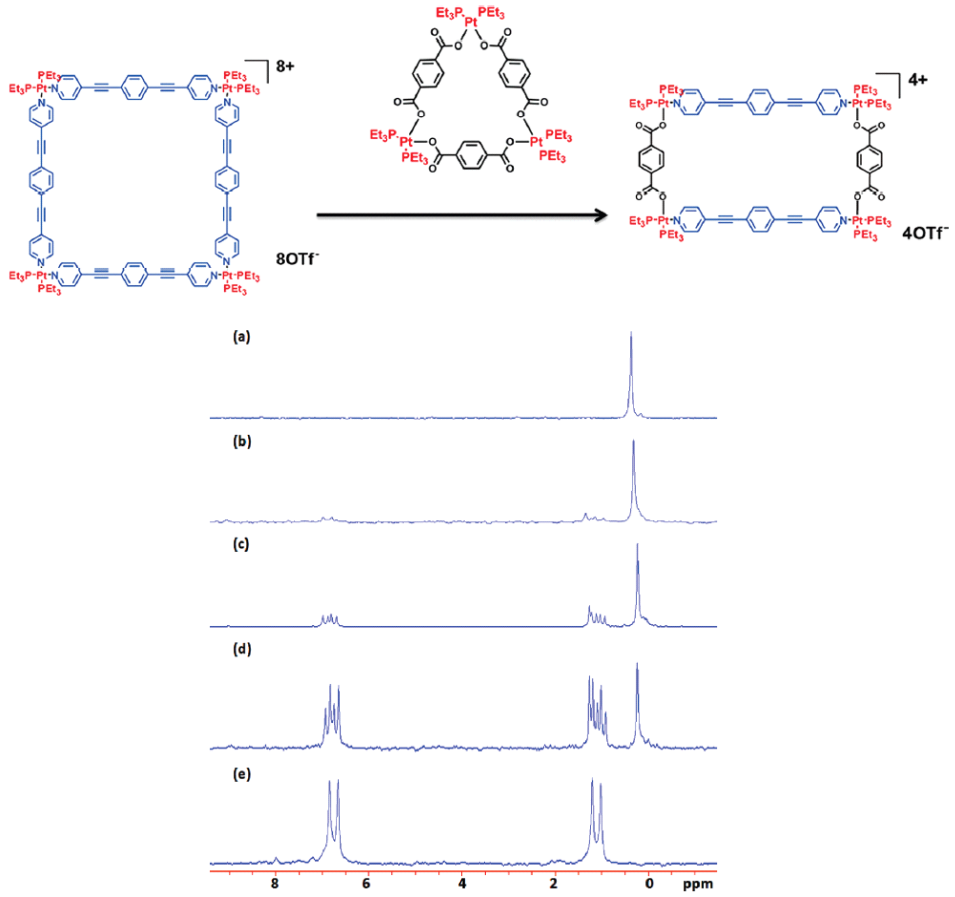

Figure 2. Supramolecular trasformation of a pyridyl-square into a multi-component rectangle upon addition of a carboxilate-triangle.

[7] (a) S.-S.Sun, C. L. Stern, S. T. Nguyen, J. T. Hupp, *J. Am.Chem. Soc.* **2004**, *126*, 6314-6326; (b) J. Heo, Y.-M. Jeon, C. A. Mirkin, *J. Am. Chem. Soc.* **2007**, *129*, 7712-7713.

This multi-component self-assembly approach has served, for example, for designed modification of two-component supramolecular structures,[8] or for the direct self-assembly of a catenane from ten different building-blocks (Figure 3).[9]

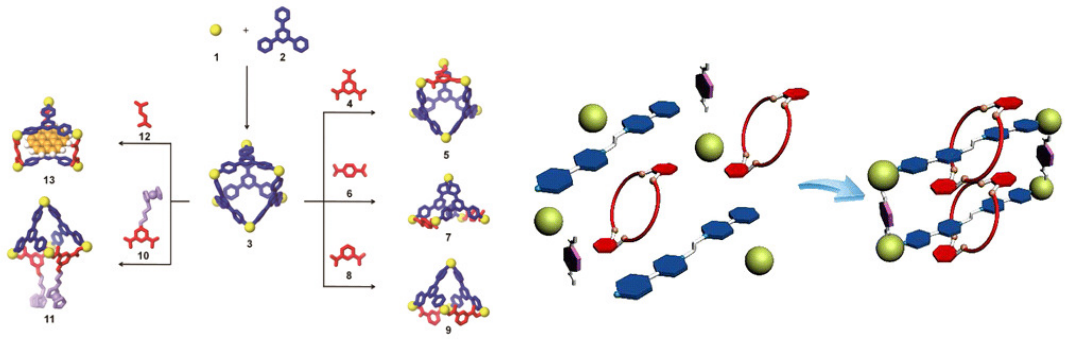

Figure 3. Examples of the applications of metal-directed multi-component self-assembly.

The main objective of this chapter is the application of metal directed multi-component self-assembly to the supramolecular organization of chromophores in three-dimension structures. The initial objectives of this thesis, according to the corresponding section (see page 18) envisaged to focus on the supramolecular organization of SubPcs. However, along the progress of the work, we decided to include also the work on porphyrin chromophores, which was developed during a predoctoral stay at the University of Utah under the guidance of Prof. Stang.

Therefore, the first section of the chapter is dedicated to the self-assembly of tetragonal prisms (Figure 4) where the top and down faces are 5,10,15,20-tetra (4-pyridyl) porphyrins (tpyP). Six dicarboxylate ligands of different flexibility and length will be employed to study the impact of these features in the properties of the self-assembled structures. Moreover, five series of these prisms, differing in the metal located at the cavity of the porphyrin, will be prepared.

[8] Y.-R. Zheng, W.-J. Lan, M. Wang, T. R. Cook, P. J. Stang, *J. Am. Chem. Soc*, **2011**, *133*, 17045-17055.
[9] S. Li, J. Huang, T. R. Cook, J. B. Pollock, H. Kim, K.-W. Chi, P. J. Stang, *J. Am. Chem. Soc,* **2013**, *135*, 2084-2087.

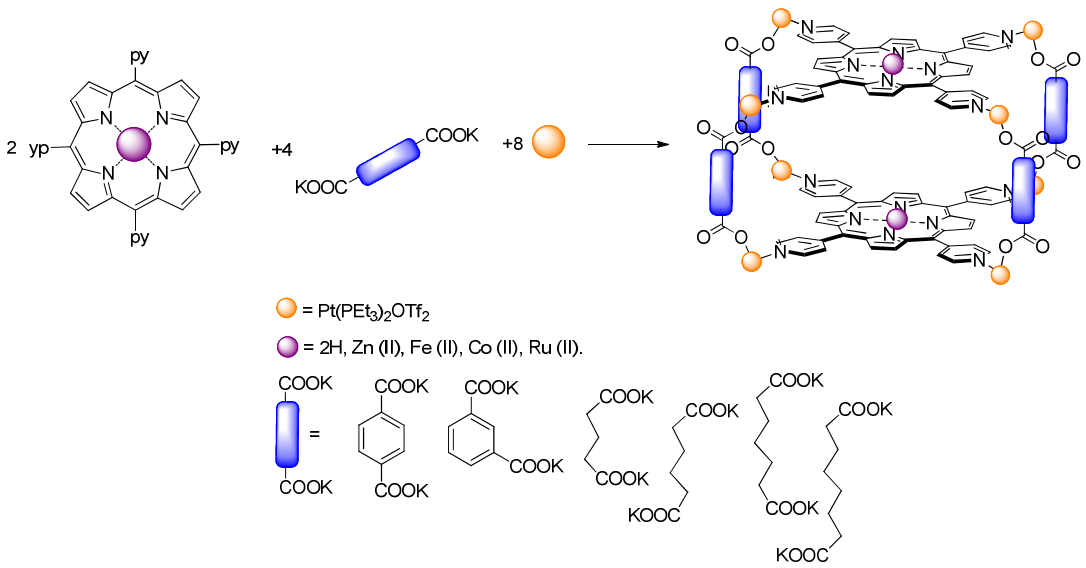

Figure 4. Porphyrin-based prisms.

Such compounds might find applications as catalysts in water splitting reactions, (Figure 4) and their activity may be modulated by the redox properties of the metal inside the porphyrin. Additionally, the flexibility of prisms and distance between the porphyrins, parameters which are determined by the dicarboxylate ligands, may also tune the catalytic activity, and at the same time allow to gain some insight into the mechanism or possible intermediates of the reaction.

Secondly, we addressed the study of multicomponent self-assembly on SubPcs. (Figure 5) Namely, hexapyridyl-substituted SubPc had been previously prepared in our group with the aim of self-assembling homodimeric capsules with Pd (II) salts. However, the formation of the desired capsule could not be confirmed.

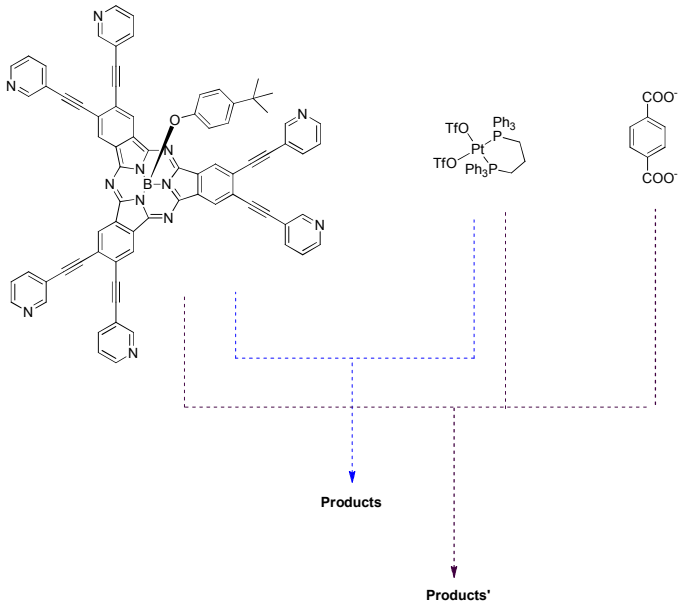

Figure 5. Scheme of the study of self-assembly of hexapyridyl SubPc.

The proximity of two pyridines on the same benzene ring of the SubPc may lead to the formation of chelated structures, where these two pyridines coordinate to the same metal center. This product may compete with the formation of a homodimeric capsule. Hence, we decided to employ the additional thermodynamic stabilization that heteroleptic coordination to Pt (II) metal centers provides in order to prevent this possible chelate effect, and thus, organize hexapyridyl SubPc into a homodimeric capsule which, moreover, will possess a bigger cavity than the one arising from self-assembly with only metal centers. The possibilities this cavity offers in host-guest chemistry, catalysis, etc will not be addressed, as they are out of the scope of this work.

To sum up, the objectives of the second section of the present chapter will be the study of coordination-driven self-assembling properties of hexapyridyl-SubPc in the context of homo- and heteroleptic coordination. Additionally, we intend to achieve some insight into the thermodynamic and kinetic features of the products formed.

2. Multicomponent self-assembly of Porphyrin-based prisms

2.1. Self-assembly

2.1.1. Free-base porphyrin prisms

The first attempts to obtain free-base porphyrin prisms **18a-f** (Figure 6) were carried out following the procedure described in the literature.[5] Firstly, the building-blocks were stirred at 70ºC in a mixture of acetone and water (4:1). This mixture provides an accurate medium to make soluble the dicarboxylate salts as well as the neutral organic dipyridyl ligand and the Pt complex. After 4 hours of stirring, some products of coordination of both ligands to Pt are observed, but many intermediates or incomplete assemblies remain due to the presence of water. Hence, solvents were evaporated, and the mixture was again stirred at 70ºC in acetone for 4 hours more. Despite the success of this procedure in simpler multicomponent assemblies previously prepared in the group, such conditions hardly ever worked as expected for porphyrin prisms. In general, the ^{31}P-NMR spectra showed the desired prism signals and other singlet(s) corresponding to intermediates or unreacted Pt complex.

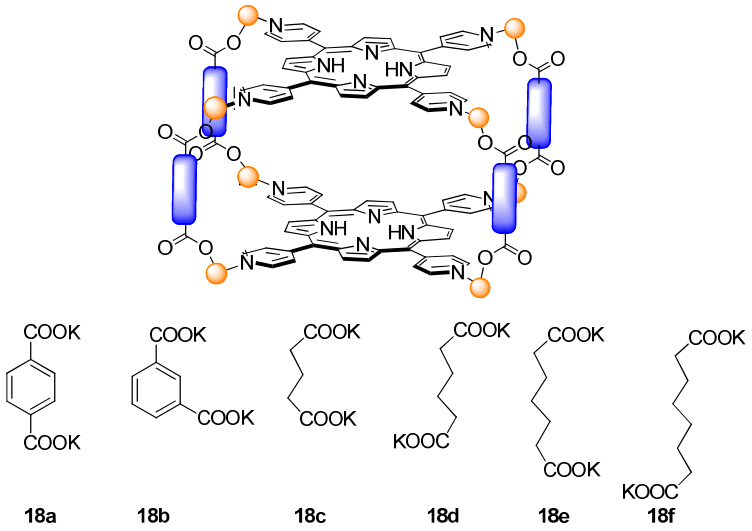

Figure 6. Serie of free-base porphyrin prisms.

Thus, the development of a new procedure for multicomponent self-assembly was necessary. Screening of different solvents was carried out (Table 1).

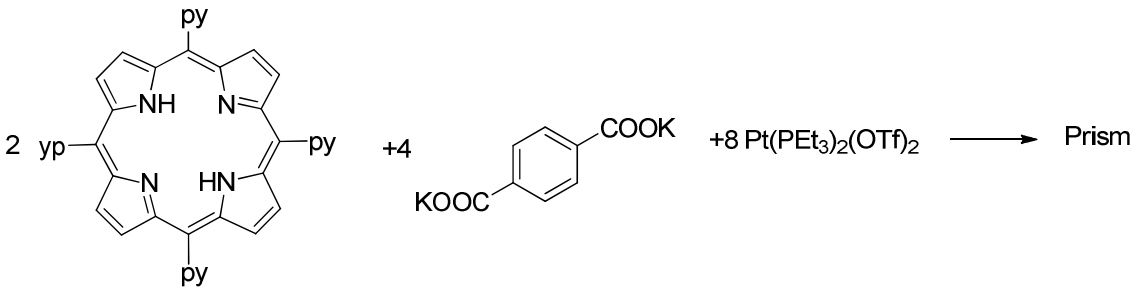

Figure 7. Self-assembly of free-base porphyrin prisms

Table 1. Screening of conditions for multi-component self-assembly.

sample	Porphyrin	Carboxilate	$Pt(dppp)OTf_2$	conditions
Blank	0.81 mg	0.64 mg	3.79 mg	1)acetone/water 8:1,4h, 65℃ 2)Acetone, 4h, 70℃
A	0.82 mg	0.66 mg	3.83 mg	1)acetone/water 8:1,4h, 65℃ 2)$MeNO_2$, 4h, 70℃
B	0.78 mg	0.60 mg	3.67 mg	1) MeCN/ water 8:1,4h, 65℃ 2)$MeNO_2$, 4h, 70℃
C	0.88 mg	0.73 mg	4.11 mg	1) $MeNO_2$/ MeOH 8:1,4h, 65℃ 2)$MeNO_2$, 4h, 70℃
D	0.77mg	0.61 mg	3.64 mg	CH_2Cl_2/ $MeNO_2$/MeCN 1:1:1, 4h, 65℃

In sample A, only the solvent employed in the second step was modified. Acetone was substituted by nitromethane, expecting that the higher coordinating power of this solvent would break more easily the H_2O-Pt bonds that might exist in the intermediates.

Samples B and C were addressed to study if replacement of acetone/water mixture in the first step was possible. In both cases $MeNO_2$ was maintained as solvent for the second step, due to the good result obtained in A (see below).

Finally, and considering that water was not necessary for the self-assembly to occur (sample C), self-assembly was attempted in a mixture of three organic solvents (sample D). Dichloromethane was incorporated to improve the initial solubility of the porphyrin; nitromethane and acetonitrile provide higher polarity to the mixture and the possibility to increase the temperature if necessary.

After 10 min heating, the solubility of the building blocks in each mixture was the following: C>D>B>A. In sample C the reagents were fully dissolved, D showed some not soluble carboxylate and porphyrin, and in A and B there was only some not dissolved porphyrin, but a higher amount than in the case of D. After one hour of reactions, all components were dissolved in all samples.

Solvents were evaporated with an air flow in all cases after the solutions were cooled down to room temperature.

^{31}P-NMR showed in all cases the two doublets corresponding to the multicomponent self-assembly. Small amounts of impurities were detected in B and C. (Figure 8)

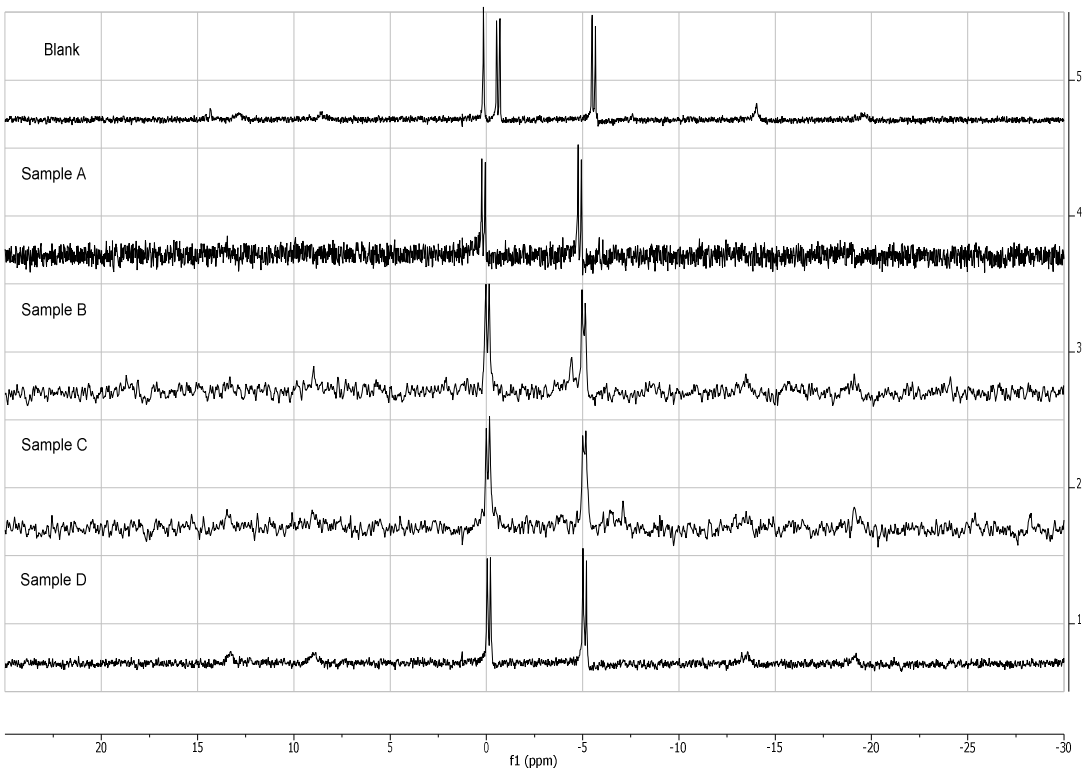

Figure 8. ^{31}P-NMR spectra of the samples employed in the screening of solvents for self-assembly.

Conditions of sample D were chosen as the optimum, since it is a one-pot procedure that allows the direct and successful assembly of the porphyrin prisms.

Prisms with C_8, C_6, terphthalic and isophthalic diacid salts were self-assembled without remarkable issues with the previously discussed one-pot procedure. In contrast, C_7 and C_5 diacid salts didn't form the prisms so easily. C_7 prism required overnight reflux to reach equilibrium, while self-assembly of C_5 prism never occurred. From these observations we conclude that odd-number alkyl chains present more difficulties to arrange themselves to fulfil the required geometry of the coordination sphere of Pt. Moreover, and in addition to this drawback, C_5 might be too short to form the prism properly. The self-assembly of a porphyrin prism with succinic acid salt (C_4 alkyl chain) failed, too, which is in good agreement with the previous explanation.

Flexibility of the dicarboxylate influences the solubility of the resulting prisms, which follows this trend: isophthalate < terphthalate < C_6 ~ C_7 ~ C_8.

Vapour diffusion of diethyl ether into a dichloromethane solution of **18f** (with PF^-_6 as counteranion) afforded small crystals, but their quality was not adequate for X-Ray diffraction analysis.

2.1.2. Zn (II) porphyrin prisms

Metallation of the porphyrin with Zn(II) was carried out directly on the prisms (Figure 9).

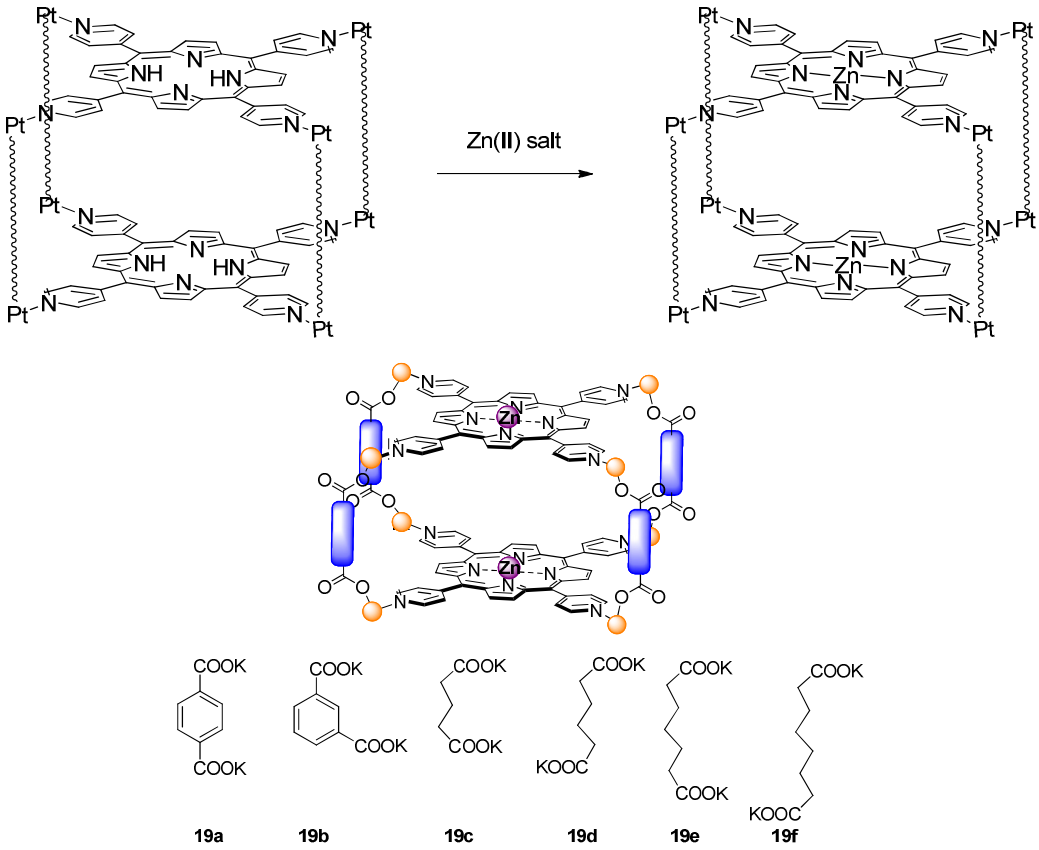

Figure 9. Metallation of porphyrin prisms with Zn (II) and schematic representation of the library of compounds obtained.

Firstly, the most common procedure to obtain zinc porphyrins (ZnP) was attempted,[10] which consists in treating the porphyrin (or the prism in this case) with an excess of $Zn(OAc)_2$ in a 3:1 mixture of chloroform and methanol.

When the reaction was carried out at room temperature, the ZnP prism was achieved in low yield (<20%). Thus, the reagents were refluxed (65ºC) in order to increase the amount of product. Unfortunately, in these conditions the prism split up. (Figure 10). The singlet observed in ^{31}P-NMR corresponds to trigonal prism **20**, containing three ZnPs and six Pt atoms.

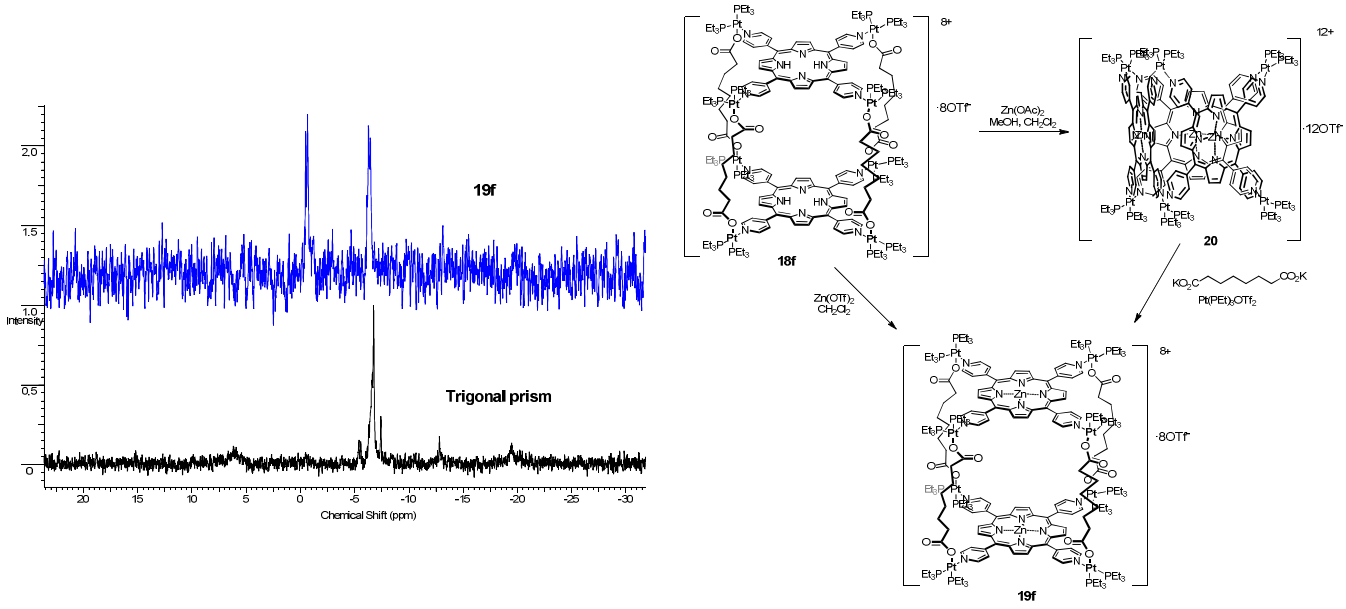

Figure 10. Scheme of the reactions attempted for obtaining the Zn (II) metalated multi-component prisms, and ^{31}P-NMR spectra of the products.

From compound **20** it was possible to re-assemble the multicomponent prism adding the corresponding amount of carboxylate and $Pt(PEt_3)_2OTf_2$. The reagents were dissolved in the CH_2Cl_2/ $MeNO_2$/MeCN 1:1:1 mixture and heated up at 50ºC for 5 hours (Figure 10).

Direct metallation of the porphyrin proceeded at room temperature (40-50% yields) treating the prisms with an excess of $ZnOTf_2$ in dichloromethane. Furthermore, the products crashed out from the solution; thus, isolation of the ZnP prisms was quite

[10] M. E. Milanesio, M. Gervaldo, L. A. Otero, L. Sereno, J. J. Silber, E. N. Durantini, *J. Phys. Org. Chem,* **2002**, *15*, 844–851.

straightforward. The use of $ZnOTf_2$ instead of $ZnOAc_2$ also prevents anion exchange during the reaction.

2.1.3. Fe (II) porphyrin prisms

In general, metallation of porphyrins with Fe (II) involves many difficulties. Firstly, it requires high temperatures (DMF or toluene are the most commonly employed solvents). On the other hand, Fe(II) oxidizes very easily to Fe(III), and in that case, NMR characterization is not possible.

Inclusion of Fe into the Porphyrin cavity was carried out before self-assembly. This synthetic pathway was chosen on the basis of the experimental procedure for porphyrin metalation with iron, which in general requires high temperatures that would cause decomposition of the prisms.

Fe (II) Porphyrin (Figure 11) was obtained refluxing the tpyP in DMF for 3 hours in the presence of $FeCl_2$.[11] This method was reported for the preparation of Fe(III) porphyrins, and as a consequence, the oxidation step involving treatment with HCl was avoided. Unfortunately, the product of the reaction could not be characterized in ^{1}H-NMR due to its low solubility in every solvent we tried.

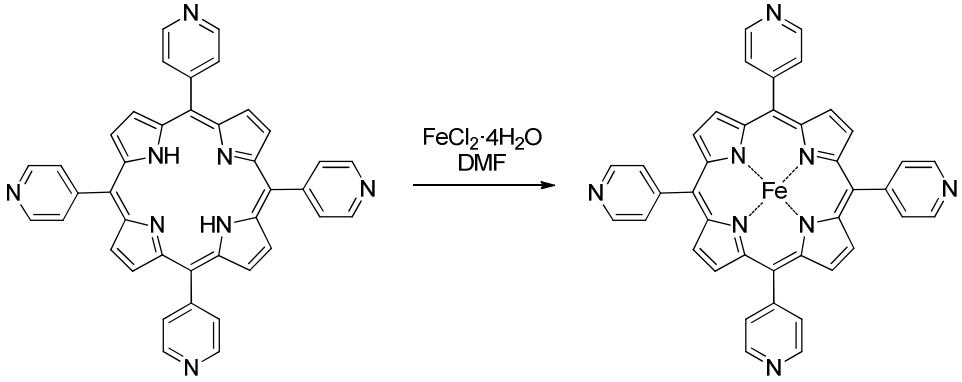

Figure 11. Metallation of tpyP with Fe(II).

Self-assembly of a porphyrin prism was then attempted blindly in the same conditions employed for free-base tpyP. Unfortunately, an important amount of material remained unsoluble, and analysis of the mixture in ^{31}P-NMR showed one singlet at ~ 0 ppm.

[11] H. Kobayashi, T. Higuchi, Y. Kaizu, H. Osada, M. Aoki, *Bull. Chem. Soc. Jpn,* **1985**, *48*, 3137-3141.

Thus, stepwise formation of the prism was attempted. Firstly, the FeP was stirred at 70ºC in $MeNO_2$ to partially dissolve it. Subsequently, the Pt acceptor was added and the mixture stirred 4h at 70ºC. ^{31}P-NMR spectrum (Figure 12) showed 2 peaks at ~ 0 and 0.5 ppm after this process. Finally, the C_8 dicarboxylate was added and the solution was again stirred at 70ºC for 4h. Four signals were then observed in ^{31}P-NMR spectrum, all of them presenting the same intensity. After stirring for 4 hours more, two of these doublets became predominant in the spectrum. Purification was carried out via anion exchange with an excess of KPF_6.

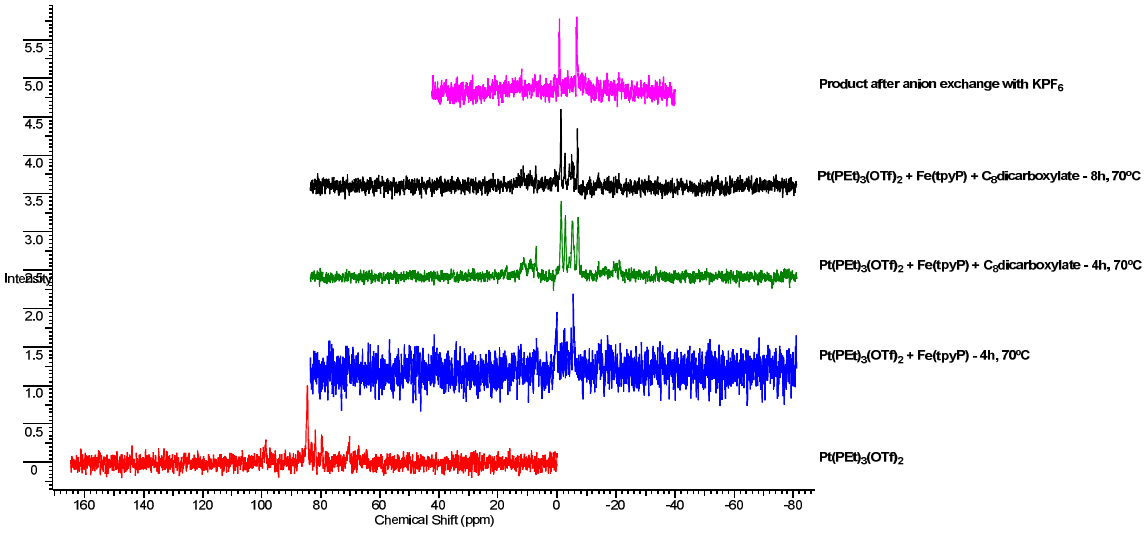

Figure 12. ^{31}P-NMR spectra obtained upon following the stepwise self-assembly of Fe(tpyP) prism with potassium octanedioate and $Pt(PEt)_3(OTf)_2$.

The other prisms bearing Fe(II) porphyrins were formed following similar procedure, although in some cases anion exchange could not fully eliminate the impurities.

2.2. Characterization

All compounds were characterized by mutinuclear NMR (^{1}H, ^{31}P), and mass spectrometry (electrospray).

Free-base Porphyrin prisms showed two doublets in ^{31}P-NMR spectra, at approximately -0.5 and -5.5 ppm. Metallation of the macrocycle with Zn (II) or Fe (II) barely affected to the position of the doublets (Figure 13). Inclusion of the metal into the Porphyrin was reflected in ^{1}H-NMR, where a small shift of the Porphyrin protons occurred and the signal of the NH protons of the free base (located at -3 ppm) disappeared after metallation. This fact was clearly observed for Zn (II) porphyrin

prisms, whereas we had a lot of difficulties to fully characterize Fe (II) porphyrin prisms in ^{1}H-NMR, most likely because of the oxidation of the metal to Fe (III). Moreover, the color of the prisms (Figure 13) changed from brown to green when the Porphyrin was metallated with Zn (II).

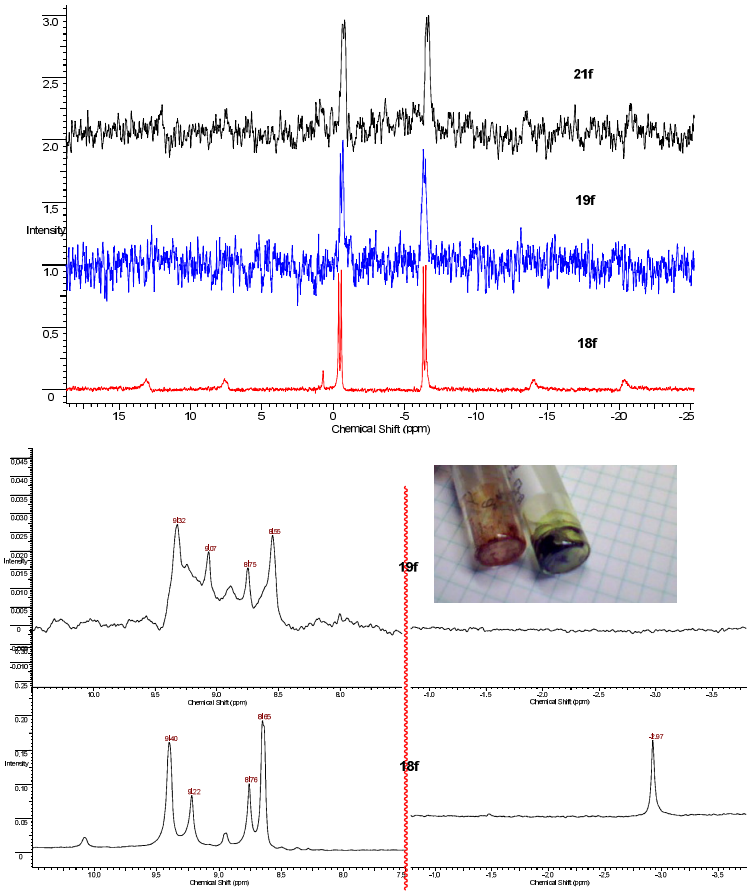

Figure 13. ^{31}P-NMR spectra of **18f**, **19f**, and **21f** prisms; ^{1}H-NMR spectra of **18f** and **19f**. Inset shows a picture of a free-base and a Zn (II) tpyP prism.

^{1}H-NMR spectra showed in all cases the signals corresponding to the Porphyrin, the carboxylate and the ethyl groups on the phosphines. An interesting feature observed in the case of alkyl-dicarboxylate prisms was that the signals of the protons corresponding to the Porphyrin ring shifted as a function of the alkyl chain length. This effect might be related either to the distance between the porphyrins or to their relative disposition (Figure 14). In any case, this observation seems to indicate that the symmetry of the prism increases with the length of the alkyl chain.

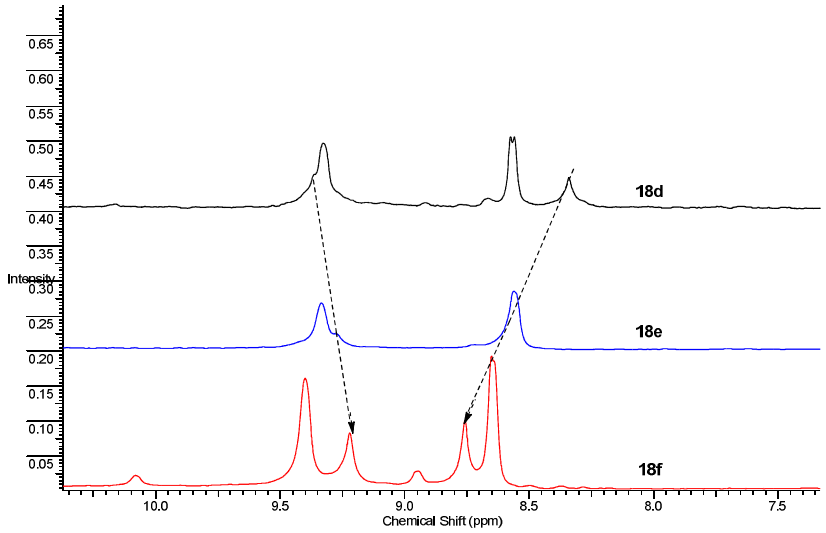

Figure 14. ^{1}H-NMR spectra of compounds **18d-f**, showing the progressive shift of signals of porphyrin protons.

Prisms self-assembled with *tert*- and *iso*- phthalates show the signals for the Porphyrin protons at approximately the same chemical shifts; 9.3-7.1 ppm and 9.3-7.3 ppm, respectively.

Finally, mass spectrometry experiments confirmed the formation of the free-base Porphyrin prisms. Namely, we could observe the signals of M-3OTf^{-} for all free-base porphyrin prisms, whose isotopic distribution fitted quite well the theoretical one (Figure 15).

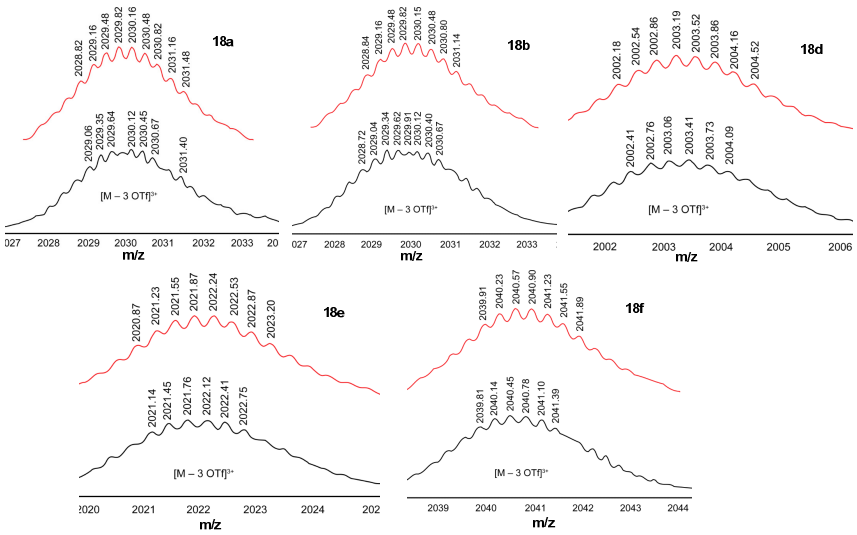

Figure 15. Peaks corresponding to [M-3OTf]$^{3+}$ of compounds **18a-f**. Theoretical (red) and experimental (black) isotopic distributions are shown.

3. Kinetic and thermodynamic aspects of multicomponent self-assembly of Hexapyridyl-Subphthalocyanine

3.1. Synthesis of Building-blocks

Synthesis of hexapyridyl SubPc (Figure 16) was addressed starting from phthalimide. This compound was treated with iodine to afford 4,5-diiodophthalimide **22** in 54% yield. Subsequently, compound **22** was stirred in ammonia to produce opening of the phthalimide. Finally, amides of compound **23** were dehydrated in the presence of thiolnyl chloride. Phthalonitrile **24** was obtained in 20% global yield.

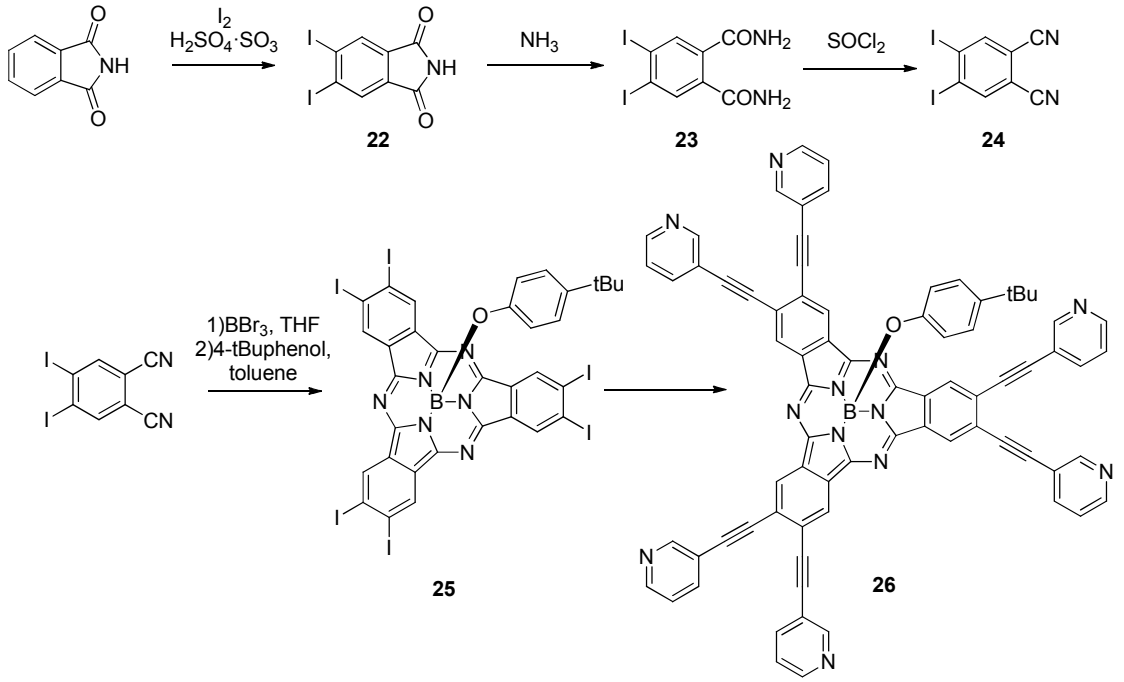

Figure 16. Synthesis of hexapyridyl-SubPc **25**.

Cyclotrimerization of 4,5-diiodophthalonitrile was carried out employing the method described by Sharman and van Lier in 2005.[12] While the common experimental procedure for the synthesis of SubPcs involves treatment of the starting material with BCl_3 at high temperature (reflux of *p*-xylene, 135°C), the low solubility and reactivity of compound **24** requires a different approach. As described in the aforementioned article by van Lier and coworkers, 4,5-diiodophthalonitrile was treated with BBr_3 1M solution in

[12] W. M. Sharman, J. E. van Lier, *J. Porphyrins Phthalocyanines,* **2005**, *9*, 651-658.

dichloromethane* at room temperature, and after 5 minutes of stirring, THF was added, and the mixture was refluxed at 60°C for one hour. Axial bromine was exchanged in situ; after removal of volatiles and solvent and without further purification, 5 equivalents of 4-*tert*-buthylphenol and a small amount of toluene were added, and the resulting mixture was refluxed until the reaction was complete (checked by TLC).

Finally, the six pyridines were incorporated by means of a Sonogashira cross-coupling reaction catalyzed by $Pd(PPh_3)Cl_2$, which afforded the desired SubPc **26** in 71% yield.

On the other hand, Pt complex **12c** was prepared as described in the previous chapter of this thesis.

Sodium *tert*phthalate was prepared by treatment of *tert*phthalic acid with an aqueous saturated solution of sodium bicarbonate.

3.2. Self-assembly

Before studying self-assembly of multi-component structures based on SubPcs, the self assembly of SubPc **26** only with the platinum complex **12c** was performed (Table 2). This process was carried out in 1:3 and 2:5 (defect of **12c**) SubPc/metal complex stoichiometries, employing dichloromethane as solvent. The products obtained in these reactions were purified by precipitation from the concentrated dichloromethane solutions and separated by gel permeation chromatography.

Table 2. Summary of the self-assembly processes studied.

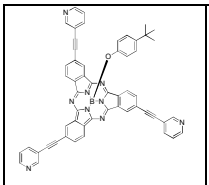	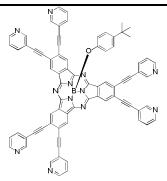	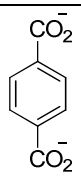	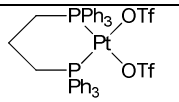
	1		3
	2		5
2		3	3
	2	6	12

* This synthetic route was optimizad by Dr. Yannik Rio in our group.

On the other hand, multi-component self-assembly was carried out in the conditions described above for Porphyrin prisms. In this case, all compounds were self-assembled with sodium *tert*phthalate. Firstly, SubPc **11** was mixed in 2:3:6 stoichiometry (SubPc/dicarboxylate/**12c**, respectively), in order to check if the dycarboxyate ligand was accurate for the self-assembly of this kind of structures.

Secondly, the behaviour of hexapyridyl-substituted SubPc **26** was examined in the context of multi-component self-assembly. Self-assembly was carried out in 2:6:12 SubPc/dicarboxylate/**12c** stoichiometry. Products crashed out from the concentrated reaction mixture upon addition of diethyl ether. Again, gel permeation chromatography allowed the separation of products and by-products present in the reaction mixtures.

3.3. ^{31}P-NMR studies and Characterization of products

3.3.1.Two-component self-assembly

When SubPc **26** and **12c** were mixed in 1:3 stoichiometry, a single product was obtained when equilibrium was reached. This product showed a singlet in ^{31}P-NMR spectrum (Figure 17), and thus, it was identified as a homodimerc capsule. This hypothesis was confirmed in mass spectrometry, where peaks at m/z = 3262.12 and 1630.3, which fit fragmentations of **27**, were found.

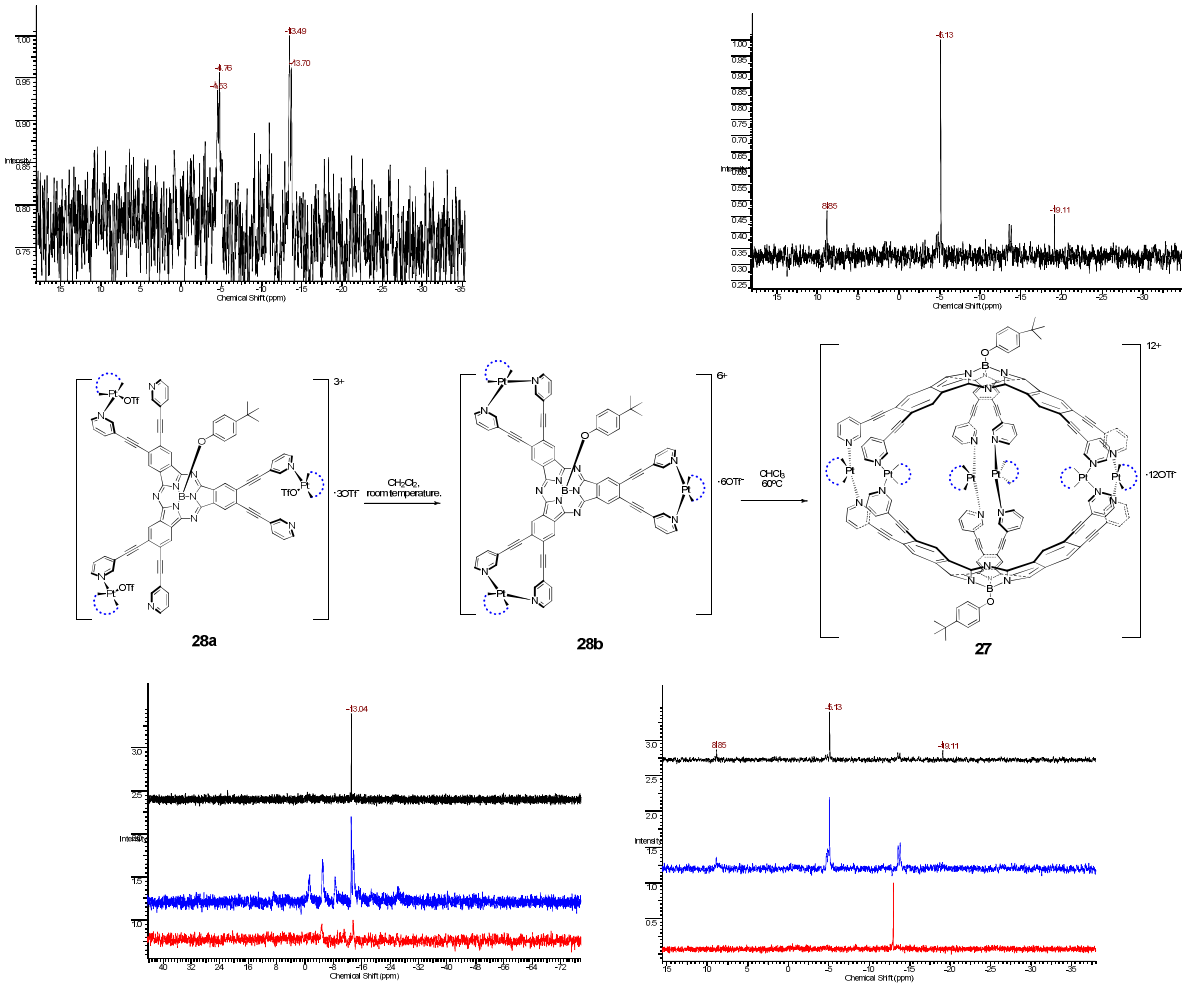

Figure 17. Top: ^{31}P-NMR of **28a** and **27**. Middle: Hypothesis explaining the signals observed in the progress of self-assembly of SubPc **27** and **12c**. Low: Evolution of ^{31}P-NMR spectra during self-assembly.

Along the progress of this self-assembly other peaks were noted in ^{31}P-NMR (Figure 17). Gel permeation chromatography of the non equilibrated mixture allowed the separation of two products: firstly, the aforementioned homodimeric capsule **27**, and secondly, another compound (**28a**) that shows two doublets in its ^{31}P-NMR spectrum. If **27** is left in dichloromethane solution for two days, it slowly equilibrates to **28b** (Figure 17), which shows only one singlet in ^{31}P-NMR. On the basis of ^{31}P-NMR spectra, the structure of **28a** should be a compound where Pt centers present heteroleptic coordination. Mass spectrum of this product showed the same signal as the one for **27** at m/z = 1631.30, plus an additional one, also +2 cation, at m/z = 1320.15, which fits a product coming from the fragmentation of a structure formed by one SubPc and three Pt complexes; $[M\text{-}Pt(dppp)\text{-}4OTf^-]^{2+}$. Mass spectrum of **28b** presented the same signals. Thus, our hypothesis to explain these data is that in **28a** three Pt centers are coordinated to three pyridyl moieties (Figure 17). Then, this compound slowly evolves

to a structure, **28b**, which is more stable due to the chelate effect that arises from the coordination of the two pyridines on the same benzene ring to the metal.

Moreover, both **28a** and **28b** evolved to **27** after one hour of chloroform reflux.

In the case of the self-assembly in 2:5 stoichiometry, which involves a defect of **12c**, the same singlet at -5.08 ppm in ^{31}P-NMR was also found as major product, which corresponds to **27** (Figure 17). Additionally, ^{31}P-NMR shows some couples of doblets, which may be consistent with the formation of species of similar structure as **28a**. None of this species could be isolated in enough quantity to be fully characterized.

3.3.2. Three-component self-assembly

The study of multi-component self assembly on SubPcs started with the formation of the capsule **29** (Figure 18), which was performed mainly to check the accuracy of the chosen dicarboxylate ligand (*tert*phthalate).

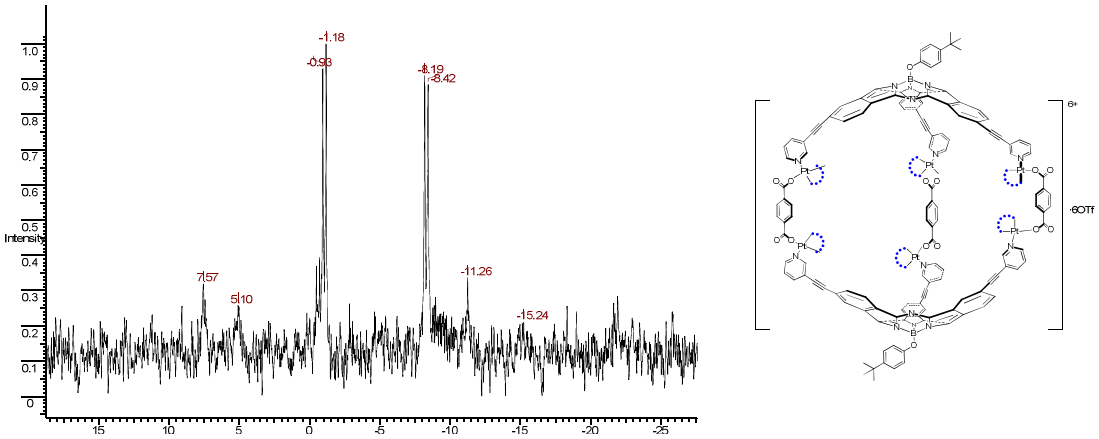

Figure 18. ^{31}P-NMR spectrum and structure of **29**.

Subsequently, multi-component self-assembly was carried out with SubPc **26**. After one night of reaction at 60 ºC, ^{31}P-NMR spectrum of the mixture showed, surprisingly, four doublets instead of the two we expected. This is consistent with the formation of capsule **30** (Figure 19) as a mixture of two isomers that arises from the possible conformations of the pyridines.

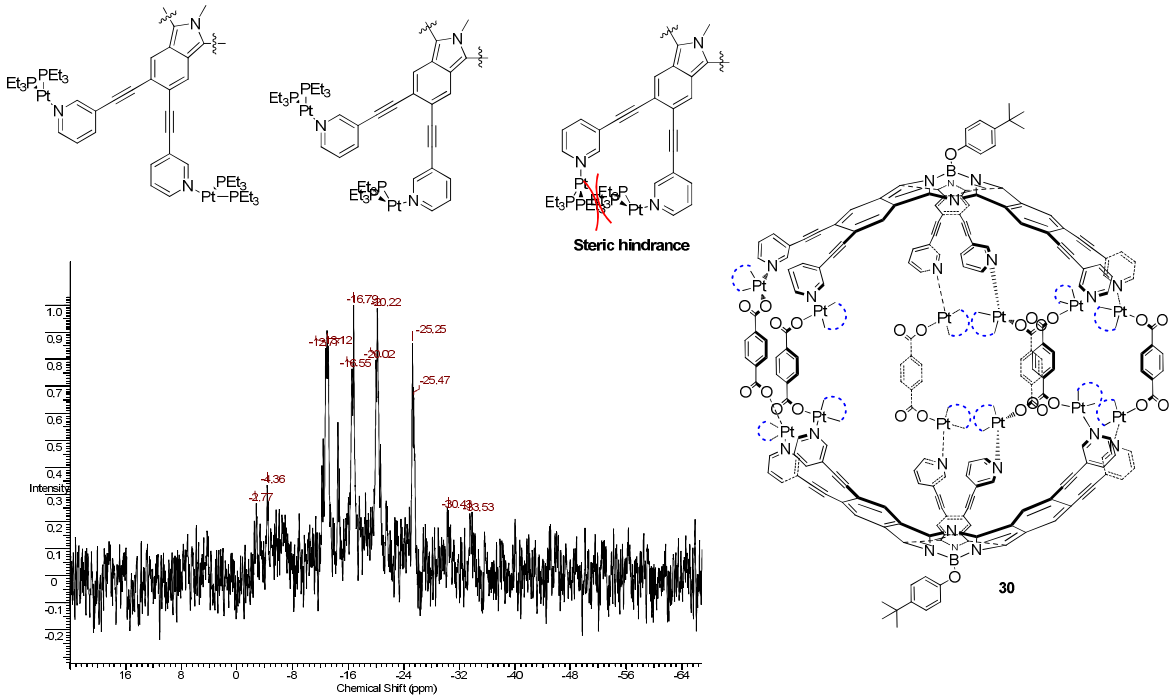

Figure 19. Representation of the conformations that can be adopted by the pyridines of SubPc **26**; Capsule **30** and ^{31}P-NMR spectrum of the final product of multi-component self-assembly of SubPc **26**.

During the course of the reaction, especially at the first stages, some amount of **27** and other intermediates that could not be identified were observed in ^{31}P-NMR.

In view of these results, we can establish a qualitative trend in the thermodynamic stability of the products of self-assembly of hexapyridyl-substituted SubPc: **28a** < **28b** < **27** < **29**.

4. Summary and Conclusions

Along this chapter, metal-directed organization of pyridyl-substituted chromophores has been studied.

In the first section, porphyrin prisms were prepared, whose distance between the porphyrin moieties was tuned via the dicarboxylate ligand, thus also allowing different degrees of flexibility. In this context, a one-pot procedure for the self-assembly of multi-component pyridyl-carboxylate structures was developed. The use of dicarboxylate ligands of different flexibility allowed the observation of a marked trend in the solubility of the resulting prisms. Moreover, in the particular case of alkylic dycarboxylates, the success of self-assembly was determined to be dependent on the odd or even number of carbon atoms. This effect was explained by the different arrangement of the coordinating groups in each case; that implies that even-numbered alkylic dicarboxylates fit better the coordination geometry of the Pt centers.

Corresponding prisms bearing Zn (II) and Fe (II) into the cavity of the prisms were also prepared envisaging future application of these compounds as catalysts of redox reactions. Zn (II) was included by direct treatment of the free-base porphyrin prisms with $Zn(OTf)_2$. Inclusion of Fe (II), in contrast, was carried out through metallation of the porphyrin before self-assembly. Unfortunately, the easy oxidation of Fe (II) to Fe (III) prevented complete characterization of the prisms.

On the other hand, in the second section of this chapter, a study of the properties of hexapyridyl-substituted SubPc **26** was addressed. This compound was studied firstly in the direct self-assembly with a Pt (II) complex, in a similar way to the formation of homodimeric capsules described in Chapter 1. In that case, two kinetic products could be isolated and identified. The thermodynamic product of this process was the corresponding homodimeric capsule **27**, which might render an interesting structure for host-guest chemistry, for example.

Multi-component self-assembly of SubPcs was also studied, and in this case two new capsules were prepared and characterized, the first one with tripyridyl-substituted SubPc and the second one with hexapyridyl-SubPc. During the multi-component self-assembling process of hexapyridyl-SubPc **26**, capsule **27** was observed as a kinetic

product. Qualitatively, all these experiments lead to an ordering of these compounds in a series, according to their thermodynamic stability.

5. Experimental section

General procedure for multi-component self-assembly: Pyridyl-substituted compound (1 eq), sodium or potassium dicarboxylate (1 eq) and $Pt(PPEt_3)OTf_2$ (1 eq) were placed in a vial and the solvent ($MeCN/MeNO_2/CH_2Cl_2$ 1:1:1) was added. The mixture was stirred at 65°C for 4 h and then at room temperature overnight. The solution was concentrated and diethyl ether was added. The product crashed out and was filtered and washed with water and diethyl ether.

Compound 18a

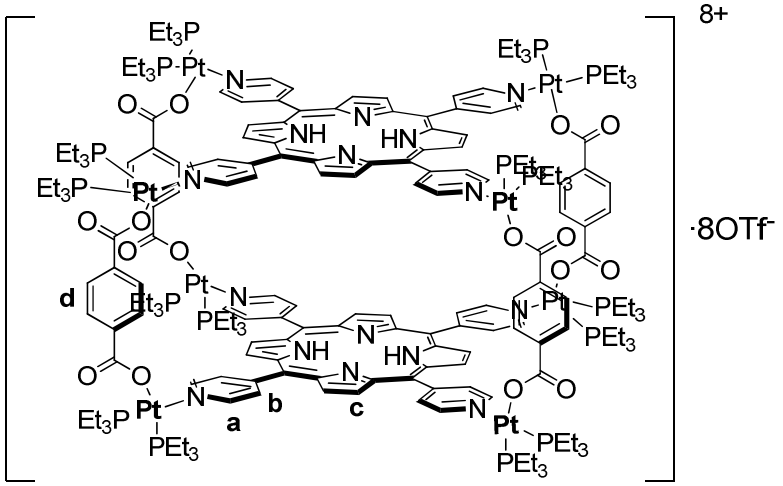

tpyP (0.88 mg, 1.38 mmol), potassium *tert*phthalate (0.77 mg, 3.67 mmol), $Pt(PEt_3)_2OTf_2$ (4.11 mg, 5.64 mmol), 1 mL solvent. Compound **18a** was obtained as brown powder (4.2 mg, 93%). ^{1}H-NMR (300 MHz, Acetone-d6, 298 K): δ = 9.38 (d, 16H, J = 4.1 Hz, H*a*), 9.30 (s, 8H, H*c*), 8.42 (d, 16H, J = 4.1 Hz, H*b*), 8.07 (s, 16H, H*d*), 7.06 (s, 8H, H*c*), 2.36-2.19 (m, 96H, P*CH*$_2$CH$_3$), 1.56-1.39 (m, 144H, PCH$_2$*CH*$_3$), -3.30 ppm (bs, 4H, NH). ^{31}P NMR (119 MHz, Acetone-d6, 298 K): δ = -0.13 (d, $J_{P\text{-}P}$ = 21.06 Hz), 13.40 and -13.59 (^{195}Pt satellites, $J_{Pt\text{-}P}$ = 3289 Hz), -5.11 (d, $J_{P\text{-}P}$ = 21.06 Hz), 9.02 and -19.22 ppm (^{195}Pt satellites, $J_{Pt\text{-}P}$ = 3429 Hz). MS (ESI, acetone): *m/z* = 2030.12 (M-3OTf).

Compound 18b

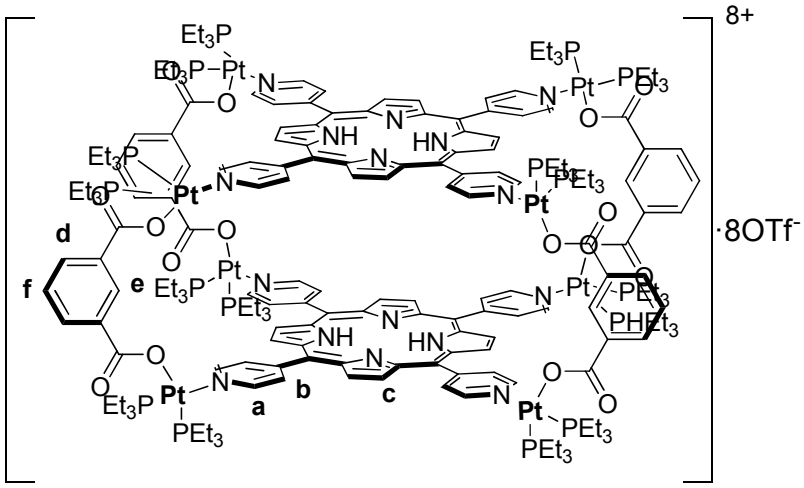

tpyP (1.96 mg, 2.72 mmol), potassium *iso*phthalate (1.14 mg, 5.44 mmol), $Pt(PEt_3)_2OTf_2$ (7.88 mg, 10.81 mmol), 2 mL solvent. Compound **18b** was obtained as brown powder (8.2 mg, 94%). ^{1}H-NMR (300 MHz, Acetone-d6, 298 K): δ = 9.40 (s, 16H, H*a*), 9.34 (s, 8H, H*c*), 8.91 (s, 4H, H*e*), 8.43 (s, 16H, H*b*), 8.12 (d, 8H, J = 6.7 Hz, H*d*), 7.74 (s, 8H, H*c*), 7.33 (t, 4H, J = 6.5 Hz, H*f*), 2.35-2.21 (m, 96H, P$CH_2$$CH_3$), 1.48 (m, 144H, PCH_2CH_3), -3.29 ppm (s, 4H, NH). ^{31}P NMR (119 MHz, Acetone-d6, 298 K): δ = 0.85 (d, $J_{P\text{-}P}$ = 20.8 Hz), 14.22 and -12.42 (^{195}Pt satellites, $J_{Pt\text{-}P}$ = 3236 Hz), 5.29 (d, $J_{P\text{-}P}$ = 21.3 Hz), 8.88 and -19.50 ppm (^{195}Pt satellites, $J_{Pt\text{-}P}$ = 3458 Hz). MS (ESI, acetone): *m/z* = 2029.91 (M-3OTf).

Compound 18d

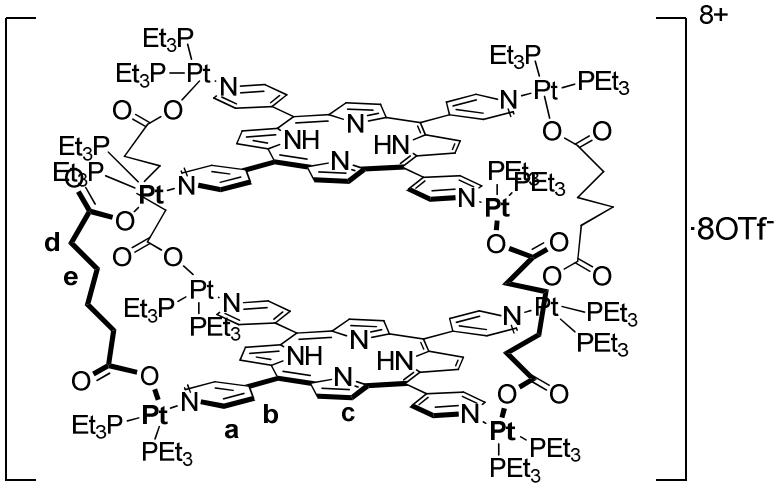

tpyP (2.01 mg, 3.16 mmol), potassium hexanedioate (1.30 mg, 6.19 mmol), $Pt(PEt_3)_2OTf_2$ (9.22 mg, 12.65 mmol), 2 mL solvent. Compound **18d** was obtained as brown powder (9.2 mg, 90%). ^{1}H-NMR (300 MHz, Acetone-d6, 298 K): δ = 9.36 (s, 8H, H*c*), 9.33 (d, 16H, *J* = 4.7 Hz, H*a*), 8.55 (d, 16H, *J* = 4.7 Hz, H*b*), 8.34 (s, 8H, H*c*), 2.81 (bs, 16H, H*d*), 2.22 (m, 96H, P*CH*$_2$CH$_3$), 1.62 (m, 16H, H*e*), 1.43 (m, 144H, PCH$_2$*CH*$_3$), -3.01 ppm (m, 4H, NH). ^{31}P NMR (119 MHz, Acetone-d6, 298 K): δ = 0.11 (d, $J_{P\text{-}P}$ = 20.8 Hz), 13.56 and -13.39 (^{195}Pt satellites, $J_{Pt\text{-}P}$ = 3274 Hz), 5.42 (d, $J_{P\text{-}P}$ = 21.3 Hz), 8.15 and -19.89 ppm (^{195}Pt satellites, $J_{Pt\text{-}P}$ = 3405 Hz). MS (ESI, acetone): *m/z* = 2003.41 (M-3OTf).

Compound 18e

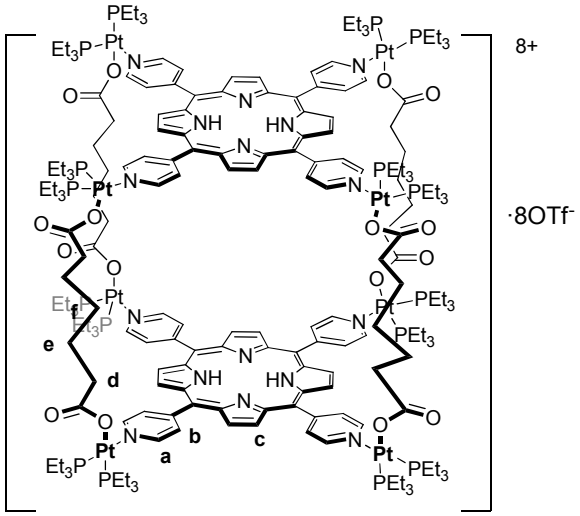

tpyP (1.95 mg, 3.06 mmol), potassium heptanedioate (1.29 mg, 6.09 mmol), $Pt(PEt_3)_2OTf_2$ (8.73 mg, 11.98 mmol), 2 mL solvent. Compound **18b** was obtained as brown powder (8.8 mg, 91%). ^{1}H-NMR (300 MHz, Acetone-d6, 298 K): δ = 9.33 (s, 16H, H*a*), 9.28 (s, 8H, H*c*), 8.56 (s, 24H, H*b*, H*c*), 2.79 (m, 16H, H*d*), 2.15 (m, 96H, P*CH*$_2$CH$_3$), 1.63 (m, 24H, H*e*, H*f*), 1.37 (m, 144H, PCH$_2$*CH*$_3$), -3.05 ppm (s, 4H, NH). ^{31}P NMR (119 MHz, Acetone-d6, 298 K): δ = -0.26 (d, $J_{P\text{-}P}$ = 18.9 Hz), 13.22 and -13.76 (^{195}Pt satellites, $J_{Pt\text{-}P}$ = 3274 Hz), -6.36 (d, $J_{P\text{-}P}$ = 20.1 Hz), 7.73 and -20.26 ppm (^{195}Pt satellites, $J_{Pt\text{-}P}$ = 3398 Hz). MS (ESI, acetone): *m/z* = 2022.12 (M-3OTf).

Compound 18f

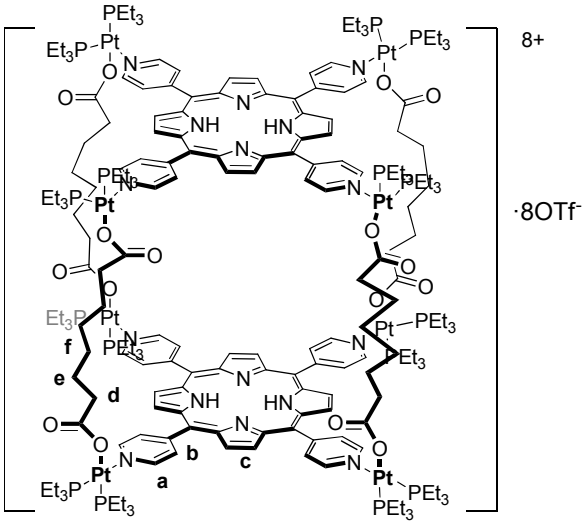

tpyP (1.94 mg, 3.06 mmol), potassium octanodioate (1.31 mg, 6.11 mmol), $Pt(PEt_3)_2OTf_2$ (8.75 mg, 12.02 mmol), 2 mL solvent. Compound **18b** was obtained as brown powder (9.0 mg, 91%). ^{1}H-NMR (300 MHz, Acetone-d6, 298 K): δ = 9.34 (bs, 16H, H*a*), 9.17 (s, 8H, H*c*), 8.71 (s, 8H, H*c*), 8.60 (d, 16H, J = 5.5 Hz, H*b*), 2.79 (m, 16H, H*d*), 2.16(m, 96H, P*CH*$_2$CH$_3$), 1.57 (m, 16H, H*e*), 1.41 (m, 144H, PCH$_2$*CH*$_3$),1.22 (m, 16H, H*f*), -2.79 ppm (s, 4H, NH). ^{31}P NMR (119 MHz, Acetone-d6, 298 K): δ = -0.45 (d, $J_{P\text{-}P}$ = 21.4 Hz), 13.12 and -14.05 (^{195}Pt satellites, $J_{Pt\text{-}P}$ = 3289 Hz), -6.37 (d, $J_{P\text{-}P}$ = 21.4 Hz), 7.65 and -20.38 ppm (^{195}Pt satellites, $J_{Pt\text{-}P}$ = 3404 Hz). MS (ESI, acetone): *m/z* = 2040.45 (M-3OTf).

General procedure for metallation of prisms 18a-f with Zn (II): Free-base prism (1 eq) and $Zn(OTf)_2$ (1.2 eq) were placed under N_2 atmosphere and stirred in CH_2Cl_2 for 1-2 hours. The resulting green precipitate was collected and washed with water, CH_2Cl_2 and diethyl ether.

Compound 19a

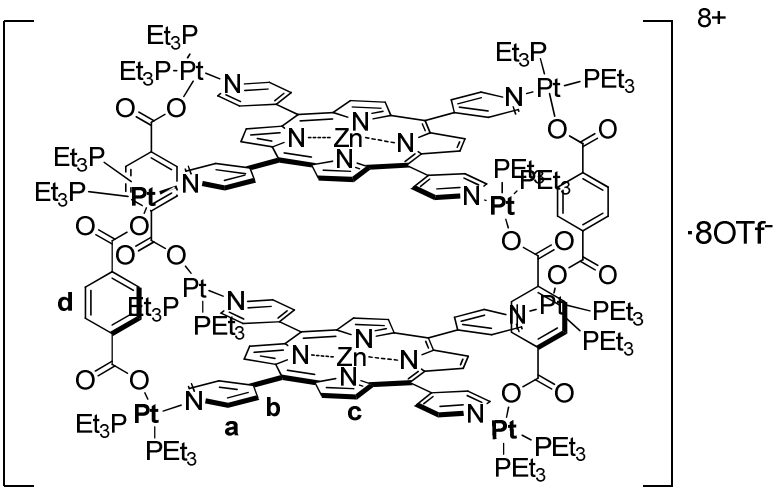

18a (4.97 mg, 0.00075 mmol), $Zn(OTf)_2$ (0.61 mg, 0.0016 mmol), 1.5 mL solvent. Compound **19a** was obtained as a green powder,1.99 mg, 40 %. ^{1}H-NMR (300 MHz, $MeNO_2$-d3, 298 K): δ = 9.34 (bs, 16H, H*a*), 8.35 (s, 8H, H*b*), 8.08 (s, 24H, H*c*, H*e*), 7.11 (d, 8H, H*c*), 2.22 (m, 96H, PCH_2CH$_3$), 1.47 ppm (m, 144H, PCH$_2$$CH_3$). ^{31}P NMR (119 MHz, Acetone-d6, 298 K): δ = -1.67 (d, $J_{P\text{-}P}$ = 17.7 Hz), -6.75 (d, $J_{P\text{-}P}$ = 18.2 Hz); ^{195}Pt satellites could not be observed. ESI-MS spectrum could not be recorded.

Compound 19b

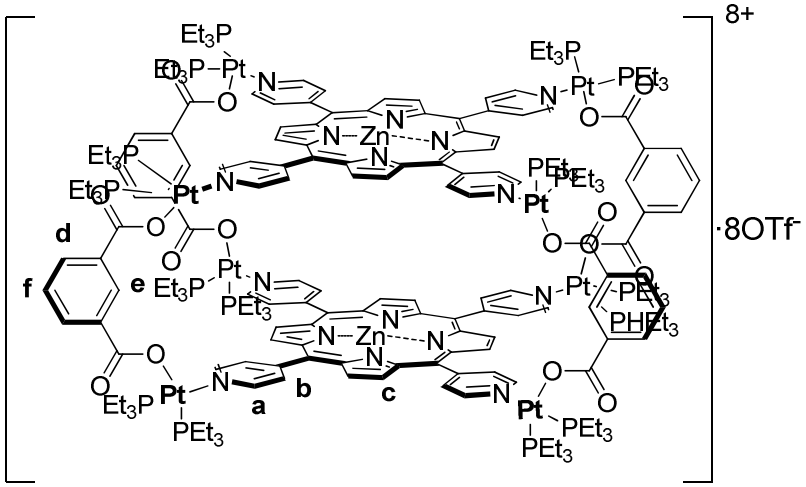

18b (5.01 mg, 0.00075 mmol), $Zn(OTf)_2$ (0.64 mg, 0.0017 mmol), 1.5 mL solvent. Compound **19b** was obtained as a green powder, 1.97 mg, 39 %. ^{1}H-NMR (300 MHz, Acetone-d6, 298 K): δ = 9.40-8.00 (m, 32H, H*c,d,e,f*), 7.71 (s, 16H, H*a*), 7.62 (d, 16H, H*b*), 2.11 (m, 96H, PCH_2CH$_3$), 1.77 ppm (m, 144H, PCH$_2$$CH_3$). ^{31}P NMR (119 MHz, Acetone-d6, 298 K): δ = -1.67 (d, $J_{P\text{-}P}$ = 17.7 Hz), -6.75 (d, $J_{P\text{-}P}$ = 18.2 Hz); ^{195}Pt satellites could not be observed. ESI-MS spectrum could not be recorded.

Compound 19d

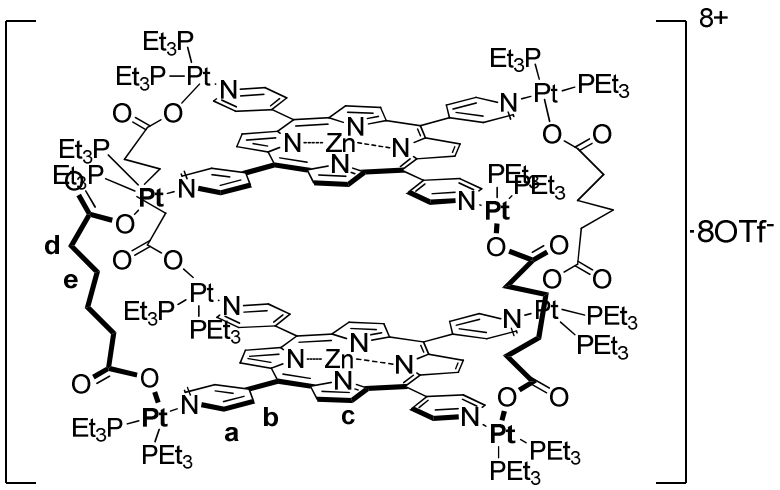

18d (4.89 mg, 0.00075 mmol), $Zn(OTf)_2$ (0.62 mg, 0.0016 mmol), 1.5 mL solvent. Compound **19d** was obtained as a green powder, 2.05 mg, 41 %. ^{1}H-NMR (300 MHz, Acetone-d6, 298 K): δ = 9.28 (bs, 16H, H*a*), 9.17 (s, 8H, H*c*), 8.49 (bs, 16H, H*b*), 8.37 (s, 8H, H*c*), 2.82 (bs, 16H, H*d*), 2.21 (m, 96H, P*CH*$_2$CH$_3$), 1.64 (m, 16H, H*e*), 1.43 (m, 144H, PCH$_2$*CH*$_3$). ^{31}P NMR (119 MHz, Acetone-d6, 298 K): δ = -0.15 (d, $J_{P\text{-}P}$ = 21.1 Hz), 13.44 and -13.66 (^{195}Pt satellites, $J_{Pt\text{-}P}$ = 3292 Hz), -6.18 (d, $J_{P\text{-}P}$ = 19.8 Hz), 7.71 and –20.15 ppm (^{195}Pt satellites, $J_{Pt\text{-}P}$ = 3384 Hz). ESI-MS spectrum could not be recorded

Compound 19e

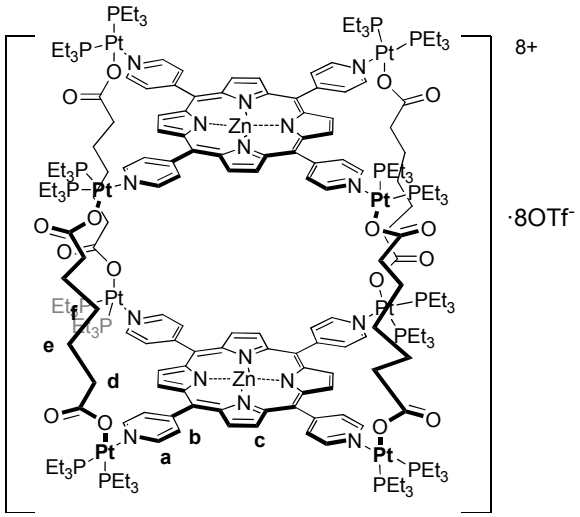

18e (5 mg, 0.00076 mmol), $Zn(OTf)_2$ (0.60 mg, 0.0016 mmol), 1.5 mL solvent. Compound **19e** was obtained as a green powder, 2.00 mg, 40 %. ^{1}H-NMR (300 MHz, Acetone-d6, 298 K): δ = 9.31 (s, 16H, H*a*), 8.63 (s, 16H, H*c*), 8.51 (s, 16H, H*b*), 2.81

(m, 16H, H*d*), 2.18 (m, 96H, P*CH*$_2$CH$_3$), 1.69 (m, 24H, H*e,* H*f*), 1.42 (m, 144H, PCH$_2$*CH*$_3$). ^{31}P NMR (119 MHz, Acetone-d6, 298 K): δ = -1.51 (d, $J_{P\text{-}P}$ = 19.8 Hz), -7.65 ppm (d, $J_{P\text{-}P}$ = 20.7 Hz). ^{195}Pt satellites could not be observed. ESI-MS spectrum could not be recorded.

Compound 19f

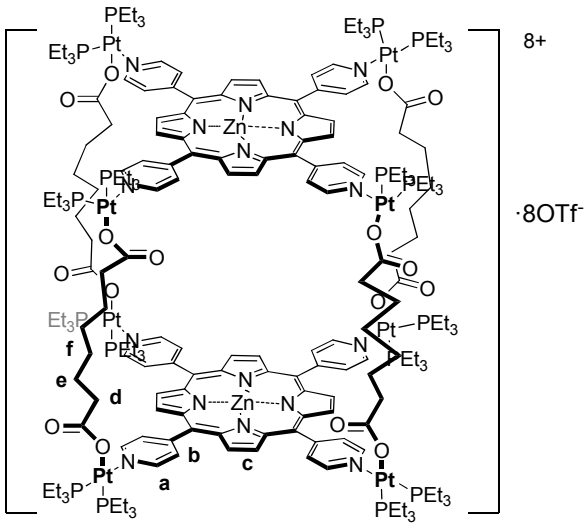

18f (5 mg, 0.00076 mmol), Zn(OTf)$_2$ (0.55 mg, 0.015 mmol), 1.5 mL solvent. Compound **19f** was obtained as a green powder, 2.54 mg, 47 %. ^{1}H-NMR (300 MHz, Acetone-d6, 298 K): δ = 9.32 (bs, 16H, H*a*), 9.07 (s, 8H, H*c*), 8.75 (s, 8H, H*c*), 8.55 (bs, 16H, H*b*), 2.45 (m, 16H, H*d*), 2.22 (m, 96H, P*CH*$_2$CH$_3$), 1.1-1.9 ppm (m, 176H, H*e*, PCH$_2$*CH*$_3$, H*f*). ^{31}P NMR (119 MHz, Acetone-d6, 298 K): δ = 6.98 (d, $J_{P\text{-}P}$ = 21.3 Hz), 19.93 and -6.19 (^{195}Pt satellites, $J_{Pt\text{-}P}$ = 3301 Hz), 1.17 (d, $J_{P\text{-}P}$ = 20.7 Hz), 14.50 and -12.68 ppm (^{195}Pt satellites, $J_{Pt\text{-}P}$ = 3173 Hz). ESI-MS spectrum could not be recorded.

Compound 20

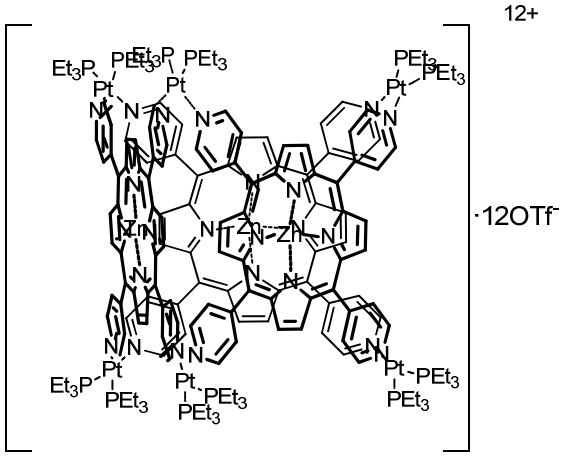

18f (5 mg, 0.00076 mmol), and $Zn(OAc)_2$ (0.38 mg, 0.0019 mmol), were refluxed in $MeOH/CH_2Cl_2$ 1:1. Compound **20** was obtained as a green solid 2.18 mg, 45 %. ^{31}P NMR (119 MHz, Acetone-d6, 298 K): δ = -6.31 (s), 6.30 and -25.92 ppm (^{195}Pt satellites, $J_{Pt\text{-}P}$ = 3907 Hz).

General procedure for the self-assembly of Fe(II) porphyrin prisms: FeP was stirred at 70°C in $MeNO_2$. Subsequently, the Pt acceptor was added and the mixture stirred 4h at 70°C. Finally, the C_8 dicarboxylate was added and the solution was again stirred at 70°C for 8h. The solution thus obtained was poured onto a concentrated solution of KPF_6, and the product crashed out as a brown-orange solid.

Compound 21a

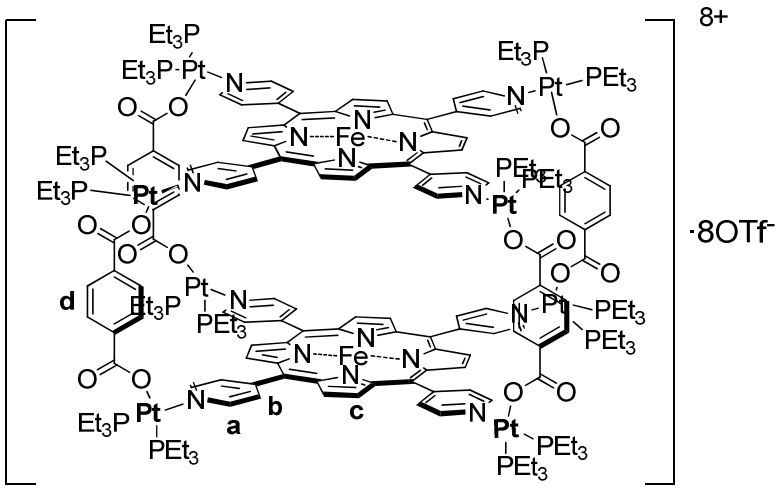

FeP (0.93 mg, 1.38 mmol), potassium *tert*phthalate (0.77 mg, 3.67 mmol), $Pt(PEt_3)_2OTf_2$ (4.11 mg, 5.64 mmol), 1 mL solvent. Compound **21a** was obtained as a brown powder (4.7 mg, 38%). ^{31}P NMR (119 MHz, Acetone-d6, 298 K): δ = 0.91 (d, $J_{P\text{-}P}$ = 14.0 Hz), -4.55 (d, $J_{P\text{-}P}$ = 14.7 Hz), 7.67,-0.59, -5.40 ppm (impurities). ^{195}Pt satellites could not be observed. ESI-MS spectrum could not be recorded

Compound 21b

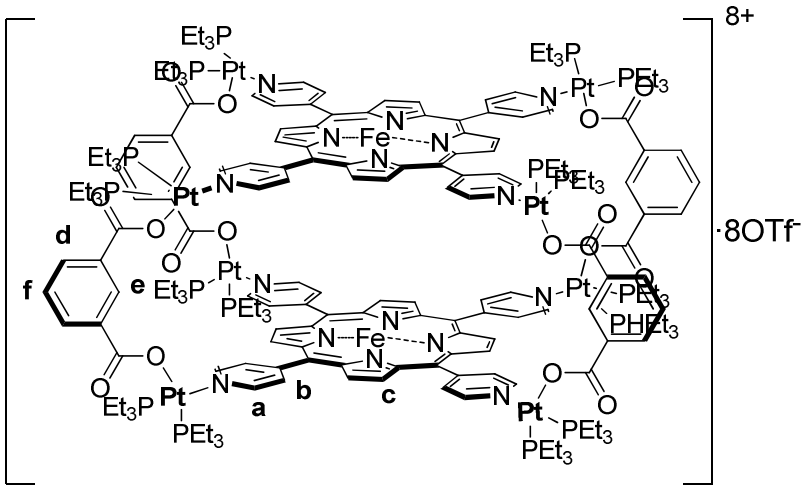

FeP (0.95 mg, 1.38 mmol), potassium *iso*phthalate (0.74 mg, 3.67 mmol), $Pt(PEt_3)_2OTf_2$ (4.21 mg, 5.77 mmol), 1 mL solvent. Compound **21b** was obtained as a brown powder (2.93 mg, 32%). ^{31}P NMR (119 MHz, Acetone-d6, 298 K): δ = -0.25 (d, $J_{P\text{-}P}$ = 19.1 Hz), -4.82 (d, $J_{P\text{-}P}$ = 21.4 Hz), 7.22,-0.60, -1.06, -7.80 ppm (impurities). ^{195}Pt satellites could not be observed. ESI-MS spectrum could not be recorded

Compound 21d

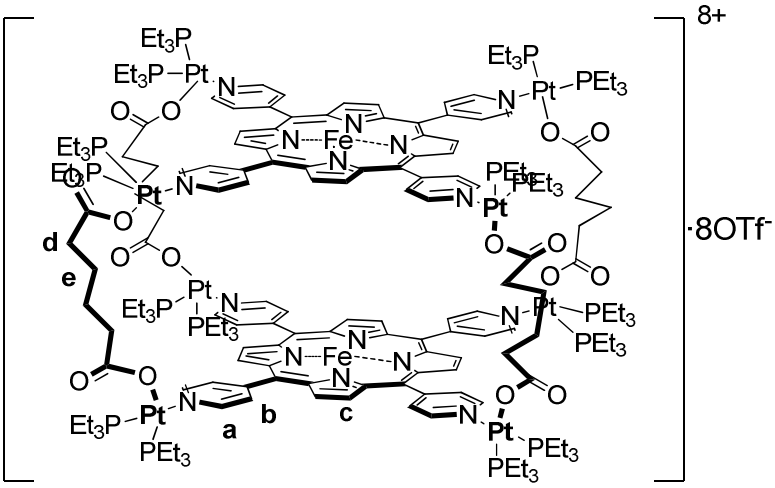

FeP (0.96 mg, 1.42 mmol), potassium hexanedioate (0.81 mg, 3.67 mmol), $Pt(PEt_3)_2OTf_2$ (4.14 mg, 5.68 mmol), 1 mL solvent. Compound **21d** was obtained as a brown powder (3.35 mg, 36%). ^{31}P NMR (119 MHz, Acetone-d6, 298 K): δ = -0.54 (d, $J_{P\text{-}P}$ = 17.1 Hz), 15.19 and -13.18 (^{195}Pt satellites, $J_{Pt\text{-}P}$ = 3456 Hz), -6.23 (d, $J_{P\text{-}P}$ = 21.4

Hz), 7.81 and -16.31 (^{195}Pt satellites, $J_{Pt\text{-}P}$ = 2998 Hz), -5.14 ppm (impurities). ^{195}Pt satellites could not be observed. ESI-MS spectrum could not be recorded

Compound 21f

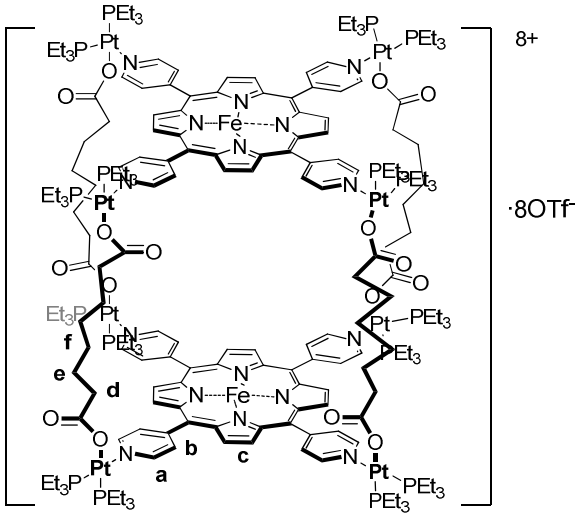

FeP (1.03 mg, 1.52 mmol), potassium octanedioate (0.75 mg, 3.04 mmol), $Pt(PEt_3)_2OTf_2$ (4.40 mg, 6.03 mmol), 1 mL solvent. Compound **21f** was obtained as a brown powder (3.96, 39%). ^{31}P NMR (119 MHz, Acetone-d6, 298 K): δ = 1.67 (d, $J_{P\text{-}P}$ = 17.1 Hz), -7.36 ppm (d, $J_{P\text{-}P}$ = 21.4 Hz). ^{195}Pt satellites could not be observed. ESI-MS spectrum could not be recorded

4,5-diiodophthalimide[13] (22)

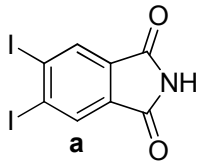

To a stirred suspension of phthalimide (15 g, 0.1 mol) in fuming sulphuric acid (60 mL), iodine (50.8g, 0.2 mol) was slowly added. The reaction mixture was heated to 60°C for 24 h. After cooling to room temperature, the mixture was poured onto ice and the brown solid formed was collected and washed with water, a 2% solution of K_2CO_3, saturated solution of $Na_2S_2O_3$ and water again. After drying, the solid was extracted in a Soxhlet for 48 h with acetone. Upon concentration and addition of water, a white precipitate containing 4,5-diiodophthalimide and 4,5-dichlorophthalic acid crashed out. Purification of the product was carried out by column chromatography on silica gel ($CHCl_3$/Ethyl acetate 4:1). 27 g, 68% yield. m. p. =219-222°C (described: 220-222°C); ^{1}H-NMR (300 MHz, $CDCl_3$, 298 K): δ = 8.39 (s, 2H, H*a*), 7.83 ppm (s, 1H, NH).

[13] D. S. Terekhov, K. J. M. Nolan, C. R. Arthur, C. C. Leznoff, *J. Org. Chem*, **1996**, *61*, 3034.

4,5-diiodophthalamide[13] **(23)**

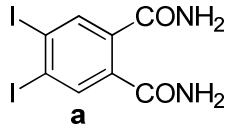

a

A suspension of **22** was stirred at 50-60ºC for 2 hours. The white solid formed was filtered, washed with water and vacuum-dryed. m. p. <250ºC; ^{1}H-NMR (300 MHz, $CDCl_3$, 298 K): δ = 8.43 (s, 2H, H*a*), 7.71 (s, 2H, H*a*), 7.49 (bs, 2H, NH_2).

4,5-diiodophthalonitrile[13] **(24)**

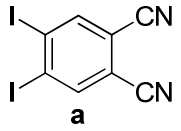

a

To a suspension of 4,5-diiodophthalamide in a dioxane/pyridine 10:1 mixture (165 mL), trifluoroacetic anhydride was slowly added. After the addition was complete, the reaction was warmed up to room temperature and stirred 16 hours. The resulting mixture was poured onto ice and extracted with ethyl acetate (5x30 mL). The organic layer was then washed with water (1x50 mL), HCl 1M (2x50 mL), Na_2CO_3 10% (2x50 mL) and dried over $MgSO_4$. After filtration of the drying agent, the solvent was evaporated. The product was redissolved in a minimum amount of CH_2Cl_2 and hexane was added. Compound 24 was obtained as a white solid. m. p. =215-218ºC (described: 216-217ºC); ^{1}H-NMR (300 MHz, $CDCl_3$, 298 K): δ = 8.32 ppm (s, 2H, H*a*).

Phenoxy-[2,3,9,10,16,17-hexaiodo-7,12:14,19-diimino,-21,5-nitrilo-5H-tribenzo[c,h,m][1,6,11]triazacyclopentadecinato-(2)-κN^{22},κN^{23},κN^{24}]-boron(III)[12] **(25)**

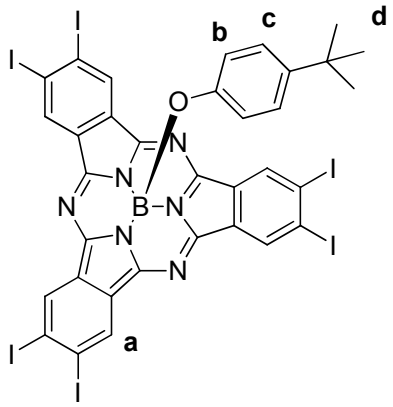

785 mg of 4,5-diiodophthalonitrile were disolved in 1 mL of chlorobenzene. 2 mL of BBr_3 1M in dichloromethane were incorporated though a syringe at room temperature. After 5 minutes of stirring, 0.5 mL of THF was added and the reaction mixture was refluxed for 1 hour. After completion, the solvent was evaporated, and 1 mL of toluene and 700 mg of 4-tertbuthylphenol were added. The resulting mixture was refluxed until the reaction was complete (Check by TLC). Solvent was again removed, and the purple solid was washed with MeOH/H_2O 1:1. Purification was carried out by column chromatography in silica gel, CH_2Cl_2/Hexane 1:1. Product was obtained as a purple solid (706 mg, 62%). m. p. >250°C. ^{1}H-NMR (300 MHz, $CDCl_3$, 298 K): δ = 8.94 ppm (s, 6H, H*a*), 6.76 (d, 2H, *J* = 8.2 Hz, H*b*), 5.31 (d, 2H, *J* = 8.1 Hz, H*c*), 1.07 ppm (s, 9H, H*d*). UV-vis ($CHCl_3$): λ_{max} (log(ε)) = 296 (4.03), 583 nm (4.71).

Phenoxy-[2,3,9,10,16,17-hexapyridylethynyl-7,12:14,19-diimino,-21,5-nitrilo-5H-tribenzo[c,h,m][1,6,11]triazacyclopentadecinato-(2)-κN^{22},κN^{23},κN^{24}]-boron(III) (6a) **(26)**

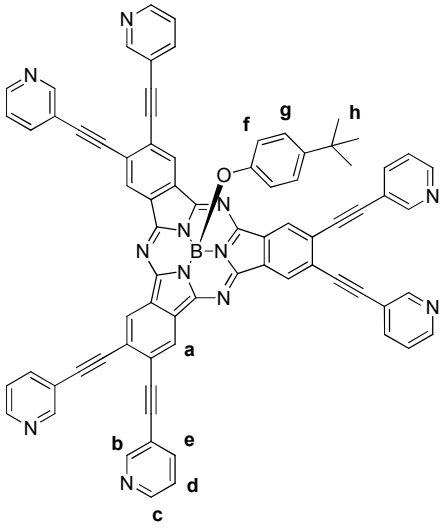

SubPc **25** (40 mg, 0.03 mmol), 3-ethynylpyridine (25 mg, 0.24 mmol), $PdCl_2$ (7 mg, 0.009 mmol), and CuI (1.72 mg, 0.009 mmol) were disolved in toluene/NEt_3 1:2 (3 mL) and stirred at 40°C overnight. 10 mL of water were added and the product was extracted with dichloromethane. The combined organic layer were dried over $MgSO_4$. After filtration, the solvent was evaporated and the product was purified by column chromatography in silica gel (AcOEt/$CHCl_3$/MeOH 8:8:1). Compound **26** was obtained as a blue solid (19 mg, 53%). ^{1}H-NMR (300 MHz, $CDCl_3$, 298 K): δ = 9.02 (s, 6H, H*a*), 8.87 (s, 6H, H*b*), 8.68 (d, 6H, *J* = 4.7 Hz, H*c*), 7.88 (d, 6H, *J* = 7.8 Hz, H*e*), 7.35 (dd, d, 6H, *J* = 7.5 Hz, *J'* = 4.8 H*d*), 6.81 (d, 2H, *J* = 8.6 Hz, H*g*), 5.42 (d, 2H, *J* = 8.6 Hz, H*f*), 1.10 ppm (s, 9H, H*h*). ^{13}C-NMR (300 MHz, $CDCl_3$, 298 K): δ = 152.34, 151.32, 149.62, 149.35, 138.52, 129.87, 126.42, 126.31, 125.92, 123.32, 119.91, 117.87, 92.78, 91.27, 31.31 ppm. UV/Vis ($CHCl_3$): λ_{max} (nm) (log(ε))= 382 (4.38), 612 nm (4.78). MS (MALDI), DCTB): *m/z* = 1151 $[M]^+$, 1002 [M-axial]$^+$.

General procedure for self-assembly of compounds 27-28: SubPc **26** and **12c** were dissolved in dichloromethane in the corresponding stoichiometric amounts. The solution was refluxed for 4 hours and then at room temperature overnight. Addition of diethyl ether on the concentrated solution provoked precipitation of a blue solid that was collected and washed with hexane and diethyl ether. If a mixture of products is obtained, they can be separated by gel permeation chromatography (Bio Beads S-X1, 200-400 mesh) in dichloromethane.

Compound 27

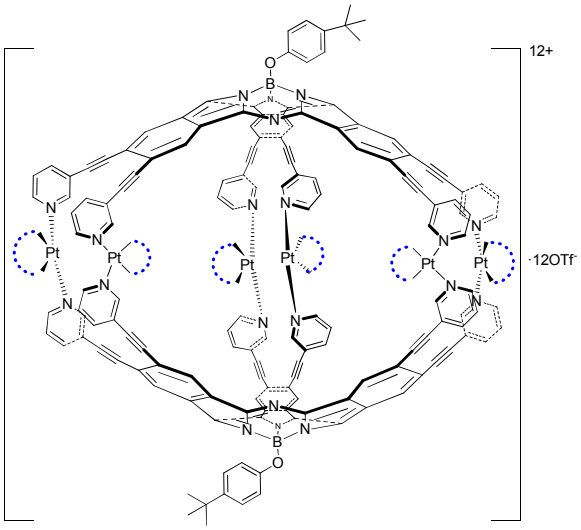

SubPc **26** (4 mg, 0.0035 mmol), **12c** (8.5 mg, 0.01 mmol), CH_2Cl_2 (1.5 mL). Compound **27** was obtained as a blue solid (9.4 mg, 76%). ^{1}H-NMR (300 MHz, Acetone-d6, 298

K): δ = 9.16 (m, 24H, H*a*, H*b*), 8.67 (m, 48H, H*c*, H*e*), 8.11-7.4 (m, 132H, Ph, H*d*), 6.92 (m, 4H, H*g*), 5.53 (m, 4H, H*f*), 3.64-3.40 (m, 32H, H*j*, H*i*), 1.12 ppm (bs, 18H, H*h*). ^{31}P NMR (119 MHz, Acetone-d6, 298 K): δ = -5.13 ppm (s), 8.85, -19.11 (^{195}Pt satellites, $J_{Pt\text{-}P}$ = 3397 Hz). MS (ESI, acetone): *m/z* = 1631.30 [M-2Pt(dppp)-4OTf]$^{2+}$/2.

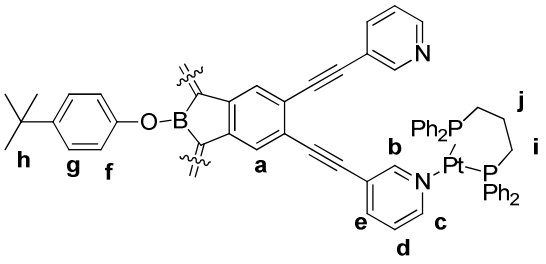

Compound 28a

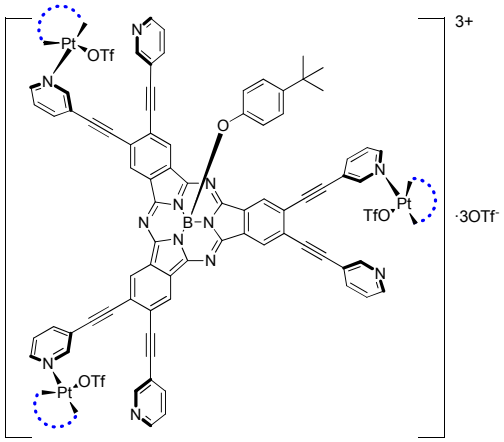

SubPc **26** (4 mg, 0.0035 mmol), **12c** (8.5 mg, 0.01 mmol), CH_2Cl_2 (1.5 mL). Compound **27** was obtained as a blue solid (1.8 mg, 30%). ^{1}H-NMR (300 MHz, Acetone-d6, 298 K): δ = 9.04-8.81 (m, 12H, H*a*, H*b*), 8.67 (m, 18H, H*c*, H*d,* H*e*), 8.11-7.4 (m, 60H, Ph), 6.85 (m, 4H, H*g*), 5.53 (m, 4H, H*f*), 3.08 (m, 32H, H*j*, H*i*), 1.16 ppm (s, 18H, H*h*). ^{31}P NMR (119 MHz, Acetone-d6, 298 K): δ = -4.76 (d, $J_{P\text{-}P}$= 26.7 Hz), -13.49 ppm (d, $J_{P\text{-}P}$= 25.2 Hz) . MS (ESI, acetone): *m/z* = 1320 [M-2Pt(dppp)-4OTf]$^{2+}$.

Compound 28b

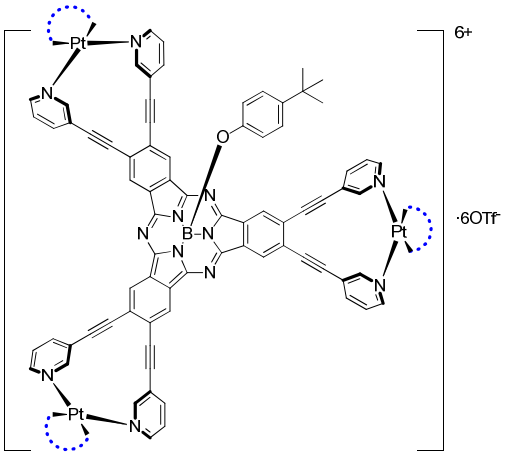

Compound **28a** was left in dichloromethane solution for 2 days. ^{31}P NMR (119 MHz, Acetone-d6, 298 K): δ = -13.04 (s), -1.53, -25.56 ppm (^{195}Pt satellites, $J_{Pt\text{-}P}$ = 2984 Hz) . MS (ESI, acetone): *m/z* = 1320 [M-2Pt(dppp)-4OTf]$^{2+}$.

Compound 29

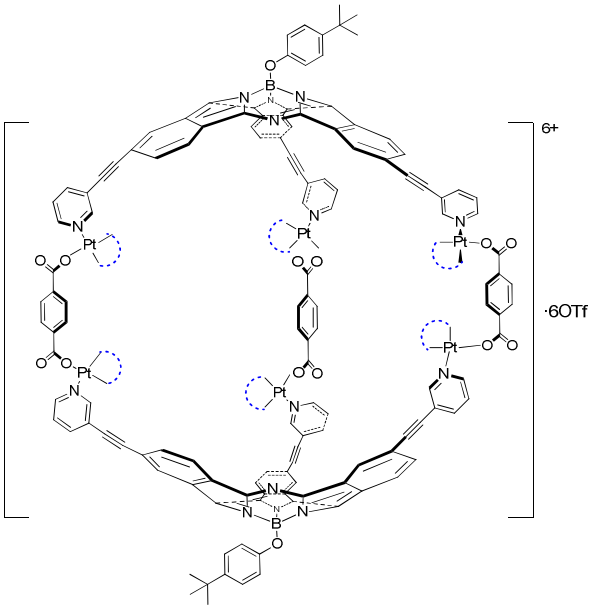

SubPc **11** (5 mg, 0.006 mmol), sodium tertphthalate (1.8 mg, 0.009 mmol), **12c** (16.2 mg, 0.018 mmol), $MeNO_2$/MeCN/CH_2Cl_2 1:1:1 (1 mL). Compound **29** was obtained as a purple solid (18 mg, 90%). ^{1}H-NMR (300 MHz, Acetone-d6, 298 K): δ = 8.93 (s, 6H, H*a*), 8.83 (d, 6H, *J* = 8.1 Hz, H*g*), 8.55 (d, 6H, H*e*), 8.39 (bs, 6H, H*b*), 8.11 (m, 12H, H*d*, H*c*), 7.96 (d, 6H, *J* = 8 Hz, H*f,* H*terphthalate*); 7.80-7.00 (m, 60H, H*Ph*, 6.73 (d, 4H, *J* = 8.6 Hz, H*h*), 5.34 (d, 4H, *J* = 8.6 Hz, H*i*), 4.25 (m, 6H, H*l*), 3.08 (m, 12H, H*k*); 1.16 (s, 18H, H*j*) ppm. ^{31}P NMR (119 MHz, Acetone-d6, 298 K): δ = -1.17 (d, $J_{P\text{-}P}$= 28.2 Hz),

7.58, -11.26 (^{195}Pt satellites, $J_{Pt\text{-}P}$ = 2288 Hz), -8.19 (d, $J_{P\text{-}P}$= 28.2 Hz), -5.11, -14.86 ppm (^{195}Pt satellites, $J_{Pt\text{-}P}$ = 2427 Hz).

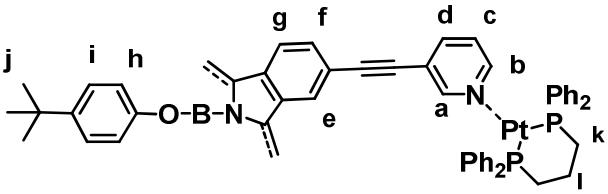

Compound 30

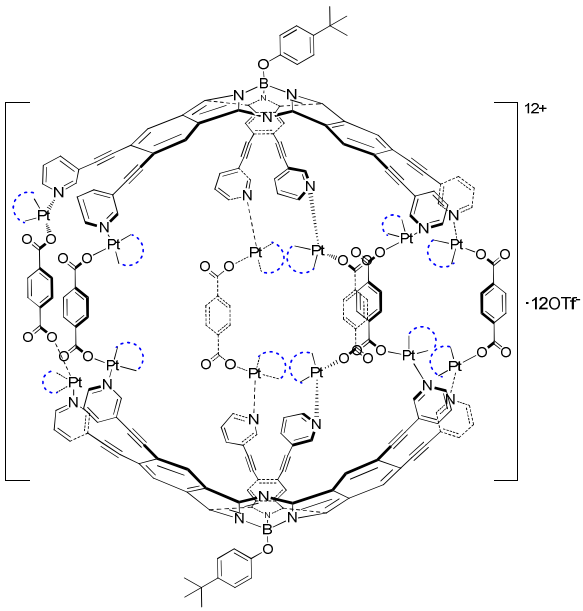

SubPc **26** (5 mg, 0.006 mmol), sodium tertphthalate (1.8 mg, 0.012 mmol), **12c** (21.24, 0.026 mmol), $MeNO_2$/MeCN/CH_2Cl_2 1:1:1 (1.5 mL). Compound **30** was obtained as a blue solid. ^{1}H-NMR (300 MHz, Acetone-d6, 298 K): δ = 9.01-8.55 (m, 48H, H*a,b,c,e*), 7.75-7.09 (m, 156H, H*d*, H*tertphthalate*, Ph), 6.85 (m, 4H, H*g*), 5.48 (m, 4H, H*f*), 3.03 (m, 60H, H*i*, H*j*), 1.02 ppm (s, 18H, H*h*). ^{31}P NMR (119 MHz, Acetone-d6, 298 K): δ = -12.97 (d, $J_{P\text{-}P}$= 24.1 Hz), -16.79 (d, $J_{P\text{-}P}$= 25.4 Hz), -20.02 (d, $J_{P\text{-}P}$= 24.1 Hz), -25.25 (d, $J_{P\text{-}P}$= 25.4 Hz), -2.77, -4.36, -30.43, -33.53 ppm (^{195}Pt satellites). λ_{max} (nm) (log(ε))= 611 nm (4.48).

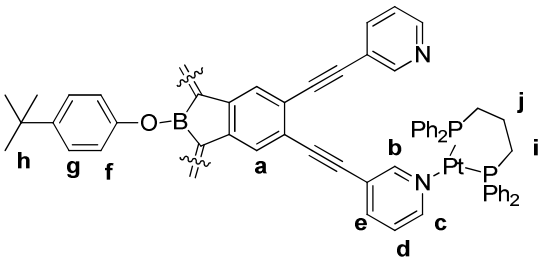

Incorporation of a tricationic subphthalocyanine in an organic photovoltaic device.

Irene Sánchez-Molina[a], Alejandra Soriano[b], Christian G. Claessens[a,*], Tomás Torres[a,c,*], Henk J. Bolink[b, *]

[a]*Departamento de Química Orgánica Universidad Autónoma de Madrid, Cantoblanco 28049-Madrid, Spain.*

[b]*Instituto de Ciencia Molecular, Catedrático José Beltrán 2, 46980 Paterna-Valencia, Spain*

[c]*IMDEA-Nanociencia, c/Faraday 9, Campus de Cantoblanco, 28049 Madrid, Spain.*

ABSTRACT: A new tricationic subphthalocyanine was synthesized and employed as light-harvesting and donor material in an ionic solid state organic photovoltaic cell.

KEYWORDS: Subphthalocyanines, Organic Photovoltaics, ionic compounds

INTRODUCTION

Subphthalocyanines[1] (SubPcs) are 14 π-electron aromatic macrocycles comprising three 1,3-diiminoisoindol units N-fused around a boron atom. They display an intense absorption band in the visible region, with its maximum around 560-620 nm depending on the peripheral substitution on the macrocycle. These chromophores have been studied as donor as well as acceptor materials in organic photovoltaic devices, giving rise to excellent results in terms of efficiency and processability, especially in the case of vacuum-deposited planar heterojunction solar cells.[2] Organic photovoltaic devices have attracted much attention due to their ease of fabrication and potentially low-cost production.[3] Recently, cationic cyanine dyes have been

[1] (a) C. G. Claessens, D. González-Rodríguez , T. Torres, *Chem. Rev*. **2002**, *102*, 835; (b)T.Torres *Angew. Chem. Int. Ed.* **2006**, *45*, 2834; (c) G. de la Torre, C. G. Claessens, T. Torres *Chem. Commun.* **2007**, 2000–2015.

[2] (a) K. L. Mutolo, E. I. Mayo, B. P. Rand, S. R. Forrest, M. E. Thompson *J. Am. Chem. Soc.* **2006**, *128*, 8108; (b) H. Gommans , T. Aernouts , B. Verreet, P. Heremans , A. Medina, C. G. Claessens , T. Torres, *Adv. Funct. Mater* **2009**, *19*, 3435; (c) G. E. Morse, T. P. Bender, *ACS Appl. Mater. Interfaces*, **2012**, *4*, 5055–5068.; (d) P. Heremans, D. Cheyns , B. P. Rand . *Accounts Chem. Res.* **2009***,42,* 1740-1747; (e) G. E. Morse, M. G. Helander, J. Stanwick, J. M. Sauks , A. S. Paton , Z-H. Lu,T. P. Bender, *J. Phys. Chem.*C **2011**, *115,* 11709-11718; (f) B. Verreet, B. P. Rand, D. Cheyns, A. Hadipour , T. Aernouts , P. Heremans , A. Medina, C. G. Claessens, T. Torres, *Adv. Energy Mater.* **2011**, *1*, 565-568; (g) S. M. Menke, W. A. Luhman, R. J. Holmes, *Nat. Mater.* **2013**, 12, 152-1577.

[3] (a) M. Granstrom , K. Petritsch, A. C. Arias, A. Lux, M. R. Anderson, R. H. Friend, *Nature* **1998**, *395*, 257-260;(b) S. R. Forrest *Nature* **2004**, *428*, 911-918.

incorporated in bilayer solar cells with the aim of taking advantage of ionic movement to assist in the charge separation process.[4] Thus, a considerable research effort has been devoted to the enhancement of the efficiency of these devices through the use of new materials and the development of new device architectures. In this connection, it is of particular interest to verify if ionic SubPcs can be processed from solution. This would allowthe preparation of devices using printing or coating techniques; techniques which considerably simplify the fabrication process. To enhance the solubility, achieve the proper electronic properties, and improve the film formation of the SubPc's it is of great interest to incorporate accurate axial and peripheral groups. Our previous experience in the synthesis of pyridyl- and pyridinium-substituted SubPcs[5] motivated the choice of these groups to incorporate the positive charges in the molecule. The use of a double bond as linkage between the macrocycle and the pyridinium groups was aimed to an extension of conjugation. In this manner we expect to provoke a red-shift in the absorption bands of the SubPc, which would get closer to the wavelength range where solar radiation is maximum, and thus, the performance of the device would be better. To sum up, we report in this communication the study of a highly-conjugated SubPc **31** (Figure A1) bearing positive charges in the periphery as the donor in partially solution processed bi-layer solid-state organic photovoltaic devices. Despite the synthetic versatility and tunability of their properties through the choice of the proper substituents, and the evident interest these molecules present as light harvesters, very few examples of solution processable SubPc derivatives have been used for OPVs. [6]

RESULTS AND DISCUSSION

Synthesis and characterization of SubPc 31.

SubPc 3**1** which has been described by us was synthesized in four steps from 4-iodophthalonitrile. Condensation of 4-iodophthalonitrile in the presence of boron trichloride (1 M in p-xylene) gave rise to triiodo-SubPc as chlorine derivative.[7] In situ axial substitution of

---

[4] (a) O. Malinkiewicz, T. Grancha , A. Molina-Ontoria, A. Soriano, H. Brine, H. J. Bolink, *Adv. Ener. Mater*, **2013**, *3*, 472-477; (b) R. Hany , B. Fan, F. Araujo de Castro, J. Heier, W. Kylberg, F. Nuesch, *Prog. Photovolt. Res. Appl.* **2011**, *19*, 851-857; (c) M. Lenes, H. J. Bolink. *ACS Appl. Mater. Interfaces*, **2010**, *12*, 3664-3668.

[5] (a) L. Lapok , C. G. Claessens, D. Wöhrle, T. Torres, *Tetrahedron Lett.* **2009,** *50*, 2041-2044; (b) C. G. Claessens, M. J. Vicente-Arana, T. Torres, *Chem. Commun.*, **2008**, 6378-6380.

[6] C. E. Mauldin, C. Piliego, D. Poulsen, D. A. Unruh, C. Woo, B. Ma, J. L. Mynar, J. M. J. Fréchet *ACS Applied Materials & Interfaces,* **2010**, *2*, 2833-2838.

[7] (a) I. Sánchez-Molina, B. Grimm, C. G. Claessens, D. M. Guldi, T. Torres, submitted; (b) C. G. Claessens, D. Gonzalez-Rodriguez, B. del Rey, T. Torres, G. Mark, H.-P. Schuchmann, C. von Sonntag , J. G. MacDonald, R. S. Nohr, *Eur. J. Org. Chem.* **2003**, *14*, 2547-2551; (c) I. Sánchez-Molina, C. G. Claessens, B. Grimm, D. M. Guldi, T. Torres, *Chem. Sci,* **2013**, *4*, 1338-1344.

the chlorine atom in triiodo-SubPc employing 4-*tert*-butylphenol in toluene / THF (1:1) in the presence of substoichiometric amounts of DBU gave rise to the corresponding tert-butyl-phenoxy SubPc in 60% overall yield. This SubPc was subsequently subjected to a triple Heck cross-coupling reaction with 4-vinyl-pyridine in the presence of catalytic amounts of $PdCl_2$ and tris(orthotolyl)phosphine yielding 75% of tris-(4-pyridylvinyl)-substituted SubPc as a violet solid.[8] Finally, the desired ammonium centers were incorporated through quaternization of the nitrogen atoms[5a] of the pyridyl moieties with methyl iodide. Purification was achieved by anion exchange with ammonium hexafluorophosphate, which gave rise to SubPc **1** in 51% yield.

The new SubPc **31** was characterized by ^{1}H NMR, ^{13}C NMR spectroscopy, UV-vis spectrophotometry and mass spectrometry. The UV-vis spectra of these aromatic macrocycle show the expected Q bands at relatively high wavelengths in acetonitrile (604 nm, compared to 565 nm for unsubstituted SubPc) as a consequence of the extended conjugation brought by the three 4-ethynylpyridyl groups. MALDI-TOF mass spectrum of tricationic SubPc 1 shows peaks at m/z = 1188.4, 521.7 and 299.5 corresponding to $[M\text{-}PF6]^{+}$, $[M\text{-}2PF6]^{2+}$, and $[M\text{-}3PF6]^{3+}$, respectively.

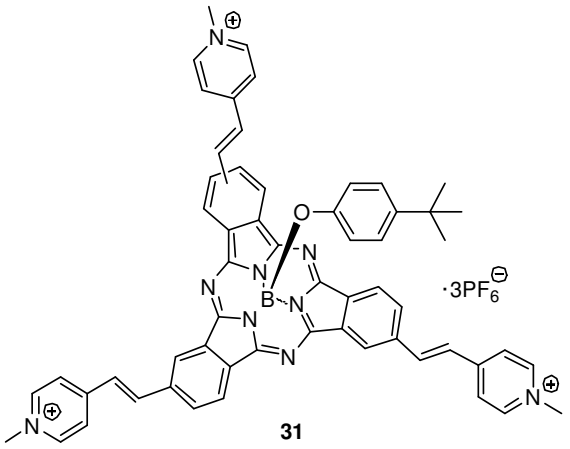

31

Figure A1. Structure of cationic SubPc **31**.

Study of SubPc 31 in bilayer solar cells

Bi-layer cells were prepared according to the layout shown in Figure A2. The dye layer is deposited on top of the hole transporting layer (HTL) poly-(3,4-ethylenedioxythiophene)-poly-

[8] C. Allain, F. Schmidt, R. Lartia , G. Bordeau , C. Fiorini-Debuisschert, F. Charra , P. Tauc, M.-P. Teulade-Fichou, *ChemBioChem* **2007***, 8*, 424-433.

(styrenesulfonate), PEDOT:PSS (Clevios AI4083, from Hereaus). The PEDOT:PSS layer was prepared by spin coating in ambient conditions. The dye layer was prepared using spin coating from an acetonitrile solution (7 mg/ml) also in ambient conditions. The acceptor layer consisted of C_{60} which was thermally evaporated under high vacuum conditions. Prior to the deposition of the Ba/Ag cathode a thin layer of (bathocuproine) BCP was evaporated. This layer of BCP is evaporated in between the C_{60} layer and the cathode to ensure a proper ohmic contact and hence an efficient charge extraction.[9]

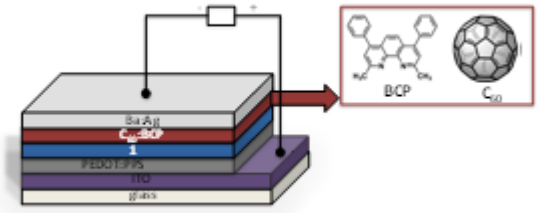

Fig.A2. Schematic picture of the device layout including the chemical structure of BCP.

The absorption spectra of **31** in acetonitrile solution and in a thin film are depicted in Figure A3. There is a slight red shift in the absorption maxima of the thin film which lies now at 600 nm. Hence, the characteristic Q-band of the light-harvester remains practically intact.

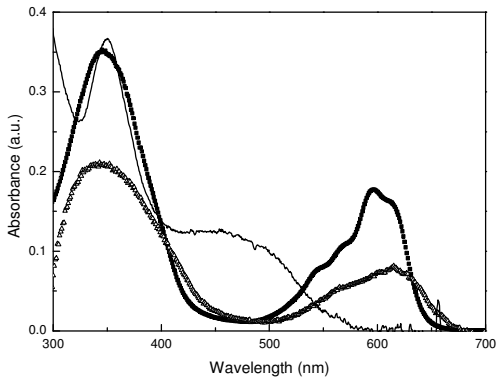

Fig. A3. Absorption spectra of **31** in acetonitrile solution (solid squares) and in a thin film (open triangles), additionally the absorption spectrum of a solid film of C60 is shown (solid line).

When the thin film of 40 nm of the Subpc **31** is integrated in the above described bi-layer solar cell the incident photon to current efficiency (IPCE) can be determined as a function of excitation wavelength (Figure A4). There are two contributions to the IPCE spectrum one

[9] H. Gommans, B. Verreet, B. P. Rand, T. Muller, J. Poortmans, P. Heremans, J. Genoe, *Adv. Funct. Mater.*, **2008**, *18,* 3-10.

around 370 nm and another around 600 nm. The first is due to the combined absorption of both C_{60} the Subpc **31** and the second is only due to absorption of the Subpc **31**. This implies that electron transfer from the excited Subpc **31** to the C_{60} occurs. This is a first requisite for efficient bi-layer solar cells. The current collected around 600 nm is less than around 370 nm. This is expected given that the absorption of the Subpc **31** around 600 nm is around 50 % less than at 350 nm, and that C_{60} itself also possesses at absorption band in this region. Therefore, at such wavelength, photocurrent can be generated either through photoinduced electron transfer from the SubPc **31** to the fullerene or from direct photoexcitation of C_{60} and subsequent hole transfer to the dye. This latter contribution appears also to be the cause for the charge generation in the wavelength regime from 450 to 500 nm where the SubPc **31** is almost not absorbing.

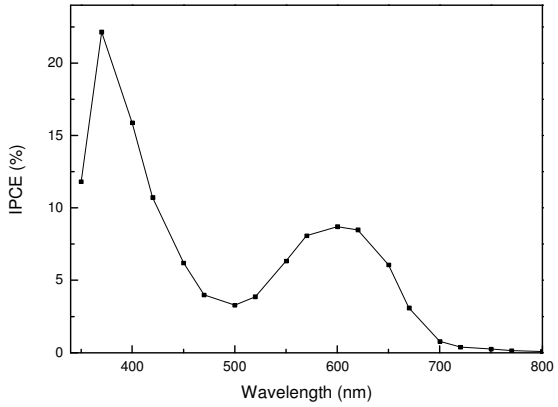

Fig.A4. Incident photon to electron conversion efficiency (IPCE) versus wavelength for the OPV using **31**.

In Figure A4, the current density (J) to voltage (V) characteristics is shown for a typical cell under an illumination of 1000 W/m^2 simulated AM1.5 solar light. The J-V curve has a slight S-shape which leads to a rather low fill factor of 23 %. The open circuit voltage (V_{oc}) and the short-circuit current (J_{sc}) are 0.72 V and 3.1 mA cm^2, respectively, leading to an estimated power conversion efficiency of 0.5 %. Hence, especially in view of the low fill-factors, this is a good preliminary result showing the potential that these cationic SubPcs have for solution processed organic photovoltaic devices.

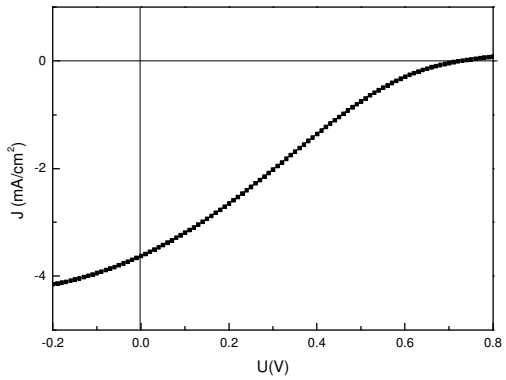

Figure A5. Current density vs voltage for the OPV using cells using Subpc 31 under an illumination of 1000 W/m^2 simulated AM1.5 solar light.

SUMMARY AND CONCLUSION

An ionic subphthalocyanine and its tripyridyl precursor was prepared in high purity and good yields. Hence, this product could be processed into an amorphous thin film via simple solution processing techniques. When integrated into a thin film organic photovoltaic device it yielded power conversion efficiencies in the range of 0.5 %, which are in good agreement with previous data obtained for other solution processable SubPcs.[18] It is expected that synthetic modifications in the structure of this cationic SubPc may enhance the quality of the films and the performance of the devices. In summary, cationic SubPcs represent a class of attractive solution processable small molecular weight organic compound for OPV.

Similar Studies are currently in progress with other cationic SubPcs (Figure A6):

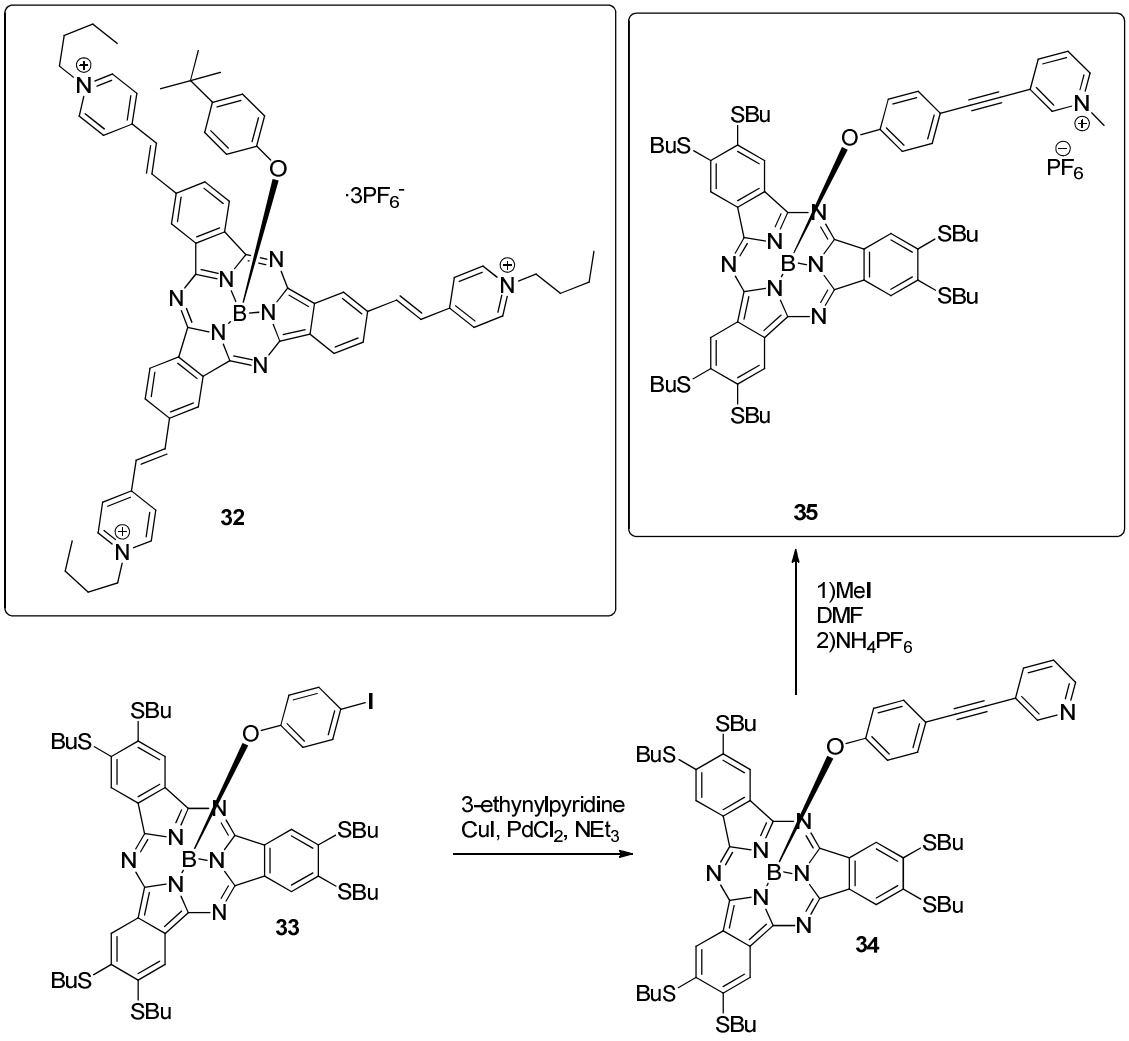

Figure A6. Strucutre of SubPcs **32** and **35**; and synthesis of the latter.

Experimental section

General Remarks

Synthesis and Characterization: UV-vis spectra were recorded with a JASCO V-660 instrument. IR spectra were recorded on a Bruker Vector 22 spectrophotometer. ESI-MS spectra were obtained with a QSTAR 6471 spectrometer, and MALDI-MS spectra with a ULTRAFLEX III spectrometer. ^{1}H, ^{13}C and ^{19}F-NMR spectra were recorded with a Bruker AC-300 equipment. Chemical shifts, δ, are indicated in ppm, using the solvent as a reference. Column chromatographies were carried out on silica gel Merck-60 (230-400 mesh, 60 Å), and TLC on aluminium sheets coated with silica gel 60 F_{254} (Merck). Chemicals were purchased from Aldrich Chemical Co and Alfa Aesar and used as received without further purification.

4-terc-butilfenolate[2,9,n-tris(methyl-3-pyridyniumethyl)-7,12:14,19-diimino-21,5-nitrilo-5H-tribenzo[c,h,m][1,6,11]triazaciclopentadecinate- κN22,κN23,κN24] boron (III) hexafluorophosphate (31)

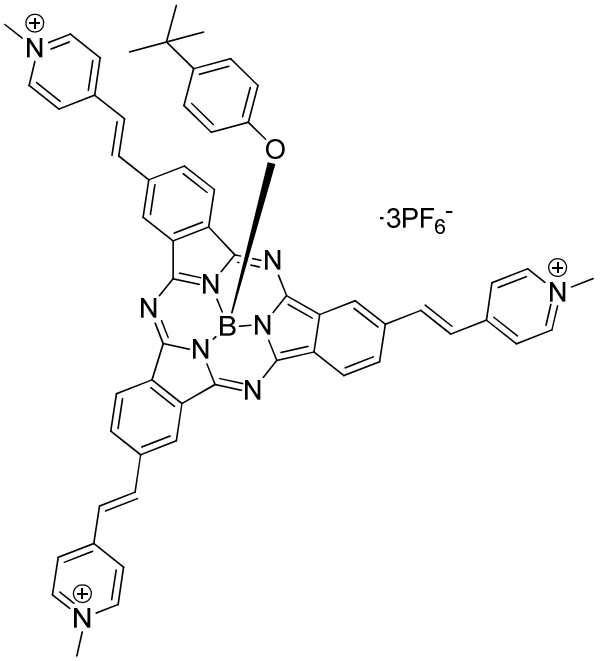

Subphthalocyanine **14** (100 mg, 0.117 mmol) was placed in a 50 ml round-bottomed flask, under argon atmosphere, and dry DMF (10 ml) was added. The system was then protected from light and methyl iodide (9.5 ml, 0.15 mol) was added. The reaction mixture was stirred for 5 hours at 50ºC. After completion (the color of the mixture turns into dark-blue), methyl iodide was evaporated under reduced pressure, as well as a part of the DMF (some ethanol can be added to smooth the progress of the DMF evaporation). At this point, 10 ml of water and a couple of spoons of NH_4PF_6 were added. The resulting mixture was stirred for 30 minutes at room temperature. Finally, another 10 ml of water were added precipitation of the product as a dark-blue solid was observed. The mixture was left overnight in the fridge to ensure completion of precipitation. The product was collected by filtration, and purification was carried out washing with water, toluene, hexane, dichloromethane and diethyl ether. Compound **31** was obtained as a bright dark-blue solid (79 mg, 51%). m.p.>250 ºC; ^{1}H NMR (300 MHz, DMSO-d_6, 298 K): δ (ppm) = 9.29 (d, 3H, *J* = 14.5 Hz, H*d*); 9.06 (m, 9H, H*a*, H*e*); 8.56-8.27 (m,12 H, H*b*, H*g*, H*f*), 8.04 (d, 3H, *J* = 14.5 Hz, H*c*), 6.91 (d, 2H, *J* = 7.7 Hz, H*i*), 5.41 (d, 2H, *J* = 7.7 Hz, H*h*), 4.41 (s, 9H, H*k*), 1.14 (s, 9H, H*j*).

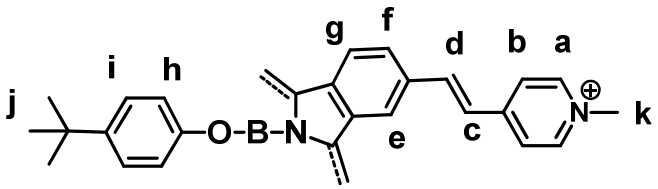

^{13}C NMR (300 MHz, DMSO-d_6, 298 K): δ (ppm) = 152.01, 145.31, 139.70, 137.79, 137.10, 130.98, 130.56, 125.58, 123.80, 121.89, 117.76, 47.09, 31.06. ^{31}P NMR (119 MHz, DMSO-d_6, 298 K): δ (ppm) = -144.21 (sept, 1P, J_{P-F} = 711.3 Hz); ^{19}F NMR (282 MHz, DMSO-d_6, 298 K): δ (ppm) = -70.2 (d, 6F, J_{P-F} = 711.3 Hz); IR (KBr): ν (cm^{-1}) = 3060, 2955, 2924, 2855, 1624, 1464, 853, 557. UV/Vis (DMSO): λ_{max} (nm) (log(ε))= 344 (4.40), 369 (4.30, sh), 400 (4.04, sh), 554 (3.91), 575 (4.04, sh), 604 (4.22), 620 (4.12, sh). MS (ESI, MeOH + 0.1% formic acid): *m/z* = 1188.4[M-PF_6^-]$^+$, 521.7 [M-2PF_6^-]$^{2+}$, 299.5 [M-3PF_6^-]$^{3+}$. Exact mass: 299.4715 (Calculated), 299.4786 (Experimental).

4-terc-butilfenolate[2,9,n-tris(buthyl-3-pyridyniumethyl)-7,12:14,19-diimino-21,5-nitrilo-5H-tribenzo[c,h,m][1,6,11]triazaciclopentadecinate-κN22,κN23,κN24] boron (III) hexafluorophosphate (32)

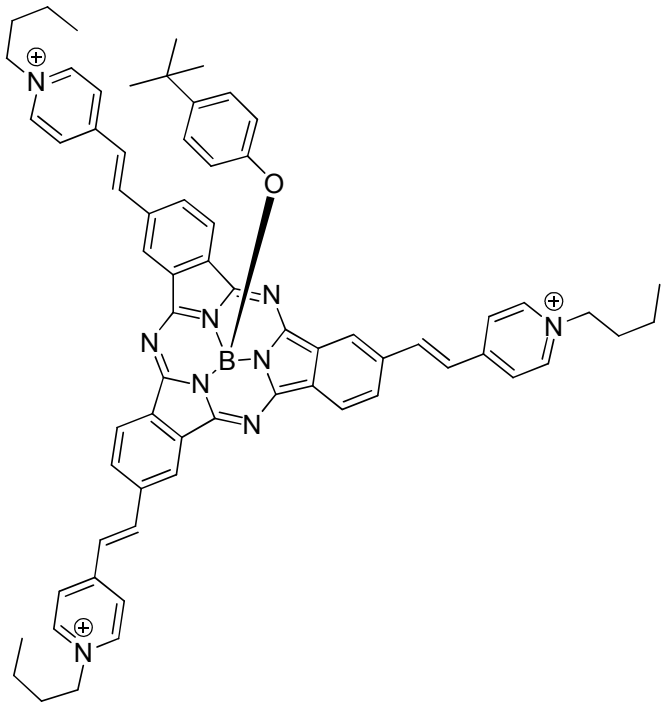

Subphthalocyanine **14** (64 mg, 0.075 mmol) was placed in a 50 ml round-bottomed flask, under argon atmosphere, and dry DMF (4 ml) was added. The system was then protected from light and buthyl bromide (2 ml, 0.019 mol) was added. The reaction mixture was stirred for 5 hours at 50ºC. After completion (the color of the mixture turns

into dark-blue), methyl iodide was evaporated under reduced pressure, as well as a part of the DMF (some ethanol can be added to smooth the progress of the DMF evaporation). At this point, 10 ml of water and a couple of spoons of NH_4PF_6 were added. The resulting mixture was stirred for 30 minutes at room temperature. Finally, another 10 ml of water were added precipitation of the product as a dark-blue solid was observed. The mixture was left overnight in the fridge to ensure completion of precipitation. The product was collected by filtration, and purification was carried out washing with water, cold toluene, hexane, and diethyl ether. SubPc **32** was obtained as a dark-blue solid (70 mg, 64%). m.p.>250 ºC; ^{1}H NMR (300 MHz, DMSO-d_6, 298 K): δ (ppm) = 9.23 (s, 3H, H*e*); 9.03 (d, 6H, *J* = 6.5 Hz, H*a*); 8.93 (m,6 H, H*g*, H*f*), 8.42 (d, 3H, *J* = 15.3 Hz, H*d*), 8.36 (d, 6H, *J* = 6.5 Hz, H*b*), 7.98 (d, 3H, *J* = 15.3 Hz, H*c*), 6.77 (d, 2H, *J* = 8.5 Hz, H*i*), 5.31 (d, 2H, *J* = 8.5 Hz, H*h*), 4.54 (m, 6H, H*k*), 1.93 (m, 6H, H*l*), 1.32 (m, 6H, H*m*), 1.03 (s, 9H, H*j*), 0.94 (t, 18H, *J* = 7.1 Hz, H*n*).

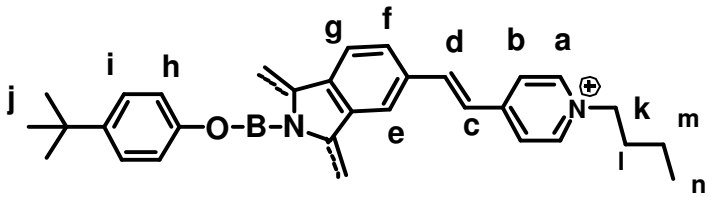

^{13}C NMR (300 MHz, DMSO-d_6, 298 K): δ (ppm) = 152.03, 145.61, 139.63, 137.82, 137.10, 131.22, 130.64, 125.62, 123.99, 121.85, 117.56, 48.10, 33.24, 32.18, 31.06, 28.35. ^{31}P NMR (119 MHz, DMSO-d_6, 298 K): δ (ppm) = -144.23 (sept, 1P, $J_{P\text{-}F}$ = 711.4 Hz); ^{19}F NMR (282 MHz, DMSO-d_6, 298 K): δ (ppm) = -71.3 (d, 6F, $J_{P\text{-}F}$ = 711.4 Hz); IR (KBr): *v* (cm^{-1}) = 3060, 2950, 2922, 2865, 1620, 1465, 850, 560. UV/Vis (DMSO): λ_{max} (nm) (log(ε))= 344 (4.42), 369 (4.29, sh), 400 (3.96, sh), 554 (3.92), 575 (4.09, sh), 604 (4.25), 620 (4.15, sh). MS (ESI, MeOH + 0.1% formic acid): *m/z* = 584.77 [M-2PF_6^-]$^{2+}$, 341.53 [M-3PF_6^-]$^{3+}$.

4-iodophenolate-[2,3,9,10,16,17-hexabuthylthio-7,12:14,19-diimino,-21,5-nitrilo-5H-tribenzo[c,h,m][1,6,11]triazacyclopentadecinato-(2)-κN^{22},κN^{23},κN^{24}]-boron(III) (33)

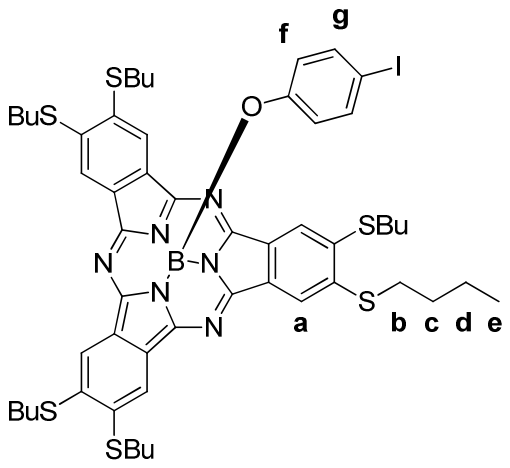

m.p.>250 ºC; ^{1}H NMR (300 MHz, $CDCl_3$, 298 K): δ (ppm) = 8.55 (s, 6H, H*a*), 7.04 (d, 2H, *J* = 8.1 Hz, H*g*), 5.21 (d, 2H, *J* = 8.1 Hz, H*f*), 3.23 (m, 12H, H*b*), 1.80 (m, 12H, H*c*), 1.58 (s, 12H, *J* = 6.8 Hz, H*d*), 1.01 (t, 18H, *J* = 6.8 Hz, H*e*). ^{13}C NMR (300 MHz, $CDCl_3$, 298 K): δ (ppm) = 150.74, 140.83, 138.53, 138.00, 128.33, 121.75, 119.56, 118.11, 33.43, 30.66, 22.24, 13.82 ppm; MS (MALDI, DCTB): *m/z* = 1142.3 $[M]^+$ (experimental), 1142.2 (calculated), 923.24 $[M\text{-axial}]^+$.

4-(3-pyridylethynyl)phenolate-[2,3,9,10,16,17-hexabuthylthio-7,12:14,19-diimino,-21,5-nitrilo-5H-tribenzo[c,h,m][1,6,11]triazacyclopentadecinato-(2)-κN^{22},κN^{23},κN^{24}]-boron(III) (34)

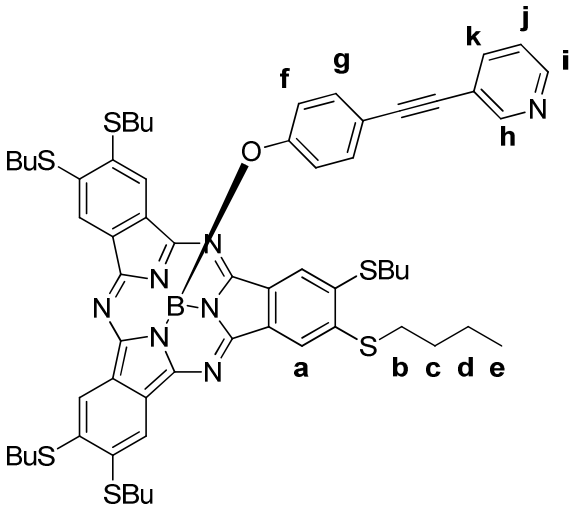

m.p.>250 ºC; ^{1}H NMR (300 MHz, $CDCl_3$, 298 K): δ (ppm) = 8.61 (s, 1H, H*h*), 8.56 (s, 6H, H*a*), 8.45 (d, 1H, *J* = 3.6 Hz, H*i*), 7.65 (d, 1H, *J* = 6.6 Hz, H*k*), 7.19 (m, 1H, H*j*), 7.00 (d, 2H, *J* = 7.3 Hz, H*g*), 5.45 (d, 2H, *J* = 7.3 Hz, H*f*),), 3.23 (m, 12H, H*b*), 1.80 (m, 12H, H*c*), 1.58 (s, 12H, *J* = 6.8 Hz, H*d*), 1.00 (t, 18H, *J* = 6.8 Hz, H*e*); ^{13}C NMR (300 MHz, $CDCl_3$, 298 K): δ (ppm) = 153.64,152.07, 150.63, 148.23, 140.58, 138.57,

138.34, 132.83, 128.40, 123.09, 119.65, 118.18, 115.55, 92.78, 84.98, 33.45, 30.67, 22.39, 13.89. MS (ESI, MeOH + 0.1% formic acid): *m/z* = 1119.3 $[M]^+$ (experimental), 1118.4 (calculated), 922.02 $[M\text{-axial}]^+$.

4-(methyl-3-pyridiniumethynyl)phenolate-[2,3,9,10,16,17-hexabuthylthio-7,12:14,19-diimino,-21,5-nitrilo-5Htribenzo[c,h,m][1,6,11] triazacyclopentadecinato -(2)-κN^{22},κN^{23},κN^{24}]-boron(III) hexaflourophosphate(35)

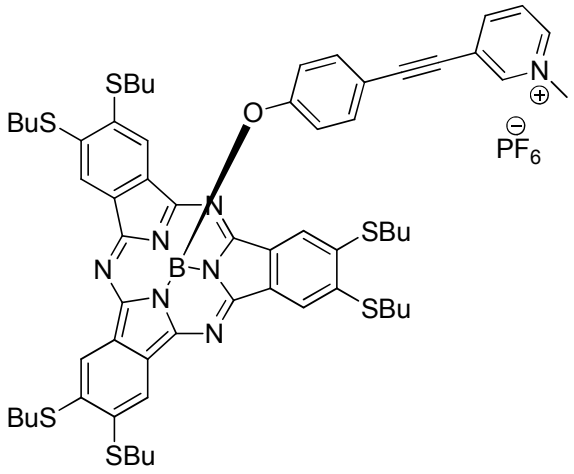

m.p.>250 ºC; ^{1}H NMR (300 MHz, $CDCl_3$, 298 K): δ (ppm) = 8.56 (s, 6H, H*a*), 8.50 (bs, 1H, H*i*), 8.47 (s, 1H, H*h*), 8.14 (d, 1H, *J* = 7.9 Hz, H*k*), 7.81 (t, 1H, *J* = 6,6 Hz, H*j*), 6.98 (d, 2H, *J* = 7.9 Hz, H*g*), 5.43 (d, 2H, *J* = 7.9 Hz, H*f*), 4.30 (s, 3H, H*l*), 3.21 (m, 12H, H*b*), 1.82 (m, 12H, H*c*), 1.60 (q, 12H *J* = 7.1 Hz, H*d*), 0.99 ppm (t, 18H, *J* = 7.1 Hz, H*e*). m.p.>250 ºC; ^{13}C NMR (300 MHz, $CDCl_3$, 298 K): δ (ppm) = 155.10, 150.72, 145.79, 143.19, 140.71, 133.48, 128.23, 127.99, 126.00, 119.48, 119.35, 112.93, 99.67, 49.01, 33.30, 30.49, 22.22, 13.73 ppm; . ^{31}P NMR (119 MHz, $CDCl_3$, 298 K): δ (ppm) = -144.50 (sept, 1P, $J_{P\text{-}F}$ = 711.3 Hz); ^{19}F NMR (282 MHz, $CDCl_3$, 298 K): δ (ppm) = -70.7 (d, 6F, $J_{P\text{-}F}$ = 711.3 Hz); MS (ESI, MeOH + 0.1% formic acid): *m/z* = 1132$[M\text{-}PF_6^-]^+$.